1975

Mechanisms Of Corona Quenching And Sparkover Phenomena In Electrostatic Precipitation

Mahfoz Baki Awad

MECHANISMS OF CORONA QUENCHING AND SPARKOVER PHENOMENA IN ELECTROSTATIC PRECIPITATION

by

Mahfoz Baki Awad

Faculty of Engineering Science

Submitted in partial fulfillment

of the requirements for the degree of

Doctor of Philosophy

Faculty of Graduate Studies

The University of Western Ontario

London, Ontario

June, 1975

ACKNOWLEDGEMENTS

Foremost amongst those who shared to my joy and pain in the past three years stands my advisor Professor G.S. Peter Castle. His invaluable advice, encouragement, and great interest throughout the course of this work have been a constant source of inspiration for me. The material presented in this thesis has been appreciably refined through hundreds of hours of useful discussions with him.

Thanks are also extended to Professor P.A. Fraser for his helpful discussions and invaluable advice.

Gratitude is also expressed to Mr. Dave Waytowich of the Engineering Mechanical Shop for his good fabrication of the apparatus.

To all the members of the electrical group, it is my pleasure to express a sincere appreciation for the very nice time I have enjoyed working with them. I acknowledge the N.R.C, for their financial support.

Last, but not least, I am greatly indebted to my wife Ragaa for her warm support, great confidence and never failing open mindedness.

M.B. AWAD

linear corona current density varies appreciably in the axial direction of the precipitator depending upon the charging and collection processes.

Experiments were carried out to investigate the effect of the inlet specific surface area on the collection efficiency at fixed total air flow rate and fixed applied voltages. The results showed that for low values of initial corona current densities, as the inlet specific surface area increases, the efficiency decreases. For higher values of initial corona current densities however, as the inlet specific surface area increases, the collection efficiency increases slightly. Another set of efficiency experiments were made using a fixed inlet specific surface area of 14.7 m^2/m^3 to study the relative importance of the applied voltage and the corona current. The results showed that for low values of initial corona current densities the magnitudes of both the applied voltage and the corona current are significant. For higher values of initial corona current densities however, the value of the corona current is the main factor with the applied voltage having only a slight effect.

The second part of this work was devoted to a study

of the sparkover voltage and the maximum pre-sparking corona current as affected by the particle concentration, the corona wire diameter, the polarity of the corona and the geometry of the outer electrode (i.e tube or plate). The results showed that under the experimental condition used here positive corona has higher sparkover voltage than the negative in both geometries with and without particle space-charge effects. The particle space-charge was found to raise the sparkover voltage. The amount of increase in the sparkover voltage in a single unit precipitator is dependent on the particle concentration in the exit section and hence on the collection efficiency. However, in all the cases tested the amount of increase in the sparkover voltage was not sufficient to compensate for the reduction in the maximum pre-sparking corona current due to corona quenching. The maximum pre-sparking corona current decreases as the corona wire diameter increases in the positive corona. In the negative corona however, the maximum pre-sparking corona current stays practically constant with the increase in corona wire diameter up to approximately 2.5 mm diameter, beyond which it decreases. Consideration of these results, coupled with a thorough review of the streamer theory of breakdown in point-to-plane geometry have led to a proposed mechanism

for the sparkover conditions under both polarities.

The third part of this study was carried out to investigate the effect of heating the corona wire on both the corona quenching and the sparking characteristics. Experiments showed that heating the corona wire counteracts the corona quenching effect on the corona voltage-current characteristics. Efficiency measurements at different particle concentrations showed that the collection efficiency increases with negative corona on heating the corona wire. The amount of increase is especially appreciable at low corona current densities. In the positive corona however, the collection efficiency decreased with heating the corona wire. In this positive case also, the sparkover voltage and the maximum pre-sparking corona current were drastically reduced by heating the corona wire. In the negative corona however, the sparkover voltage stays practically constant with a slight increase in the maximum pre-sparking corona current.

ACKNOWLEDGEMENTS

Foremost amongst those who shared to my joy and pain in the past three years stands my advisor Professor G.S. Peter Castle. His invaluable advice, encouragement, and great interest throughout the course of this work have been a constant source of inspiration for me. The material presented in this thesis has been appreciably refined through hundreds of hours of useful discussions with him.

Thanks are also extended to Professor P.A. Fraser for his helpful discussions and invaluable advice.

Gratitude is also expressed to Mr. Dave Waytowich of the Engineering Mechanical Shop for his good fabrication of the apparatus.

To all the members of the electrical group, it is my pleasure to express a sincere appreciation for the very nice time I have enjoyed working with them. I acknowledge the N.R.C, for their financial support.

Last, but not least, I am greatly indebted to my wife Ragaa for her warm support, great confidence and never failing open mindedness.

M.B. AWAD

TABLE OF CONTENTS

LIST OF TABLES

LIST OF FIGURES

NOMENCLATURE

a	=	corona wire radius and particle radius, m
A	=	total collecting surface area, m^2
A_c	=	Cunningham correction coefficient, dimensionless
Δa	=	thickness of the ionized sheath at corona onset, m
b	=	radius of the outer tube, m
c	=	one-half wire-to-wire spacing (between centers), m
d	=	distance between two parallel plates, cm
E	=	electric field, V/m
E_{av}	=	average electric field inside the ionized sheath, V/m
E_c	=	charging electric field, V/m
E_o	=	corona-starting field with clean gas, V/m
E_o'	=	corona-starting field with dusty gas, V/m
E_p	=	precipitating electric field, V/m
F_1	=	electric force acting on a charged particle, N
F_2	=	viscus drag force acting on a particle, N
$I_{max.}$	=	maximum pre-sparking corona current, A
j_l	=	linear corona current density, A/m
j_{lc}	=	linear corona current density with clean gas, A/m
J_{lc}	=	Average linear corona current density with clean gas, A/m
j	=	corona current density, A/m^2

j_{ld} = linear corona current density with dusty gas, A/m

J_{ld} = average linear corona current density with dusty gas, A/m

(j_{lc}/j_{ld}) = linear corona current suppression ratio, dimensionless

(J_{lc}/J_{ld}) = average linear corona current suppression ratio, dimensionless

K = Boltzmann's constant, $J/^{o}K$

K_i = ion mobility, $m^2/(V \cdot s)$

K_p = particle mobility, $m^2/(V \cdot s)$

L = effective length of the corona wire, m

N_o = undistorted ion concentration, m^{-3}

N_p = particle number density, m^{-3}

p = dimensionless parameter, equation (22)

P_h = heating power to the corona wire, W

q = particle charge, C

q_i = ion charge, C

$q_{max.}$ = limiting particle charge, C

Q = total gas flow rate, m^3/s

r = radial distance from tube axis, m

s = one-half plate-to-plate spacing, m

S = specific surface area of the particles, m^{-1}

S' = surface area of the particles per gram of D.O.P., cm^2/g

S_{in} = inlet specific surface area of the particles, m^{-1}

t = time, s

T_A = absolute temperature, ^oK

T_o = absolute temperature of the air flowing without heating the corona wire, ^oK

T_{av} = average absolute temperature in the ionized sheath under heating the corona wire, ^oK

V = applied voltage, V

V_o = corona onset voltage with clean gas, V

V'_o = corona onset voltage in the presence of particle space charge, V

$\bar{v}_i$ = rms ion velocity, m/s

ω = particle migration velocity, m/s

x = longitudinal distance from wire axis, m

$\bar{x}_g$ = geometric mean diameter of the particles, cm

y = transverse distance from wire axis, m

α = first Townsend's ionization coefficient, cm^{-1}

β = Townsend's ionization coefficient by ion collision, cm^{-1}

γ = second Townsend's ionization coefficient, dimensionless

Γ = dimensionless parameter, equation (42)

δ = relative gas density, dimensionless

ε_o = permittivity of free space, 8.86×10^{-12} F/m

η = collection efficiency, dimensionless, coefficient of electron attachment, cm^{-1}

κ_p = relative dielectric constant of particle, dimensionless

λ = mean free path of air ions at STP, m

ρ = density of the D.O.P., g/cm^3

ρ_i = ion space-charge density, C/m^3

ρ_p = particle space-charge density, C/m^3

σ_g = geometric standard deviation of particle radii, dimensionless

τ = charging time constant, s

CHAPTER I

INTRODUCTION

1.1. Industrial gas cleaning

The problem of air pollution is one which grows with modern civilization and is generally a direct result of it. Growth and expansion of industrial operations has given rise to the emission of large amounts of smoke, dust, and fume as well as gaseous pollutants such as sulphur dioxide, sulphur trioxide, carbon monoxide, etc. There are two fundamental reasons for gas cleaning in industry [1]:

(1) Protection of the individual working in industry, the public in general, and property from both the particulate and gaseous pollutants.

(2) Recovery of valuable materials such as copper, lead or gold or waste gases for heating and power generation.

Air pollution control equipment may be classified into two groups [2]:

(1) Equipment for controlling gaseous emissions: There are three general methods for removing gaseous constituents. Gases may be either absorbed in a liquid, adsorbed on a solid surface or changed chemically into a harmless gas by catalytic reaction or combustion.

(2) Equipment for controlling particulate matter: This may be classified broadly as mechanical and electrical. Mechanical processes include all those which depend fundamentally on inertial or mechanical forces, namely, gravity settling, centrifugal, or cyclonic separation, gas washing, or scrubbing, filtration through screens, fabric bags, or packed beds, and sonic agglomeration. The electrical process, commonly referred to as electrostatic precipitation, differs basically from all mechanical methods in that the forces of separation act directly on the suspended particles and are electrical in nature.

1.2 Electrostatic Precipitation

The separation of suspended particles from a gas by the process of electrostatic precipitation requires three fundamental steps[3]:

(1) electrical charging of the suspended particles;

(2) collection of the charged particles in an electric field, and

(3) removal of the precipitated material from the collecting electrodes.

For particle charging, the corona discharge is universally used in electrostatic precipitation. The corona is usually established between a fine wire maintained at high voltage and a cylinder or plate at ground potential. The corona discharge at the fine wire causes ions to traverse the

intervening space and to charge the particles. There are two different classifications for electrostatic precipitators:

(1) The Cottrell or single-stage precipitator, figure (1-A), is used for industrial dust collection in the electric-power industry, the cement industry, paper mills, the chemical industry, etc. These precipitators deal with gases having particle concentrations which often reaches several grams per cubic meter and the temperature of the gases may be as high as 1000°F (4). In such industrial precipitators the high voltage electrode is usually operated at a high negative voltage, because a higher voltage and a higher efficiency can be attained than with positive polarity and the generation of some ozone is not objectionable. In this case particle charging and collection occur by the same corona field.

(2) Two-stage precipitator, figure (1-B), for air conditioning purposes is operated with a positive high voltage applied to a fine wire, so that the resulting corona discharge will charge the particles. This charging stage is followed by a collection stage in which a strong electrostatic field deposits the particles on a collecting plate. Positive polarity is usually used because it generates less ozone than if the same precipitator was operated with negative polarity. In this type of precipitator the dust concentration in the incoming air is usually less than 0.02 gram per cubic meter and the air temperature is

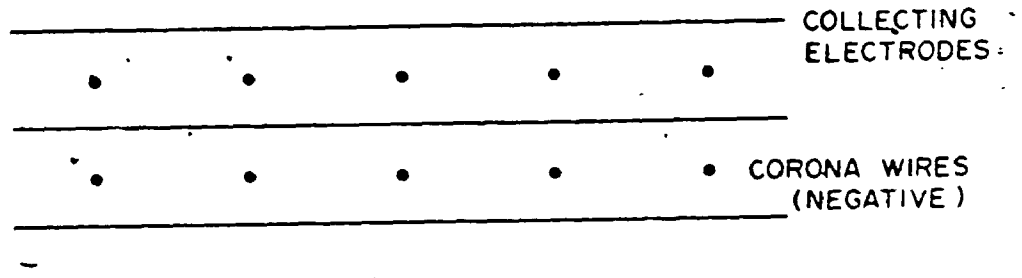

(A) SINGLE STAGE

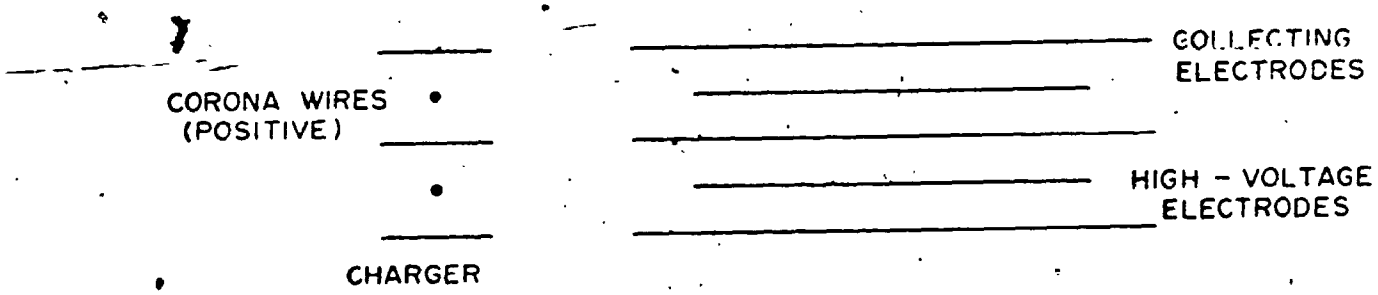

(B) TWO - STAGE

FIGURE 1. SCHEMATIC DIAGRAMS OF SINGLE - STAGE AND TWO - STAGE PRECIPITATOR WITH PLATE ELECTRODES.

usually in the range of ordinary room temperatures.

1.3 Advantages and disadvantages of electrostatic precipitation

The use of electrostatic precipitators for the collection of air contaminants has grown because of many inherent advantages, some of which are:

(1) High collection efficiency can be attained

(2) The finest particles in the submicron size range, which defy almost all other air cleaning devices, can be collected effectively[5].

(3) Pressure and temperature drops are small.

(4) Very large gas flow rates can be handled. However, the electrostatic precipitators have some drawbacks, some of which are:

(1) Initial cost is high.

(2) Some materials are extremely difficult to be collected because of extremely high resistivity causing the back corona phenomenon, or extremely low resistivity causing reentrainment.

(3) The use of a precleaner, generally of the cyclonic type, may be required to reduce the particle concentration in a precipitator. High particle concentrations in a precipitator can cause corona quenching. This phenomenon was one of the reasons for the failure in 1884

of the pioneering attempt by Lodge and Walker to precipitate lead oxide fume on a commercial scale[6].

1.4 General Objectives

Let us consider the last two drawbacks in the operation of electrostatic precipitators raised in the previous section. The first drawback is related to the behavior of the dust once it has been precipitated on the collecting electrode. This has been the subject of extensive studies by many investigators. The second is related to the behaviour of the dust prior to the deposition on the collecting electrode. Although the phenomenon of corona quenching has been observed for many years in electrostatic precipitators dealing with moderate or heavy concentrations of dust and has been the subject of considerable interest[7] to [12], it does not appear to have received the same attention in the recent literature as the previous effects. Since the present trend towards using finely ground, lower grade, coals of high ash content will probably accelerate in the next decade, it seems important to look further at the effect of the particle space-charge on the collection efficiency.

The purpose of the present work was to conduct an experimental study on the phenomenon of corona quenching to investigate:

(1) The effect of the particle concentration on the corona characteristics and compare the experimental results with some of the existing theories.

(2) The effect of some parameters such as the geometry of the outer electrode and the diameter of the corona wire on the corona quenching phenomenon and compare with some of the previous theoretical work.

(3) The effect of the particle concentration on the collection efficiency of electrostatic precipitators. This effect has found no direct answer in the literature in spite of its great practical importance.

(4) The effect of heating the corona wire on corona quenching and collection efficiency.

(5) The actual linear corona current density distribution in the axial direction of a wire-tube precipitator under conditions of corona quenching.

In addition to the above objectives, a portion of the study was devoted to an attempt to investigate the sparking characteristics for positive and negative corona of wire-tube and wire-plane geometries under the following conditions:

(1) with clean air,

(2) in the presence of corona quenching, and

(3) case (1) and (2) with heating the corona wire.

Special emphasis was given to the maximum pre-sparking corona current as influenced by different parameters due to the importance of this current on the performance of electrostatic precipitators.

CHAPTER II

THE ELECTRICAL THEORY OF ELECTROSTATIC PRECIPITATION - A CRITICAL REVIEW

2.1 General

The present study was started by undertaking a thorough literature survey of most of the electrical aspects involved in the theory of electrostatic precipitation. This chapter reviews some of this theory as developed by several previous workers and emphasises the assumptions involved and their interpretation. Only subjects that are related to the present experimental work are discussed.

The characteristics of the corona discharge utilized in the precipitator equipment is of vital importance to the processes of charging and collection of the suspended material. Of particular interest is the electric field distribution in the interelectrode spacing as related to the corona current density and the geometry of the electrodes. Attention is focused on the wire-tube and wire-plate geometries which are normally encountered in electrostatic precipitators.

2.2 Mechanisms of Corona Formation

Let us consider a system of two electrodes immersed

in a gas such as atmospheric air, one electrode is a fine wire having a much smaller radius of curvature than an outer coaxial cylinder. As the potential difference between the electrodes is raised, it has been found that the gas in the vicinity of the fine wire breaks down at a voltage less than the complete spark-breakdown value for the gap under consideration. This partial breakdown is called "corona" and the fine wire is normally called the corona wire or discharge electrode. The critical field intensity at the surface of the corona wire to start the negative corona (i.e with the corona wire having negative polarity) may be given by Whitehead's empirical formula [13]:

$$E_o = (310.2\ \delta + 9.54\ (\delta/a)^{\frac{1}{2}}) \times 10^4 \quad V/m \qquad (1)$$

Under positive corona, Whitehead's formula is

$$E_o = (337\ \delta + 8.13\ (\delta/a)^{\frac{1}{2}}) \times 10^4 \quad V/m \qquad (2)$$

and Peek's [14] empirical equation for both polarities is:

$$E_o = (300\ \delta + 9\ (\delta/a)^{\frac{1}{2}}) \times 10^4 \quad V/m \qquad (3)$$

The above three formulae were derived from experiments on fine corona wires. Comparing equations (1) and (2),

one can see that for the normal corona wire sizes encountered in electrostatic precipitators, E_o for negative corona is higher than that for positive corona, and this is in agreement with the observations in previous published work [15] that the negative corona has a slightly higher onset voltage than the positive for the wire-tube geometry. Equation (3) does not allow for any polarity effect.

Townsend's investigations of electron ionization in gases led to the concept of the electron avalanche in which each new electron produced generates further new electrons by ionization. The first Townsend's ionization coefficient α, which governs this avalanche, is dependent upon the type of the gas, the electric field strength, and the gas density. At constant gas temperature, α for any given gas is given by:

$$\alpha/p = f\ (E/p) \qquad (4)$$

The functional form of equation (4) must be evaluated experimentally for each gas of interest [3]. An experimental curve for air as found by Townsend [16] is shown in figure (2). From this curve one can see that α increases rapidly with E and fairly rapidly with the gas temperature.

The corona discharge in the negative case is initiated

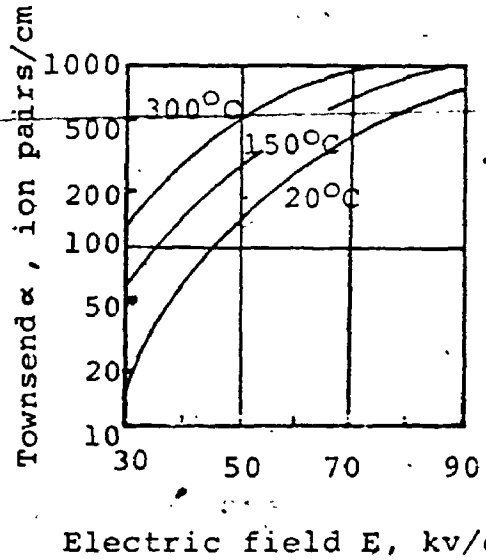

FIGURE 2. TOWNSEND IONIZATION COEFFICIENT FOR AIR AT 760 mm PRESSURE (3)

by electrons that are sufficiently accelerated in the high field-intensity region near the corona wire surface to produce electron avalanches. Ultimately, electrons created in the avalanche move to the region of low field intensity, where they attach to neutral molecules and form negative ions. Positive ions left behind in the avalanche move towards the wire, and are neutralized on contact with it. In addition to electrons and positive ions, excited molecules are also present[17], as the result of electron collisions. These give up their excess energy in the form of photon radiation. Positive ions, as well as photons, imparted on the corona wire surface create secondary-emission electrons which help to maintain the self-sustained discharge. The visual appearance of the negative corona is a series of localized glow points or tufts which appear in a rapid motion on the corona wire surface[3]. The discharge tuft has been found on a theoretical basis to be composed of two layers around the corona wire. Inside this layer, because of the much higher mobility of the electrons with respect to the positive ions, the net ion space charge is mainly positive. In the outer layer, the electrons become attached to gas molecules forming negative ions. At the outside of this layer, almost all the electrons will have become attached.

In the positive corona discharge, the primary electrons occurring at or just beyong the outer boundary of the ionized sheath are attracted to the positive corona

wire and, in moving through this high field region produce electron avalanche which generate many new electron-positive ion pairs and no appreciable electron attachment occurs; i.e $\eta=0$. The electrons are collected at the wire, while the positive ions are driven to the passive electrode. As in the negative corona, the build up of the positive ion space charge in the passive zone stabilizes the discharge. The most probable source of the primary electrons required to maintain the positive corona is the release of electrons from the gas molecules through photo-ionization by ultra-violet light quanta radiated from the visible glow region. Therefore, the positive corona is considered to be entirely a gas process. The wire itself serves merely as a collecting electrode for the electrons. The visual appearance of the discharge zone in this case is in striking contrast to the negative corona. The localized tufts are normally replaced by a uniform ionized sheath covering the surface of the corona wire. However, with the presence of scratches, sharp edges, or material deposits at the surface of the corona wire, some form of a localized discharge, similar in shape to the tufts of negative corona, may be formed.

When the corona occurs in each of the above two cases, the electric field at the corona wire surface should be modified by the ion space charge field. However, it has normally been assumed that this field strength stays constant at the corona onset level when the applied voltage is higher than the value necessary for corona onset[16] [17] [19]. Recent experimental[20] and

theoretical[18] work has shown that in the negative corona the field strength at the corona wire surface at the position of a corona tuft may fall to 30% below the onset value. Midway between the tufts the field strength should be just below the onset gradient. In the positive corona the fall in the field at the corona wire surface depends upon the form of the discharge. For a uniform glow discharge the field at the corona wire surface stays constant at its onset value independent of the applied voltage. If localized discharges or streamers are formed in this positive case, the field may fall by as much as 15% below the onset value.

Many attempts have been made to arrive at the thickness of the ionized sheath and the voltage drop across it as affected by the applied voltage. Townsend[16] in 1914 assumed that the electric field strength at the surface of the corona wire stays constant and equal to E_o, and the electric field strength at the outer edge of the ionization zone is 30 kV/cm (an approximate value of field at which cumulative ionization results in breakdown). Cobine[21] in 1941 used Townsend's assumptions and derived an expression for the thickness of the ionized sheath at the corona onset to be:

$$(\Delta a) = 9/300\ (a)^{\frac{1}{2}} \quad m \qquad (5)$$

at standard temperature and pressure. Note that the validity of both of these assumptions by Townsend are

questionable.

A comparison between the thickness of the uniform ionized sheath in positive corona and the thickness of the localized tufts in negative corona was made by Castle and Awad[15] based upon consideration of the physical nature of the discharge in both polarities. The existance of localized visible tufts in negative corona is evidence of long ionized paths of electrons. The outer boundary of the tuft is determined by the commencement of the region where most of the electrons created in the ionization zone have low energy and attach to neutral molecules to form negative ions. This occurs at a relatively low field region from the corona wire where $\alpha = 0$ and η is large enough. In the positive corona however, the outer boundary of the sheath is limited by the high electric field region required to keep energetic electrons able to cause ionization i.e $\eta = 0$ and α is very high. Therefore, because of the difference in the outer boundary conditions of the tufts and the uniform sheath, the thickness of the negative corona tuft should be appreciably higher than the thickness of the positive corona uniform sheath at the same applied voltage. Recent experimental work[22] has confirmed this polarity effect.

Loeb[23] in 1953 and Colli et al[24] in 1954 showed on a theoretical and experimental basis respectively that

the voltage drop across the ionized sheath stays constant at its onset value and equal in magnitude to the corona onset voltage. Troost[25] in 1954 reported also high values for this voltage drop (15 kV for cylindrical precipitator 30 cm diameter and 34 kV for duct precipitator 33 cm plate-to-plate spacing). On the other hand, Lowe and Lucas[26] in 1954 claimed that this voltage drop is negligible. White[3] in 1963 reported also that the ionization region near the wire acts only as an ion source and that the remaining space is filled with unipolar ions which "consume most of the voltage applied to the electrodes". During the author's work in 1973 on ozone generation by the corona discharge[27], the voltage drop across the ionized sheath near the corona onset based upon Townsend's and Cobine's assumptions was estimated as the product $E_{av}\ \Delta a$. For example, a corona wire of diameter 6.4×10^{-2} m (0.025") gave $(E_{av}\ \Delta a) = 2.87$ kV whereas the onset voltage was approximately 12 kV. This implies that this voltage drop may be a fraction of the onset voltage but may not be negligible especially close to the corona onset.

From the above it can be seen that there is no definitive answer to the question of the voltage drop across the ionized sheath. If one considered that this zone has much higher conductivity and much less thickness than the outer passive zone, it looks unreasonable that

the voltage drop across this region can reach these high values. On the other hand, it can not be negligible since there should be appreciable amount of electrical power dissipated inside this sheath to cause ionization, to supply the resulting chemical reactions, and to release electro magnetic radiation and mechanical energy as acoustic waves.

The following equations which describe the unipolar ion space-charge zone, were written[17] [28] as follows:

$$\nabla.\bar{E} = \rho_i/\varepsilon_o \qquad (6)$$

$$\nabla.\bar{j} = 0 \qquad (7)$$

$$\bar{j} = K_i \rho_i \bar{E} \qquad (8)$$

$$\bar{E} = -\nabla V \qquad (9)$$

Equation[8] is for the corona current density and should be applied only for low fields[29] similar to those in the passive zone. These equations can be combined in a single third-order non-linear partial differential equation as follows[28]:

$$\text{div } (\nabla V \nabla^2 V) = 0 \qquad (10)$$

Solutions of the above equations under different conditions for the wire-tube and wire-plate geometries will be considered in the next two sections. Equation[7] justifies taking j_{1c} as constant.

2.3 The electric field distribution in wire-tube geometry under particle free condition

Let us consider an infinitely long wire of radius a at the center of a tube of radius b (b≫a). Prior to the corona onset, $\rho_i = 0$ and $j = 0$, and equations (6) to (9) lead to:

$$\nabla . \bar{E} = 0$$

and $$\bar{E} = - \nabla V$$

Taking V as the applied voltage at the surface of the wire and grounding the outer tube, integration will give:

$$E = V/r \ \ln(b/a)$$

which represents the electrostatic field distribution in the gap.

Above the corona onset, equations (6) to (9) for this geometry give:

$$\frac{1}{r} \frac{d}{dr} (rE) = \rho_i/\varepsilon_o \qquad (11)$$

$$E = - \frac{dV}{dr} \qquad (12)$$

$$j_{lc} = 2\pi r K_i \rho_i E \qquad (13)$$

Eliminating ρ_i from equation (11) using equation (13) gives:

$$rE(dE/dr) + E^2 - (j_{lc}/2\pi\varepsilon_o K_i) = 0 \qquad (14)$$

This equation is integrated to:

$$E^2 = (dV/dr)^2 = (j_{lc}/2\pi\varepsilon_o K_i) + C^2/r^2$$

where C is an integration constant which was evaluated on the assumptions:

(1) The field at the surface of the corona wire stays constant at its onset value E_o.

(2) The ionized sheath is only a source of ions of negligible thickness and voltage drop so that $r_i \simeq a$, $E_i = E_o$, and all the applied voltage is consumed by the unipolar ion space charge which fills all the gap.

Based upon those assumptions the well-known equation:

$$E = (j_{lc}/2\pi\varepsilon_o K_i) + (a/r)^2(E_o^2 - (j_{lc}/2\pi\varepsilon_o K_i)) \qquad (15)$$

is obtained.

For sufficiently large r ($r \gg a$) and j_{lc} (far from the corona onset voltage), equation (15) simplifies to:

$$E = (j_{lc}/2\pi\varepsilon_o K_i)^{\frac{1}{2}} \qquad (16)$$

which is independent of r.

From the above one can see that, because of the assumptions involved, the validity of equations (15) and

(16) to represent accurately the actual field distribution in the gap is questionable in any particular case.

An attempt was made by Cooperman[30] to check the validity of equation (15) experimentally. The technique he used was based upon shooting a ball of fixed diameter through the passive zone of the discharge and to a Faraday cage where the charge picked up was measured by an electrometer. The ball was fired at different velocities so that a plot was obtained as shown in figure (3). This plot represents the Pauthenier charging equation (see section 2.5) in its reciprocal form. Therefore, the intersection with the ordinate was equated with the reciprocal value of the theoretical maximum charge acquired by a particle by the ion bombardment mechanism in a uniform space charge field, (see equation (20) section 2.5). From this equality, the electric field at certain firing position of the ball was obtained and compared with the calculated value using equation (15). The results showed a 10% variation in the experimentally estimated fields and the calculated values from equation (15). However, the technique as described by Cooperman "was not pushed to a high level of accuracy". Therefore, equation (15) may be used only for estimating purposes of the electric field distribution in the wire-tube geometry.

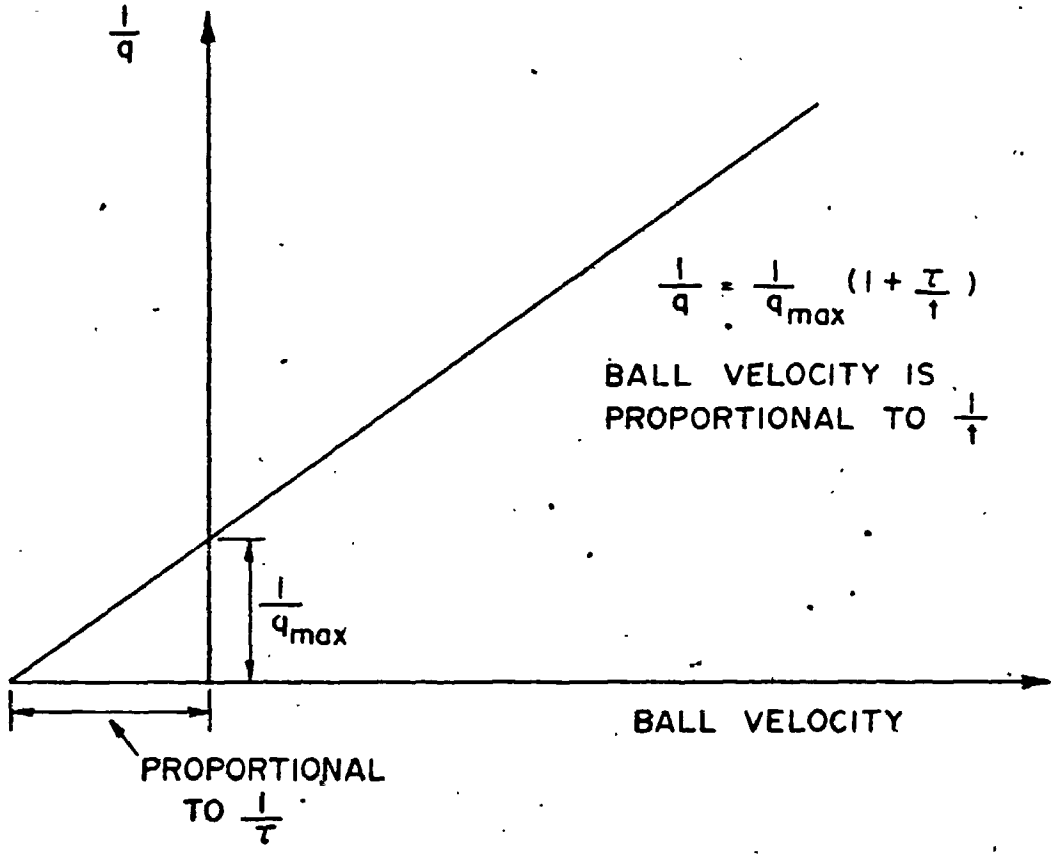

FIGURE 3. COOPERMAN'S TECHNIQUE FOR THE ESTIMATION OF THE ELECTRIC FIELD.

2.4 The electric field distribution in wire-plate geometry under particle-free condition

Apart from the simple wire-tube configuration discussed in the previous section, it is very difficult to obtain analytical solutions for the electric field distribution in the wire-plate geometry from the general equations (6) to (9). The work in the literature regarding this has been found in two main areas:

(1) Electrostatic Precipitation.

(2) High-voltage unipolar transmission lines.

Prior to the corona onset voltage, the electrostatic potential distribution in the duct, figure (4a) is given by Cooperman[31] in terms of the rapidly converging infinite series:

$$V(x,y) = V \frac{\sum_{m=-\infty}^{\infty} \ln \frac{\cosh(\pi(y-2mc)/2s)-\cos(\pi x/2s)}{\cosh(\pi(y-2mc)/2s)+\cos(\pi x/2s)}}{\sum_{m=-\infty}^{\infty} \ln \frac{\cosh(\pi mc/s) \quad -\cos(\pi a/2s)}{\cosh(\pi mc/s) \quad +\cos(\pi a/2s)}} \qquad (17)$$

Attempts to find the electric field distribution in this geometry under the presence of the ion-space charge distortion can be classified into theoretical and experimental.

(A) Theoretical

In solving equations (6) to (9) for the wire-plate geometry, it is normally assumed that the ion-space charge

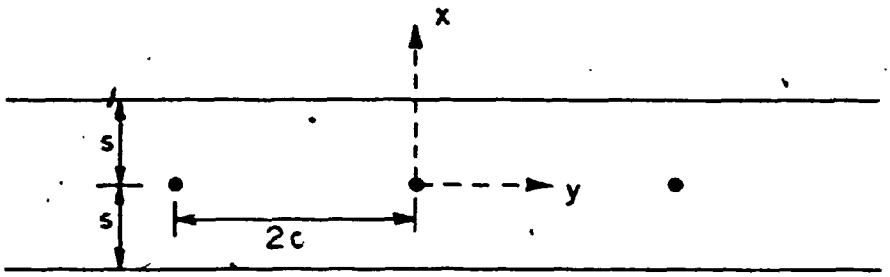

(a)

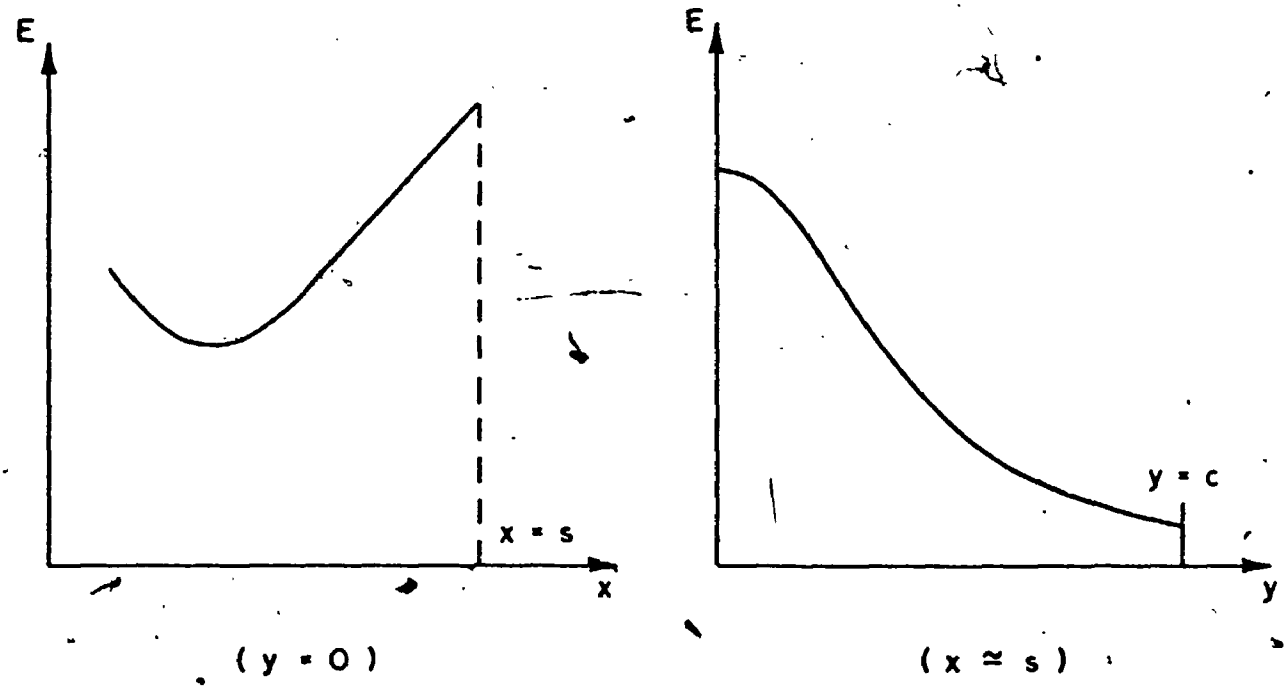

(y = 0)

(x ≃ s)

(b)

(c)

FIGURE 4. DUCT PRECIPITATOR AND ELECTRIC FIELD DISTRIBUTION.

affects only the magnitude but not the direction of the electric field[32] [33]. Based upon this assumption, if $\bar{E}$ is the electric field at any point in the presence of ion-space charge and $\bar{E}'$ the space-charge-free field at this point, then

$$\bar{E} = \xi \bar{E}' \tag{18}$$

where ξ is a scalar function. In this case, the electric field at any point can be obtained by solving equations (6) to (9) simultaneously and the gradient of the potential (i.e the potential is measured with the presence of the ion-space charge) at any point must give a value for the electric field that completely satisfies Poisson's equation. This assumption and the method of solving equations (6) to (9) simultaneously is correct for wire-tube geometry because the angular deviation of the flux lines between the ionized and the space-charge free field is zero. However, in the case of the wire-plate configuration, this angular deviation may take important values due to the asymmetrical geometry[34] [35]. In this case the ion-space charge affects both the magnitude and direction of the electric field and hence equation (18) is not valid and solving equations (6) to (9) simultaneously should yield only an approximate result. If one obtained the potential distribution by solving equations (6) to (9) then

the gradient of this potential gives an electric field in the direction of the electrostatic field having a magnitude not equal to the actual total field. However, without this assumption, the analysis of ionized fields would be extremely difficult as it would require numerical solution of nonlinear partial differential equations in complex geometries[32].

Based upon solving equations (6) to (9) numerically, the general trend of the electric field was found to be as shown in figure (4,b,c,)[29].

Regarding the corona current density distribution at the plane, theoretical[36] and experimental[36] [37] work indicated the general trend shown in figure (5). Note that the electric field distribution at the outer electrode follows the pattern of the corona current density distribution at this electrode, figure (4c).

(B) Experimental

Cooperman[30] in 1956 developed the method of shooting balls through the corona region described in the previous section. Penney[38] in 1960 developed the method of using a fine wire as a probe for the potential distribution at any section in the corona region. Both techniques were difficult to carry out resulting in considerable uncertainty in the measurements. The electric field distribution at a plane parallel to the outer electrode and close to it as obtained by these results is shown in figure (6). Penney's results agree with the results of the theoretical analysis[29]

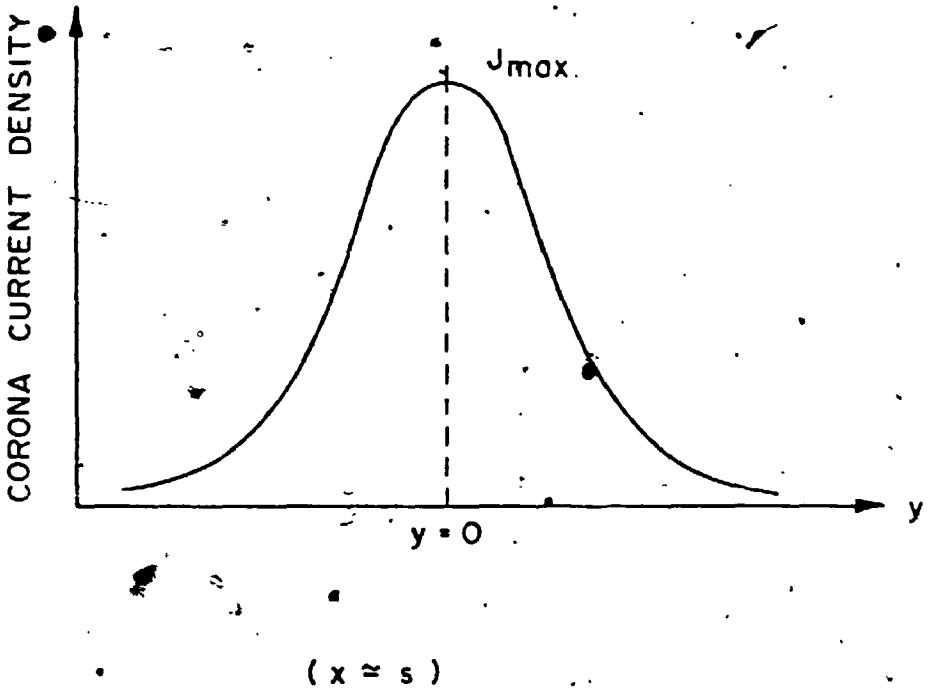

FIGURE 5. CURRENT DENSITY DISTRIBUTION AT THE COLLECTING ELECTRODE.

in the general trend whereas Cooperman's results do not. One can possibly explain this important discrepancy as follows: The electric field at any point as predicted by Cooperman's method should be representative of the actual total field at this point. This is because this field is obtained from charge measurement. Penney's results were based upon assuming that the ion-space charge does not affect the direction of the electric field and hence was obtained by taking the potential gradient. Penney[38] stated "the charge associated with the corona current has very little effect on the direction of the equipotential line at any point in space". Penney's results agreed with the theoretical results[29] because both were based upon the same assumption. Therefore, one can say that Cooperman's results may at least give a realistic general trend for the total field distribution.

It is interesting to note that one of the tests carried out by these two authors had close conditions. Comparison of the results obtained indicates a reasonable agreement only for the value of the electric field close to the outer electrode opposite to the corona wire and a wide disagreement at all other points as can be seen from figure (6).

From the above, it appears that predicting the actual field distribution in wire-plate geometry even for the

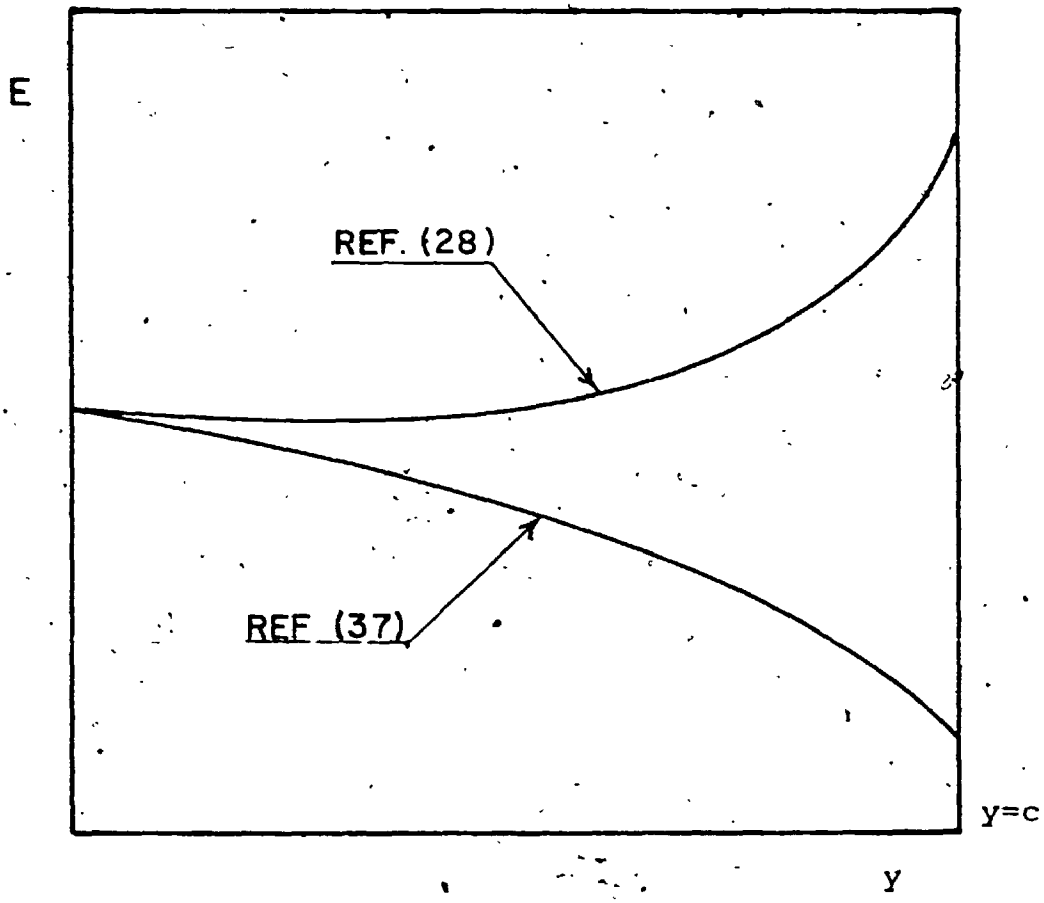

FIGURE (6) THE GENERAL TREND OF THE ELECTRIC FIELD DISTRIBUTION IN THE VICINITY OF THE OUTER ELECTRODE

simple case of only ion-space charge present in the gap (i.e with no particle-space charge) is a very difficult task.

2.5 Particle Charging

As previously stated, the interelectrode spacing between the corona wire and the outer electrode contains a cloud of rapidly moving gaseous ions, of the same polarity as the corona wire. The charging of the dust particles is attributed to some portion of the ionized gas molecules coming into collision with, and attaching themselves to, the dust particles. It is considered that a collision between the ionized molecule of gas and the dust particle can be brought about by either of two distinct mechanisms, the field or bombardment charging and the ion diffusion charging. In practice however, both are operative at the same time and have relative importance dependent upon the conditions in any given case. The first investigation of the field charging process was due to Pauthenier and Moreau-Hanot[39]. In the diffusion charging process, the first significant work was made by Arendt and Kallman[40]. Both theories were refined by White[3]. Examples of more recent refinements are the work by Hignett[41] in the field charging process and by Liu et al[42] in the diffusion charging process.

The field charging process which predominates for particles larger than approximately 0.5 micrometer

diameter assumes:

(1) Interaction effects between the charged particles are neglected. This assumption may be justified if the average particle separation is at least several particle diameters.

(2) The electric field and the ion concentrations are uniform in the volume of the precipitator. Because of the non-uniformity of the electric field and the ion concentration normally encountered in electrostatic precipitators this assumption cannot be justified in any particular case.

(3) The magnitudes of the charging field and ion concentrations are the undistorted values originally present in the gap without the presence of particle space-charge distortion. This may be a satisfactory assumption only for a situation of low particle space charge with respect to the ion space charge originally present in the gap.

(4) The particles are spherical. The effect of the non-spherical particles on the charging process may be to distort the field in the vicinity of the particle in a some-what different manner from that caused by spherical particles. Smith and Penney[43], found experimentally that non-spherical particles introduce only a very slight change from the charge acquired by spherical particles of equal surface area. Hence, this assumption may be acceptable.

Under these assumption the charge acquired by a spherical particle is given by:

$$q = q_{max} \quad t/(t+\tau) \tag{19}$$

$$q_{max} = 4\pi\varepsilon_o p E a^2 \tag{20}$$

$$\tau = 4\varepsilon_o/q_i K_i \tag{21}$$

and $$p = 2((K_p-1)/(K_p+2)) + 1 \tag{22}$$

Equations (20) and (22) show that the limiting charge q_{max} carried by a particle, of a definite material, is directly proportional to the surface area of the particle and to the strength of the charging field. Equation (21) shows that the charging time constant τ is inversely proportional to the ion space-charge density present in the gap and hence one can see that the higher the corona current density the faster will be the charging rate. With the ion space-charge densities commonly found in industrial precipitators, the charging time constant is very brief compared with the treatment time of the gas in the precipitator.

In the diffusion charging process which predominates for particles smaller than about 0.2 μm diameter, the particle in an ionized gas acquires a charge by the random thermal motion of the ions and their consequent collision with and attachment to the particle. White[3], making

use of the Kinetic theory, developed an expression for the charge acquired in time t by an initially uncharged particle as follows:

$$q = (4\pi\varepsilon_o a\ K\ T/q)\ \ \ln((aN_o q^2\ \bar{v}_i\ t/4\varepsilon_o\ KT_a) + 1) \qquad (23)$$

Laboratory measurements of particle charging in unipolar corona as compared with the previous theoretical equations have been made by many investigators for a wide range of conditions[41] [42]. These results show that particle charging theory for spherical particles may be considered to be reasonably satisfactory for particles larger than 0.5 μm diameter and smaller than 0.2 μm. For the range of particle sizes between 0.2 to 0.5 μm diameter, combined bombardment and diffusion charging must be considered. Cochet[44] derived the following equation that agreed with his experimental data:

$$q = \ \ (1 + \lambda/a)^2 + \frac{2}{(1 + \lambda/a)}\ \ \frac{K_p - 1}{K_p + 2}\ \ x$$

$$4\pi\varepsilon_o\ E\ a^2\ (t/t+\tau) \qquad (24)$$

2.6 Particle collection and efficiency calculation

Particle collection in an electrostatic precipitator has been the subject of extensive studies by many investigators. A thorough review for this work is presented by White[3] and Robinson[6].

Particle collection is essentially a process of mass transfer from the gas moving through an electrostatic precipitator in a direction normal to the collecting surface. In a laminar flow precipitator, the only collecting force acting on the charged particle is due to the electric field i.e Coulomb force. However, all industrial precipitators operate with various degrees of turbulence. Under gas-turbulence condition forces due to the turbulent diffusion of aerodynamic and electrodynamic origin are also operating besides the Coulomb-force.

The force F_1 acting upon a particle carrying a charge q in a precipitating field strength E_p is given by:

$$F_1 = q\, E_p \tag{25}$$

For particles charged by ion bombardment to the limiting value as given by equation (20), the electric force F_1, is given by:

$$F_1 = 4\pi\varepsilon_o\, pa^2\, E_c\, E_p \tag{26}$$

From Stokes' low, the viscous drag force F_2 acting upon

a spherical particle having a Reynolds number less than unity is given by:

$$F_2 = 6\pi\mu\, a\omega \qquad (27)$$

At steady state conditions, the force due to the electrical field and the viscous force are equal, hence

$$\omega = 2p\varepsilon_o\, E_c\, E_p\, a\, /3\mu \qquad (28)$$

If the particle size is comparable with the mean free path of the gas molecules ($\simeq$ 0.1 μm in atmospheric air), there is a greater tendency for particles to slip between molecules and ω as given by equation (28) should be modified by the Cunningham correction coefficient and becomes:

$$\omega = (2p\varepsilon_o\, E_c\, E_p\, a/3\mu)\ (1 + A_c\, \lambda/a) \qquad (29)$$

However, it is significant to note that equation (29), which is normally accepted in the literature, considers the Cunningham correction coefficient but not diffusion charging for this size range of particles.

Under realistic precipitating conditions, calculations of the particle-migration velocity are difficult because of the absence of any adequate theory for calculating the electric field distribution inside the precipitator even under clean gas condition. The situation is further complicated by the presence of variable particle concentrations

at different sections of the precipitator. This will be discussed in section (7.2). In calculating ω assuming ion-bombardment charging, it has been argued that the maximum field near the wires be used for E_c in equation (27) since turbulence may be supposed to carry most particles into the high field region at some point before collection[6].

According to White[3] and Deutsch[45] the collection field E_p must be assigned that value of electric field intensity at the wall which acts upon particles entering the collection sublayer beside the wall. On the other hand, according to the diffusion theories of precipitation, E_p should be assigned the average value of the field in the gap since particle convection is considered active throughout the cross section[6].

On the basis of assuming uniform particle concentrations at any cross section of the precipitator, which implies complete and continuous mixing of particles, the Deutsch efficiency equation is given by:

$$\eta = 1 - e^{-A\omega/Q} \qquad (30)$$

This uniform particle distribution is in conflict with the recent theories of precipitation by various investigators as presented in reference (6).

CHAPTER III

DISTURBING EFFECTS IN ELECTROSTATIC PRECIPITATORS

3.1 General

In spite of the amount of literature devoted to the subject of electrostatic precipitation and of the successful performance of modern precipitator plants, the present state of the theory of the subject is unsatisfactory, and many phenomena encountered in industrial precipitators are imperfectly understood. Many of these phenomena, if present, disturb the operation of an existing precipitator and thus reduce its collection efficiency and require using a larger size precipitator to achieve a given collection efficiency. For example:

(1) In the precipitation of high resistivity dusts, the phenomenon of back corona may be present. The back corona discharge occurs at the passive electrode covered with the high resistivity deposits. Such discharges reduce the precipitator collection efficiency by lowering the sparkover voltage. In addition it produces ions of opposite sign to the main ions originating from the vicinity of the corona wire thus reducing the effective particle charging.

(2) If a precipitator is operating without back

corona, the particles must be losing charge by conduction. If the particles have moderate resistivity (but still below the value 10^9 Ohm-m required for back corona) the ionic current will maintain some negative charge which will provide a force of adhesion that prevent reentrainment of the particles with the gas stream. On the other hand, if particles have a very low resistivity (the lower limit usually quoted for effective precipitation is 10^2 Ohm-m) a charge of the same sign as the collecting electrode will be induced and this will produce a force tending to remove them from the collecting electrode.

Extensive reviews for the previous two disturbing effects which have been studied by numerous investigators have been given by White[3] and Robinson[6].

(3) If a precipitator is dealing with high particle concentrations i.e high particle surface area per unit volume of the gas, the problem normally encountered is named "corona quenching". This phenomenon has been the subject of study by many investigators. Since the present study is mainly concerned with this phenomenon, more detail will be given to previous contributions in this subject in the following section.

3.2 Corona quenching in Electrostatic Precipitators

3.2.1 Practical aspects of corona quenching

It is well-known that zinc oxide and other industrial fumes from furnaces or roasters if present in moderate or heavy concentration in the gas entering an electrostatic precipitator would severely reduce the corona current to a value of the order of one percent of its normal value. In this case the collection efficiency is severely reduced. This situation is normally called "severe corona quenching" and was examined in detail by Deutsch more than 40 years ago[45]. Disqussing the effect of such dense fume upon precipitator performance, Deutsch wrote "In electrical precipitation practice, it has been known for several years that in spite of very high potentials impressed upon the electrodes, essentially no discharge current can be made to flow through the dust-gas mixture; the collection efficiency (under these conditions) is relatively low, although a considerable part of the suspended material is still separated from the gas". Sproull[7] distinguished the previous case of severe corona quenching from a relatively mild quenching. Mild corona quenching was first studied by Pauthenier and Moreau-Hanot[10]. This case occurs in various degrees in most precipitators dealing with moderate concentrations of the suspended material.

3.2.2 Mild corona quenching

Suspended dust particles become highly charged as they enter the ionized corona field of an electrostatic precipitator. The resulting change in the space-charge distribution can play a role on the electric field distribution in the gap and the performance of the precipitator. Let us focus attention on the simple wire-tube geometry.

The total linear corona current density in a precipitator consists of charges carried by both free gaseous ions and charged particles and is given by:

$$j_{ld} = 2\pi r E \, (\rho_i K_i + \rho_p K_p) \qquad (31)$$

Under certain conditions near sparkover in negative corona, an electron component may also exist. As the dust concentration increases, ρ_p increases while ρ_i decreases. It is important to note that since the particle mobility K_p is normally 2 to 3 orders of magnitude less than the ion mobility, the measured corona current although smaller than the measured current with clean gas for the same applied voltage, may be assumed carried essentially by free gaseous ions[6]. However, the low mobility particles which are charged with the same sign as the discharge electrode may cause an increase in the total space-charge and hence reduce the ionization field in the vicinity of the discharge electrode. In addition, this build up of space-charge in

the gap may enhance the collection field at the outer electrode.

From the quantitative point of view, Poisson's equation taking the particle space charge effect into account is given by:

$$\nabla.\vec{E} = (1/\varepsilon_o)\ (\rho_i+\rho_p) \qquad (32)$$

Neglecting the charged particle component in the linear corona current density, equation (31) leads to

$$\rho_i = J_{ld}/2\pi rK_i\ E \qquad (33)$$

Considering that the particles are charged to the limiting value by the ion-bombardment process and taking the sum of the charge over a unit volume of the gas, one can get:

$$\rho_p = \varepsilon_o\ pES \qquad (34)$$

Substituting from equations (33) and (34) into (32) and arranging:

$$(dE/dr)+(E/r)-(pES)-(j_{ld}/2\pi\varepsilon_o\ K_i\ rE) = 0 \qquad (35)$$

Solution of equation (35) gives:

$$E^2 = (C/r^2)e^{2pSr} - (j_{ld}/4\pi\varepsilon_o\ K_i)((2/pSr)+(1/(pSr)^2)) \qquad (36)$$

The boundary condition was obtained on the assumption that

the field at the surface of the corona wire stays constant at its onset value irrespective of the corona current and the specific surface area [16] [19] (i.e at r=a, E = E_o). This then gives:

$$C = a^2 E_o^2 + (j_{1d}/4\pi\varepsilon_o K_i (pS)^2) \quad (37)$$

and

$$E(r) = \left\{\left[(a/r)^2 E_o^2 + (j_{1d}/4\pi\varepsilon_o K_i (pSr)^2)\right] e^{2pSr} - (j_{1d}/4\pi\varepsilon_o K_i)\left[(2/pSr)+(1/(pSr)^2)\right]\right\}^{\frac{1}{2}} \quad (38)$$

Lowe and Lucas [9] suggested that the constant C may be obtained from:

$$\int_a^b E\, dr = \text{Applied voltage} \quad (39)$$

where E is obtained from equation (36). They did not however, perform this integration.

Neglecting the electrostatic component of the field $(a/r)^2 E_o^2$ at the outer electrode and constraining the product (2pSr) to be much less than unity, the field at the outer electrode from equation (38) becomes:

$$E = \left\{(j_{1d}/2\pi\varepsilon_o K_i)(1+(2pSr/3))\right\}^{\frac{1}{2}} \quad (40)$$

One can see here, that there are several important assumptions and limitations used in deriving equations (38) and (40):

I. Equation (34) shows that the particles are assumed to be charged by the ion-bombardment mechanism. In other words, the application of the above analysis should be true only for the particle size range, 0.5 μm diameter and above, where diffusion charging may be neglected. This limitation is particularly suspect when it is considered that most cases of serious corona quenching occur due to the presence of large numbers of submicron particles. Strictly speaking, if the diffusion charging is occuring a correction similar to that made by Cochet[43] should be considered. In this case:

$$q_{max} = 4\pi\varepsilon_o \Gamma E a^2 \qquad (41)$$

where

$$\Gamma = (1+(\lambda/a))^2 + (2/(1+\lambda/a)\ ((K_p-1)/(K_p+1))) \qquad (42)$$

On this basis, p has to be replaced by Γ in all the above equations if diffusion charging is to be considered.

II. Neglecting the variations of the electric field at the surface of the corona wire due to the corona current and particle space-charge effects as well as neglecting the voltage drop across the ionized sheath, are questionable assumptions as has been mentioned in section (2.3).

III. (2pSr) must be assumed much less than unity so that the exponential term in equation (38) could be expanded in a power series.

IV. Moreover, if one considered the axial variation in the relative magnitudes of ρ_i and ρ_p due to the charging and collection processes and the corresponding variation of j_{1d} as will be seen in section (7.2), the validity of equations (38) and (40) to predict the electric field of any particular precipitator in spite of their wide acceptability is questionable.

Winkel and Schuetz[8] derived an expression to show the influence of corona quenching on the linear corona current density. This involved assuming the field at the outer electrode to be the same with and without dust loading and was obtained by equating the field strengths obtained from equation (40) with $S = 0$ (no loading) in one case to S finite (with loading) in the other. This gives:

$$j_{1c}/j_{1d} = 1+(2pb/3)\ S \qquad (43)$$

Equation (43) does give qualitative agreement and quantitative disagreement with their results using particles of 50 millimicrometer average diameter. The positive corona gave 5.5 times the corona current quenching predicted by the theory whereas the negative gave 4 times this theoretical value. This quantitative disagreement may be due to replacing the linear corona current density j_{1d} which varies in the axial direction

of the tube precipitator according to different factors (as will be seen in section 7.2), by an average linear corona current density j_{ld} defined as the total measured corona current with dusty gas divided by the length of the precipitator i.e

$$J_{ld} = (1/L) \int_0^L j_{ld}\, dz \qquad (44)$$

In the general case j_{ld} must be different from J_{ld} and hence quantitative agreement with equation (43) for any particular case should not be expected.

Besides the effect of the suspended particles on reducing the corona current at fixed values of applied voltage, they result in an apparent increase in the corona onset voltage. This increase in the apparent corona onset voltage may be considered as a factor indicating the degree of quenching. White[12] derived this effect as follows:

Neglecting the ion space-charge density in comparison with the particle space charge density, Poisson's equation in wire-tube geometry yields:

$$(1/r) \frac{d}{dr} (r\, dV/dr) = \rho_p/\epsilon_o \qquad (45)$$

Integrating this equation twice and substituting the following boundary conditions:

$$(dV/dr)_{r=a} = - E_o = - (V_o/a \ln(b/a))$$

and

$$V(b) = 0$$

after some rearrangement:

$$V_o' = V_o + \frac{\rho_p b^2}{4\varepsilon_o} \tag{46}$$

Substituting from equation (34) for ρ_p, one gets:

$$V_o' = V_o + \frac{pE b^2}{4} S \tag{47}$$

From equation (47) one can see that the apparent increase in the corona onset voltage is only dependent upon the interelectrode spacing and is not affected by the diameter of the corona wire. It is also linearly increasing with the specific surface area of the suspended material. Note that the transfer from equation (46) to (47) involved assuming the particles to be fully charged by the ion bombardment process. This situation is in doubt because of the relatively low corona current density near to the apparent corona onset voltage. Another way to look at the problem will be presented in section (7.2). An alternative to the above method, White[12] also used equation (38) putting r=a to get the apparent field required to start corona in the presence of particle space-charges. He wrote:

$$E_o' = E_o e^{pSr} \tag{48}$$

In a numerical example, putting r=b, White calculated E_o' to be 2.0 E_o and then concluded that a specific surface area of 2.3 m^2/m^3 can result in doubling the apparent corona onset voltage. It is clear that r=a is the right substitution to calculate the field at the corona wire surface. However, using equation (38) in the first place to get the field at the surface of the corona wire is also questionable since it represents the field distribution only in the passive zone outside the corona ionized sheath as it was obtained on the basis of assuming unipolar space-charge in Poisson's equation.

The theory of dust space-charge was extended to duct precipitators by Cooperman[11]. On a theoretical basis, he wrote:

$$V_o' = V_o + \frac{\rho_p b^2}{2\varepsilon_o} \tag{49}$$

$$= V_o + \frac{pE\,b^2}{2} S \tag{50}$$

From equations (47) and (50) it was concluded that the electrical operation of duct precipitators is more sensitive to particle space-charge than in the case of tubes.

3.2.3 Severe corona quenching

If the concentration of the dust particles is so dense that all the free gaseous ions are bound by the low mobility particles, the linear corona current density will be drastically reduced and is given by:

$$j_{ld} = 2\pi r \rho_p K_p E$$

Under this condition Deutsch[46] developed the charge acquired by a dust particle (assuming all particles to be of uniform size) to be given by:

$$q = \rho_i / N_p \qquad (51)$$

According to the Deutsch theory the reduction in the charge acquired per particle is accompanied by an equal reduction in the migration velocity. This will imply that Deutsch assumed the collection field to be constant irrespective of the relative effects of the particle and ion space-charge densities. Based upon this assumption the particle migration velocity is given by:

$$\omega = \omega_{max} \frac{\rho_i}{N_p q_{max}} \qquad (\rho_i \lesssim N_p q_{max}) \qquad (52)$$

where q_{max} is the charge that would be acquired by the field charging process (equation (19)) if the ion space-charge density originally present in the gap was large with respect to the particle concentration and ω_{max} is the associated migration velocity.

It is possible in this case, that the low mobility charged particles enhance the collection field at the outer electrode so that the percentage reduction in the migration velocity may be less than the percentage reduction in the charge per particle. It is not likely, however, in this case that the field enhancement at the collecting electrode compensates for the drastic reduction in the charge per particle.

CHAPTER IV

MECHANISMS AND MODES OF GASEOUS BREAKDOWN

4.1 General

The term "gaseous breakdown" refers to the transition from a non self-sustained discharge to a self-sustained one. Therefore, when breakdown occurs, a current will flow whose magnitude is governed by the external circuit only; that is, this current is totally independent of any external ionization. This current is known as self-sustained. There are several types of breakdown in gases. In uniform fields, the transition to breakdown will lead directly to a sparkover at which the current is theoretically infinite and breakdown between the two electrodes occurs i.e complete voltage breakdown. In non-uniform fields, however, the transition to breakdown will lead at first to currents flowing under the presence of the applied voltage which is normally known as corona or partial breakdown. Then with further increase in the applied voltage, the breakdown will lead to the sparkover condition.

This subject has been of interest and investigation by numerous Physicists and Engineers. Foremost among them is L.B. Loeb who has contributed very significantly to this subject. The published work was thoroughly reviewed

β being "Townsend's second ionization coefficient".

(2) Cathode processes usually referred to as γ-processes, in which electrons are liberated from the cathode by the action in the gas.

When dealing with gas processes Townsend's criterion of breakdown in uniform fields is:

$$(\alpha/\beta) = e^{\alpha d} \tag{53}$$

This process does not have a sound physical meaning because of the inability of ions to ionize by collision and is therefore not satisfactory. Cathode processes lead to a similar criterion of breakdown in a uniform field which is given by:

$$\gamma\, e^{\alpha d} = 1 \tag{54}$$

For a non-uniform field, such as in the corona, the condition is:

$$e^{\int_0^x \alpha dx} = 1/\gamma \tag{55}$$

As a result of some of the assumptions made in deriving the above theoretical expressions, some limitations of the Townsend's mechanism were found and can be summarized as follows[48]:

(a) The time required for the formation of a channel

by Loeb[47] and more recently by Nasser[48].

In the early 1900's, Townsend developed a theory for the mechanism of gaseous breakdown based upon the concept of electron avalanche. Since the 1920's some weaknesses in the application of this mechanism were discovered. Another mechanism of breakdown was then developed and called "streamer breakdown". In this chapter both mechanisms will be considered briefly and then attention will be focused on the corona modes in some of the non-uniform field geometries.

4.2 Townsend's theory of breakdown

According to this theory, the primary process that contributes to the breakdown of the gas is the electron avalanche. The first Townsend's ionization coefficient α which governs this avalanche is defined as the number of new electrons produced by one primary electron moving a unit length in the gas under the effect of the electric field. As mentioned in section (2.3) it is mainly a function of the relative gas density and the prevailing electric field.

The secondary processes that aid the development of a self-sustained discharge as assumed by Townsend are:

(1) Gas processes in which gaseous ionization by ion collision are effective. This is termed β-process,

of a self-sustaining discharge, which is normally called the formative time lag, has been found experimentally to be much shorter than Townsend's mechanism with any secondary action.

(b) The effect of the space-charge left behind the electron avalanche generation on the initial electric field was completely neglected. In many instances, the concentration of ions can reach very appreciable values that distort the initial field to a great extent. This might lead to local augmentation of electron energies and ionization, with a resultant α above that resulting from the static field alone.

(c) In non-uniform fields, the cathode material seems to have little or no influence at all on the breakdown values. This throws doubt on any mechanism involving cathode participation as proposed by Townsend.

These factors make it difficult to reconcile much of the experimental observations with the theory of breakdown based on the Townsend's mechanism although this theory supplied excellent interpretation of various observed phenomena. Thus, the other breakdown mechanism does not seek to replace Townsend's methanism completely; but rather supplements it in the various instances where it does not apply.

Note that the corona characteristic as represented

by the voltage-current relationships in electrostatic precipitators is based upon Townsend's theory of breakdown (3) (6)

4.3 The streamer theory of breakdown

Although a great deal of work has been devoted to studying the so-called streamer mechanism of breakdown, the processes are still far from being fully understood.

In non-uniform fields, breakdown can be locally contained and therefore more conveniently observed. Here the formation of channels of ionization is distinctly different from the electron avalanches predicted by Townsend and has indicated that another process must be taking place. The ionization channels or "streamers" are filamentary, branched, and capable of reaching large distances. If breakdown occurs by a transition from a streamer to a spark, the mechanism involved is sometimes referred to as the streamer breakdown mechanism. This mechanism has been studied under various wave forms of the applied voltage;

(1) An impulse voltage within which the ionic space-charge drift and accumulation can be neglected because of the short-lived applied voltage. A review for this case can be found in detail in reference (48) and will not be of concern here.

(2) A D.C. voltage, with which the ionic space-

charge accumulation must be considered as a factor governing the total electric field. This is the case of interest here and will be considered in more detail.

The physical processes that occur and lead to the formation of the streamers are always easier to be discussed for uniform fields, but the general concept may still be applied in many cases to the non-uniform fields.(48). If in a parallel-plane geometry, an electron starts at the cathode, it will initiate an electron avalanche which results in an accumulation of positive ions. During the build up of this primary avalanche, excitation of gas atoms takes place at the same time the ionization has been occuring. Photons will be emitted from these excited gas atoms as they return to the ground state. These photons will be heading in all directions and will be absorbed at various distances from their origin, depending on the absorption coefficient of the gas. The absorption of photons may lead to a photoionization process which produces photo-electrons. These new photo-electrons will advance toward the anode causing a "~~second-generation auxiliary~~ avalanche". This auxiliary avalanche will emit photons that can participate in developing further generation of auxiliary avalanches. The charge of the auxiliary avalanches helps the growth of the accumulated positive ions created by the primary

avalanche towards the cathode. This process constitutes the formation and growth of an ionized channel from anode to cathode.

Comparing these two mechanisms, it can be seen that the streamer mechanism provides a faster ionization and space-charge accumulation process than Townsend's mechanism through the development of photons and photo-electrons and their auxiliary avalanches. In the next two sections dealing with the corona modes, the process of streamer formation will be considered in non-uniform fields.

4.4 Corona modes in point-plane geometry

4.4.1 Anode corona

(a) Onset Pulses

When the electric field strength at the surface of the point reached a critical value for the corona onset, the discharge appears in the form of onset streamers or burst pulses. Onset streamers may be followed or preceded by the burst pulses. The onset streamers are a form of discharge directed radially from the electrode and it has a luminous stem in the high field region and some branching of less intensity in the low field region. These branches are responsible for the formation of photo-electrons in this low field region which in turn

form negative ions. The field in this case is distorted by both positive and negative ions. A new streamer cannot develop before these negative ions are cleared from the gap. Sometimes a streamer starts to propagate into an area that has not been cleared of the space-charges and thus get "choked". This will be a short streamer with a slower rise and smaller magnitude than the onset streamer and is called burst corona. Loeb[47] called the burst pulses "frustrated streamers".

(b) The steady Glow (Hermstein's glow):

When the voltage is raised further, streamer occurance becomes more frequent until all transient activities stop and a thin glow is formed. The transition from the intermittent onset streamer mode to the steady glow occurs when sufficient negative ion space-charges accumulate around the anode. In the spacing between the anode surface and the negative ion cloud a steady positive glow is formed.

(c) Breakdown streamers:

This intermittent mode develops from the glow when the field becomes adequately high. Breakdown streamers resemble the onset streamers but they are much stronger. If these breakdown streamers reached the plane with enough energy, they might cause electron emission from the cathode. This is called the "return stroke". The conductivity increases in the gap and the spark occurs.

If the return stroke is not formed, a new stronger ionization wave called the "leader channel" is formed and it is sufficient for sparkover.

The occurance of the above three modes or some of them is dependent on the field distribution i.e on the radius of the point, the gap separation, and the applied voltage. This situation is best illustrated by figure (7).(48)

4.4.2 Cathode Corona

(a) Trichel Pulses:

When the electric field strength at the surface of the point reaches a critical value for the corona onset, electrons are ejected from the cathode surface by some mechanism such as field emission or positive ion bombardment. These electrons cause electron avalanche forming positive ions. The positive ions further provide an additional source of electrons through bombardment of the cathode surface. The electron avalanche is choked off in a very short time by the negative ion space-charge which forms by electron attachment just outside the ionization region and reduces the field in that region below the avalanche threshold. The rise time of the pulse is extremely short in the order of 10^{-9} second. The electron avalanche remains off until the negative space-charge is removed by the electric field a sufficient

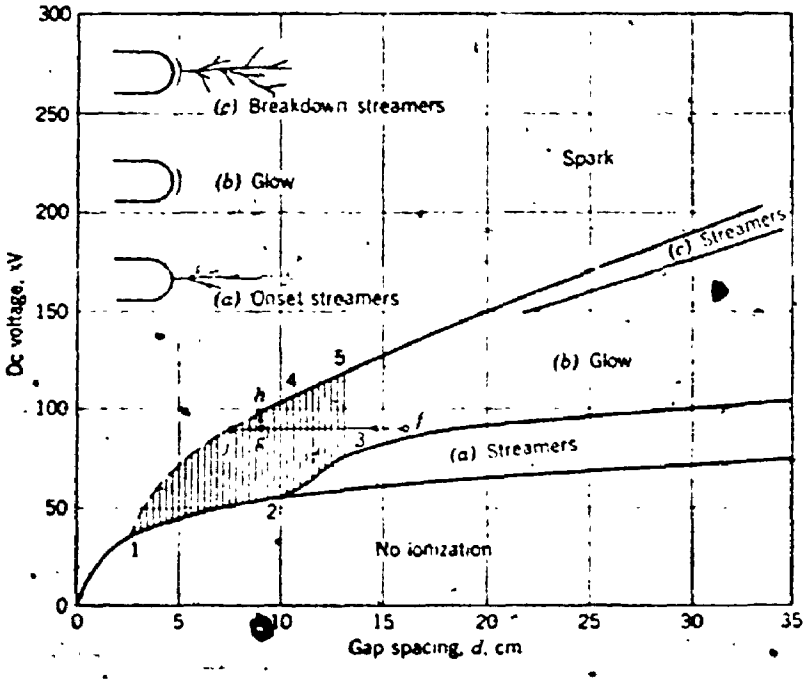

FIGURE (7) THRESHOLD CURVES FOR THE VARIOUS MODES OF ANODE CORONA AND FOR SPARK BREAKDOWN FOR A SPHERICAL ANODE OF 1-cm RADIUS. 1-2 SPARK THRESHOLD; 2-3 SPARK OR GLOW THRESHOLD; 4-5 GLOW-SPARK TRANSITION; 1-4 (ARTIFICIAL) GLOW-SPARK TRANSITION.(48)

distance. The time required for this clearing is called "the clearing time" for the field in the ionization region to regain its critical value. As the applied voltage increases, the clearing time decreases and the pulse frequency increases. However, this frequency cannot increase indefinitely and will reach a critical value which is dependent on the radius of the point. As the diameter of the point increases the critical frequency decreases.

(b) The steady Glow:

With further voltage increase the Trichel pulses, after reaching the critical frequency, change to the steady glow mode.

(c) Negative streamers:

Negative streamers called "Feathers" represent the last mode of corona before sparkover. The Feather current consists of a D.C. component and superimposed pulses. The rise time of these pulses is very long in comparison with any other corona pulses. This implies a slow advance of the streamer head. The length of the Feathers increases with the voltage until one of them cross the gap causing a breakdown, or a retrograde streamer initiates from the anode and meets the Feathers. It is most likely that the positive streamers initiated from the anode in this case are responsible for completing the breakdown.

4.5 Corona modes in wire-tube and wire-plane geometries

These geometries have been of interest in the areas of various industrial applications utilizing the corona discharge as in electrostatic precipitators, electrophotography etc. and in the high voltage and extra-high voltage transmission lines.

In the field of electrostatic precipitation, because of the discovery by Cottrel[49] in 1908 that negative corona is far superior to positive corona for electrical precipitation purposes, negative corona is used almost without exception for industrial precipitation. White[3] mentioned "It is not unusual to find that the sparkover voltage for the negative corona is as much as twice that for the positive corona".

Penney[50] in 1960 mentioned that with corona from a clean metal point-to-plane, sparkover occurs at a considerably lower voltage if the point is positive and because of this it is frequently assumed that positive corona will always result in the lowest sparkover voltage. However, he showed that this situation can be reversed under the presence of some deposits on the electrodes. For example, high resistivity material deposited at the surface of the outer electrode causes more pronounced reduction in the negative sparkover voltage than the positive which in this case resulted in higher sparkover voltage. On the contrary, high resistivity material on the corona wire has a

relatively small effect with negative corona but a very large effect with positive corona.

Cooperman[51] in 1964 carried out experimental measurements of sparkover voltage using clean air at room temperature in wire-tube geometry. His results showed that for tube diameters in the range of 6.3×10^{-2} m(2.5") to 12.6×10^{-2}m(5") and corona wires of diameters 2.54×10^{-4}m(0.010") to 27.5×10^{-4}m(0.109"), the positive corona has higher sparkover voltage than the negative. He concluded that the major barrier to the practical application of positive corona is the formation of dust deposits at the surface of the corona wire. This dust deposits produces "flares" and appreciably lowers the positive sparkover voltage.

Vuhuu and Comsa[52] in 1969 made laboratory studies for the corona modes in wire-plane geometry as a model for an EHV transmission line. Their results showed that the corona mode is dependent upon the diameter of the corona wire as well as the gap separation and can be summarized as follows:

(1) for positive thin corona wires of diameters less than 16×10^{-4}m, as the voltage is increased the corona modes are; burst pulses, glow and sparkover i.e no streamers were observed.

(2) for positive thick corona wires of diameters larger than 16×10^{-4}m using short gap distances (0 → 5cm), or

very long gap distances (above 16 cm to 20 cm) the sequences is the same as the case of thin wires. There exists, however, a critical range of gap distances (5 to 16 cm) for which as the voltage is increased streamers are formed with the burst pulses. This critical range of gap distances was divided into two sub-ranges. For gaps (5→ 10 cm) these onset streamers cause sparkover at voltages only slightly higher than the burst pulse onset level. For gaps (10→16 cm) they do not produce sparkover, but as the voltage is increased further, the glow takes over and the streamers disappear. The explanation of this dependence of the corona modes on the gap separation is rather difficult. However, it is significant to note that for the range of gap distances (5→10 cm) which is the normal spacing for electrostatic precipitators, the sparkover voltage under positive polarity is lower than the value under negative polarity.

From this one can conclude that positive corona may be applied in industrial electrostatic precipitators for high sparkover voltage than with the negative corona provided the corona wire has a diameter less than 16×10^{-4} m. This significant result may be emphasized by Penney's[53] results that dust deposits of high resistivity on a positive thin corona wire surface has a relatively small effect on the sparkover voltage. In other words, the fear of the

presence of streamers due to dust deposits at the corona wire surface should also be small for this size range of corona wires.

(3) For thin (less than 16×10^{-4}m) or thick (above 16×10^{-4}m), negative corona modes under all gap distances, were the same as with the point-to-plane geometry as has been mentioned in section (4.4.2).

CHAPTER V

Experimental Set-up

5.1 General Description of the Apparatus

The experimental arrangement used is shown schematically in figure (8) and can in general be described briefly as follows:

Relatively clean air at room temperature was used to atomize the Dioctyl phthalate (D.O.P.) in an aerosol generator. The smoke coming out of the aerosol generator was diluted with a given quantity of a relatively clean air at room temperature such that the total air flow inside the corona section was maintained constant at any desired value. A venturi expansion section followed by a long intermediate acrylic tube was used between the aerosal inlet and the precipitator to ensure the homogeneity of the flow. At the corona section, a high voltage D.C. power supply was connected to the corona wire while the outer electrode was grounded through a multi-range ammeter* for the corona current measurement. This meter was protected against excessive currents close to sparkover by two solid state

---

*Multimeter, Avometer, Model 8.

Figure (8) Experimental Set-Up

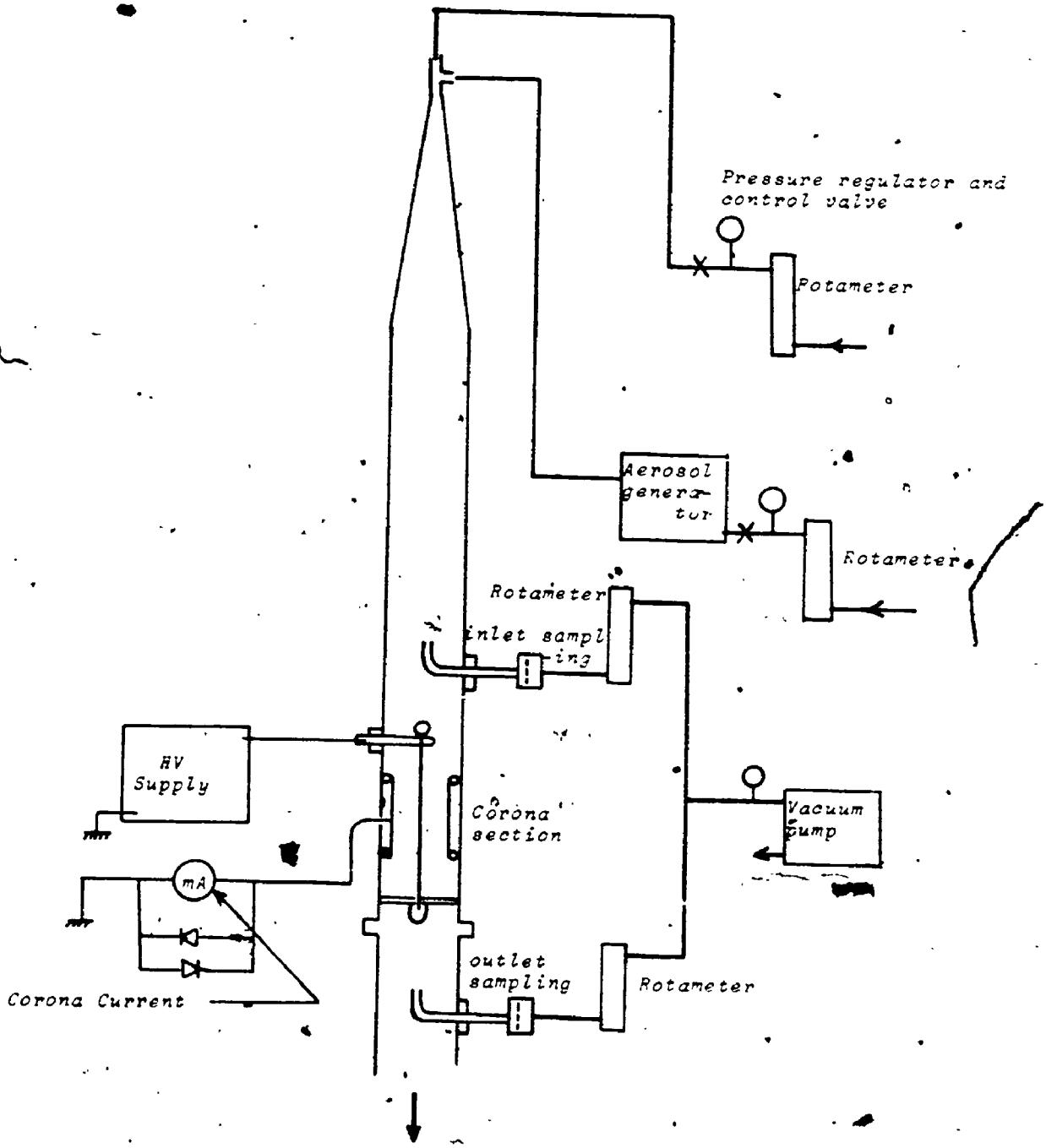

diodes mounted back-to-back having a threshold voltage of 500 millivolts. Upstream and downstream of the precipitator, two sampling nozzles were connected to a vacuum pump through filter papers. The aerosol coming out of the system was exhausted to the atmosphere outside the room. Photograph of the overall test facility is shown in view (9). In the next sections of this chapter, brief description of each component of the system will be considered.

5.2 Air Supply:

Air was supplied by the central compressor system which used outside air as its source. To eliminate pressure fluctuations caused by compressor cycling, the air was passed through a pressure regulating valve at the inlet to the system. Oil from the compressor, water droplets from the air line, and particulate materials were removed before being admitted to the apparatus by two stages of mechanical filtration. The first consisted of a pressure vessel packed tightly with "Viskonaire" filter media. This was followed by an enclosed membrane filter of pore size 0.1 micrometer diameter and surface area of approximately $0.25 m^2$ to remove the remaining intermediate and small sized particles. The secondary air flow rate was monitored with a rotameter and could be varied over the range 1.9 to 18.9 L/s. The aerosol generator air flow rate was also monitored with a rotameter and could be

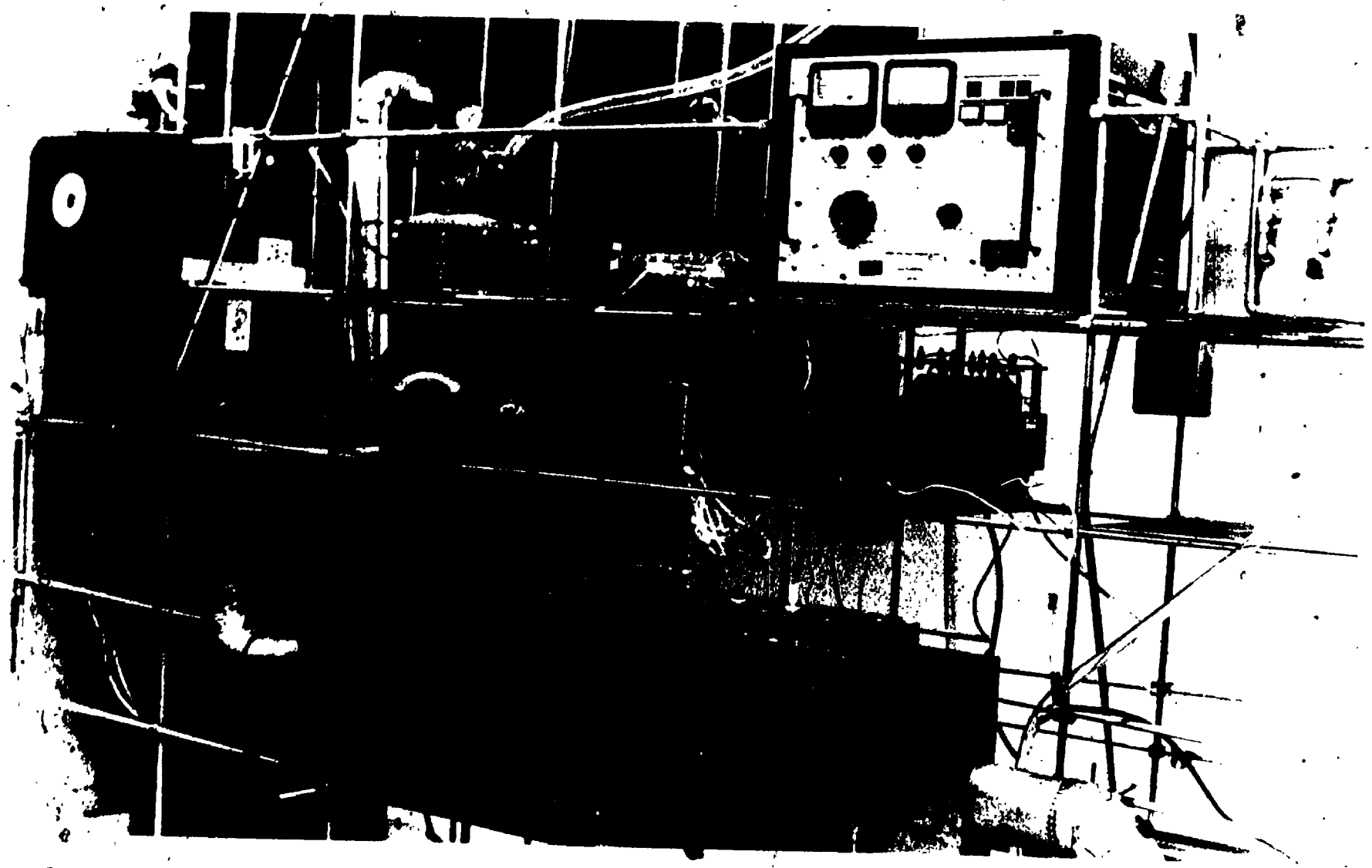

VIEW (9) OVERALL TEST FACILITY

varied over the range 0.5 to 10.8 L/s. The air temperature was that of the ambient and ranged from 20 to 26°C and the relative humidity ranged from 20 to 30% throughout the tests.

5.3 Aerosol Generator:

A Royco D.O.P atomizer, Model 258 was used. Some of the properties of the D.O.P. as obtained from reference (54) are listed in Appendix (A). The smoke was generated by passing air through one or more jet nozzles that are immersed in the liquid D.O.P. in the generator. It has been experimentally determined by the manufacturer that 1.75 Kg/cm^2 (25 pSi) is an optimum pressure for repeatable mass concentration with efficient dispersion of minimum particle size. The test smokes produced by this generator have been shown to be reproducible in particle size distribution and mass concentration[55]. The amount of aerosol can be easily varied by selecting one to six jets. Taking into account the air added by the aerosol generator, the secondary air flow rate was adjusted so that the total air flow rate was kept constant for most of the experiments at 7.1 L/s (15 $ft.^3/min.$).

5.4 Fluorometer:

For the purpose of measuring the collection efficiency and estimating the specific surface area of the suspended material, the technique used was based upon using uranine

2 3

OF/DE

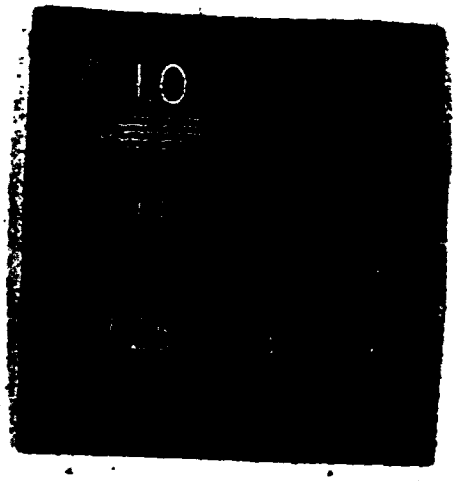

(sodium fluorescein) material as a tracer dissolved in the D.O.P. and using a fluorometer as a detector. The aerosol droplets collected on the filter papers were dissolved with a known quantity of ethyl alchol (between 10 and 100 milliliters). The washings were analysed for the presence of uranine on a Turner fluorometer, Model 111.

The instrument was calibrated using carefully prepared solutions of uranine in ethyl alchol. Linear calibration curves were obtained for uranine concentrations from 0.02 ppm to 0.5 ppm. The instrument was as accurate in the ppb range as in the ppm range. The presence of some D.O.P. did not affect the readings. (See Appendix (B) for the specifications and calibration of the fluorometer).

5.5 Sampling train

The efficiency of aerosol removal was determined from concentration measurements taken at the inlet and outlet sampling points. Each sampling point was fitted with sampling bushings. The sampling nozzles, 1.1 cm I.D. copper tubing, could be adjusted to any radial position by moving it through the holder. For a total air flow rate of 7.1 L/s (15 $ft.^3/min.$) in 10.2×10^{-2}m(4") diameter acrylic tube, the suction rate required for isokinetic sampling was calculated to be 0.083 L/s. A suction pump was used to establish the isokinetic

sampling rates.*

Two rotameters were calibrated using a wet test meter** and adjusted for the required suction rates for the two nozzels.

Gelman Instrument Company Model 2220 in line filter holders were used to hold the filter papers. Gelman Instrument Company Type E glass filter papers were used. This type is specially recommended by the manufacturer for experimental work using the Royco D.O.P. atomizer Model 258 WA.

5.6 Corona Apparatus

Three test units were constructed:

Unit (A) was a wire-tube precipitator. The diameter of the outer cylinder was 7.6 cm (3") and its length 15.3 cm (6"). The cylinder was made of brass with its ends flared and smoothed to eliminate end effects and the possibility of back corona. Sealing at the ends was achieved with an O ring contact between the support ring and mounting tube. Five corona wires of different diameters supported in the center of the outer cylinder were used. Table (1) shows the diameters and materials of these corona wires.

---

*Millipore filter corporation pump, 1/6 H P

**Manufactured by Precision Scientific Corporation.

Table (1) diameters and materials of the corona wires used:

corona wire diameter		Material
0.025 cm	(0.010")	Chromel-A
0.165 cm	(0.065")	Stainless steel
0.236 cm	(0.093")	Steel alloy (17% Chrome)
0.475 cm	(0.187")	Stainless steel
0.635 cm	(0.250")	Stainless steel

Unit (B) was a duct precipitator. The plate-to-plate spacing was 7.6 cm (3") and its length normal to the direction of the flow was 30.6 cm (12"). A homogenizing section was inserted ahead of the precipitator having the dimension of 7.6x30.6x60 cm with an inside perforated plate to introduce low scale turbulence and ensure uniform flow distribution. The ends of the collection plates were flared and smoothed. The same five corona wires as used in the wire-tube precipitator were also employed in this unit.

Unit (C) was a segmented wire-tube precipitator. It was dimensionally identical to Unit (A) except that the outer cylinder was divided into 15 segments separated by thin Acrylic rings 0.0762 cm (0.030") thick. For the purpose of measuring the corona current density distribution in the axial direction under different conditions of particle concentration, each segment was connected to a double-pole switch so that it was either connected to ground or through the microammeter to ground.

5.7 High voltage power supply

Positive and negative polarity can be obtained from the high voltage D.C. power supply* and the potential was

---

*Model #BAL-100-18 of the Universal Voltronics Corporation.

continuously adjustable from zero to 100 kV with a maximum output current of 18 mA. The voltage was measured using the meter provided on the control panel of the power supply after checking its accuracy with an electrostatic voltmeter reading from zero to 30 kV.

5.8 Heating circuit of the corona wire

Experiments with heated corona wire were carried out by applying the high voltage to the outer cylinder of Unit (A) while the corona wire was grounded. A 110 volts, 60-Hz A.C. supply controlled by a variac was used through a 1:1 isolation transformer for heating the corona wire at different heating currents. For estimating the heating power, the wire resistance was measured using a bridge* with an accuracy of 0.2% under no heating conditions.

---

*General Radio Company, 1970, Type 1656, Impedance bridge.

CHAPTER VI

Test Procedures

6.1 Corona current-voltage characteristics

Initial tests were made on each unit to ensure the absence of any end effects and back corona. This was done by darkening the laboratory and raising the applied voltage up to sparkover. The spark was always observed to occur inside the corona test unit. The test started by opening the required number of jets on the smoke generator, adjusting the air pressure to the smoke generator at 1.75 Kg/cm^2 (25 lb/in^2), adjusting the secondary air flow rate to the desired value so that the total air flow rate was kept constant at 7.1 L/s (15 $ft.^3/min.$), and checking that there were no leaks of the smoke from the system. The corona voltage-current characteristic was then measured under both polarities from corona onset up until sparkover. Two runs were made for each test. The results obtained were found to be very reproducible within approximately ± 3%. This was an indication of the reproducible operation of the aerosol generator, the air system, and the high voltage power supply. Accumulation of the oil on the collecting electrode did not show any effect on the voltage-current characteristics. This was an indication

droplets collected on the outlet filter paper were dissolved with 15 or 20 milliliter of ethyl alchol. This was to make both of the readings appear on the same scale on the fluorometer. For the rest of the collection efficiency measurements, each experiment was carried out at least twice. Several experiments were made under different conditions in one day. The filter papers were kept in the jars marked by the number of the test after adding the appropriate amount of ethyl alchol using accurate graduated cylinders. At the measurement time of the concentrations, 4.5 milliliters were transferred from the jars to special cuvate sampling tubes recommended by the manufacturer of the fluorometer. A blank tube containing only ethyl alchol was also prepared to use as a reference for the zero adjustment of the fluorometer. The sampling tubes after the test were thoroughly cleaned using distilled water and then ethyl alchol for several runs and then completely air dried in an oven.

6.3 Estimation of the specific surface area of the suspended material

The smoke produced by this type of aerosol generators was found[55] to consist of polydisperse droplets having a log-normal size distribution with a geometric mean diameter $\bar{x}g$ = 0.36 μm and geometric standard deviation

$\sigma g = 1.66$ as shown in figure (10).

The specific surface area per gram of the D.O.P. assuming spherical droplets obeying the log-normal size distribution is given by[57]:

$$S' = \frac{6}{\bar{x}_{va}\,\rho} \qquad cm^2/g$$

where ρ = density of the D.O.P.

$= 0.98$ gram/cm^3 (see Appendix (A))

$\bar{x}_{va}$ was obtained from the following equation:

$$\ln \bar{x}_{va} = \ln \bar{x}g + 2.5 \ln^2 \sigma g$$

By substituting the values of $\bar{x}g$ and σg

$$\bar{x}_{va} = 8.93 \times 10^{3} \text{ cm}$$

The aerosol surface area per unit volume of the air flowing is given by:

S_{in} = S' x D.O.P. generated per minute x. (air flow rate)$^{-1}$

The amount of the D.O.P. generated per minute using 1,2,3 and 4 jets of the aerosol generator was determined experimentally as in Appendix (C). The specific surface area of the inlet aerosol at fixed total air flow was then found to be:
14.7 m^2/m^3 using 1 jet, 29.4 m^2/m^3 using 2 jets, 36.7 m^2/m^3 using 3 jets, and 44.1 m^2/m^3 using 4 jets.

that the resistivity of the D.O.P. oil is not so high to cause back corona, as also previously reported by Penney[56]. As a precaution corona test section was regularly cleaned after every 4 runs.

6.2 Measurements of the collection efficiency

Initial tests were carried out to check:

(1) The homogeneity of the flow. For this purpose experiments were made with the precipitator off. Runs were made for periods of 10 to 20 minutes using a stop watch. The inlet and outlet filter papers were then carefully transferred to jars where ethyl alchol was added and the jars were tightly closed. The concentration measured at different points in the radial direction by adjusting the position of the nozzle was practically constant within ± 2% indicating good homogeneity of the smoke. The inlet and outlet concentrations were also practically the same within ± 2%.

(2) The reproducibility of the measurements. This was done by carrying out several experiments under certain fixed conditions of particle concentration, total air flow rate, applied voltage and corona current. Each experiment was made at least three times. The aerosol droplets collected on the inlet filter paper were dissolved with 100 milliliter of ethyl alchol while the aerosol

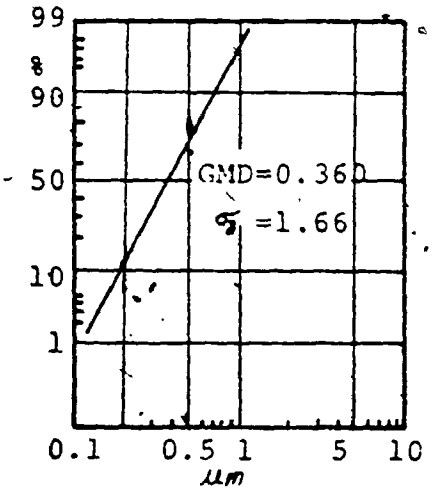

FIGURE 10. CUMULATIVE FREQUENCY DISTRIBUTION OF THE PARTICLE SIZE OF AN AEROSOL PRODUCED BY A ROYCO MOD. 258 WA GENERATOR

CHAPTER VII

Corona quenching: Theory, results and discussion

7.1 General

The theory and the mathematical model describing the mild corona quenching phenomenon presented in section (3.2.2), have several simplifying assumptions. In this chapter a description of the effects of the particle space-charge on the corona current-voltage characteristics and the collection efficiency of electrostatic precipitators will be presented without making these simplyfing assumptions. This theoretical consideration is based upon the physical character of the precipitation process under the influence of certain particle concentration. This will be followed by presenting and discussing the experimental results obtained. Some of these results will be compared with the known theories in the literature.

7.2 Theory

Consider a cylindrical corona apparatus having a (V-I) characteristic under clean gas condition as shown in figure (11), curve 1.

Let us assume uncharged particles having an inlet specific surface area S_{in} are passed through the corona

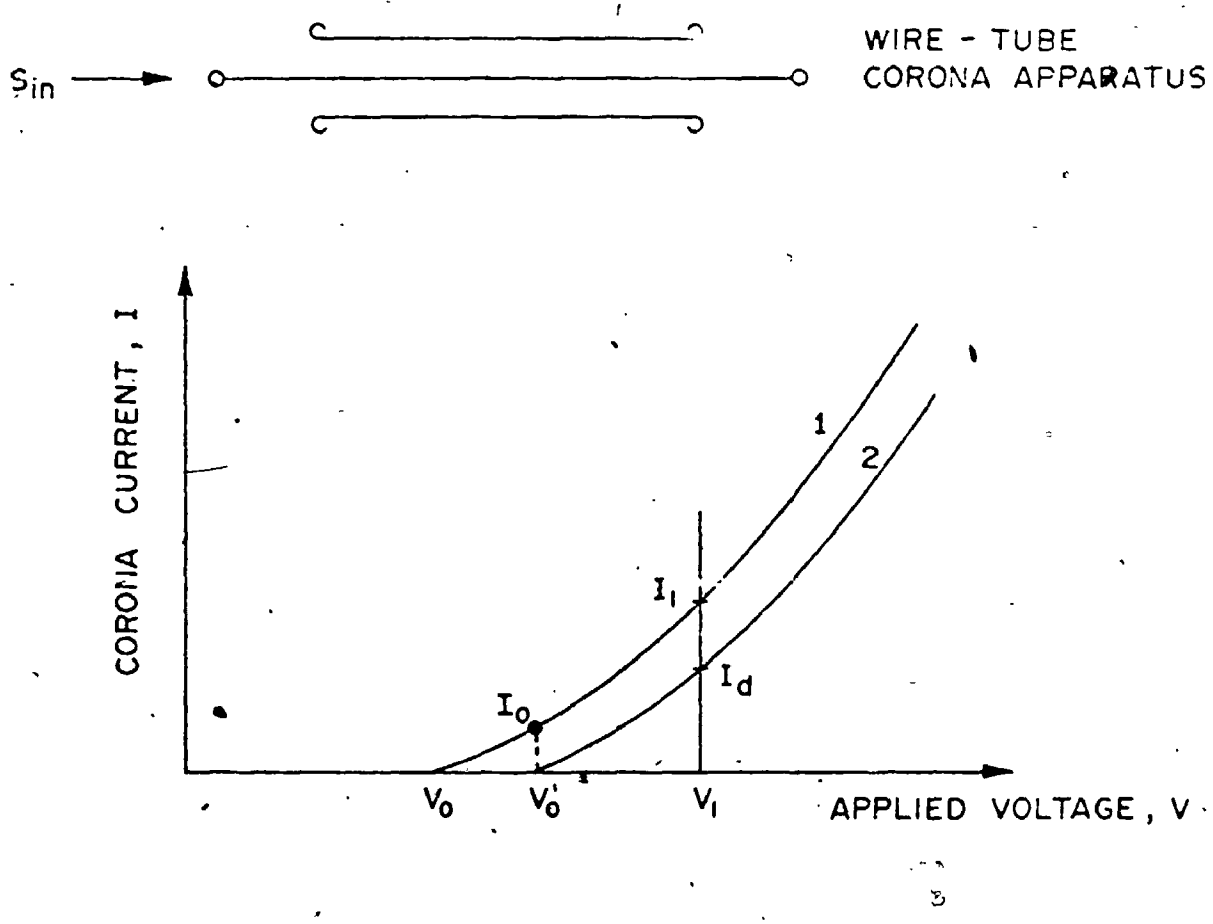

FIGURE II. CORONA VOLTAGE - CURRENT CHARACTERISTICS
CURVE (1) WITHOUT PARTICLE SPACE - CHARGE
CURVE (2) WITH PARTICLE SPACE - CHARGE

apparatus. Starting with zero applied voltage and increasing under the presence of the suspended particles, a value of applied voltage V_o will be reached at which the field at the surface of the corona wire reaches a critical value E_o given by:

$$E_o = V_o/a \ln(b/a) \qquad V/m$$

at which an electron avalanche starts and results in the production of ions and a corona current. However, these weak avalanches and resulting corona current are quickly quenched by the suspended particles i.e most of the ions are bound by the low mobility particles and the corona is apparently choked off. With a further increase in the applied voltage, more ionic current is generated from the ionized sheath and most of the ions are bound by the particles. A value of the applied voltage V_o' will be reached at which the original corona current I_o with clean gas will be quenched to give a certain total measured corona current defining an apparent corona onset voltage as shown in figure (11). In this situation, the particle space-charge effect on the field distribution in the gap should be much greater than the gaseous ion space-charge effect. For this reason, if one would like, for example, to solve Poisson's equation right at the

apparent corona onset, it should be sufficient to consider the particle space-charge effect only. This procedure was followed by White[3] as indicated previously in section (3.2.2). The apparent increase in the corona onset voltage was then found to be:

$$V_o' = V_o + (pES/4)\, b^2$$

However, as mentioned in section (3.2.2), this was based upon assuming that the particles are charged according to Pauthenier's ion-bombardment mechanism.. Such a mechanism should not be applied in this case because of the limited availability of free gaseous ions near the apparent corona onset with respect to the specific surface area. This case should be considered as a severe quenching in which the charge per particle as mentioned in section (3.2.3) is given by:

$$q = (\rho_i/N_p) = (\rho_p/N_p)$$

Substituting in equation (46) obtained from solving Poisson's equation, then

$$V_o' = V_o + (\rho_p/4\varepsilon_o)\, b^2$$

$$= V_o + (\rho_i/4\varepsilon_o)\, b^2 \qquad (56)$$

where ρ_i is the ion space-charge density originally present in the gap with clean gas. This ion space-charge density was just sufficient to produce the corona current defining the apparent corona onset voltage after being carried by certain value of inlet specific surface area. One may express this value ρ_i as a function of the inlet specific surface area S_{in} for wire-tube geometry as follows:

Let us assume:

(1) The average linear corona current density J_{ld} is approximately equal to the linear corona current density j_{ld} since particle collection is relatively small near the corona onset.

(2) The total corona current defining the apparent corona onset with dusty gas is a fixed quantity indicating onset of corona under different particle concentrations.

$$J_{ld} = 2\ \mu A$$

$$= 2 \times 10^{-6}\ A$$

(3) In general the corona current suppression ratio is a function of the inlet specific surface area. Hence,

$$(J_{lc}/J_{ld}) = f(S_{in}) \qquad (57)$$

and

$$I_{lc} = 2\times10^{-6}\, f(S_{in})$$

$$= 2\pi r l \rho_i K_i E$$

Therefore,

$$\rho_i = (2\times10^{-6}\, f(S_{in}))/2\pi r l K_i E \qquad (58)$$

Substituting in equation (56), then

$$V_o' = V_o + (2\times10^{-6}\, f(S_{in})\, b^2)/2\pi r l K_i E(4\epsilon_o)$$

$$V_o' = V_o + (9\times10^3\, f(S_{in})\, b^2)/rEK_i L \qquad (59)$$

The difficulty in this approach is that the function $f(S_{in})$ is dependent upon the charging process of the particles and is difficult to be determined. Note that the amount of increase in the corona onset voltage is inversely proportional to the length of the corona wire. This is reasonable because as the length of the corona wire increases the linear corona current density defining the apparent corona onset voltage decreases and hence the apparent corona onset can be obtained at lower voltage. This factor does not appear in White's equation (47).

Let us try to apply the above analysis to the duct precipitator. The apparent corona onset voltage as predicted theoretically by Cooperman[11] is given by:

$$V_o' = V_o + (\rho_p/2\epsilon_o)\, b^2$$

Replacing ρ_p by ρ_i for severe corona quenching, then

$$V_o' = V_o + (\rho_i/2\varepsilon_o)\ b^2$$

Substituting the value of ρ_i from equation (58), hence

$$V_o' = V_o + (2\times10^{-6}\ f(S_{in})\ b^2)/2\pi r l K_i\ E\ (2\varepsilon_o)$$

$$= V_o + (4.5\times10^3\ f(S_{in})\ b^2)/rEK_i\ L \qquad (60)$$

Comparing equation (59) with equation (60), one can observe that for the same inlet specific surface area, interelectrode spacing, and effective length of corona wire the duct precipitators are twice as sensitive to particle space-charge as wire-tube precipitators. This is the same as Cooperman's [11] result. However, the main differences are:

(1) Particles are charge limited under the conditions of severe quenching and not by Pauthenier's relationship.

(2) The effective length of the corona wire appears in the equations (59) and (60) and must be taken into consideration for the comparison between the two geometries.

Let us return to figure (11) and assume uncharged particles are placed in that corona apparatus having initial conditions with clean gas of applied voltage V_1, total corona current I_1, original average electric field E_1 and ion concentration N_1. Particles moving in the corona

region will be charged either by the ion-bombardment mechanism or the ion-diffusion mechanism or both as mentioned in section (2.5). In any case, inside this charging zone some free gaseous ions will be bound by the low mobility particles and the corona current will be quenched. In addition to this effect of mobility on reducing the corona current, as the particles proceed in the axial direction they gain more charge and hence reduce the ionization field in the vicinity of the discharge electrode due to their space-charge. The first Townsend's ionization coefficient α will be reduced as can be predicted from figure (2) of section (2.2) and hence the ion generation rate from the ionized sheath will be reduced. As the specific surface area increases the charging time constant increases and the maximum charge per particle decreases due to the decrease in the ion concentration and the charging field. In addition, as the specific surface area increases, local field interactions may also take place resulting in a further reduction in the effective charging field. At the end of this charging process, the particles are essentially fully charged and hence the rest of the precipitator should be mainly devoted to the collection process. In this region, the charged particles should not pick up any significant

number of free ions. However, this space-charge reduces the ionization field and the ionic current generated from the sheath, thus reducing the measured corona current. The collection field at the surface of the outer electrode is influenced by the electrostatic component, the ionic component of current, and the particle space-charge effect. If the relative reduction in the ionic current component due to the charged particles passing by the collection zone is not large, then the collection field should be enhanced by the particle space-charge effect.

One can see from the above that the increase in the inlet specific surface area should result in a lower particle charge but at the same time may result in an enhanced collection field. The question which arises is what will be the net effect of the particle space-charge on the collection efficiency of electrostatic precipitator. The answer to that will be seen by the experimental results later in this chapter.

Returning to the mathematical model for the quantitative evaluation of the electric field distribution under the presence of particle space-charge and the corona current suppression ratio as presented in section (3.2.2), and comparing with the above proposed mechanism one can note the following:

(1) The magnitudes of the ion space-charge and the particle space-charge densities, ρ_i and ρ_p respectively, are functions of the axial position. This will imply that the electric field distribution in the gap between the two electrodes should be dependent on the axial position of the section under consideration and the prevailing particle concentration in it.

(2) The average linear corona current suppression ratio (J_{lc}/J_{ld}) should be dependent on several factors, among them:

(A) The collection rate:

The higher the collection rate the lower should be the average corona current suppression ratio because of the larger portion at the precipitator exit with very low particle concentration.

(B) The diameter of the corona wire:

Since a significant part of the corona quenching is due to a reduction of the ionization field then the corona wire diameter may have an effect on the average corona current suppression. For example, the smaller the corona wire diameter, the higher the electrostatic field for certain voltage and the lower will be the relative effect of the particle space charge. Note that (J_{lc}/J_{ld}) is generally different from the linear corona

current suppression ratio j_{1c}/j_{1d} as mentioned in section (3.2.2). The later varies in the axial position inside the precipitator according to the variation in the specific surface area of the particles.

7.3 Results and discussion

7.3.1 Effect of the particle concentration on the corona voltage-current characteristics

A series of tests were carried out using different particle concentrations under both positive and negative corona. From these tests the corona voltage-current characteristics were obtained. The five corona wires of different diameters listed in table (1) were used in both the tube and the duct units.

Figures (12) to (19) show the (V-I) characteristics for two corona wires of different diameters. Similar results to those of the smaller wire 0.165×10^{-2}m(0.065") were obtained for the other corona wires and tabulated in Appendix (D).

One can notice that, as the inlet specific surface area increases, the apparent corona onset voltage increases and the total corona current decreases at any fixed value of applied voltage. The only case that showed intermediate sparks before the final sparkover was with using a corona wire of diameter 0.63×10^{-2}m (0.250") as indicated by the

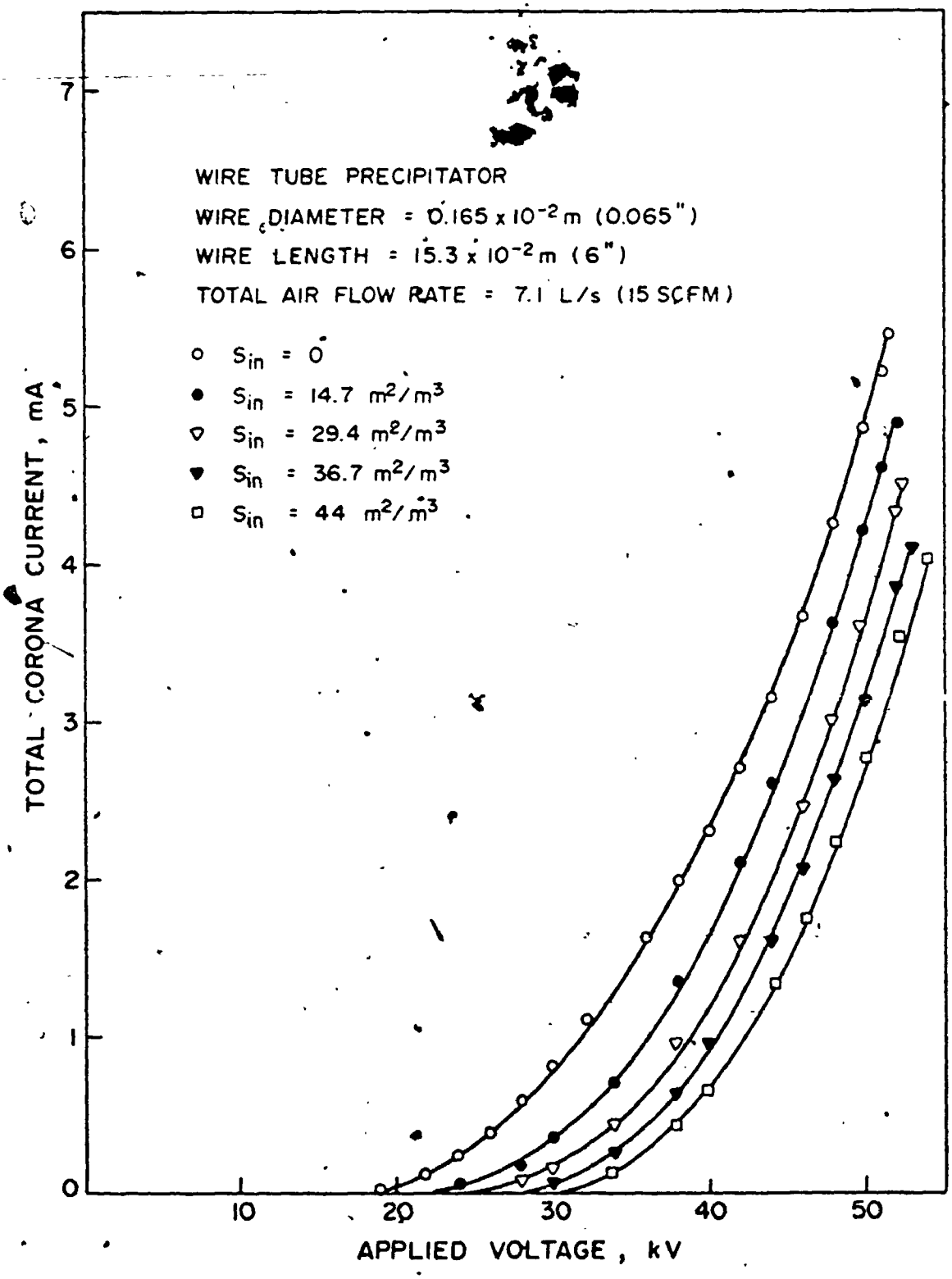

FIGURE 12. NEGATIVE CORONA VOLTAGE - CURRENT CHARACTERISTICS.

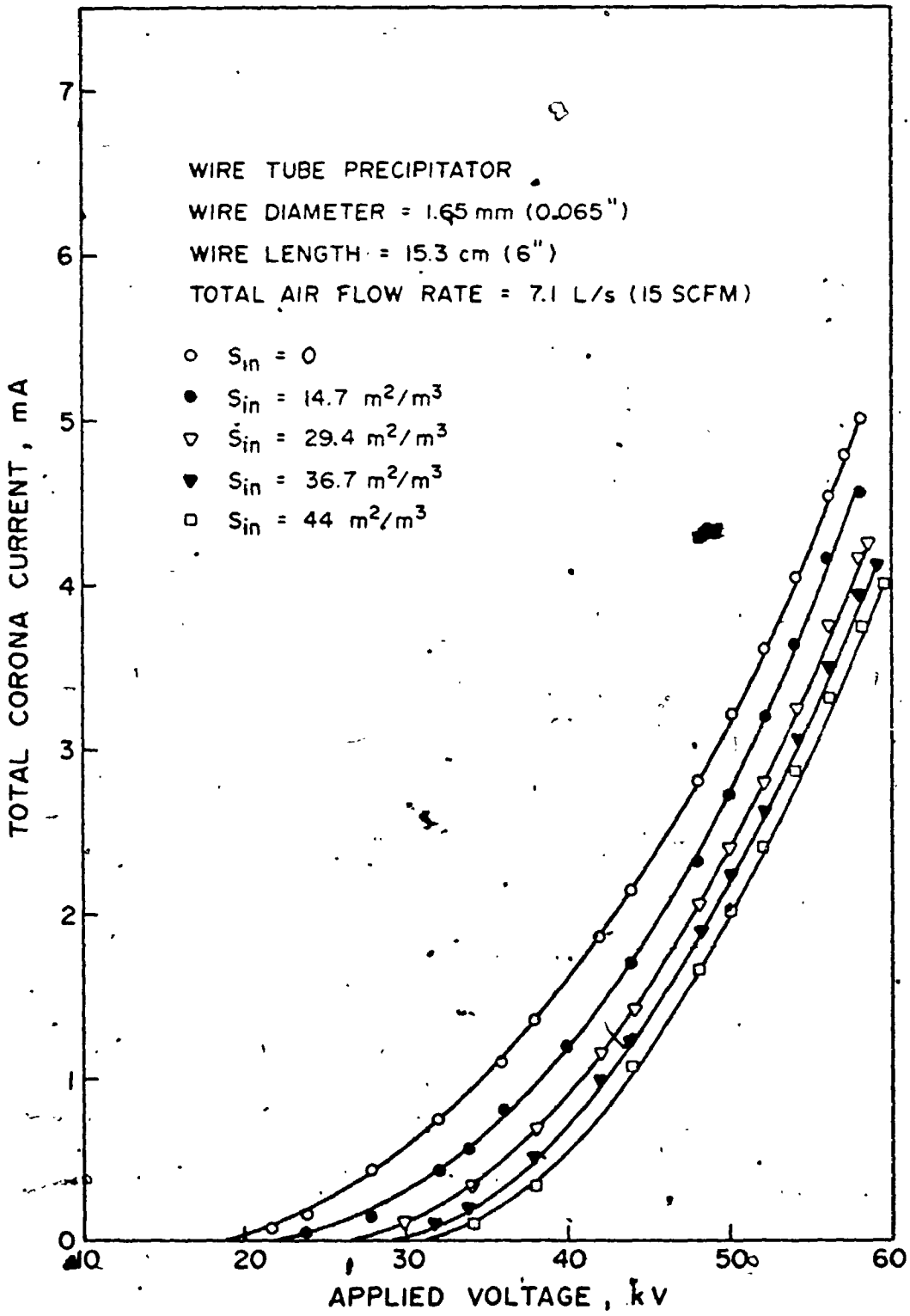

FIGURE 13. POSITIVE CORONA VOLTAGE - CURRENT CHARACTERISTICS.

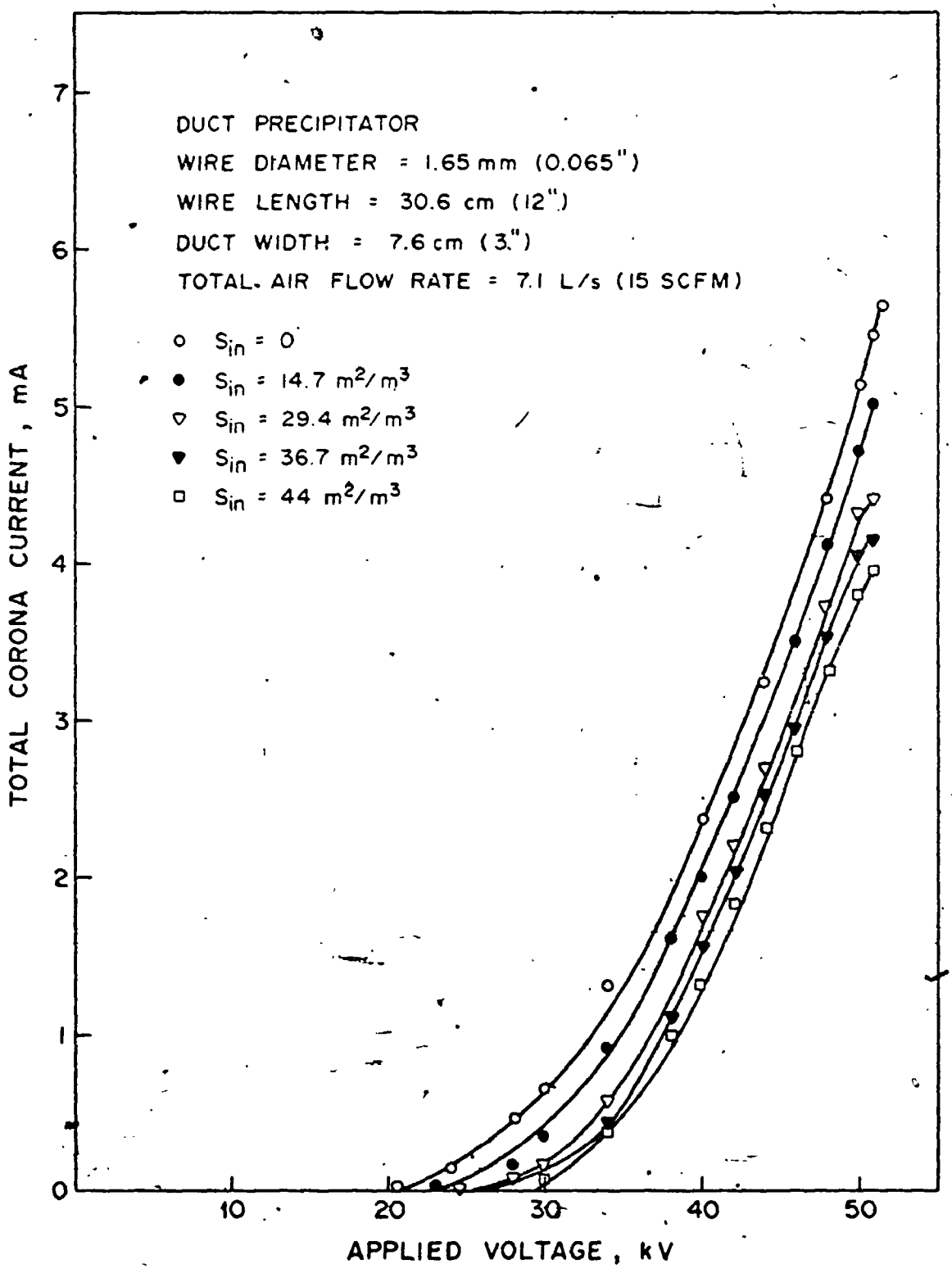

FIGURE 14. NEGATIVE CORONA VOLTAGE – CURRENT CHARACTERISTICS.

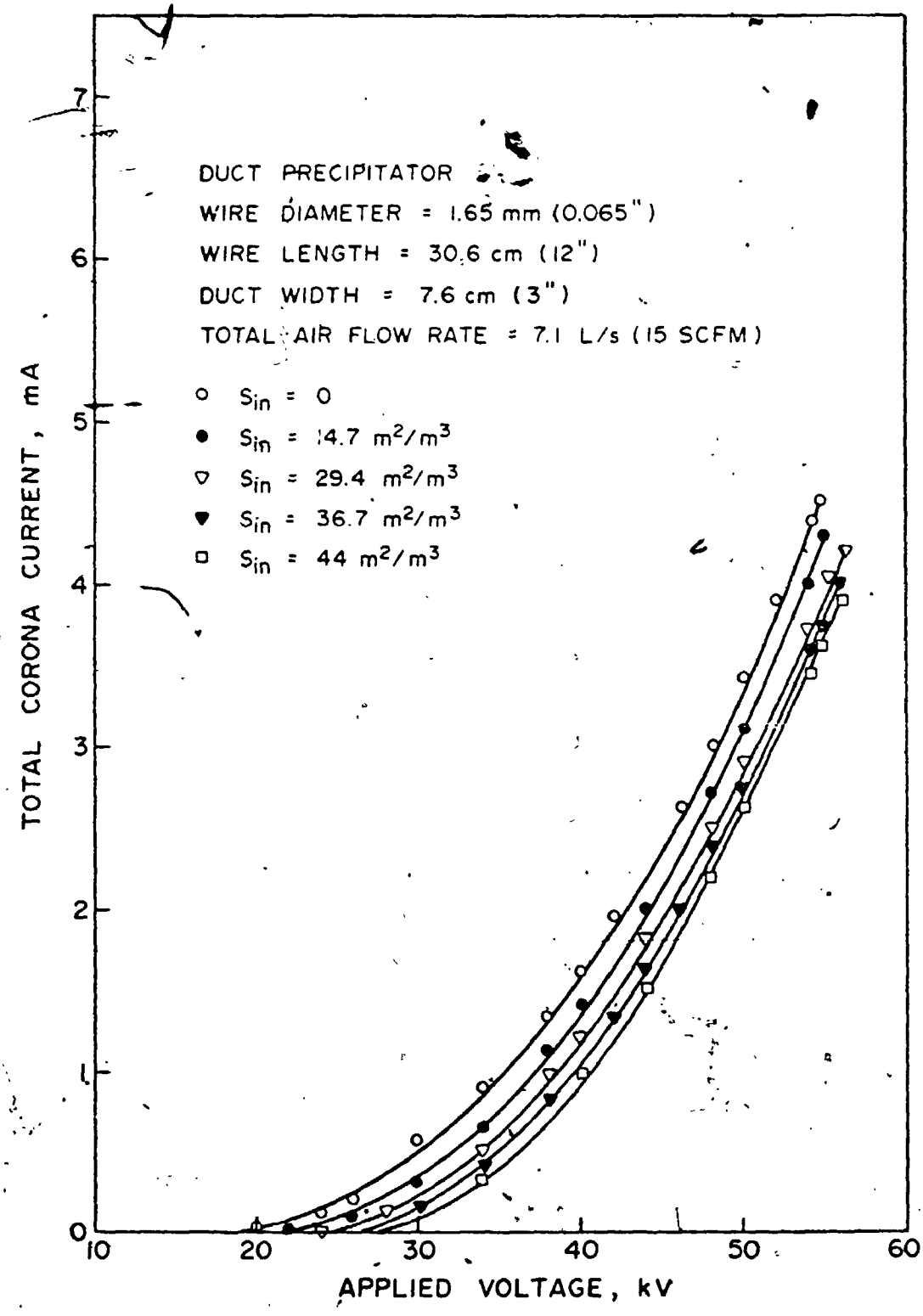

FIGURE 15. POSITIVE CORONA VOLTAGE - CURRENT CHARACTERISTICS.

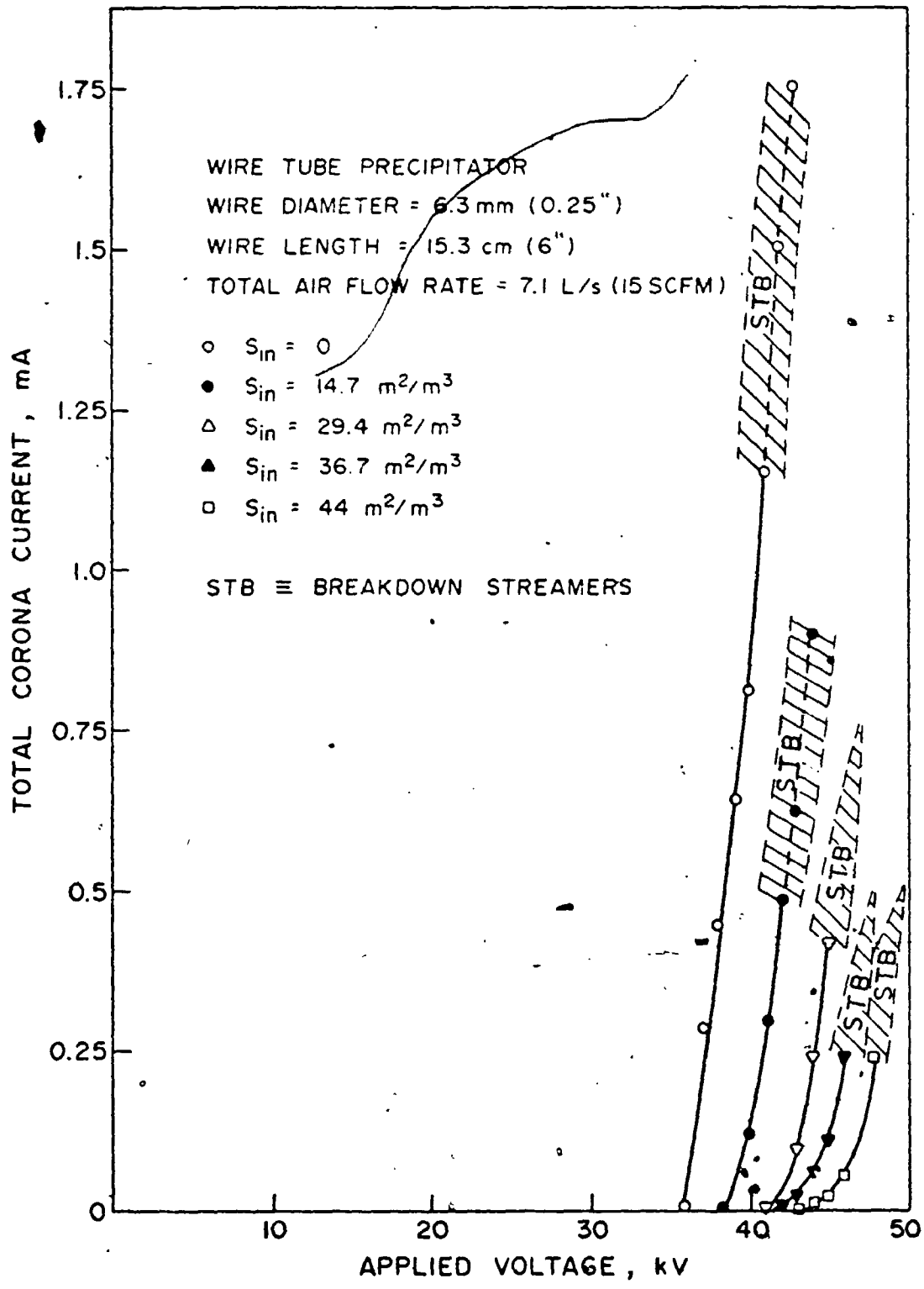

FIGURE 16. NEGATIVE CORONA VOLTAGE - CURRENT CHARACTERISTICS.

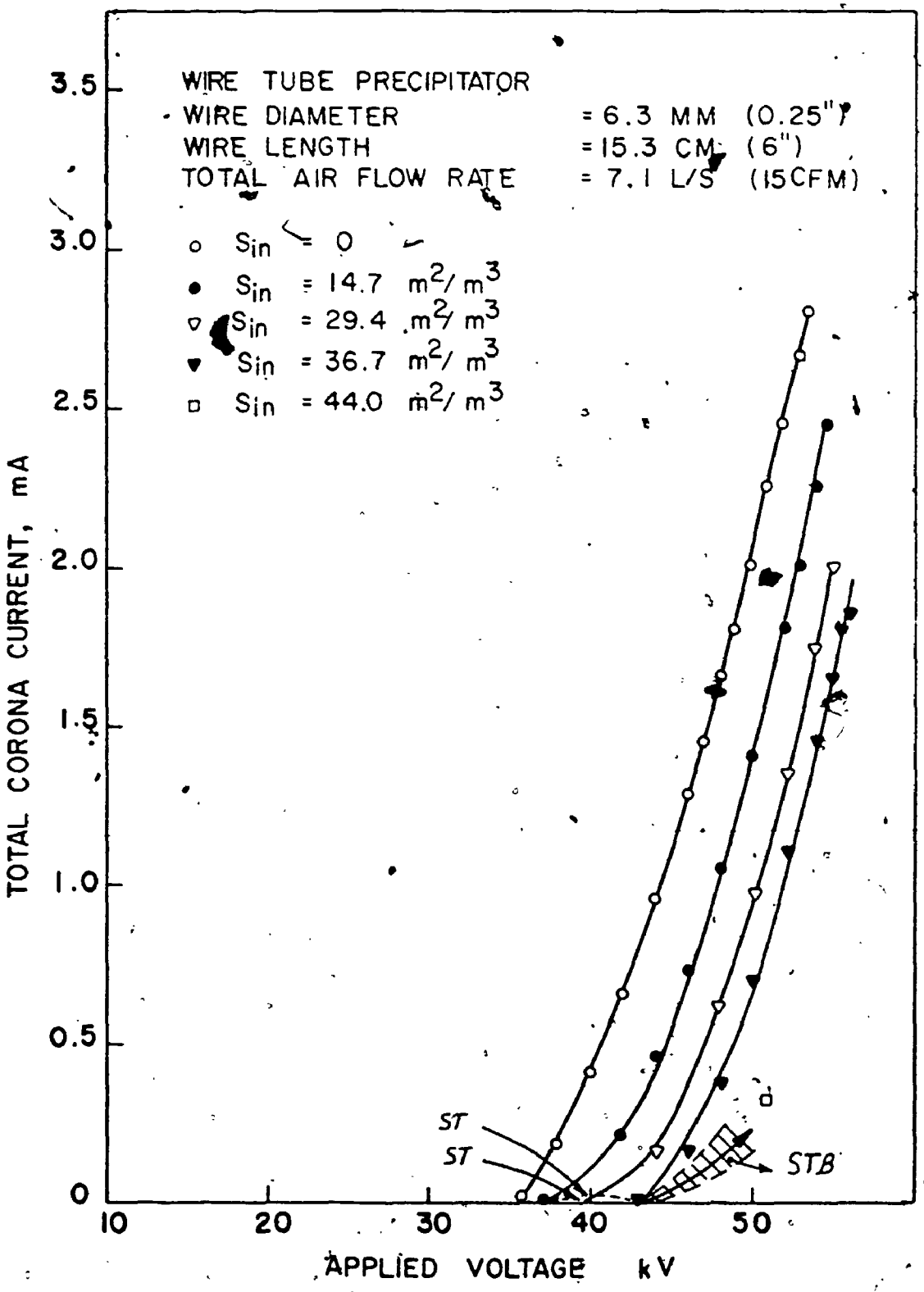

FIGURE (17) POSITIVE CORONA VOLTAGE CURRENT CHARCTERISTICS

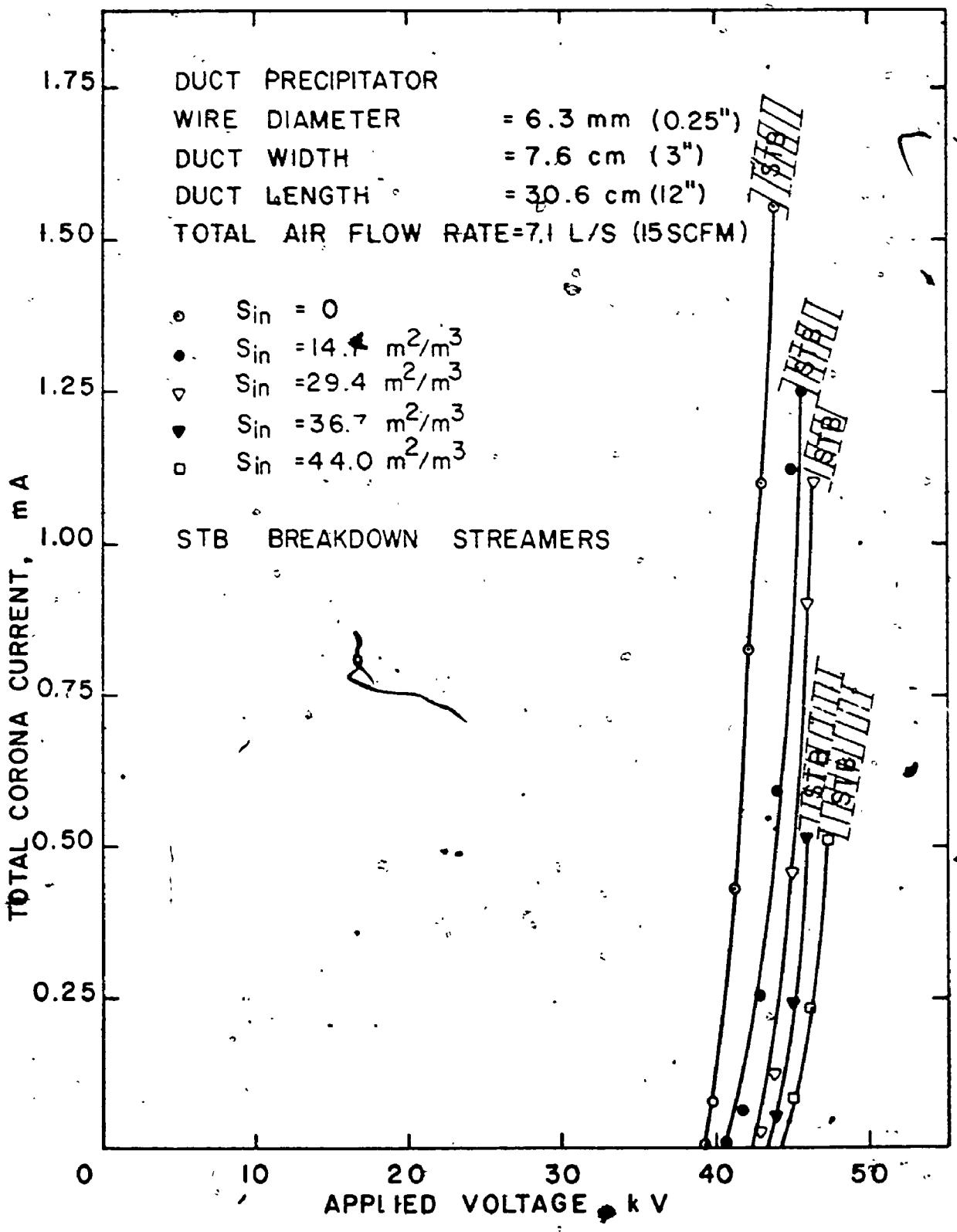

FIGURE (18) NEGATIVE CORONA VOLTAGE CURRENT CHARACTERISTICS

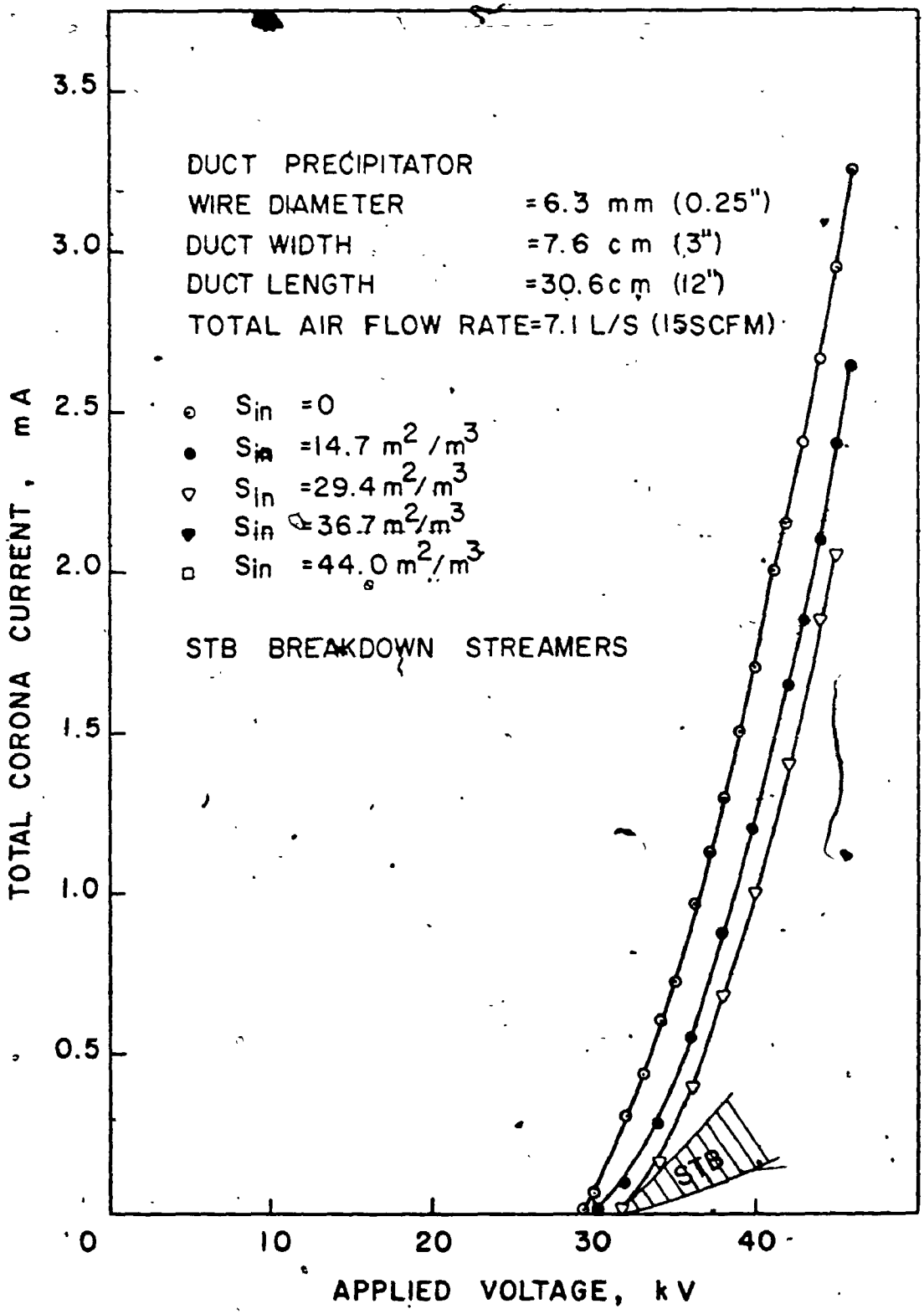

FIGURE (19) POSITIVE CORONA VOLTAGE CURRENT CHARACTERISTICS

dashed regions, ST (onset streamers) and STB (Breakdown streamers) in figures (16) to (19). These forms of instability, which occured only for this corona wire, will be discussed in the appropriate sections of this chapter.

The following interpretation of the apparent corona onset voltage and the average corona current suppression ratio in sections (7.3.2) and (7.3.3) of this chapter were made on the basis of measuring the (V-I) characteristics.

.7.3.2 Effect of the particle concentration on the apparent corona-onset voltage

Figure (20) for the tube precipitator shows the measured corona onset voltage for the cases of positive and negative corona (based on an onset of 2 μA corona current) as a function of the inlet specific surface area of the aerosol. It can be observed that the negative corona has a slightly greater increase than the positive corona and also appears to increase linearly. This polarity effect may be attributed to the higher suppression of the ionization current in the negative corona due to the higher probability of the capture of free electrons emanating from the localized tufts than in the positive case.

FIGURE (20) WIRE-TUBE PRECIPITATOR

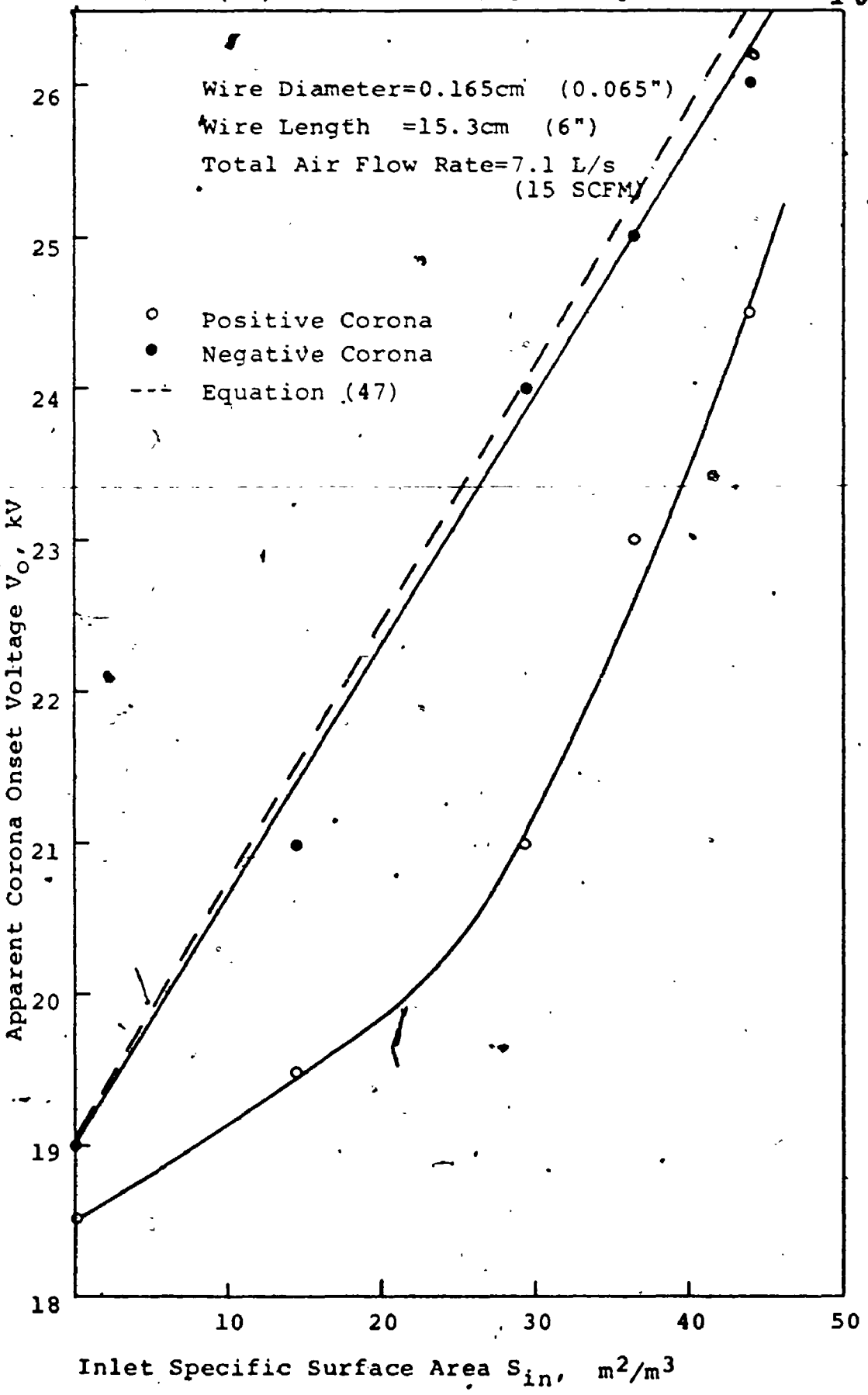

In figure (20) also, observe the comparison between the experimental results and White's equation (47) assuming an average electric field E of 3 kV/cm and a dielectric constant of the D.O.P. of 2.2 (see Appendix (A)). One can notice a good agreement of the theory with the experimental results of negative corona, only on the basis of this assumed value of the electric field which may be comparable to values found in normal precipitators.

Figure (21) shows the apparent corona onset voltage versus the specific surface area for the duct unit. One can observe here also the slightly greater increase in the negative corona than the positive.

Comparison of the results of figure (20) and (21) shows that the maximum increase in the apparent corona onset (i.e with the maximum particle concentration) in the cylindrical and the duct units was almost the same (6.5 to 7 kV with negative corona and 5.5 to 6 kV with positive corona). The results using the other wires (with the exception of the largest wire used of diameter 0.63×10^{-2}m (0.250")) showed the same amount of increase in the apparent corona onset i.e it confirms that the amount of increase in the corona onset voltage is independent of the corona wire

diameter.

From the first look at these results, one may observe that they do not seem to agree with White's[3] and Cooperman's[11] conclusion that the duct precipitator gives double the increase in the apparent corona onset voltage of the tube precipitator for the same inlet specific surface area. However, with the new approach presented in section (7.2) which has the effective corona wire length as a factor in equations (59) and (60), one can find an explanation for these experimental results. The length of the corona wire used in the duct precipitator was double that used in the tube precipitator. In short the duct precipitator should be twice as sensitive as the tube precipitator to the particle space-charge provided both have the same effective length of corona wire.

Before commenting on the special case of the presence of heavy onset streamers under positive corona with some high particle concentrations for the corona wire of diameter 0.63×10^{-2}m (0.250"), a comparison will be made between the point-to-plane geometry and the wire-tube geometry regarding the corona mode close to the onset. Let us limit this discussion at first to the positive corona. As has been mentioned in

section (4.4.1), the onset streamers and/or burst pulse corona normally appear close to the corona onset in the point-to-plane geometry. It has been also mentioned in section (4.5) that onset streamers and/or burst pulses are formed close to the corona onset for "thick" corona in wire-to-plane geometry depending on the gap length[52]. For thin corona wires only burst pulses are formed in a narrow range of applied voltage close to the onset without onset streamers. The main difference between the fine electrode (point or wire) and a relatively large electrode is that in the former case the electric field at the surface of the electrode is higher and decreases with distance from the electrode faster than with the larger electrode. Therefore, secondary ionizations from the primary avalanche in the case of very fine point occur in a smaller region and only negative ions can be formed around the point with the positive glow in between. With a larger electrode however, a main streamer channel is formed at the tip of the point as well as smaller streamers to the side regions. Therefore, for a fixed value of electric field intensity at the surface of the smaller conductor (point or wire), as the diameter increases the strength and size of the streamers increases.

From this one can see that the presence or absence of onset streamers is dependent upon the magnitude of the electric field at the surface of the smaller electrode at the corona onset as well as the degree of non-uniformity of that field i.e the field gradient in the vicinity of that conductor. The lower this electric field near the corona onset and its gradient, the stronger the onset streamers. More details regarding the onset streamers will be given in section (8.2).

Figures (17) and (19) for the largest corona wire size used 0.63×10^{-2}m (0.25"), show the presence of onset streamers, which led to complete sparkover in some cases in both the tube and the duct units under the presence of high particle concentrations. This may be explained as follows: As mentioned before, the space-charge of the particles reduces the field at the surface of the corona wire and enhances the field at the outer electrode. Therefore, their effect is to reduce the field at the corona wire surface and the non-uniformity of the field distribution in the gap. Hence the onset streamers have more chance to be formed as proposed in the mechanism mentioned. Note that these onset streamers were not observed with the smaller corona wires used (i.e with

higher electric fields) under the presence of the same particle concentrations. For this relatively large corona wire, in cases where these onset streamers do not lead to sparkover as indicated by ST in figure (17), with the increase in the applied voltage the audible noise of the streamers disappear. Apparently the ordinary stable glow regime starts and readings of the applied voltages and the corona currents could be taken. In cases where these onset streamers were so strong that they lead to sparkover, as indicated by STB in figures (17) and (19), the particle space-charge effect on the field apparently was so great to permit no corona regime at all i.e the corona wire used effectively appears as a larger one that can not permit corona before the sparkover.

On the other hand, under negative polarity, Trichel pulses should be formed for any geometry. The presence of particles with different concentrations did not show any onset streamers or any form of instability close to the corona onset voltage in this case.

7.3.3 Effect of the inlet particle concentration on the average corona current suppression ratio

Figures (22) and (23) show the average corona current suppression ratio as influenced by the inlet specific surface area of the suspended material for the tube and the duct units respectively under both positive and negative polarities at a fixed intermediate voltage of 34 kV.

From these figures one can observe:-

(1) The average corona current suppression ratio increases non-linearly with the increase in the inlet specific surface area. The higher suppression rate at the highest particle concentrations may be due to more pronounced particle space-charge effects on reducing the ionization field and the corona current generation rate from the ionized sheath.

(2) The negative corona has a slightly higher suppression for the corona current than the positive for the same applied voltage and the same inlet specific surface area. This may be due to the electron component in the total corona current in the negative case. The capture of these high mobility electrons results in an appreciable reduction in the corona current.

Figure (24) shows the average corona current

FIGURE (21) DUCT PRECIPITATOR

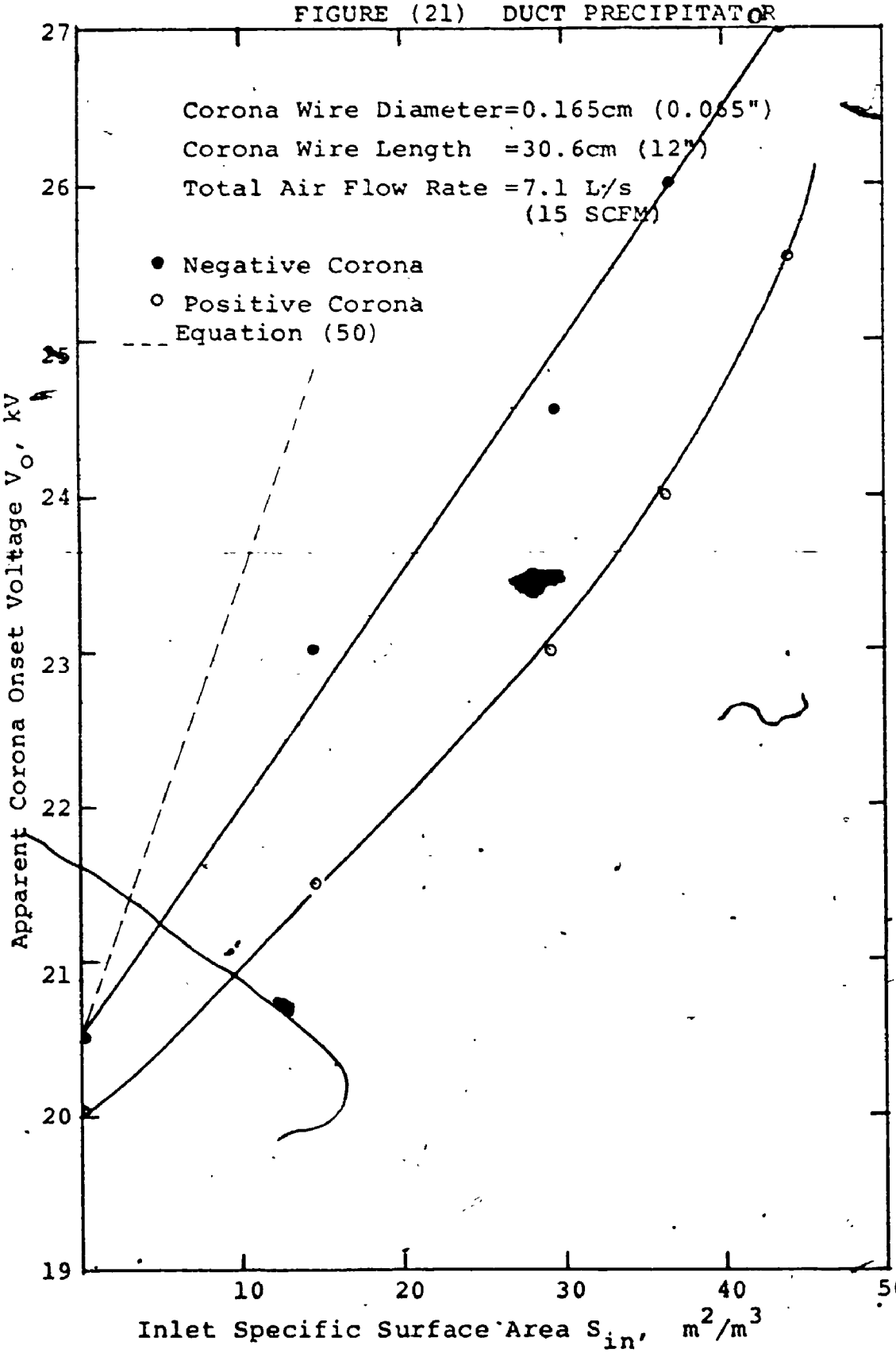

FIGURE (22) WIRE-TUBE PRECIPITATOR

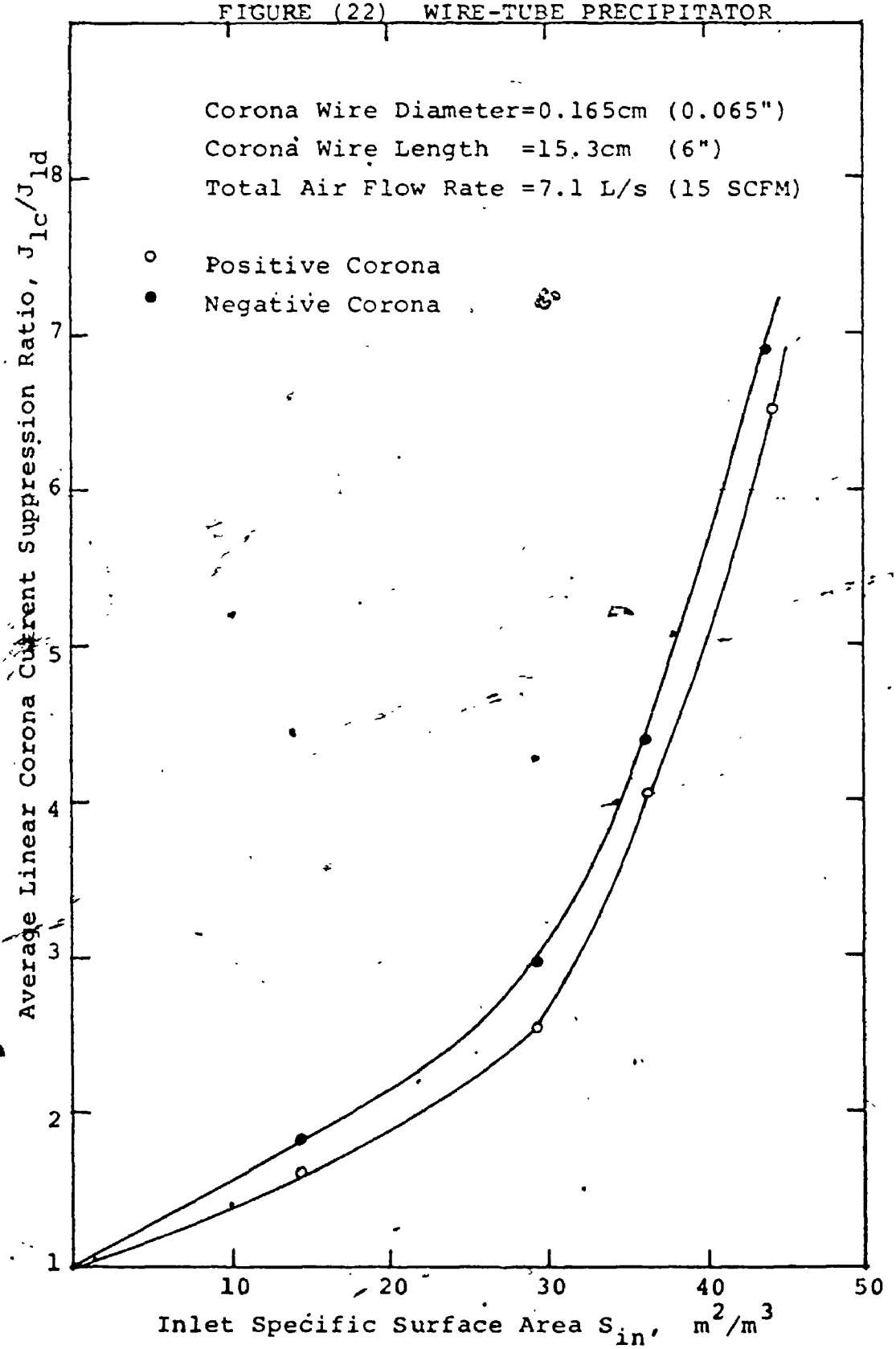

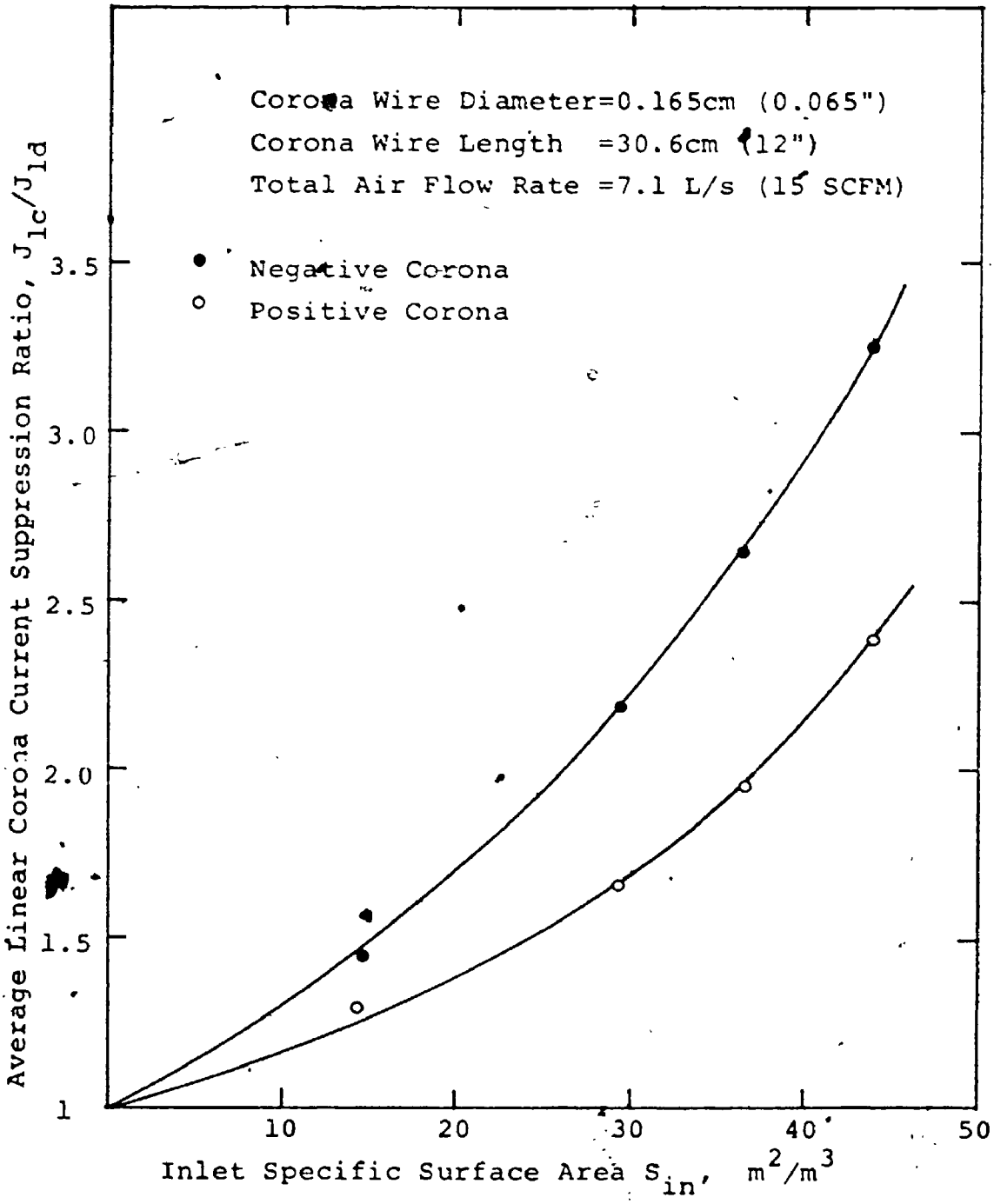

FIGURE (23) DUCT PRECIPITATOR

FIGURE (24) WIRE-TUBE PRECIPITATOR

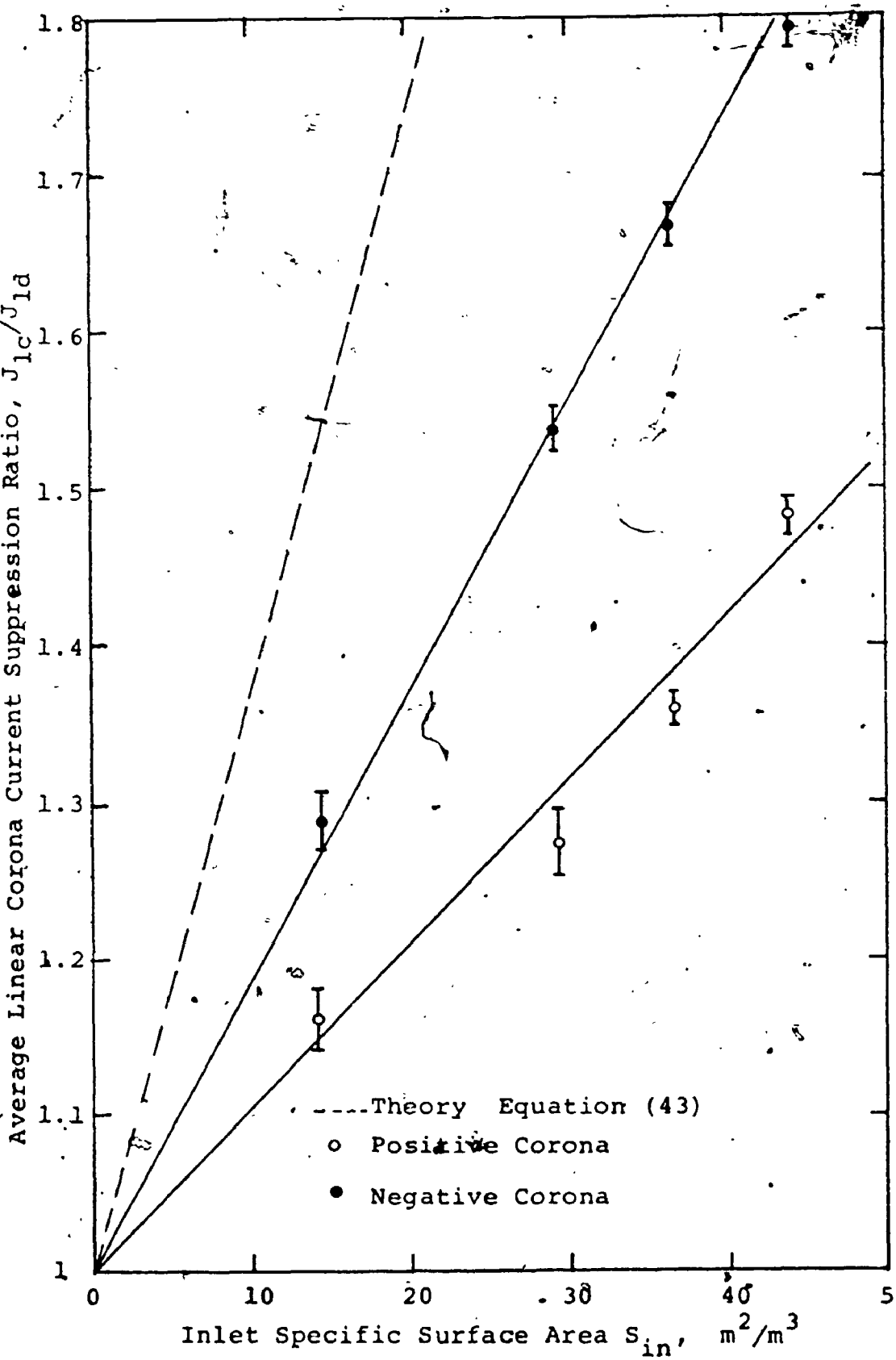

suppression ratio close to sparkover as affected by the inlet specific surface area in the tube unit. The dotted line represents the equation:

$$j_{lc}/j_{ld} = 1+(2pS/3)\ b$$

One can notice that there is only a qualitative agreement with the experimental results. The quantitative disagreement is not surprising because of the difference between the linear corona current suppression ratio (j_{lc}/j_{ld}) which varies in the axial direction with the variation in the specific surface area as mentioned in section 7.3.9and the measured average corona current suppression ratio J_{lc}/J_{ld}. Comparison of figures (22) and (24) for the tube unit shows a much lower suppression close to sparkover than at 34 kV because of the higher collection rate in the former case and the creation of a zone approximately free from particles and corona suppression at the exit of the precipitator.

Figure (25) for the duct unit close to sparkover shows also an approximate linear relationship. Note the lower average corona current suppression in this case compared with the tube unit. This is because of the higher collection efficiency due to the larger collection area (0.09 m^2) of the duct unit than the collection area of the tube unit (0.036 m^2). The larger collection area

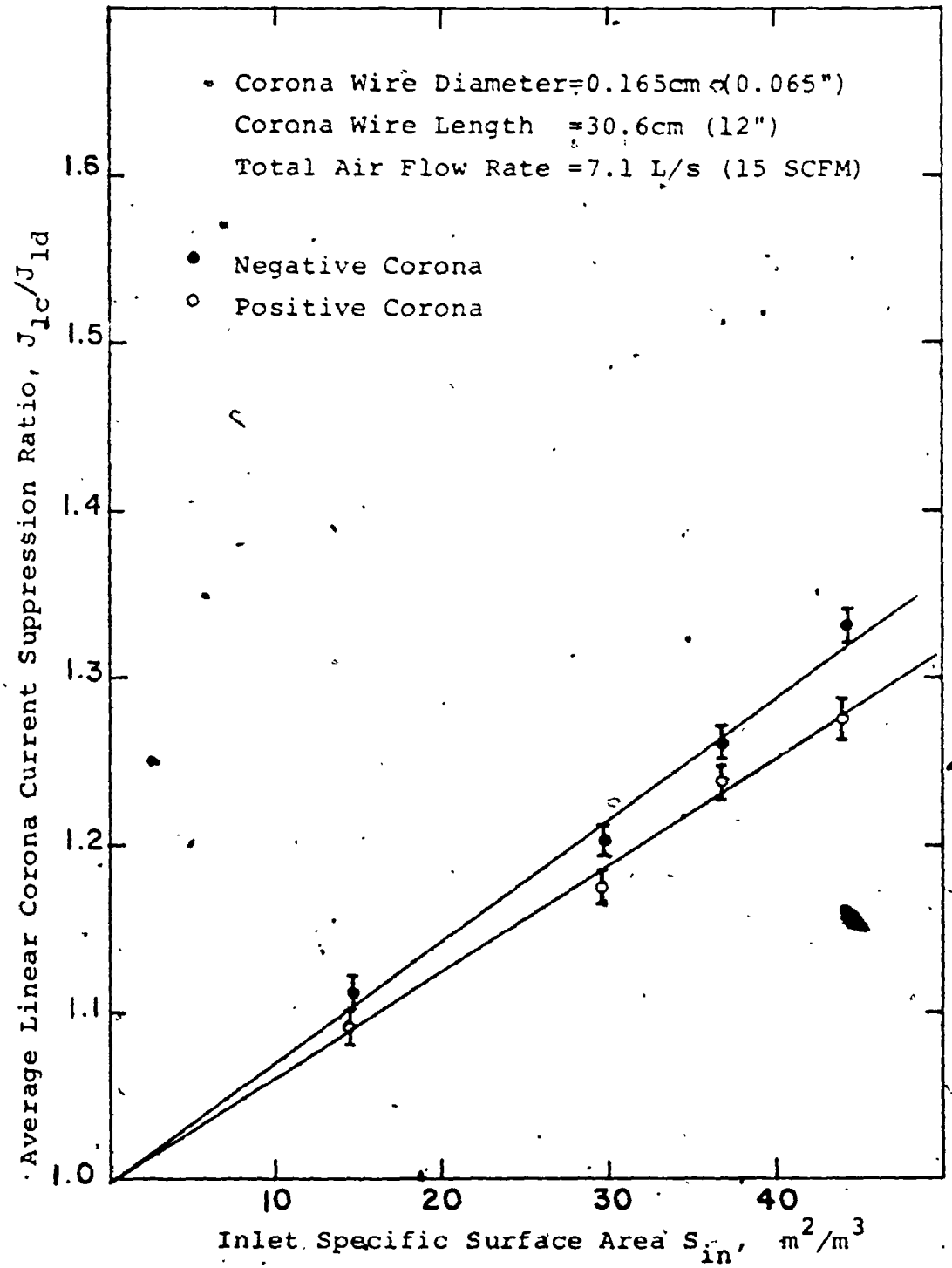

FIGURE (25) DUCT PRECIPITATOR (NEAR SPARKOVER)

for the same total air flow rate implies larger effective treatment time for the particles.

Figures (26) and (27) show the average corona current suppression ratio versus the inlet specific surface area under certain fixed original linear corona current density with clean air of 6.66 mA/m (2 mA/ft.) for the tube and the duct units respectively irrespective of the applied voltage at which this current will be obtained.

One can observe that for the same linear corona current density the negative corona has higher average corona current suppression ratio than the positive. The difference is greater than the case of fixed applied voltage shown before in figures (22) and (23).

7.3.4 Effect of the total air flow rate at fixed inlet specific surface area on the corona quenching characteristics

Under clean gas conditions, it is well-known that the volumetric gas flow rate does not appreciably affect the corona voltage-current characteristic since the radial velocity of the ions under the action of the electric field is much greater than any variations in the axial velocities of the flow. Yet, under the presence of suspended material in the gas, one can observe from the results of section (7.3.3) that the average corona current suppression ratio is appreciably affected by

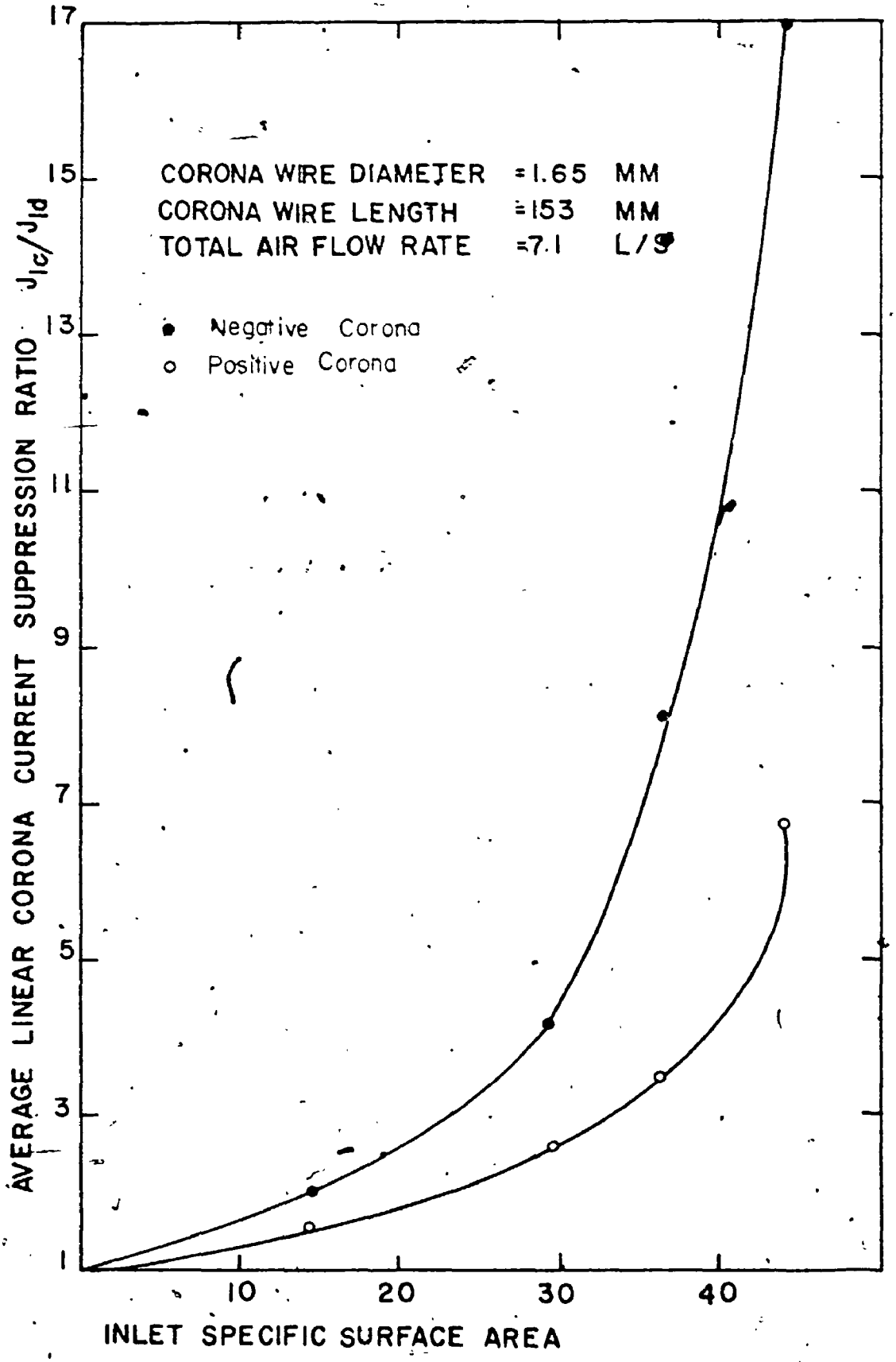

FIGURE (26) WIRE-TUBE PRECIPITATOR (J_{lc}=6.6mA/m)

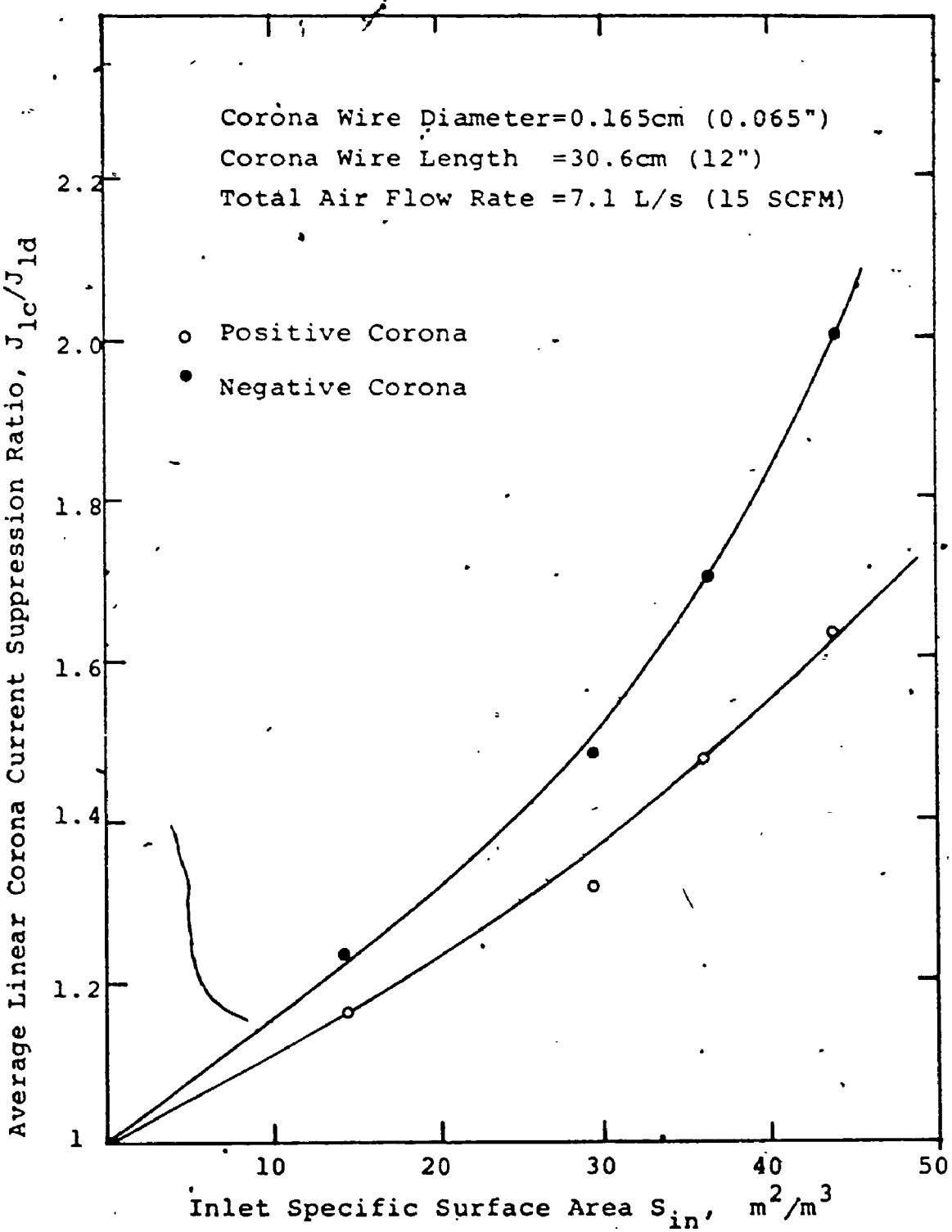

FIGURE (27) DUCT PRECIPITATOR (AT FIXED J_{lc}=6.66 mA/m)

the value of the applied voltage and hence the collection efficiency. A deduction from that will be, unlike the case of clean gas, the total air flow as it affects the collection efficiency should also affect the corona quenching characteristics of the precipitator under test. Experiments were carried out to investigate this effect. The inlet specific surface area was kept constant by increasing the known amount of the aerosol in proportion to the clean air. In these experiments the inlet specific surface area was kept constant at 14.7 m^2/m^3 at different values of the total air flow.

Figures (28) to (31) show the corona voltage-current characteristics for the tube and the duct unit respectively under this situation. One can note the following:

(1) As the total air flow rate increases keeping the inlet specific surface area constant, the apparent corona onset voltage stays constant. Note that at the apparent corona onset voltage particle charging may take place but no significant collection.

(2) As the total air flow increases, keeping the inlet specific surface area constant, the corona current is reduced at fixed values of applied voltage. This may be attributed to the reduction in the collection efficiency with the increase in the total air flow rate

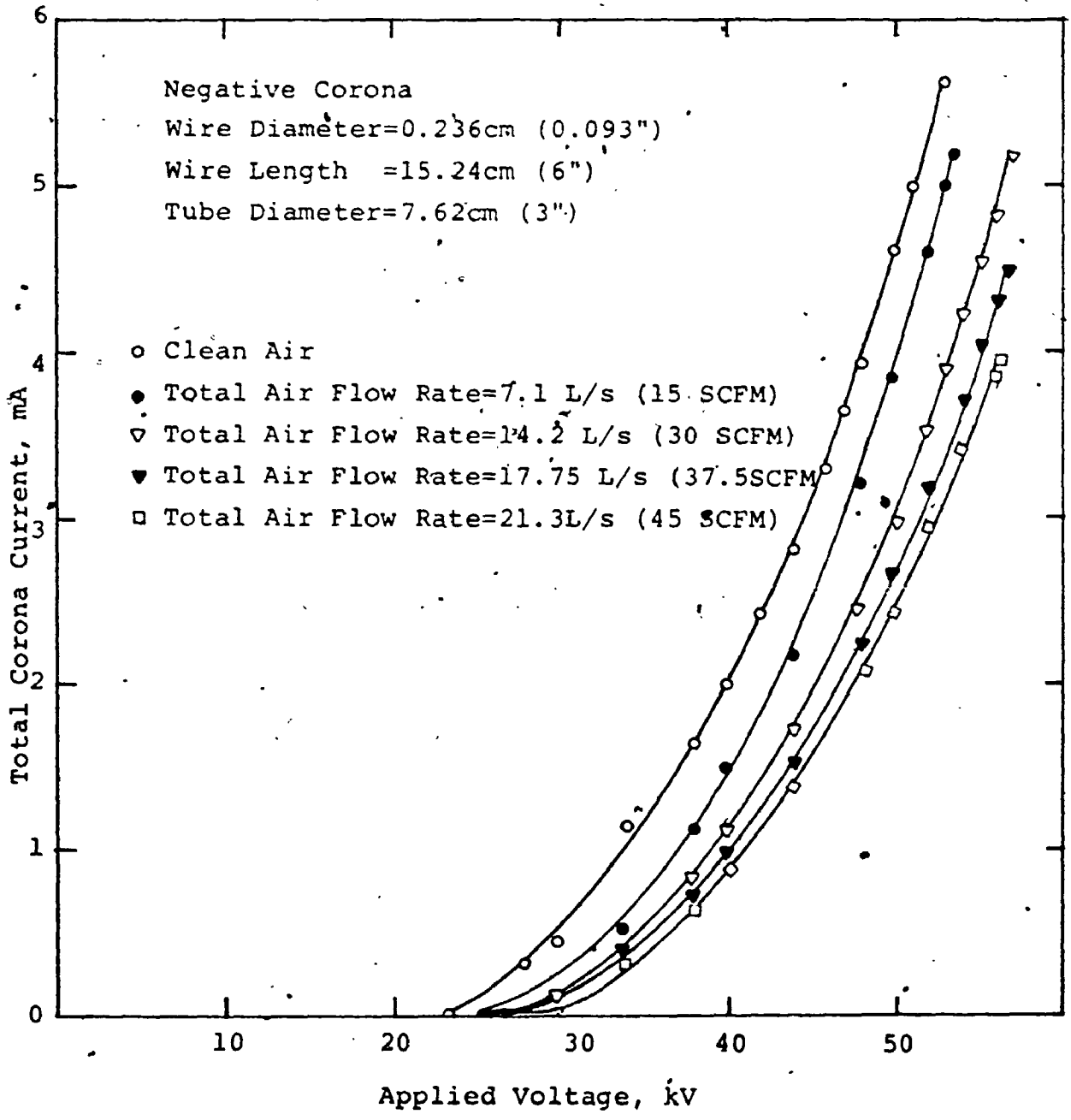

FIGURE (28) WIRE-TUBE PRECIPITATOR (AT FIXED S_{in}=14.7 m^2/m^3).

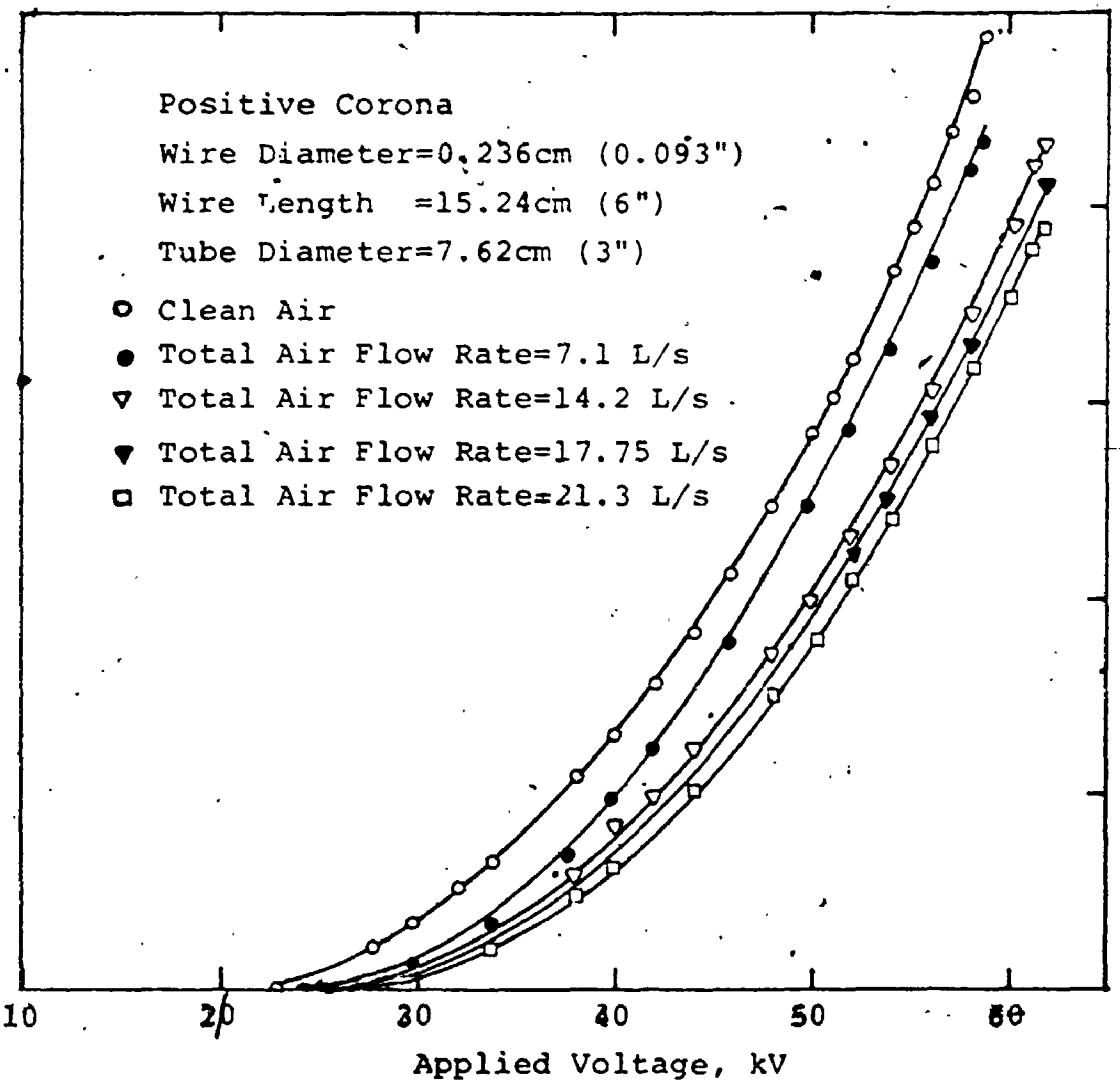

FIGURE (29) WIRE-TUBE PRECIPITATOR (AT FIXED S_{in}=14.7 m^2/m^3

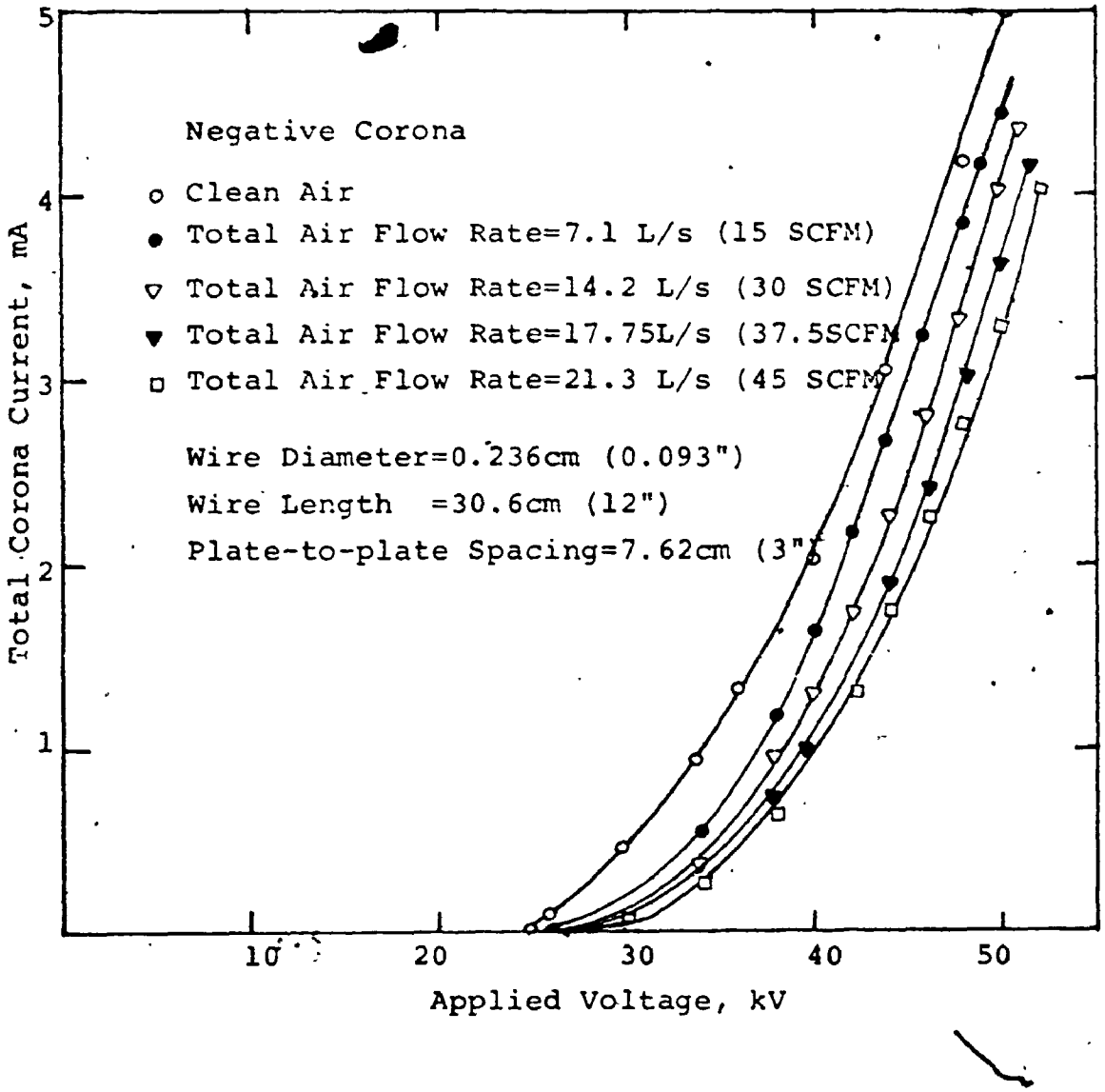

FIGURE (30) DUCT PRECIPITATOR (AT FIXED S_{in}=14.7 m^2/m^3)

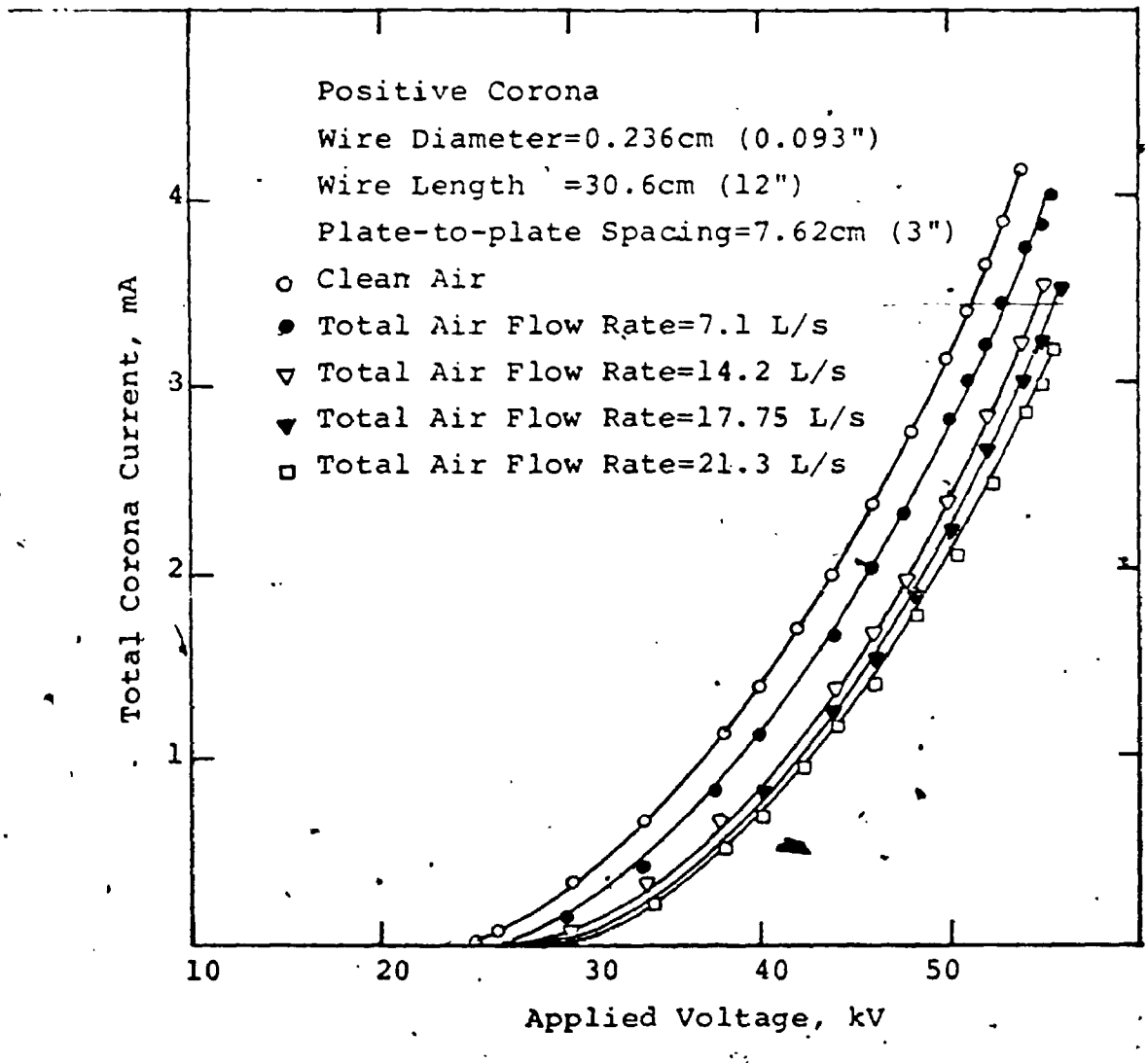

FIGURE (31) DUCT PRECIPITATOR (AT FIXED S_{in}=14.7 m^2/m^3)

and hence the charged particles stay longer time in the collection zone before being collected and result in more reduction in the corona current generated from the ionized sheath.

One explanation for the increase in corona quenching by the increase in the flow rate for the same inlet specific surface area is that the portion of the charged particles entrained with the flow outside the precipitator increases with the increase in the total air flow rate thus resulting in less corona current for the same applied voltage. However, if one considers that the particle mobility is much lower than the ion mobility and hence the corona current measured under the presence of suspended material is mainly carried by free gaseous ions, this explanation is not likely to occur.

The effect of the total air flow rate at fixed inlet specific ourface area on the sparkover voltage and the maximum pre-sparking corona current as can be observed in figures (28) to (31) will be mentioned and explained in the appropriate section.

7.3.5 Effect of the corona wire diameter on the average corona current suppression ratio

As indicated before, the quenching of the corona current by the particles suspended in the gas results from: (A) the capture of the free gaseous ions (B) the electric field reduction in the ionization region in the vicinity of the corona wire by the particle space-charge effect. Since the relation between the electric field inside the ionized sheath and the first Townsend's ionization coefficient is non-linear having the form shown in figure (2) then this second effect for corona quenching should be dependent on the original value of the ionization field with no particles present as well as the reduction in that field by the particle space-charge. As the diameter of the corona wire varies, this original value of the electric field in the ionization region varies and hence one may expect the diameter of the corona wire to have some effect on the quenching of the corona current. Note that the mathematical model mentioned in section (3.4.3) for the linear corona current suppression ratio shows that the only dimension affecting this ratio is the interelectrode spacing. However, this mathematical model was based upon focusing the attention on certain section and assuming the field inside the ionization zone

to stay constant as mentioned before in section (7.2).

Figures (32) to (35) show the average corona current suppression ratio versus the inlet specific surface area for both the tube and the duct units under positive and negative corona near sparkover. The values of the applied voltage are indicated between brackets beside each case. Because of the instability obtained with the largest corona wire used 0.63×10^{-2}m (0.25") under the presence of particles, the results of this wire are excluded from this comparison. One can observe that:

(1) Close to sparkover, as the diameter of the corona wire increases the average corona current suppression ratio increases. This may be attributed to two effects: (A) The ionization field reduction which should increase as the corona wire diameter increases. (B) The collection efficiency which should decrease as the wire diameter increases due to the lower original corona current density.

(2) The results of the corona wire of diameter (0.187") are far from linear in a similar way to those of figures (22) and (23) of low original corona current density. This shows that the relation between (J_{1c}/J_{1d}) and S_{in} may be approximately linear only if the original ion space-charge density is high enough with respect to the particle space-charge density.

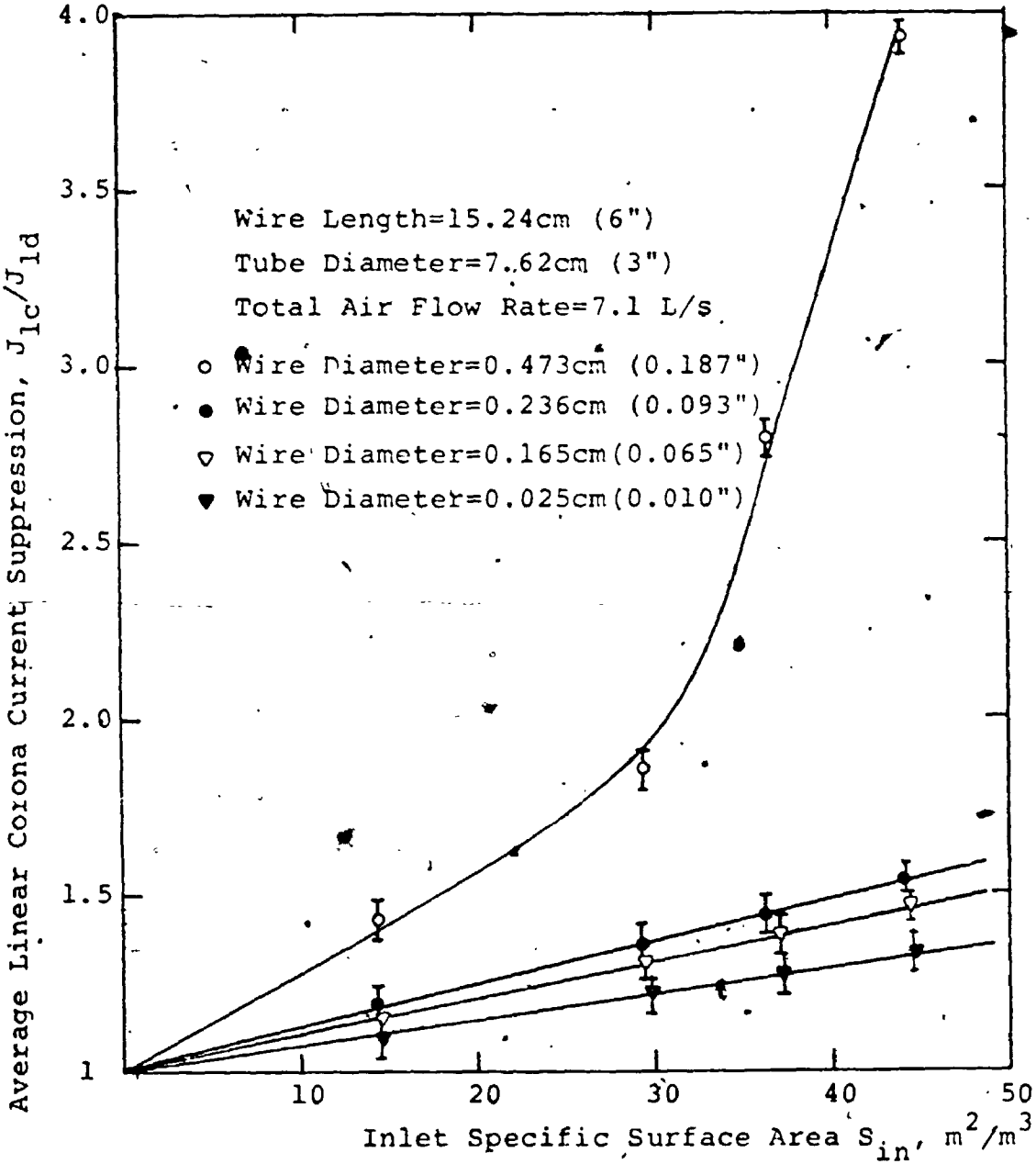

FIGURE (32) WIRE-TUBE PRECIPITATOR (NEGATIVE CORONA)

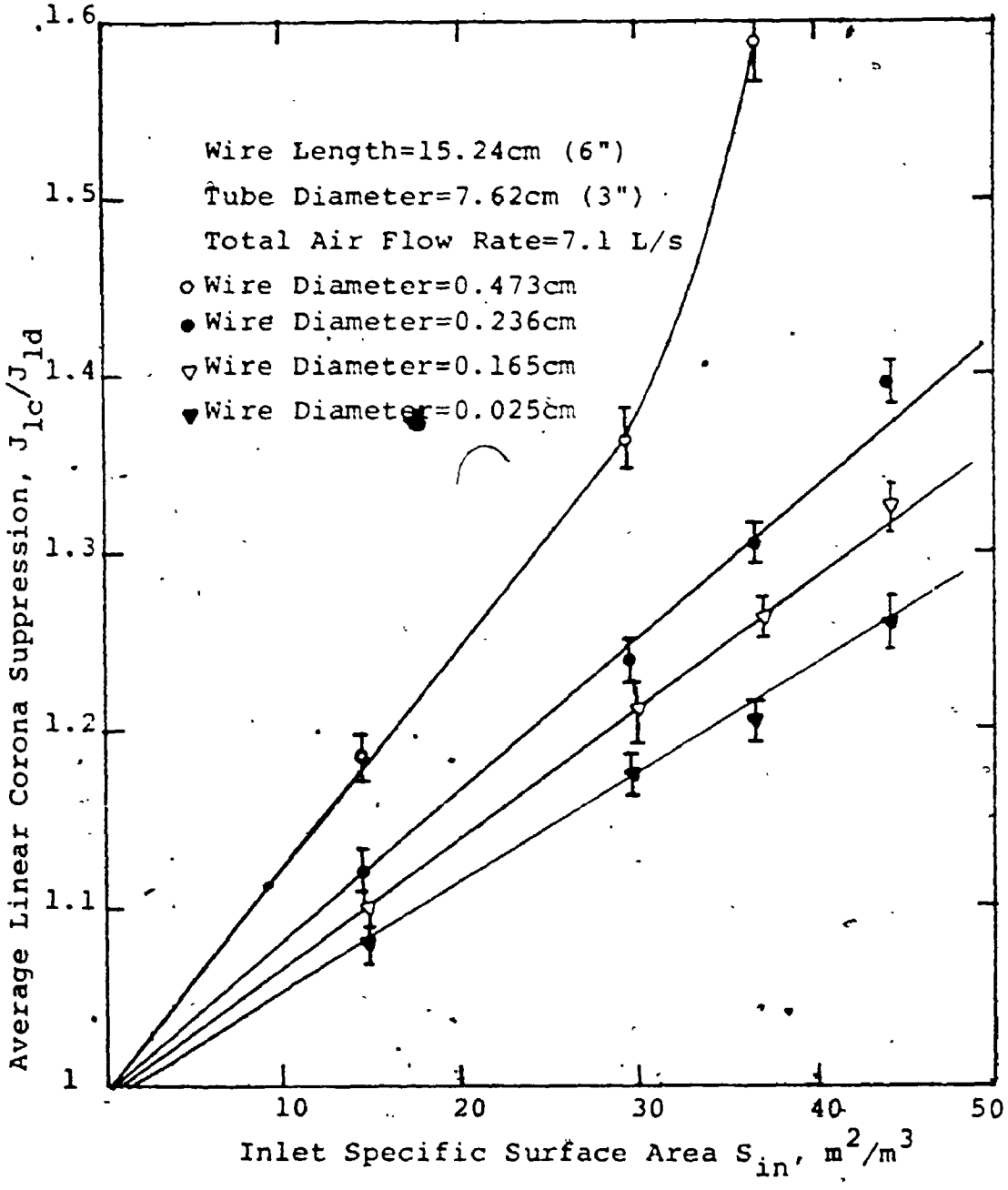

FIGURE (33) WIRE-TUBE PRECIPITATOR (POSITIVE CORONA)

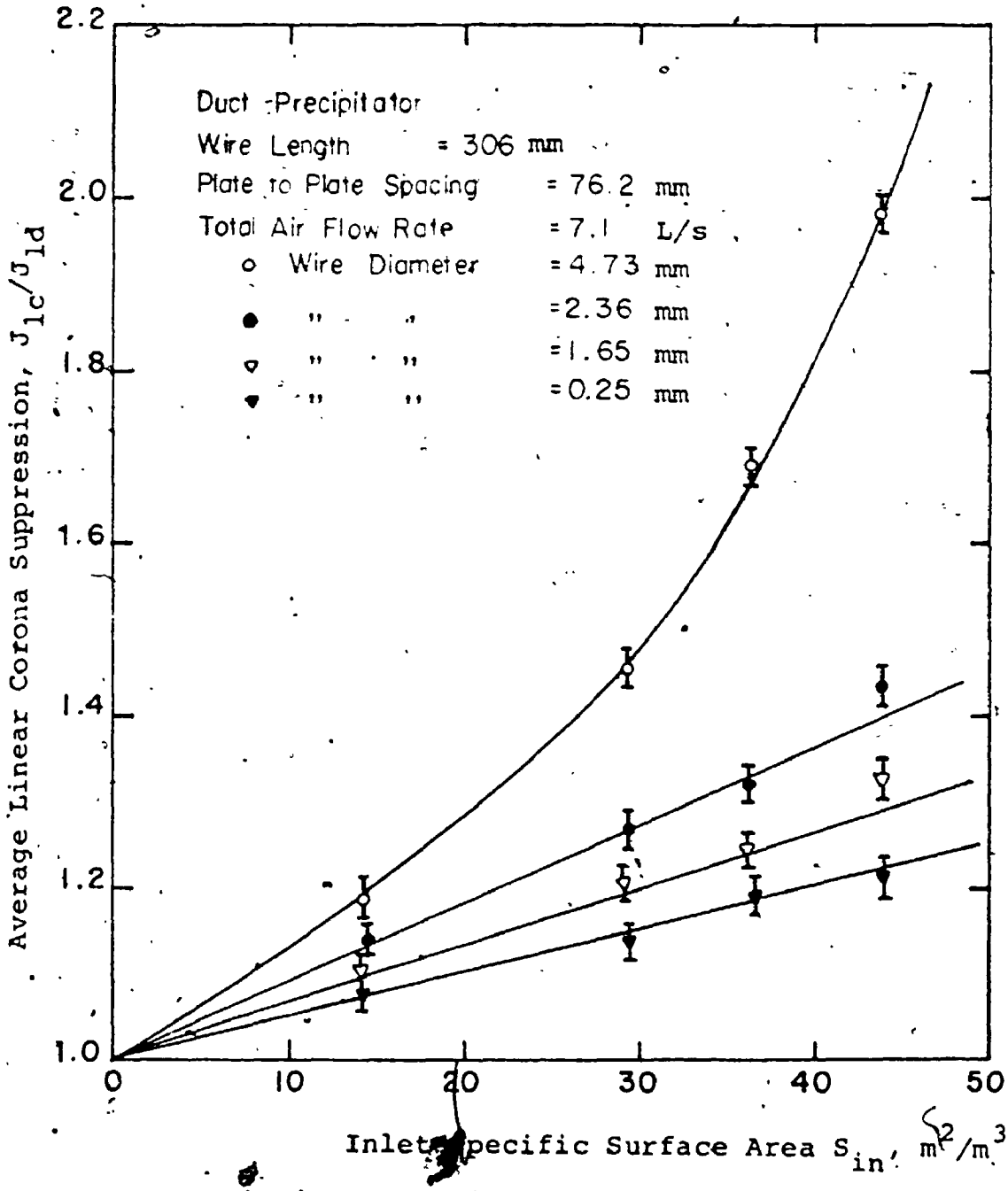

FIGURE (34) EFFECT OF THE CORONA WIRE DIAMETER ON THE AVERAGE CORONA CURRENT SUPPRESSION RATIO VERSUS THE INLET SPECIFIC SURFACE AREA NEAR SPARK-OVER IN NEGATIVE CORONA.

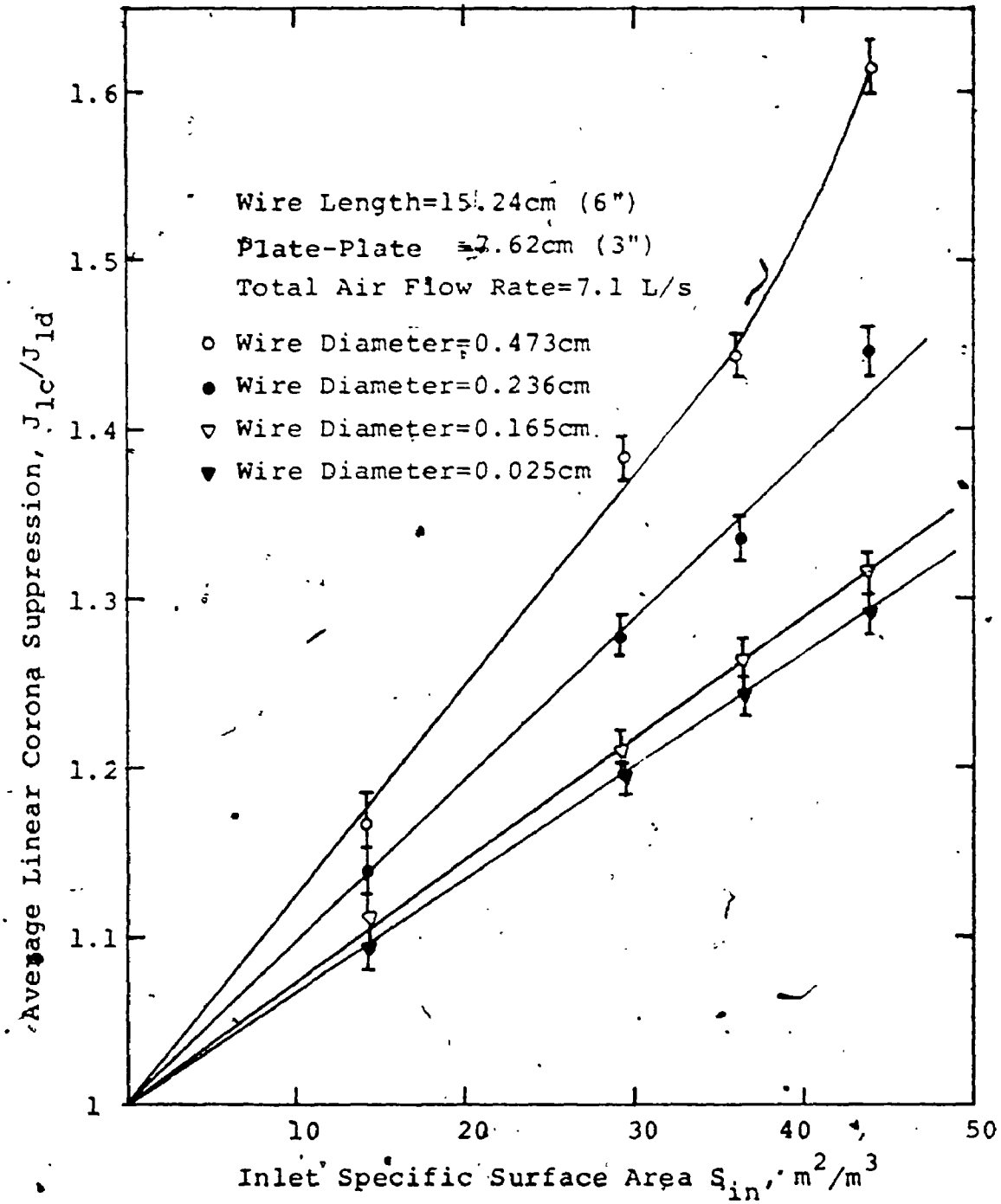

FIGURE (35) DUCT PRECIPITATOR (POSITIVE CORONA)

To reduce the effect of the collection efficiency on the influence of the corona wire diameter on the average corona current suppression ratio versus the inlet specific surface area, this relation was replotted as a fixed original value of the linear corona current density of 6.6 mA/m (2 mA/ft) for all the wires as shown in figures (36) to (39) for both the tube and the duct units. In this case also, as the corona wire diameter increases, the average corona current suppression ratio increases. The main factor for this effect should be due to the ionization field as influenced by the diameter of the corona wire. In these figures, note also the higher suppression under the negative corona than the positive.

7.3.6 Efficiency of electrostatic precipitators under conditions of corona quenching

In the previous parts of section (7.3) the results were mainly focused on the influence of the particle space-charge on the corona characteristics as measured by the external electrical circuit.

An important investigation, that is of great interest from the practical point of view, is the effect of the particle space-charge on the collection efficiency.

Figures (40) and (41) show the collection efficiency

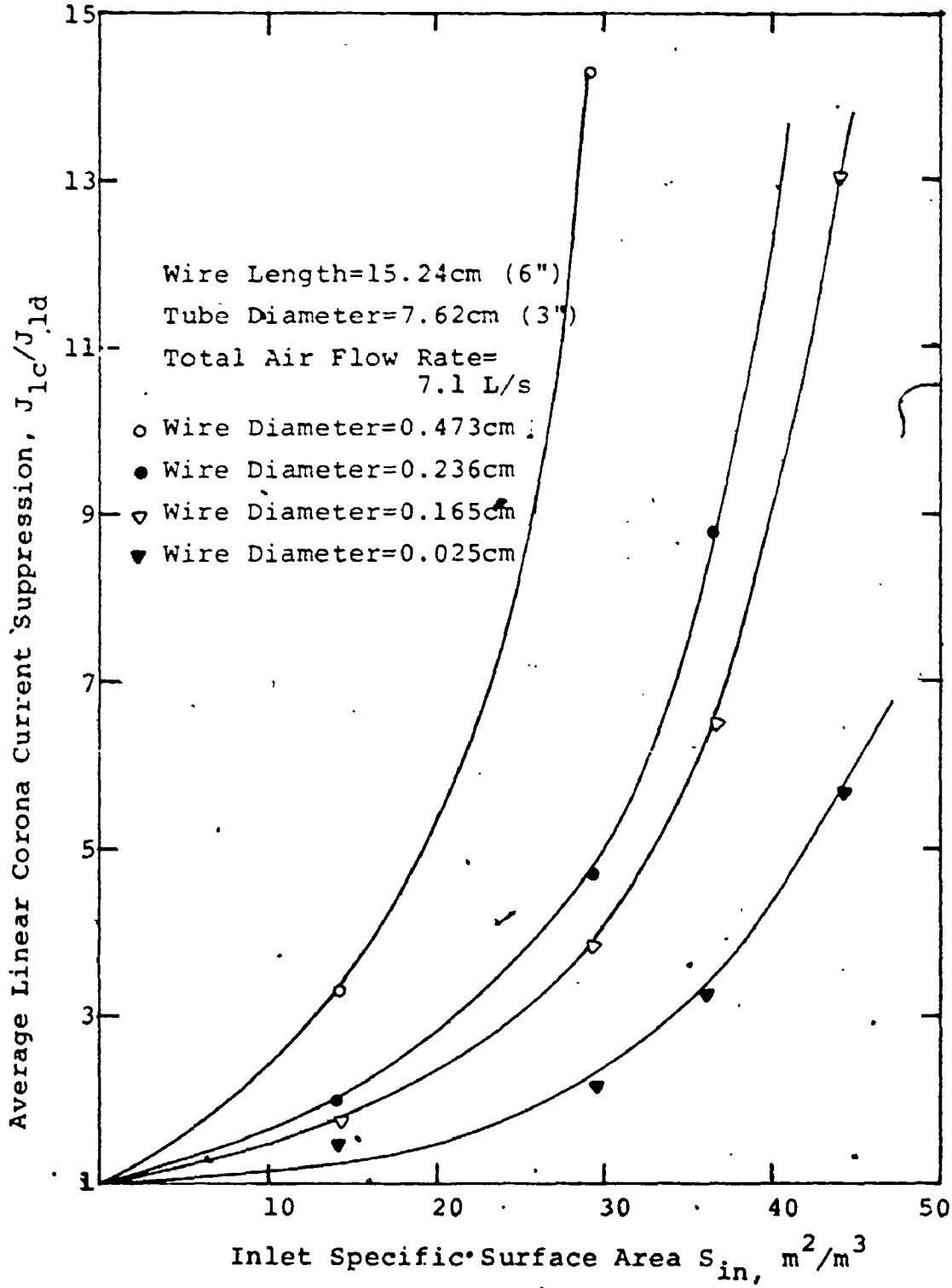

FIGURE (36) WIRE-TUBE PRECIPITATOR (NEGATIVE CORONA)

FIGURE (37) WIRE-TUBE PRECIPITATOR (POSITIVE CORONA)

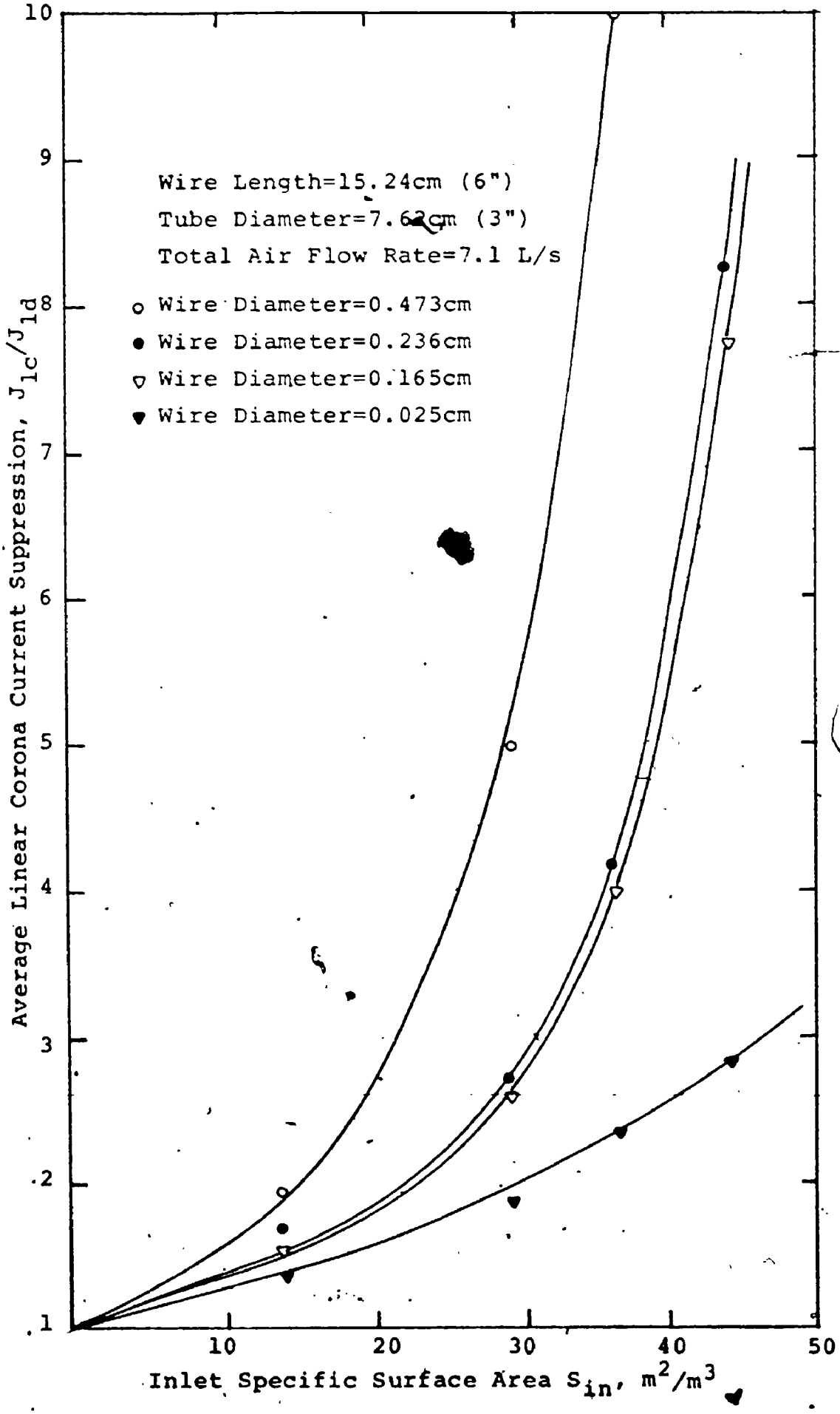

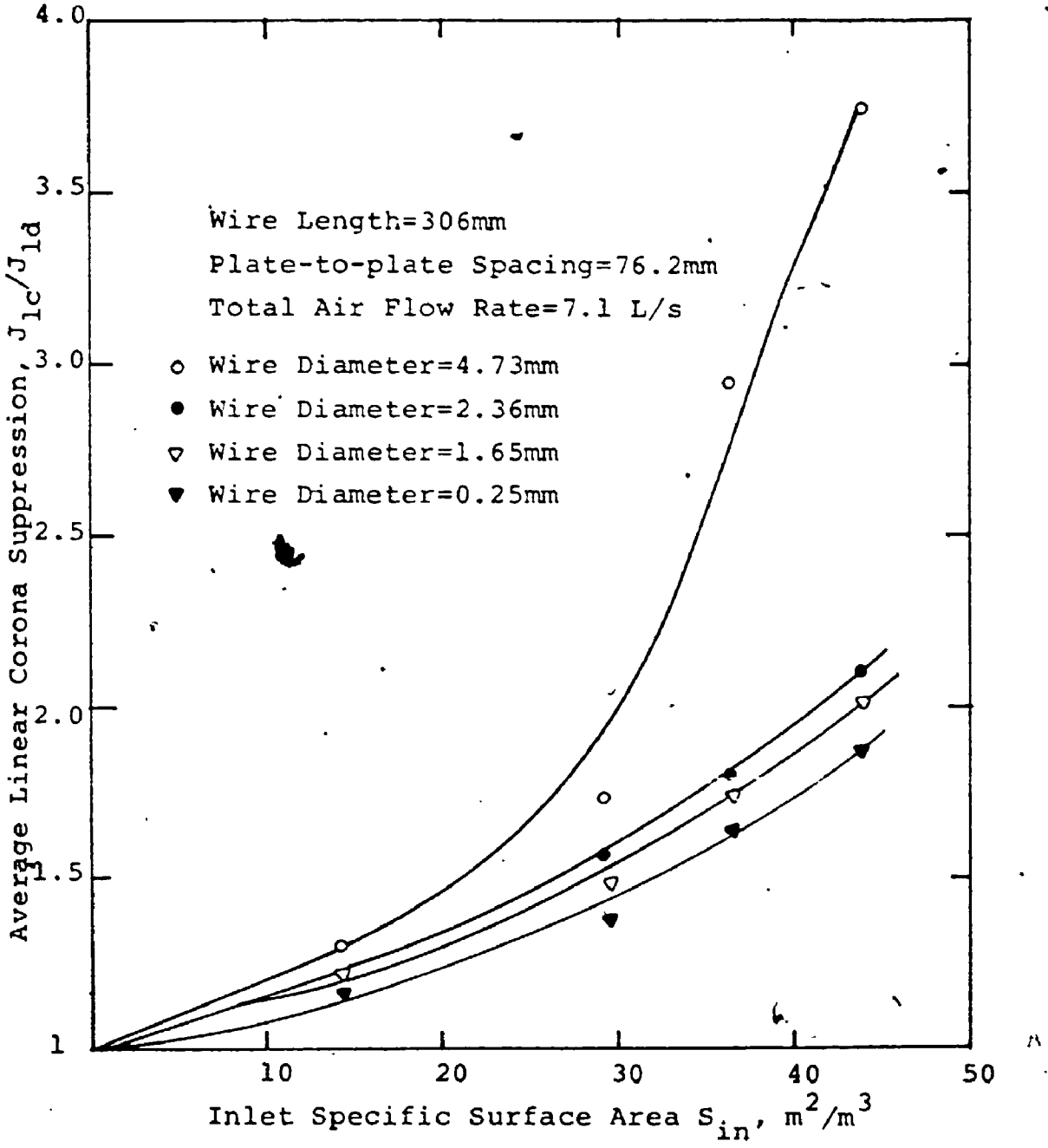

FIGURE (38) DUCT PRECIPITATOR (NEGATIVE CORONA)

FIGURE (39) DUCT PRECIPITATOR (POSITIVE CORONA)

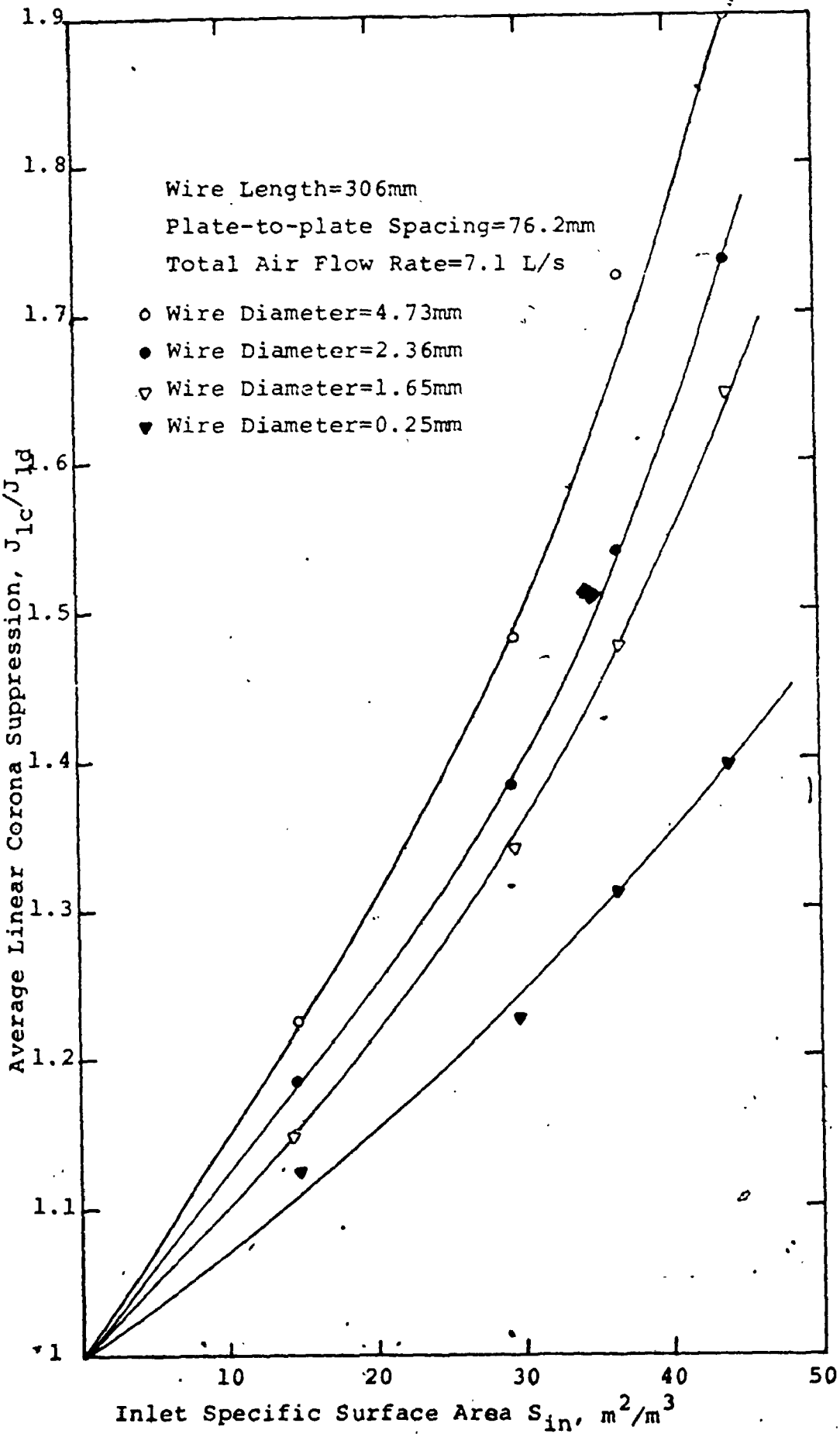

FIGURE (40) NEGATIVE CORONA
COLLECTION EFFICIENCY vs THE SPECIFIC SURFACE AREA

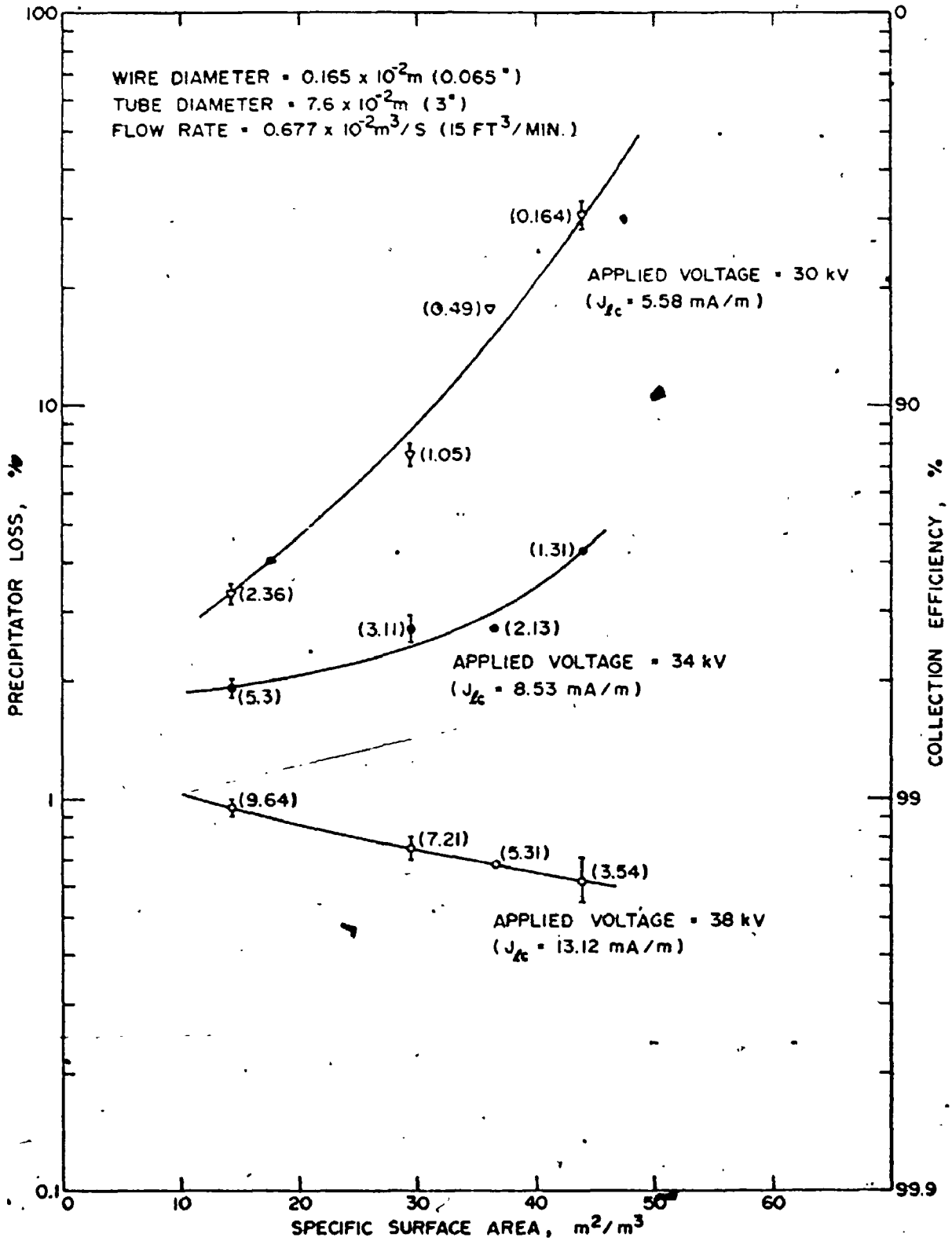

FIGURE (41) POSITIVE CORONA
COLLECTION EFFICIENCY vs THE SPECIFIC SURFACE AREA

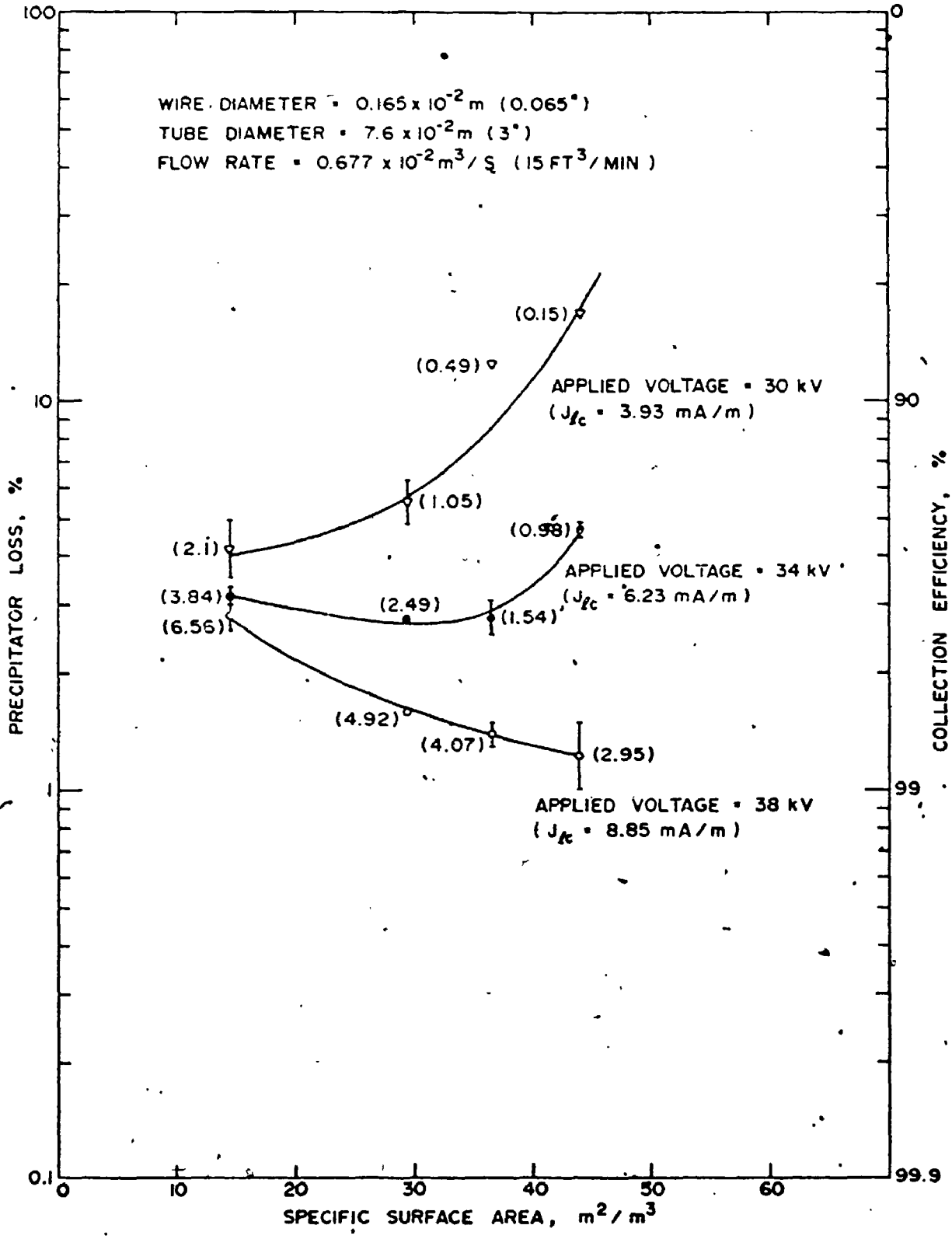

versus the inlet specific surface area of the suspended material at fixed total air flow rate for both positive and negative corona for a corona wire of diameter 0.165×10^{-2} m (0.065"). The values of the average quenched corona current density in mA/m are indicated between brackets at each point with the initial corona current densities with clean air shown under the appropriate voltage. For applied voltages of 30 and 34kV, as the inlet specific surface area increases, the average corona current density decreases and the collection efficiency decreases. This can be explained as follows: In the charging process, the charge acquired per particle decreases as the specific surface area increases. In the collection process, the collection field at the outer electrode is not enhanced enough to compensate for the reduction in the charge for the following reason. At these voltages, the original corona current density with clean air in the collection zone was relatively low and the suppression of the current generation from the ionized sheath was relatively large ($21 \gtrsim (J_{1c}/J_{1d}) \gtrsim 2$). Since the reduction in the ionic current in the presence of the suspended material is large, then the collection field component due to the ionic current is greatly reduced. However, the presence of the charged particles will give

FIGURE (42) NEGATIVE CORONA
COLLECTION EFFICIENCY vs THE SPECIFIC SURFACE AREA

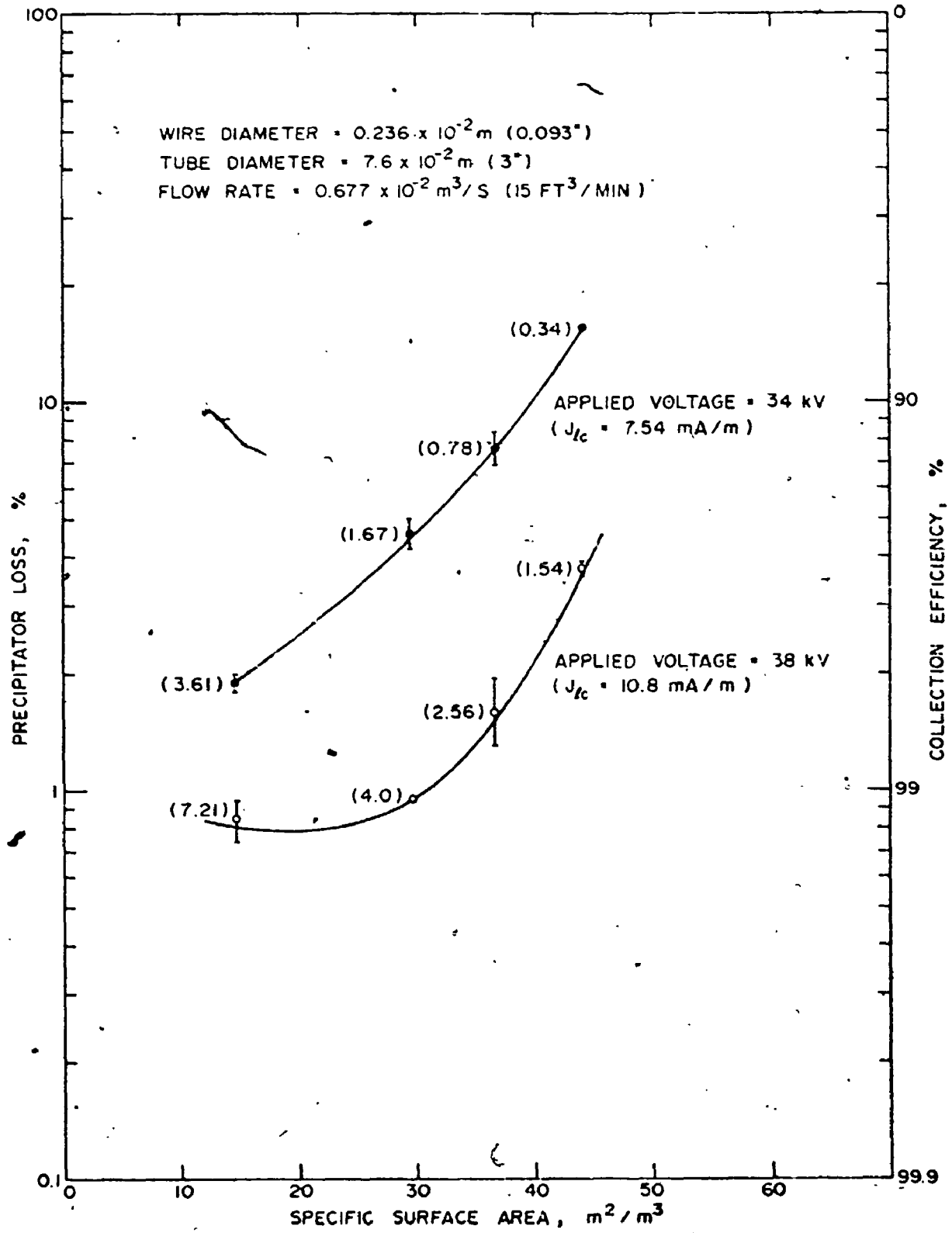

FIGURE (43) POSITIVE CORONA
COLLECTION EFFICIENCY vs THE SPECIFIC SURFACE AREA

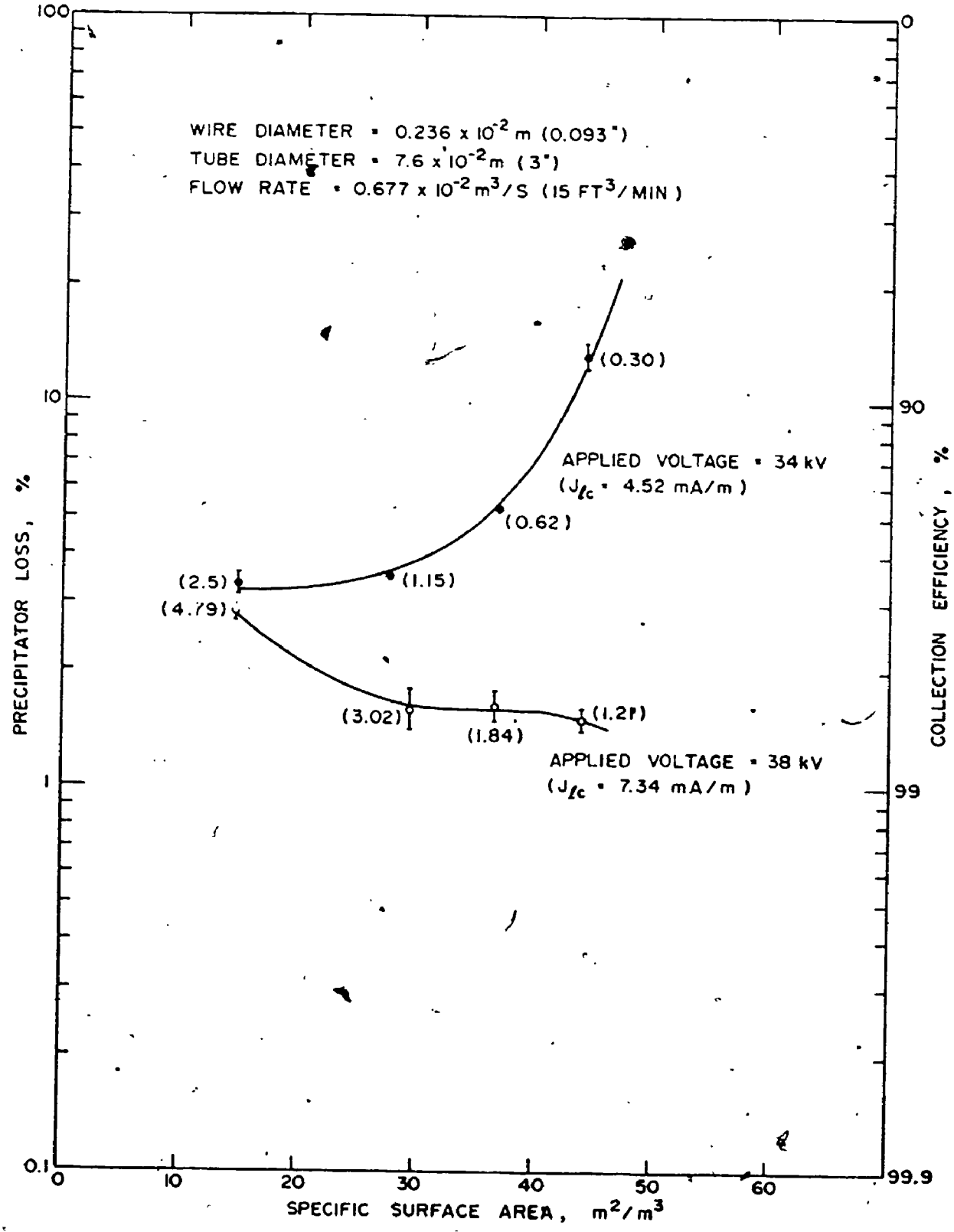

another component that adds to the electrostatic and the ionic components forming the total collection field.

On the other hand, at an applied voltage of 38 kV (i.e a higher original corona current density than in the previous two cases) the corona current suppression is relatively low ($4.47 \geqslant (J_{1c}/J_{1d}) \geqslant 1.4$) and the collection field enhancement at the outer electrode was apparently capable of compensating for the reduction in the charge per particle resulting in an increase in the collection efficiency as the inlet specific surface area increases. From the results of this corona wire, it is seen that the magnitude of the original corona current density present in the gap with clean air separates two different regimes i.e high and low current density regimes. Similar experiments were made on another corona wire of diameter 0.236×10^{-2} m (0.093"), the results of which are shown in figures (42) and (43) respectively. In figures (42) for negative corona, at applied voltages of 34 and 38 kV, as the inlet specific surface area increases the collection efficiency decreases. Note that the results with the smaller corona wire in figure (40) for negative corona at 38 kV show an increase in the collection efficiency with the increase in the inlet specific surface area. This is due to the larger original corona current density with

the smaller wire at the same applied voltage. In the positive case, however, at 38 kV the original corona current density is high enough to give an increase in the specific surface area as in the case of the smaller wire.

From the above results, one can see that a reasonable factor that may be used as an indicator for the relative effect the space-charge may have on the collection efficiency is the original linear corona current density in the gap with clean gas coupled with the inlet specific surface area of the particles. For this reason, figures (44) to (47) are plotted showing J_{lc}/S versus the collection efficiency for the two corona wires used in the negative and positive corona at fixed voltages as indicated. This indicates that a variation of the inlet specific surface area for a certain original value of j_{lc} such that the ratio is larger than approximately 0.5 $(mA/m)/(m^2/m^3)$ (i.e 0.5 mA) in the negative corona case and 0.25 mA in the positive, should not result in a reduction in the collection efficiency. This is the high corona current density regime. On the other hand, variations of the inlet specific surface area for certain original current density J_{lc} such that the ratio is less than these limits should result in a reduction in the collection efficiency. This is the low corona current

FIGURE (44) NEGATIVE CORONA
COLLECTION EFFICIENCY vs THE CORONA CURRENT DENSITY
WITH CLEAN GAS PER UNIT SPECIFIC SURFACE AREA

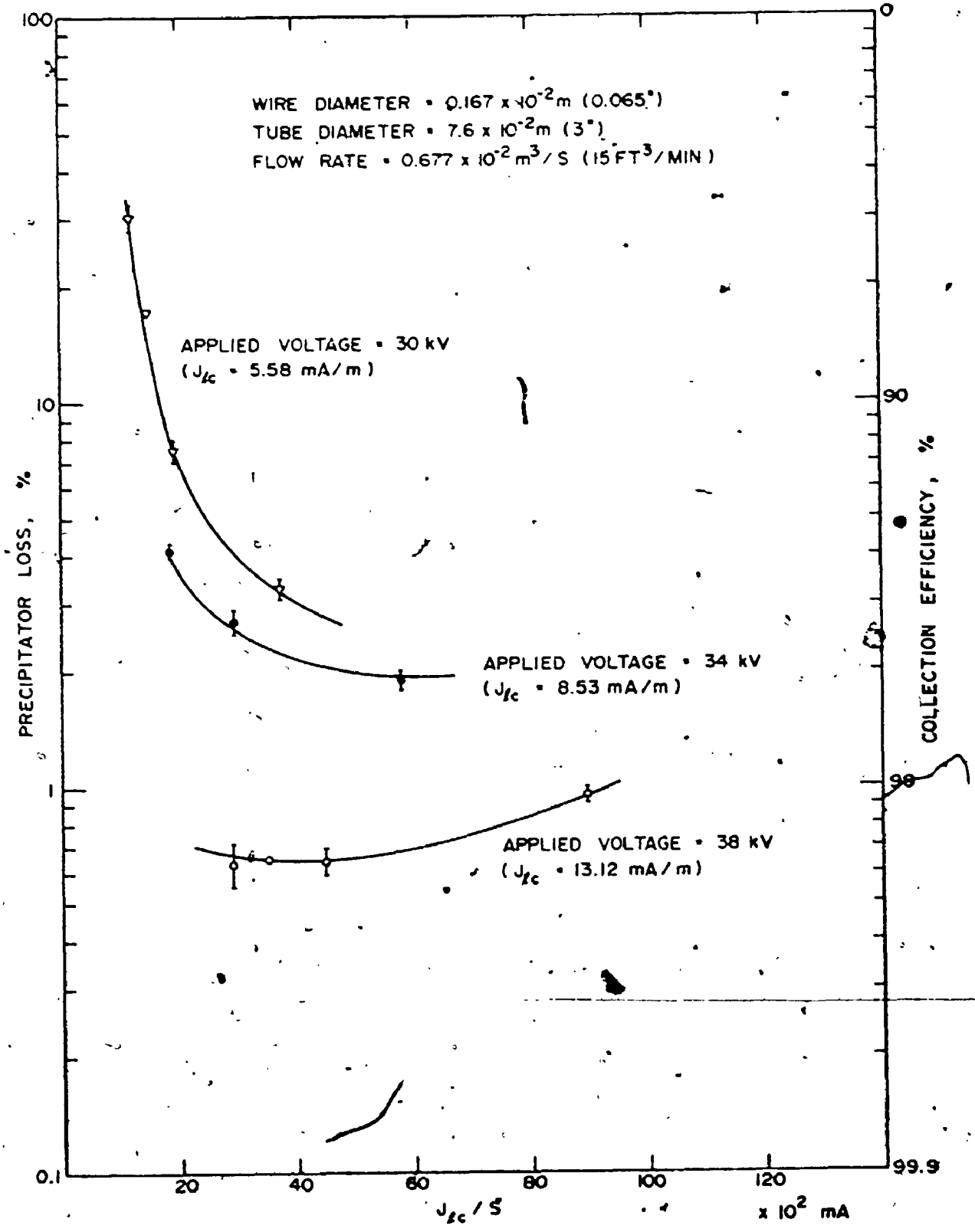

FIGURE (45) POSITIVE CORONA
COLLECTION EFFICIENCY vs THE CORONA CURRENT DENSITY
WITH CLEAN GAS PER UNIT SPECIFIC SURFACE AREA

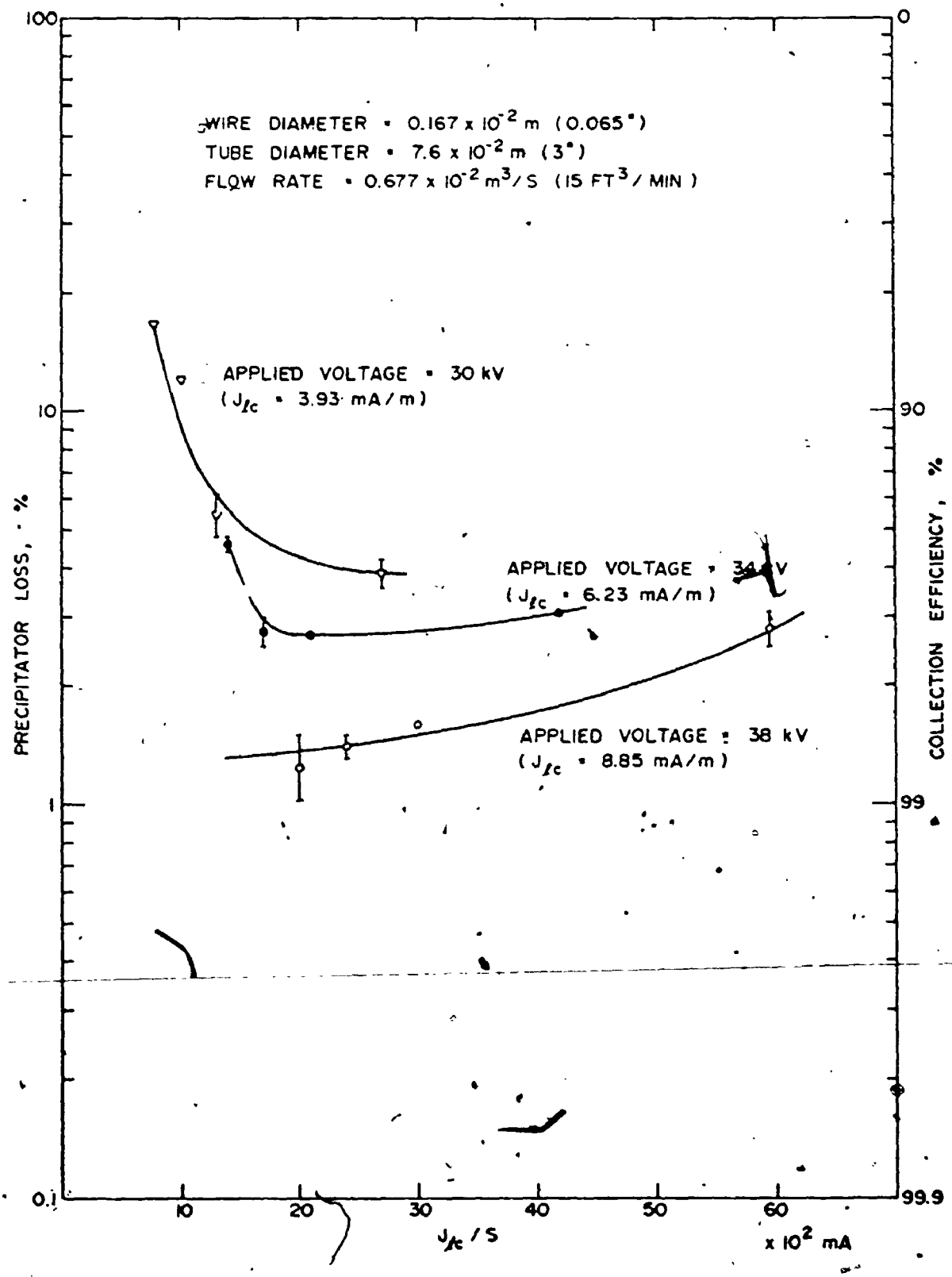

FIGURE (46) NEGATIVE CORONA
COLLECTION EFFICIENCY vs THE CORONA CURRENT DENSITY
WITH CLEAN GAS PER UNIT SPECIFIC SURFACE AREA

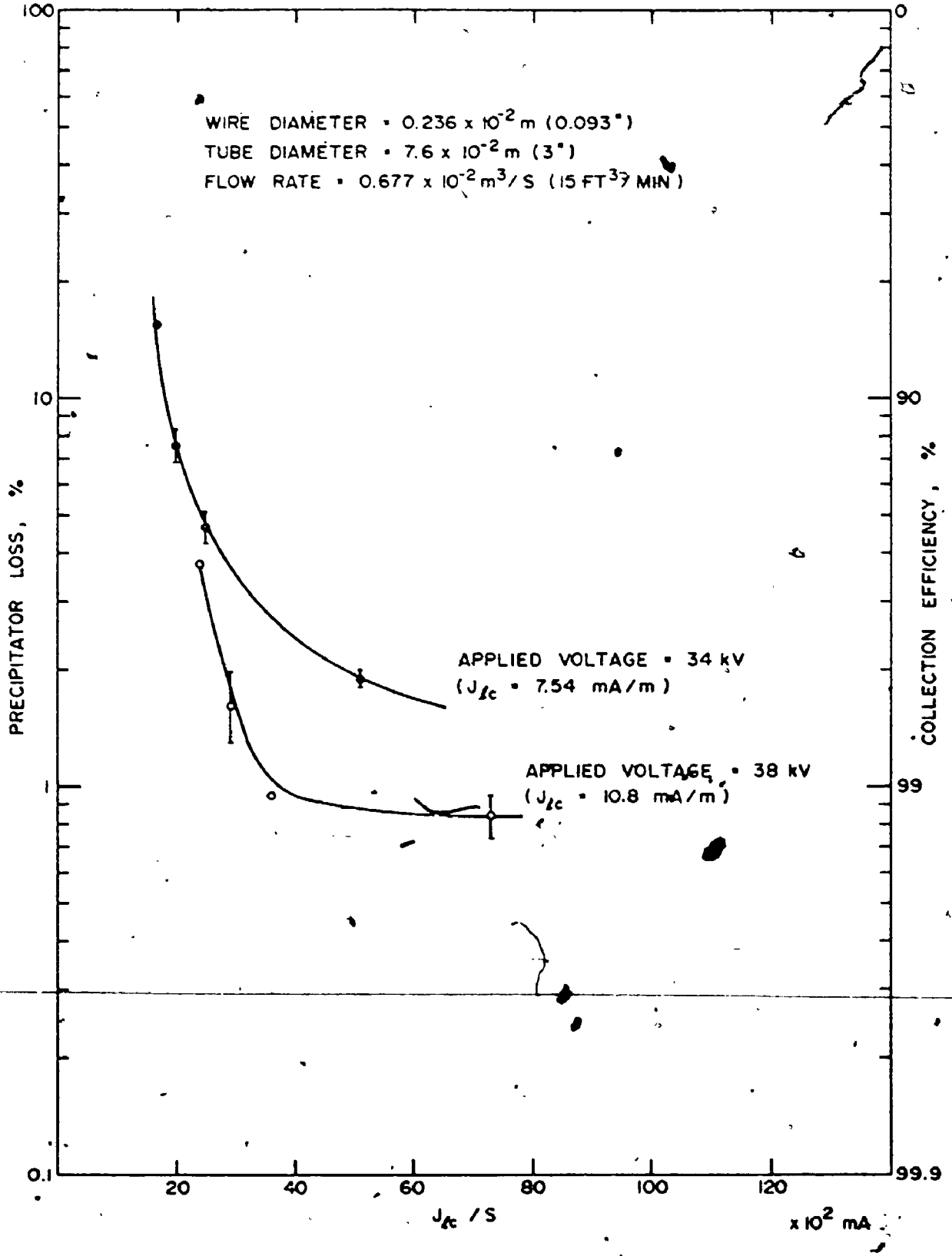

FIGURE (47) POSITIVE CORONA
COLLECTION EFFICIENCY vs THE CORONA CURRENT DENSITY
WITH CLEAN GAS PER UNIT SPECIFIC SURFACE AREA

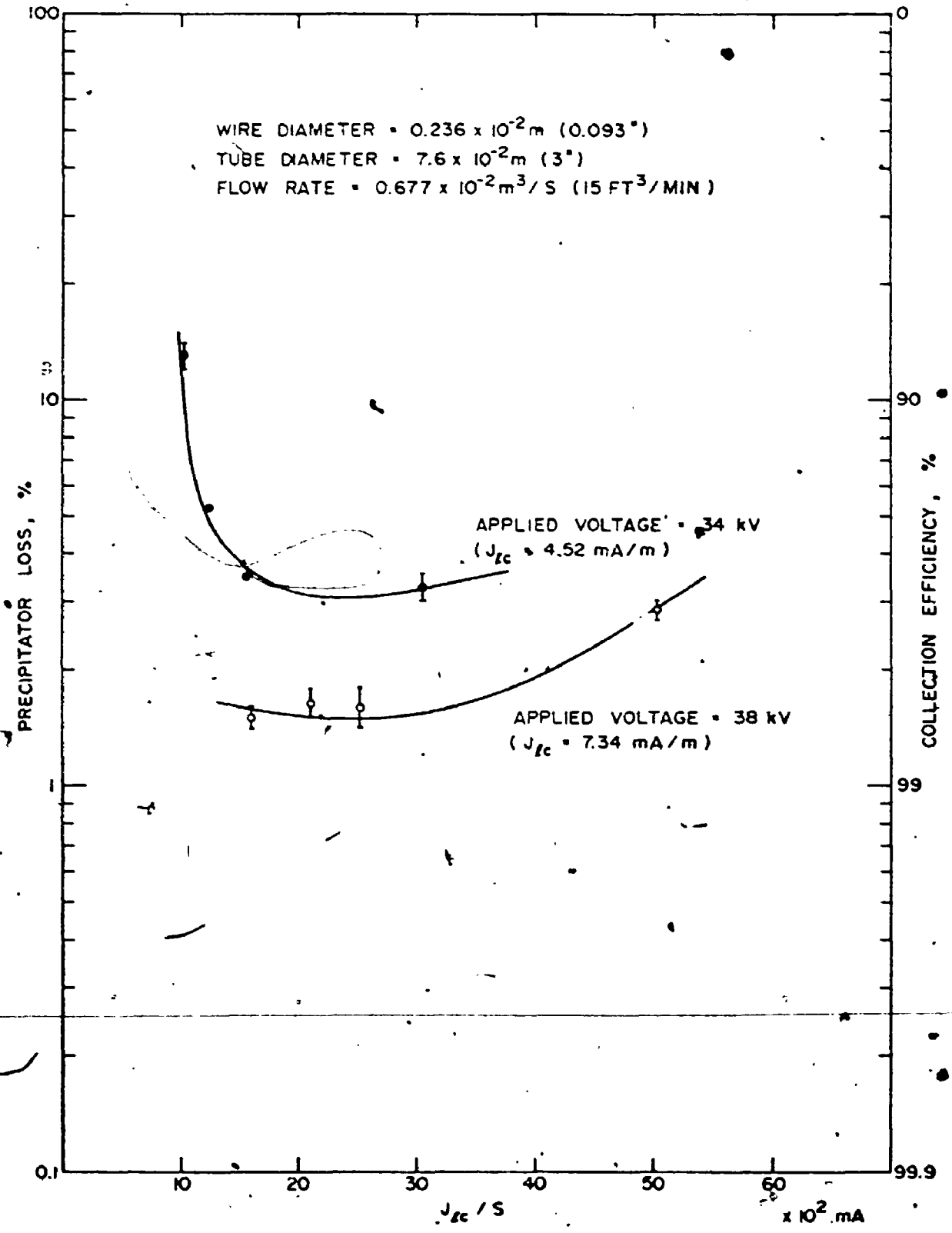

density regime.

Let us discuss the possibility of extrapolating the above experimental limits to operating size precipitators. These experimental limits should not vary appreciably with suitable variations in the corona wire diameter as the above results for the two wires of different diameters indicate. However, as the corona wire diameter increases the voltage required to attain the required value of (J_{1c}/S) will increase. On the other hand, the effect of the interelectrode spacing on these limits is not certain. However, since this ratio is actually representative of the ion space-charge per unit volume of the gas originally present in the gap (J_{1c} is proportional with ρ_i) to the total surface area of the particles per unit volume of the gas, one may expect the interelectrode spacing not to have an appreciable effect on these limits. However, as the interelectrode spacing increases the applied voltage required to attain these limits increases. Therefore, it is believed that under idealized conditions of no reentrainment or back corona the above experimental limits may be a good approximate indicator for the behaviour of the collection efficiency as affected by the inlet specific surface area. Comparison of the results shown in figures (40) and (41) for the

corona wire of diameter 0.165×10^{-2}m (0.065") indicates that for applied voltages of 30 and 34kV where J_{lc} is relatively low, the negative corona although having higher values of J_{lc} and J_{ld} gives lower collection efficiency than the positive for the same inlet specific surface areas of 29.4, 36.7, and 44 m^2/m^3 (highest three values only) and the same applied voltage. This is believed to be due to the non-uniformity of the negative corona discharge in the axial direction for low current densities and the creation of gas pockets of low ion space-charge density between the successive localized tufts. These gas pockets should result in lower charging for some portion of the suspended material. With the increase in applied voltage, the number of tufts increases and also a free electron component of the current becomes apparent. Therefore, at applied voltage of 38kV, the negative corona with its higher values of both J_{lc} and J_{ld} results in higher efficiency than the positive. Note that the results of the other corona wire as shown on figures (42) and (43) confirm this polarity effect.

It is interesting to mention that on a larger scale precipitation, Tassicker[62] confirmed that higher collection efficiencies can be obtained with increasing the ash content.

7.3.7 The relative significance of the corona current density and the applied voltage on the collection efficiency

It is well-known that to achieve optimum value of the effective migration velocity for certain particle size, one mostly aims at the highest electric field intensity at all points in the gap. Realizing this fact, industrial electrostatic precipitators normally operate at an applied voltage very close to sparkover. So, it is frequently mentioned [1] [3] that for optimum operation of electrostatic precipitator it is desirable to maintain the highest possible sparkover voltage. Some other investigators [30] [29], however, mentioned that for optimum operation of electrostatic precipitator one mostly aims at maintaining the highest possible linear corona current density. This second idea is probably based upon the fact that the linear corona current density may be the major factor for the electric field as can be indicated by the following equation:

$$E = (J_{lc} / 2\pi\varepsilon_o K_i)^{\frac{1}{2}}$$

which may be applied under certain conditions as indicated in section (2.3). The question now arises to whether the maximum pre-sparking corona current density is the main design factor of first priority or the value

of the sparkover voltage or both.

Experiments have been carried out to investigate the relative effects of the applied voltage and the linear corona current density on the collection efficiency at fixed inlet specific surface area of 14.7 m^2/m^3 and total air flow rate of 7.1 L/s (15CFM). Using corona wires of diameters 0.0254×10^{-2}m (0.010"), 0.165×10^{-2} m (0.065"), and 0.236×10^{-2} m (0.093"), the collection efficiency was measured at three fixed values of the average corona current density J_{1d}. The values chosen for J_{1d} were 1.34, 2.68, and 6.66 mA/m. The applied voltage required to get a fixed value of J_{1d} for the three corona wires of different diameters increases with the increase in the diameter of the corona wire. Figures (48) and (49) show the collection efficiency versus J_{1d} for negative and positive corona respectively. The values of the applied voltage V and the linear corona current density with clean gas at this voltage J_{1c} are indicated beside each point. From these figures note:

(1) For a fixed value of J_{1d}, as the corona wire diameter increases, the collection efficiency increases. This can be attributed to two factors: (a) higher original value of J_{1c} as can be seen from (b) higher value of the applied voltage. This results in a higher

FIGURE (48) WIRE-TUBE PRECIPITATOR (NEGATIVE CORONA)

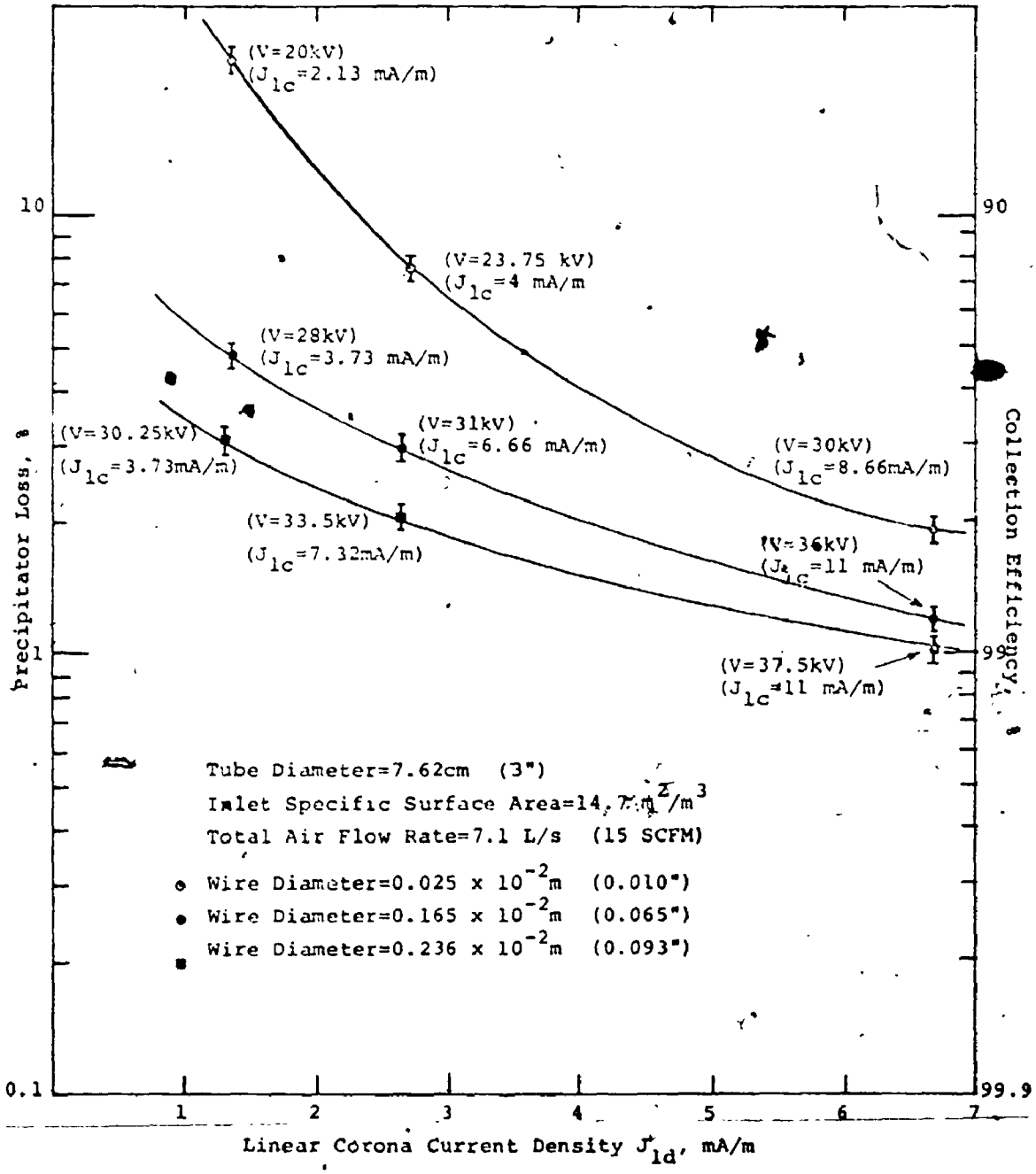

FIGURE (49) WIRE-TUBE PRECIPITATOR (POSITIVE CORONA)

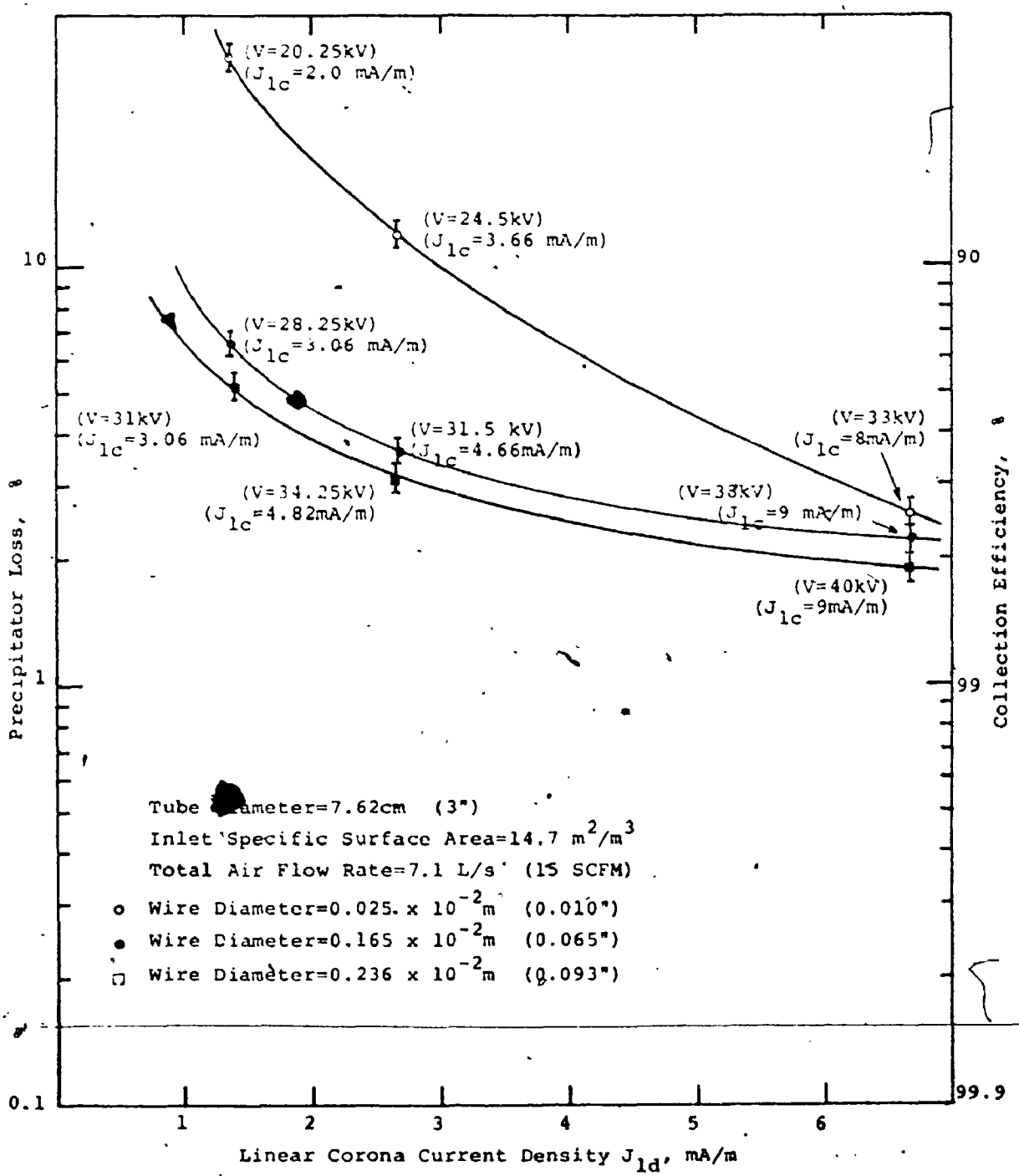

electrostatic component of the electric field.

(2) For the same value of J_{1d} and for fixed corona wire size, the negative corona gives higher collection efficiency than the positive. This may be explained by the higher value of J_{1c} under negative corona than the positive due to the electron component in the negative corona current.

Since J_{1c} is the factor directly affecting the collection efficiency as mentioned in section (7.3.6), the results were replotted against J_{1c} as shown in figures (50) and (51). These figures show that:-

(1) For low values of J_{1c}, as the corona wire diameter increases the electrostatic component of the electric field increases and the collection efficiency increases for fixed value of J_{1c}.

(2) For higher values of J_{1c}, the electrostatic component of the electric field has a relatively smaller effect and the main factor should be J_{1c}. Therefore, one can see that for low values of J_{1c}, close to the corona onset, the electrostatic component of the field as well as the ion space-charge component are both affecting the electric field and the collection efficiency, whereas for high values of J_{1c}, close to sparkover, the effect of the electrostatic component of the field may become

FIGURE (50) WIRE-TUBE PRECIPITATOR (NEGATIVE CORONA)

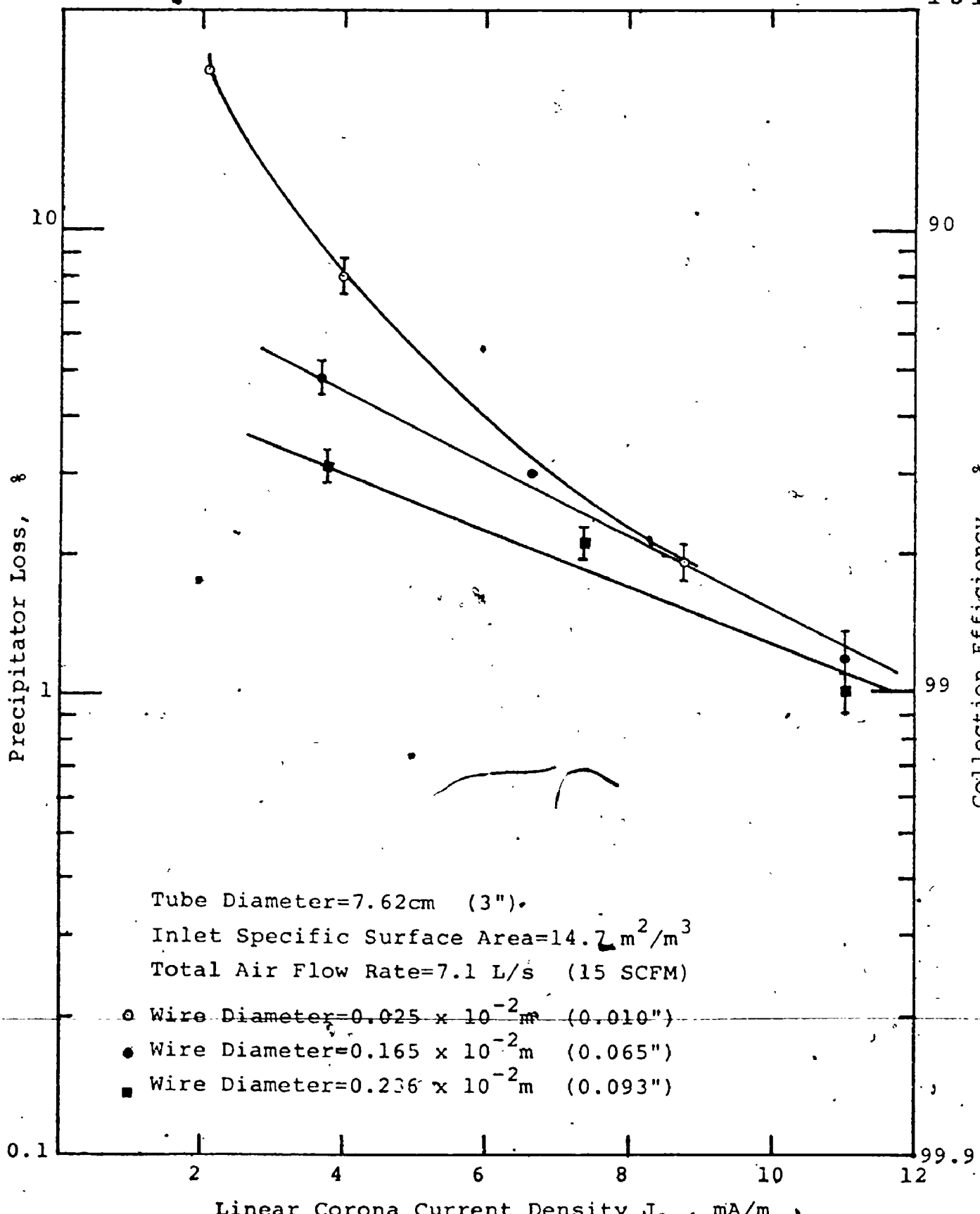

FIGURE (51) WIRE-TUBE PRECIPITATOR (POSITIVE CORONA)

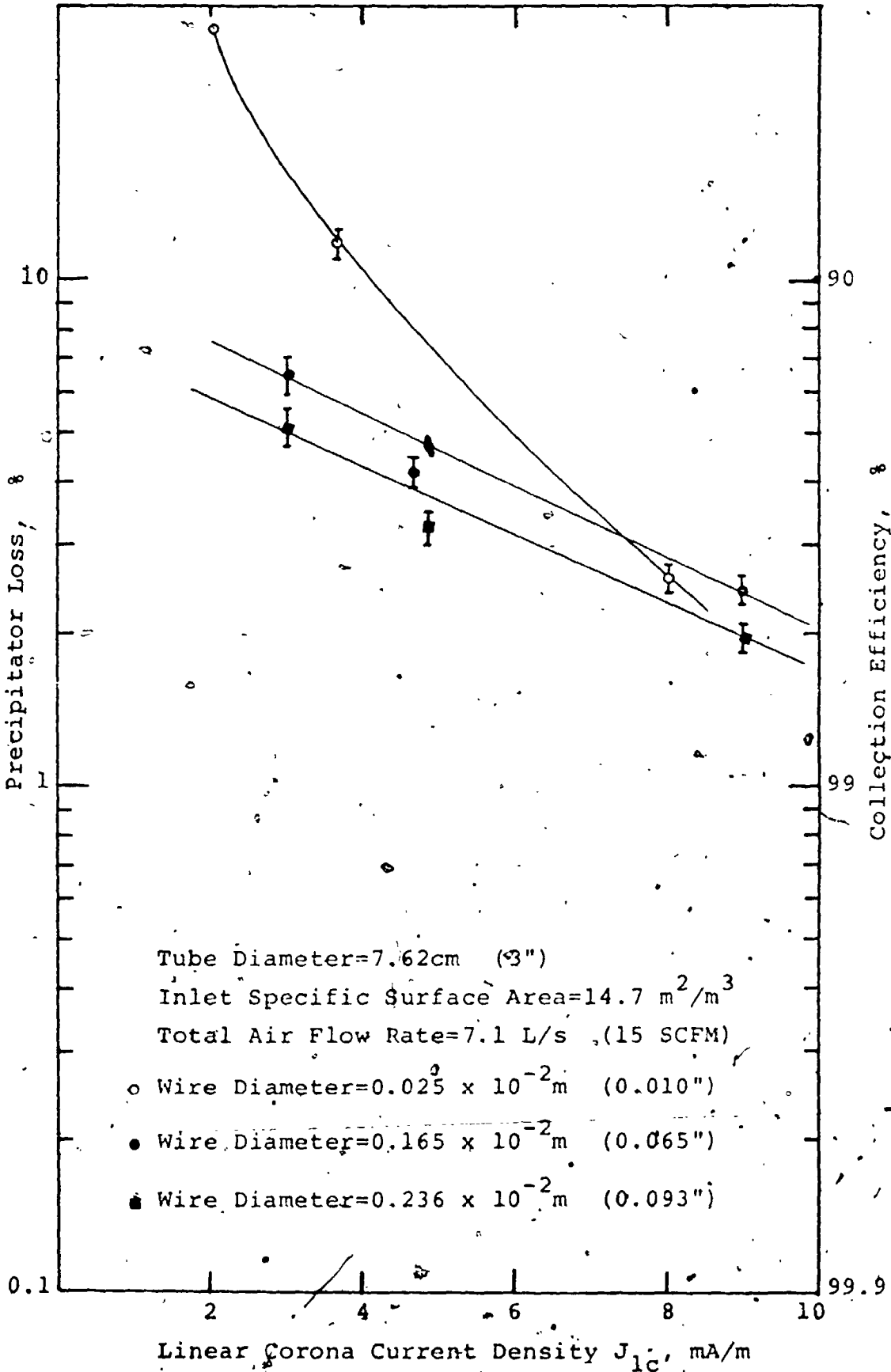

relatively small and the main factor should be J_{lc}. Hence, the purpose of maximizing the sparkover voltage is indirect and operates through its effect on the maximum pre-sparking corona current. In other words, if one can find a method that results in an increase in the maximum pre-sparking corona current while sacrificing for some reduction in the sparkover voltage, higher collection efficiency should be obtained.

7.3.8 Linear corona current density distribution in the axial direction of a wire-tube precipitator

The results of this section were obtained using the segmented corona apparatus as described in section (5.6). Positive and negative polarities were employed for cases using different particle concentrations. Because of the similarity of the general trends of both polarities, only the negative corona results will be discussed. The positive corona results are tabulated in Appendix (E).

In the presence of particles suspended in the gas, there are four effects that determine the amount of corona current collected and measured by a certain segment:

(1) The relative pick-up of the free gaseous ions by the partially charged or uncharged particles at the crossection of the segment. The higher this ion pick-up, the higher will be the quenching of the measured corona current of the segment under consideration.

(2) The ionization electric field on the discharge electrode opposite this segment. As the particle space-charge density in the interelectrode space increases, the ionization field decreases and the corona current production adjacent to the segment decreases.

(3) The collection rate of the charged particles. Under the action of the collection electric field, the charged particles disappear from the gap and deposit on the collecting electrode and hence the two effects (1) and (2), as mentioned above, will be reduced. Therefore, the higher the collection rate, the higher will be the corona current collected by a given segment at a fixed voltage.

(4) The electric field distribution in the inter-electrode spacing of this segment. Because of the assymmetry in the particle and ion space-charges in the two neighbouring segments, an electric field component may arise in the axial direction. Therefore, the total electric field at any point within the region is not

necessarily radial. This new field pattern should affect both the charging and collection rates and hence affect the above three factors.

In figures (52) to (56), the zero of the axial position as measured on the horizontal axis represents the inlet to the precipitator. Each point was taken at the center of each segment.

Figure (52) for clean air shows that for the range of applied voltages between 24kV to 44kV, the linear corona current density is constant in the axial direction except for some increase at the ends because of fringing effects. For applied voltages less than 24kV close to the corona onset voltage (19kV in this case) the end rings take less linear corona current density than the regular inner cylindrical surface. For applied voltages higher than 44kV there is a slight increase in j_{lc} in the axial direction, probably because of the higher air temperature at the segments close to the exit of the precipitator than these close to the inlet. The heat is supplied, of course, by the total corona power loss.

Figures (53) to (56) show:

(1) Applied voltages 24, 26, 28, and 30kV were very close to the apparent corona onset voltage under inlet specific surface areas of 14.7, 29.4, 36.7, and 44 m^2/m^3 respectively. In these cases as the particles

FIGURE (52) $S_{in} = 0$

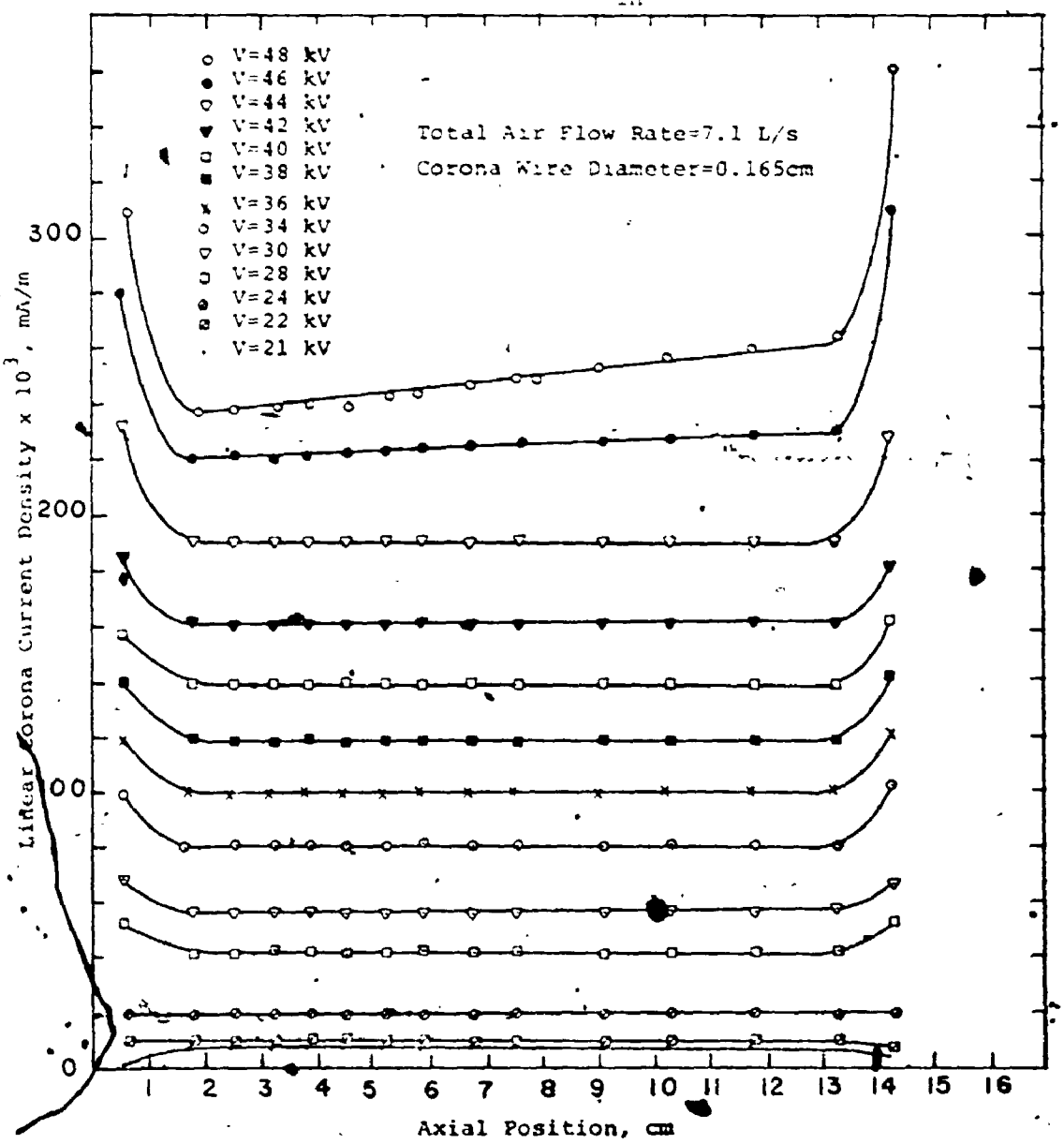

FIGURE (53) $S_{in} = 14.7\ m^2/m^3$

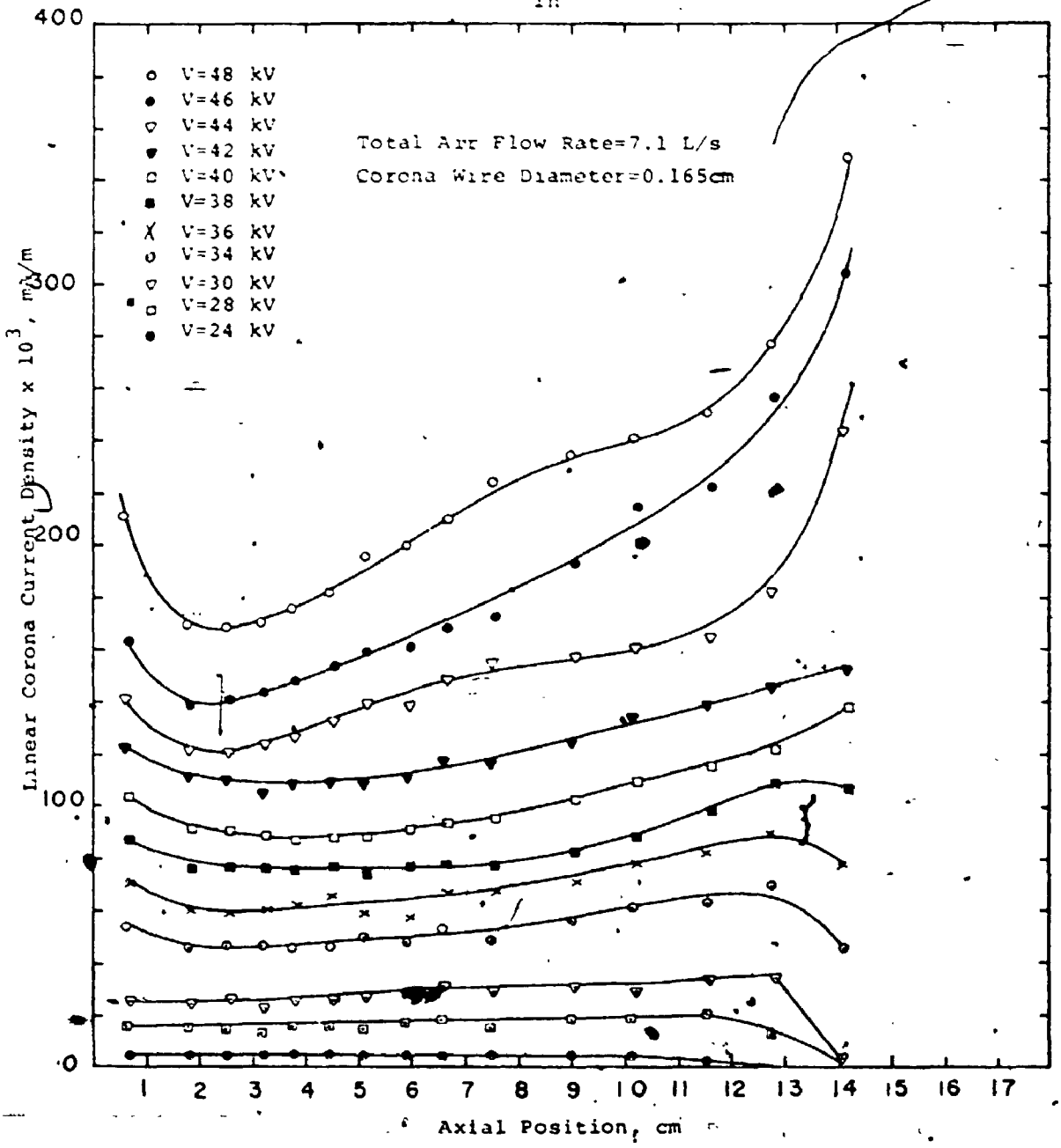

FIGURE (54) $S_{in} = 29.4\ m^2/m^3$

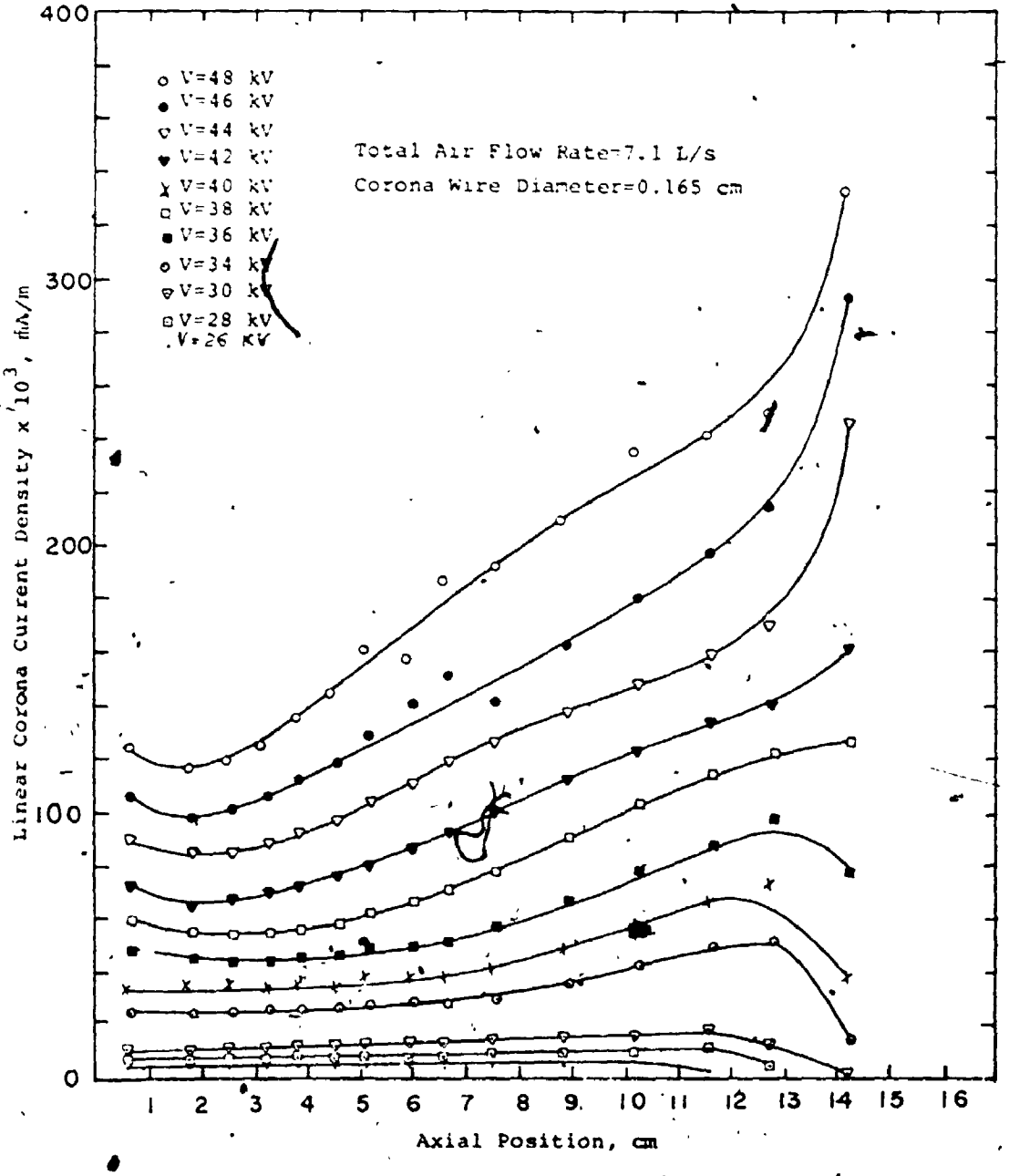

FIGURE (55) S_{in} = 36.9 m^2/m^3

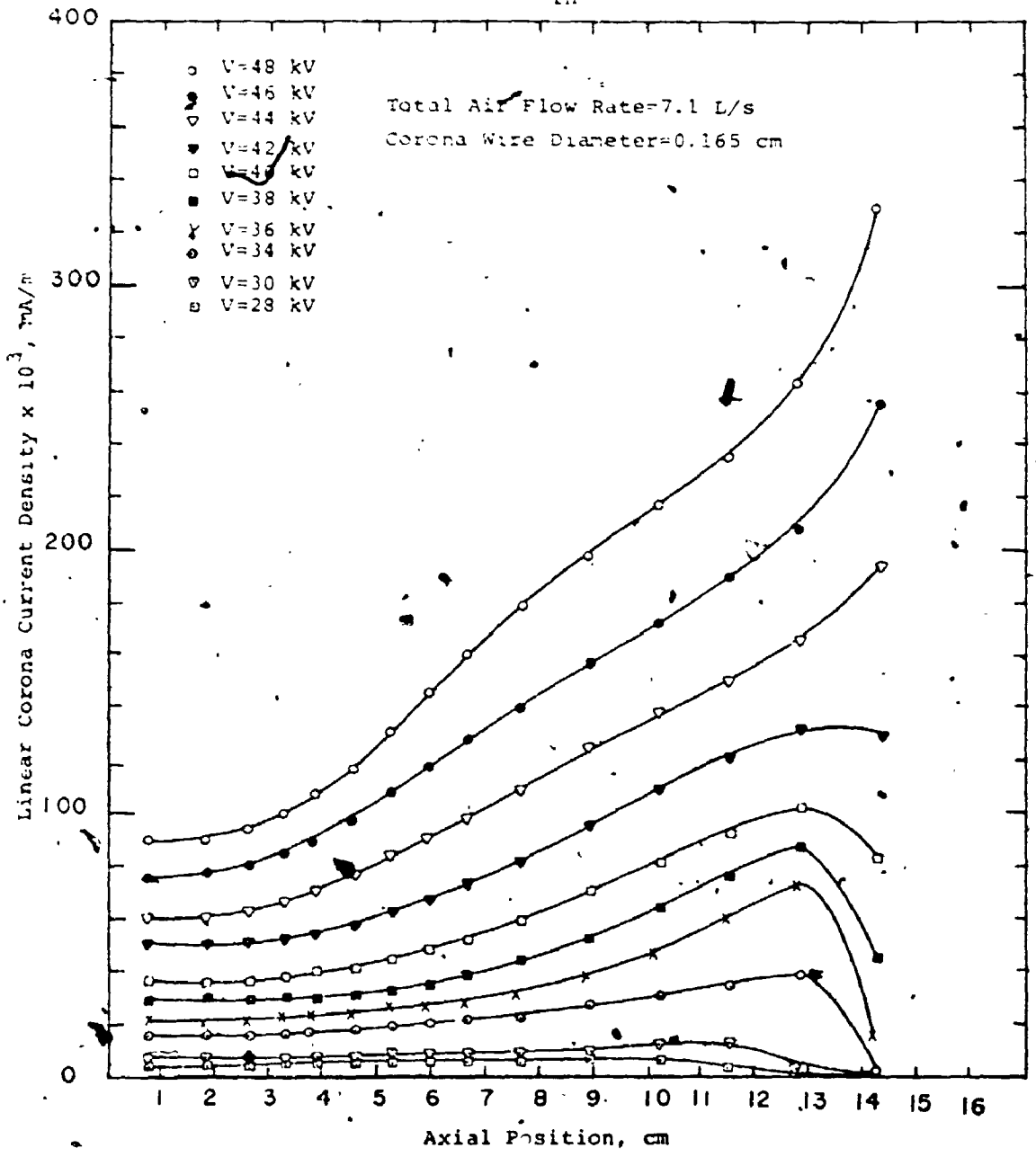

FIGURE (56) S_{in} = 44 m^2/m^3

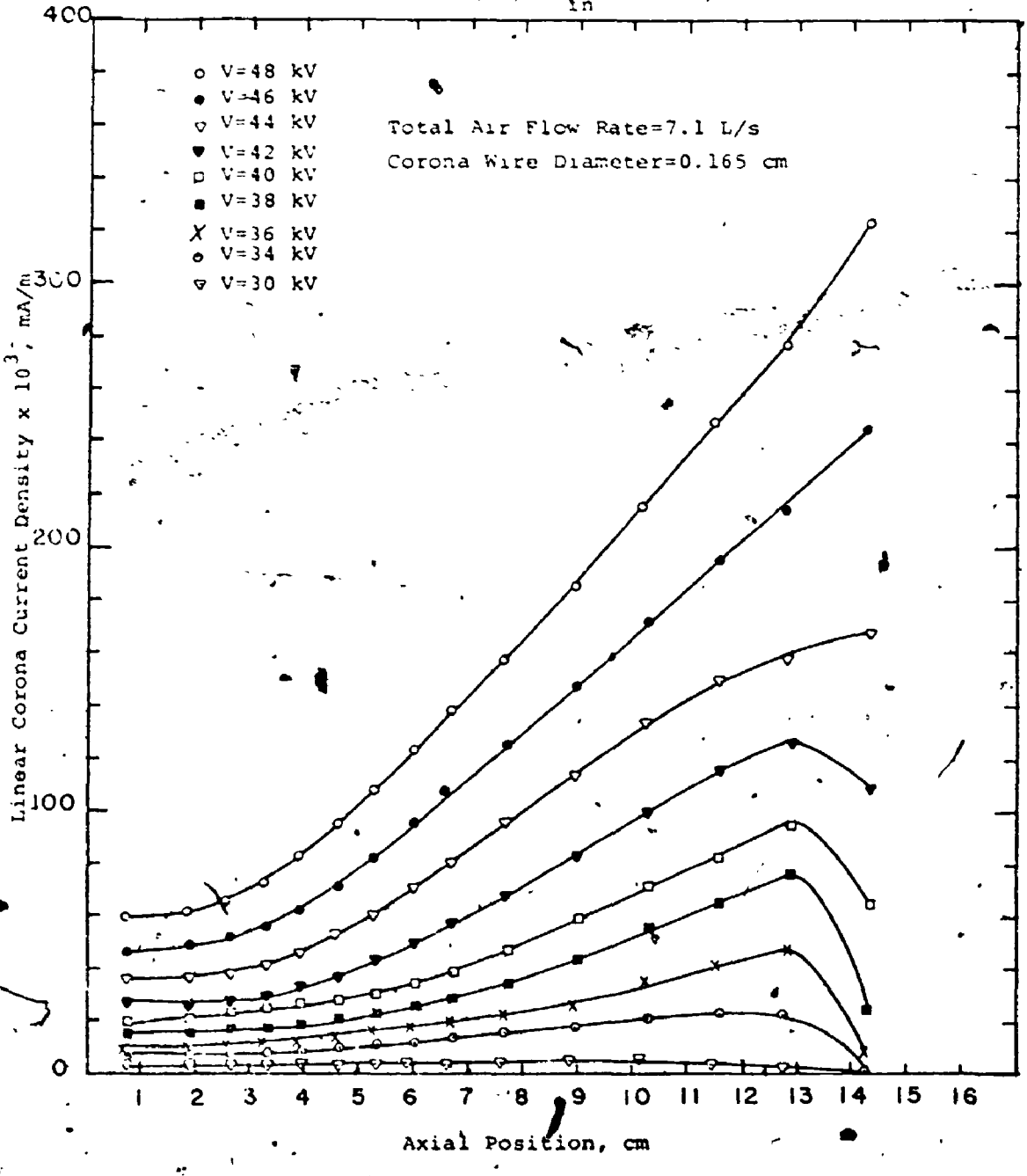

enter the precipitator and move in the axial direction their charging rate decreases while their effect on reducing the ionization field increases. Therefore, a segment close to the inlet of the precipitator should have a higher rate of particle charging (i.e larger amount of ions are picked up by the particles) and lower ionization field reduction than a segment close to the exit of the precipitator. These two effects resulted in a fairly constant value of j_{1d} for the first 12 segments. For the last three segments, an obvious dip in j_{1d} was observed. This dip may be explained by the presence of charged particles right at the outlet of the precipitator which tend to appreciably reduce the ionization field in the vicinity of the corona wire surface for some distance near the exit.

(2) With increasing the applied voltage, the collection rate increases, the particle concentration decreases in the axial direction and hence j_{1d} increases for segments downstream. With this increase in the applied voltage the particle space-charge density at the outlet of the precipitator decreases and hence they affect a shorter length of the corona wire close to the exit and the dip in j_{1d} is observed only for the last segment.

With further increase in the applied voltage, this dip entirely disappears because of the very high collection rate and the very low particle space charge density right at the outlet of the precipitator. Note that the applied voltage required to eliminate this dip increases with the increase in the inlet specific surface area. To eliminate this dip, 40kV were required for S_{in} = 14.7 and 29.4 m^2/m^3, while 44kV were required for S_{in} = 36.7 and 44 m^2/m^3. Higher than these voltages, an appreciable increase in j_{ld} at the last segment was obtained because of the very small space-charge concentration.

7.3.9 The incremental linear corona current suppression ratio

Figure (57) shows the incremental linear corona current suppression ratio j_{lc}/j_{ld} as it varies in the axial direction of the tube precipitator at 44kV. Note that as the inlet specific surface area increases the rate of reduction of j_{lc}/j_{ld} increases. This is an indication that as the inlet specific surface area increases the collection rate increases, j_{ld} increases rapidly, and hence the reduction of j_{lc}/j_{ld} per unit axial length increases. As mentioned in section (7.2), the increase in the collection rate with the increase in the inlet specific surface is due to the enhancement of the collection electric field at the outer electrode by the particle space-charge effect.

FIGURE (57) APPLIED VOLTAGE = 44 kV

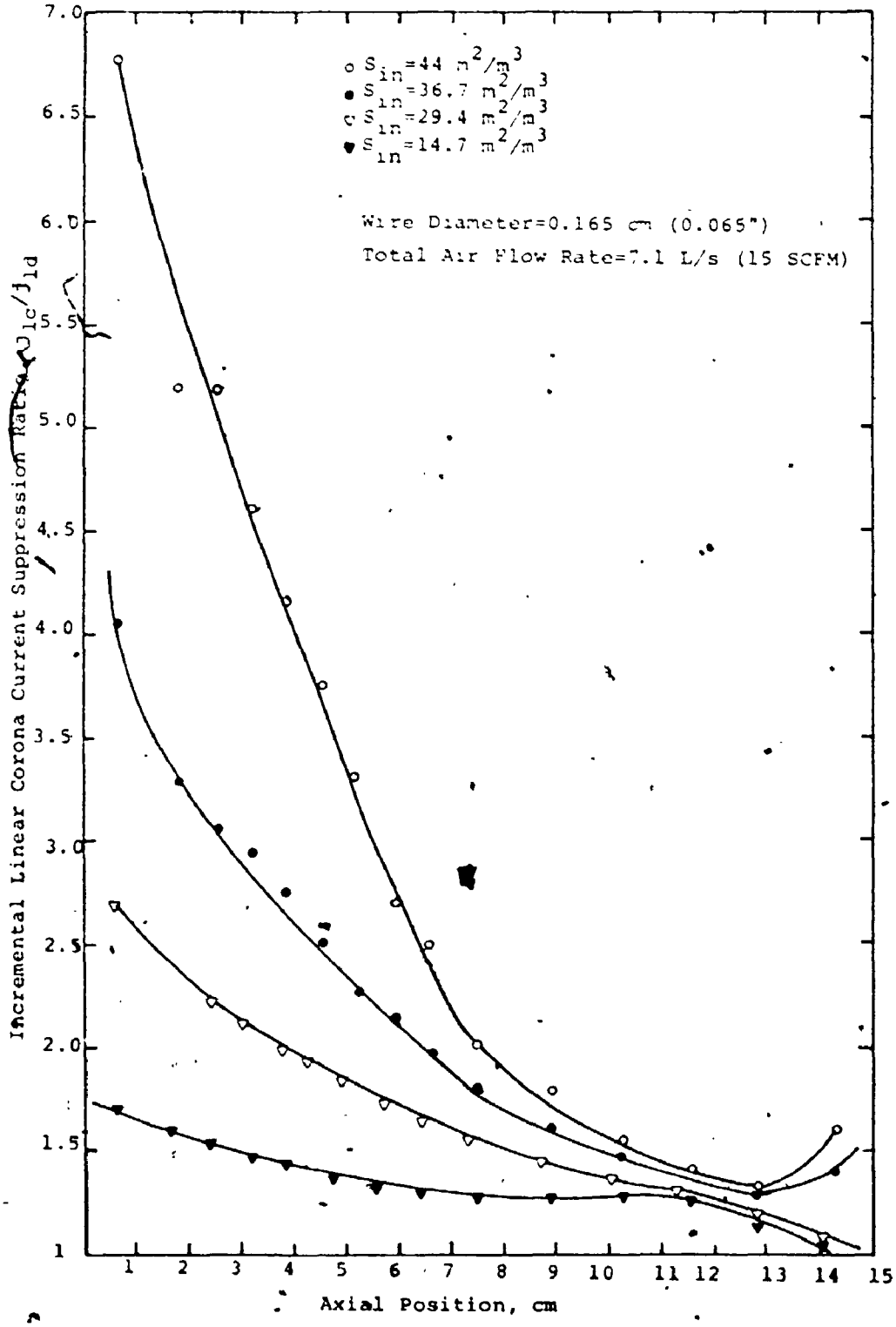

CHAPTER VIII

The sparking characteristics: Theory, results, and discussion

8.1 General

The main goal in this part of study was to generate some experimental data for the sparking characteristics for the wire-tube and wire-plate geometries under different conditions. The term sparking characteristic refers to the sparkover voltage and the maximum pre-sparking corona current. The value of the pre-sparking corona current has a special significance on the effective value of the particle migration velocity and the collection efficiency of electrostatic precipitators. Consideration of the point-to-plane corona modes and the sparking mechanisms as reviewed in section (4.1) in addition to some of the well-known discriptions of wire-plate and wire-tube coronas as mentioned in section (4.2) has led to a proposed mechanism for sparkover in wire geometries. These proposed mechanisms were used to explain the experimental results.

8.2 Theory

8.2.1 Positive corona and sparkover in wire-tube geometry

The basic requirement for corona onset is that there be a strong enough field at the surface of the corona wire to cause ionization of the air. Positive corona discharge at the threshold appear in the form of streamers and/or burst pulses. Onset streamers may be followed or preceded by the burst pulses. The positive corona modes leading to sparkover is dependent on the diameter of the corona wire and can be described as follows.

(1) For Fine Corona Wires:*

The empirical formulae for the electric field intensity E_o at the surface of the corona wire to start corona have the general form:

$$E_o = K_1 \delta + K_2 (\delta/a)^{\frac{1}{2}}$$

where K_1 and K_2 are constants.

From the above equation, one can see that the electric field at the surface of a fine corona wire right at the onset condition is very high. Using the values of 30 and

---

* Less than approximately 1.6 mm in diameter[52].

9 for the constants K_1 and K_2 as obtained by Peek[14] with the wire diameter of 1.6 mm and assuming $\delta = 1$, one can find the minimum value of E_o to be 62.4×10^5 V/m for this case. The gradient of the electric field in this case is given by[20]:

$$-(dE_o/dr) = (F_o/a) \qquad (61)$$

From equation (61) it can be seen that for this size range of wires the gradient of the field is very high having a minimum value of 78×10^8 V/m^2.

Under these conditions of very high surface field and rapid fall of this field with the radial distance r from the wire, high mobility electrons avalanche towards the wire leaving behind a positive ionic space charge. This primary avalanche is essentially a Townsend breakdown in which α, the first Townsend's ionization coefficient, is the main factor. However, several secondary processes, such as photoionization, also play an important role. Because of the fast decay of the field in the neighbourhood of the primary avalanche, negative ions will also be formed due to these secondary processes. In other words, the electrons in the secondary processes quickly spread out to encompass the conductor with a negative ion sheath. Evidently, these negative ion space charges close to the surface are required for burst pulse formation and prevent

3 3

OF/DE

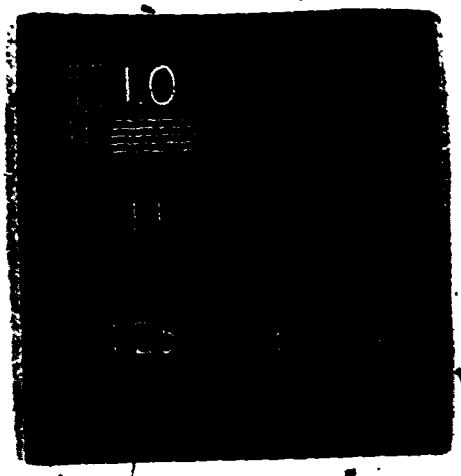

the development of radial streamers. However, the density of this charge close to onset may be not high enough to develop a steady glow so that burst pulses are formed for certain narrow regions of applied voltage close to the onset value. Above this voltage, the negative ion space charge density increases and a steady glow is formed between the surface of the corona wire and the negative ion space charge. Inside this glow region, electron avalanches take place resulting in electron and positive ion formation and one may get the well-known uniform ionized sheath of positive corona. Applying a still higher voltage, a situation will be reached at which the size of the avalanche inside the glow region increases to a critical limit at which a positive ion space charge column is formed leading to the recreation of a pulsating discharge again. However, the pulses in this case will be of greater amplitude and energy and the discharge is referred to as consisting of breakdown streamers leading to sparkover. One can see that the transition from corona to sparkover is governed by a critical field intensity and avalanche size inside the glow region.

(2) For Thick Corona Wires:

The electric field at the surface of the corona wire at the corona onset in this case is lower than in the previous case although sufficient to cause ionization. This field has a smaller gradient as can be seen from equation (61). In this case also electrons avalanche toward the wire and leave behind a positive ion space charge. This primary avalanche may be able to produce secondary avalanches due to its own photon radiation because the field in the neighbourhood is still high enough. Hence, an onset streamer may be formed as a matter of chance; i.e., sometimes burst pulses may be formed instead of the onset streamers. It all depends on the negative ion space charge density. High negative ion space charge chokes the streamer off.

Let us assume that onset streamers are formed. With an increase in the applied voltage, the pulseless glow may or may not be formed. If the diameter of the corona wire is large enough, onset streamers may lead directly to sparkover without the glow regime. This can occur if the negative ion space charge density is very small. On the other hand, for a smaller corona wire, with a further increase in the voltage, the glow may be formed and the onset streamers are apparently stopped by the negative ions. A further increase in the voltage may lead to sparkover in a similar way to the thin wires.

Note that the above description is based upon clean gas condition. The presence of particle space-charge alters the electric field distribution as described before. The reduction in the ionization field in the vicinity of the discharge electrode due to the positive space charge of the particles implies higher voltage to reach the critical field and avalanche size required for streamer formation and sparkover. In addition, if negative particle space charge is formed at the outer edge of the ionized sheath, then it will help to enlarge the glow regime and chok off the streamer propagation to the outer electrode. Therefore, one should expect that the sparkover voltage and the breakdown strength of the gap should increase as the particle concentration increases.

8.2.2 Negative Corona and Sparkover in Wire-Tube Geometry

When the onset voltage is reached in this case, a few discharge tufts first appear. Although each tuft has a noticeable pulsating nature (Trichel pulses), for a corona wire having many tufts, this pulsating nature may average out to a steady value. If the applied voltage is increased, Trichel pulse corona may change to a pulseless glow. This is because of the lower field between the negative wire and the negative ion space charge which results in a positive ion space charge build-up close to the wire causing a very high field region between it and the negative wire. With a further increase in the applied voltage, the concentration of the negative ions increases and the probability of electron attachment decreases. In other words, free electrons should be able to move longer distances in the gap. If the field at the outer electrode is enhanced enough by the negative ion space charge and a few electrons are formed close to this electrode by photo-radiation from the glow, a "retrograde" positive streamer may be formed which moves towards the negative wire and meets the negative streamer "feathers" bridging the gap. Therefore, one can see here that a primary factor for the sparkover is the creation of a positive streamer which is mainly dependent upon the critical field strength at the outer electrode.

There are three effects on the sparkover due to the particle space charge in this case:

(1) field enhancement at the outer electrode and hence the positive streamers initiated from this electrode can be triggered easier than without the charged particles. This effect should lead to a reduction in the sparkover voltage.

(2) suppression of the electron component of the total corona current close to sparkover and hence stabilize the discharge. This effect should lead to an increase in the sparkover voltage.

(3) field reduction in the ionization zone and this tends to require higher voltage to initiate negative streamers "Feathers". This effect should lead to a reduction in the sparkover voltage. Therefore, the net effect of the particle space charge should be dependent upon the relative significance of the above three effects in any particular case.

8.3 Results and discussion:

8.3.1 Effect of the corona wire diameter, polarity, and outer electrode geometry on the sparking characteristics with clean air

As mentioned in section (4.2), the earlier work of Cooperman[51] and Penney[50] showed that the positive corona has a higher sparkover voltage than the negative with clean air at room temperature in cylindrical geometry. However, the maximum pre-sparking corona current density is of primary significance in electrostatic precipitators for optimum collection efficiencies. As a result a special emphasis was given to it during this experimental work. The measurements of the sparkover voltage and the maximum pre-sparking corona current were obtained from the measurement of the (V-I) characteristics (i.e from the corona onset up to sparkover) and also from separate tests for these two values. The results indicated here are the average of at least four measurements. The values of sparkover voltage varied from the average by ± 1 kV and the values of the maximum pre-sparking corona current varied by ± 0.2 mA.

Figures (58) and (59) show the sparkover voltage for both positive and negative polarities using different sizes of corona wires in the wire-tube and wire-plate units respectively. These figures indicate higher positive

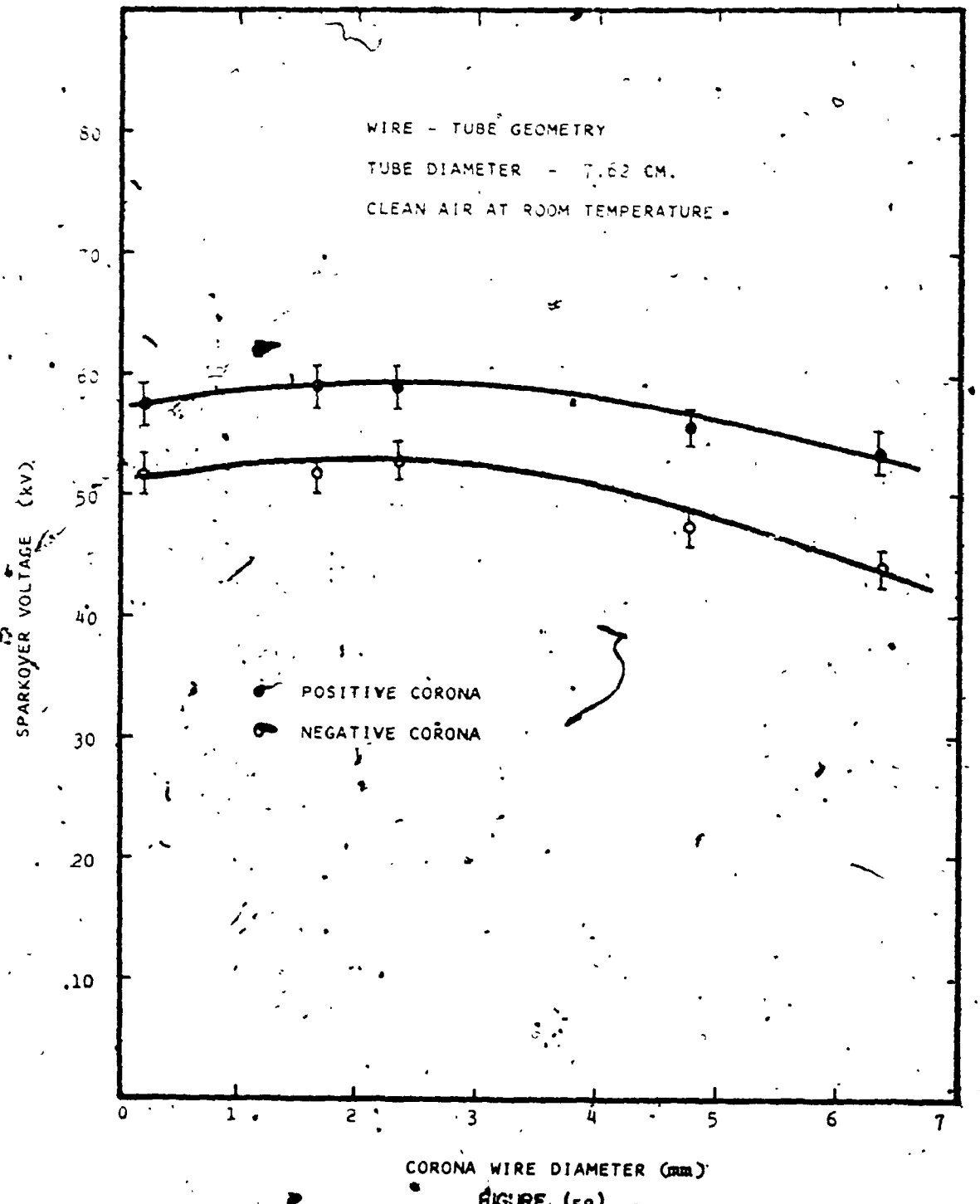
WIRE - TUBE GEOMETRY
TUBE DIAMETER - 7.62 CM.
CLEAN AIR AT ROOM TEMPERATURE
SPARKOVER VOLTAGE (kV)
80
70
60
50
40
30
20
10
0
1
2
3
4
5
6
7
POSITIVE CORONA
NEGATIVE CORONA
CORONA WIRE DIAMETER (mm)

FIGURE (58)

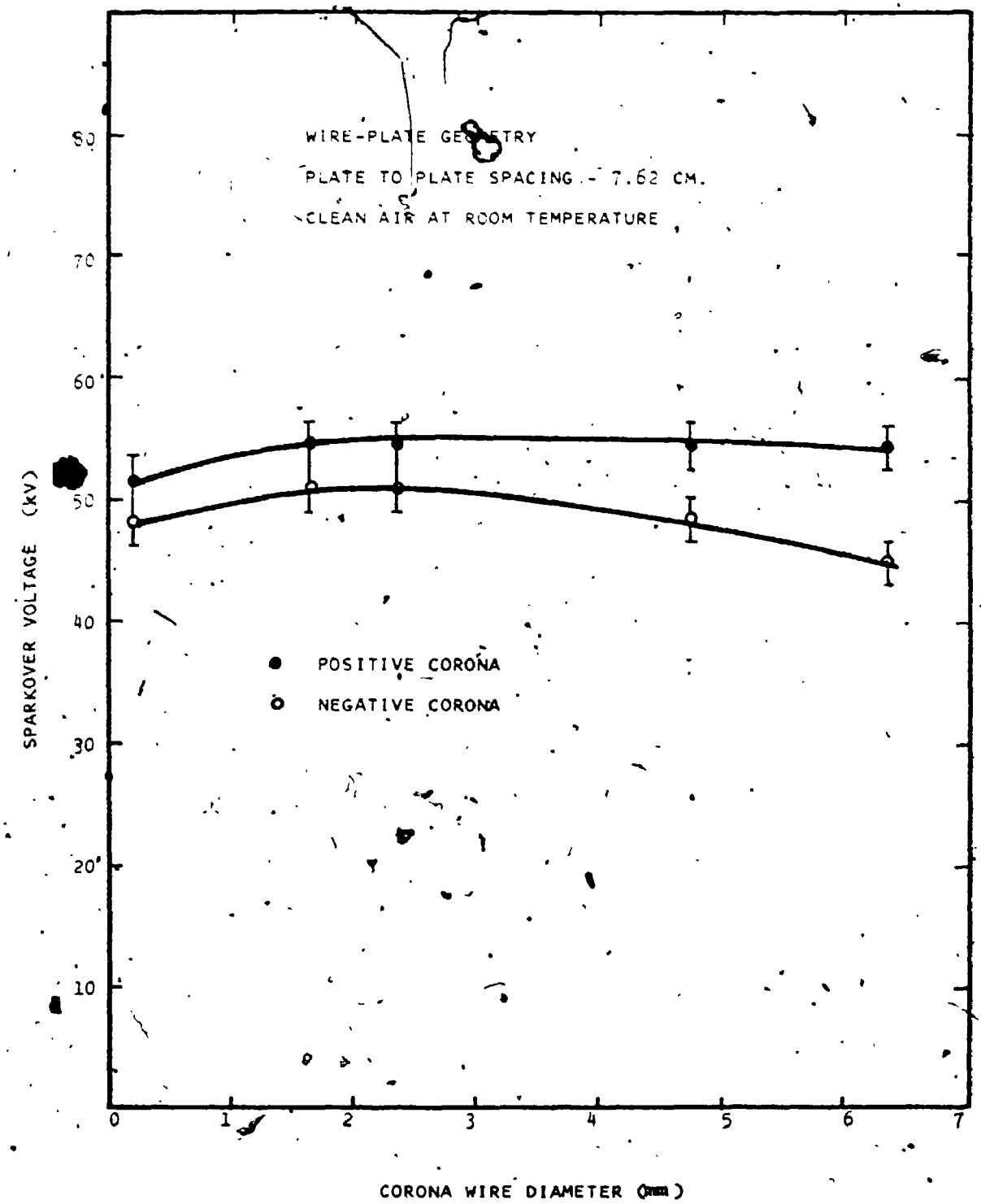
WIRE-PLATE GEOMETRY
PLATE TO PLATE SPACING - 7.62 CM.
CLEAN AIR AT ROOM TEMPERATURE
SPARKOVER VOLTAGE (kV)
80
70
60
50
40
30
20
10
0
1
2
3
4
5
6
7
POSITIVE CORONA
NEGATIVE CORONA
CORONA WIRE DIAMETER (mm)

FIGURE (59)

sparkover voltage than the negative for the size range of corona wire diameters tested. One of these wires had a diameter of 0.025 cm (0.010") the same as one of the wires used by Cooperman[51]. From Cooperman's results using this wire in a 4" cylinder, the sparkover voltages were 77 kV and 68 kV in the positive and negative corona respectively. Extrapolation of these results for a 3" cylinder the values obtained are 58 and 51 kV respectively. The corresponding values for this wire from the present experiments were 57.5 kV and 51.5 kV for the positive and negative cases respectively indicating excellent agreement.

The higher sparkover voltage under positive polarity than the negative in this case can be explained as follows: According to the streamer theory as described above, the positive corona changes to sparkover once the electric field and the avalanche size inside the sheath reaches a critical value to initiate positive streamers that are strong enough to cross the negative ion cloud around the sheath. On the other hand, the streamers initiated from the positive outer electrode in the negative corona require a lower critical field for their initiation than in the positive case because they are formed in the vicinity of much larger electrode and also they can cross the gap without the same resisting action as in the positive

case. The question arises as to how this is reconciled with the well known results at higher temperatures where the negative corona has demonstrated higher sparkover voltages (for example in electrostatic precipitators operating at approximately 200-300°F). Increasing the gas temperature results in a reduction in the relative gas density. In the positive corona, this reduction in the relative gas density results in smaller probability of attachment for the photo-electrons. Hence less negative ion space charge is formed around the wire and the breakdown streamers leading to sparkover are formed at lower voltages. In the negative case, the reduction of the relative gas density allows the electrons emanating from the ionization tufts to move longer distances in the gap before attachment i.e., an electron component appears and raises the corona current and reduces the sparkover voltage. Experience with industrial precipitators has shown that at the high temperatures and with the actual interelectrode spacing used in precipitators, the negative corona has higher sparkover voltage than the positive contrary to what has been indicated at room temperature. However, there are some doubts about the mechanisms here because of several other important parameters such as dust deposits on the corona wire surface, and deposits at the outer electrode with the possibility of back corona.

Figures (60) and (61) show the maximum presparking corona current as influenced by the corona wire diameter. One can see that there is a general trend. In the positive corona, as the corona wire diameter increases, the maximum presparking corona current decreases, whereas in the negative case it stays almost constant for the small corona wires up to a diameter of approximately 0.23 cm and then starts to decrease with the increase in diameter. This trend may be explained as follows. In positive corona the maximum presparking corona current is dependent upon the sparkover voltage and the diameter of the corona wire since the ionization electric field is the criterion for sparkover. In addition, it is known that for a fixed value of applied voltage, as the diameter of the corona wire increases the corona current decreases. Hence, the maximum presparking corona current decreases with the increase in diameter coupled with the corresponding variations in sparkover voltage as indicated in figures (58) and (59). In the negative corona however, the almost constant maximum presparking corona current for the smallest three corona wires used is evidence of the importance of the field at the outer electrode as a criterion for sparkover. Note that the field at this electrode is mainly dependent on the space charge and the

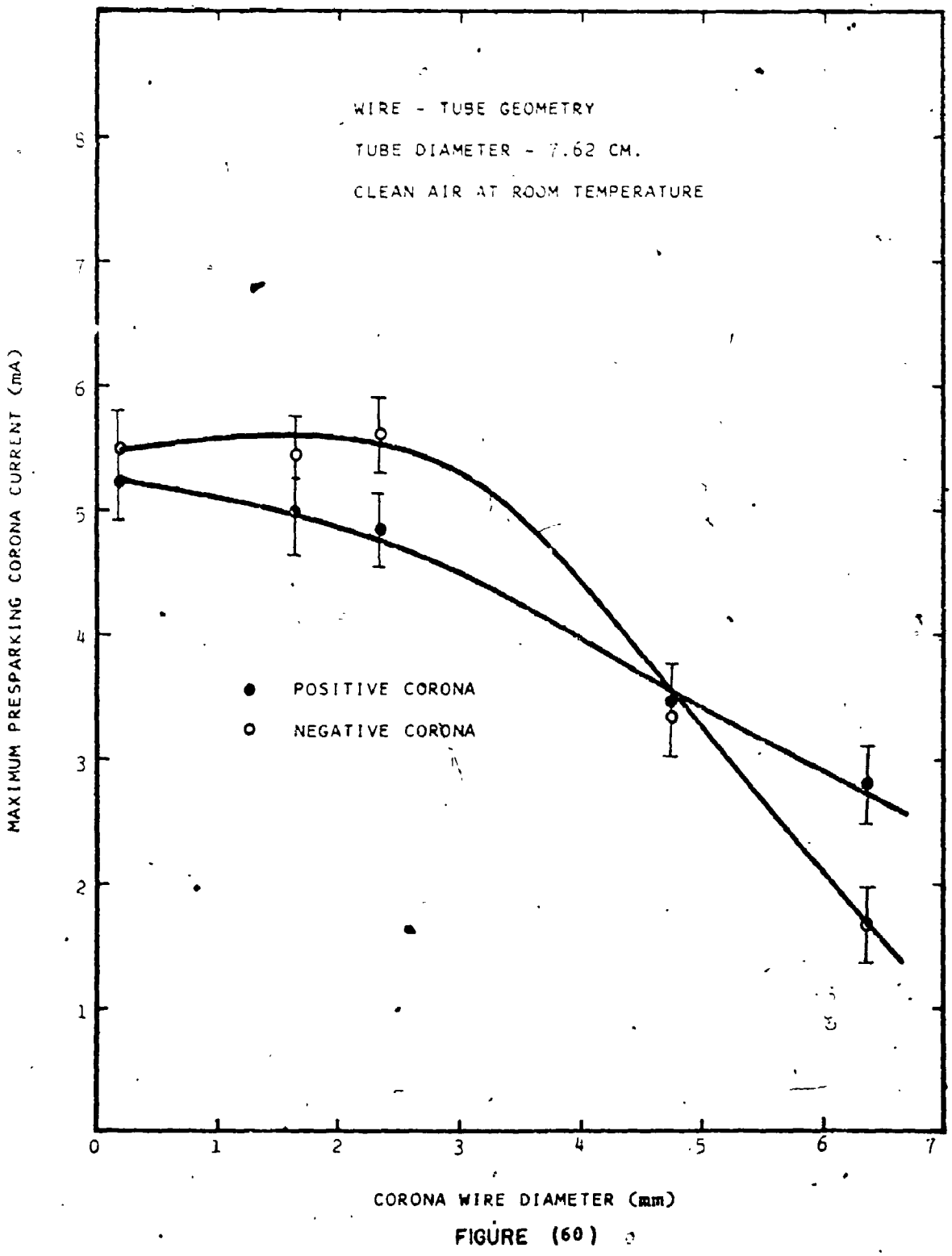
WIRE - TUBE GEOMETRY
TUBE DIAMETER - 7.62 CM.
CLEAN AIR AT ROOM TEMPERATURE
MAXIMUM PRESPARKING CORONA CURRENT (mA)
POSITIVE CORONA
NEGATIVE CORONA
CORONA WIRE DIAMETER (mm)
0
1
2
3
4
5
6
7
1
2
3
4
5
6
7
8

FIGURE (60)

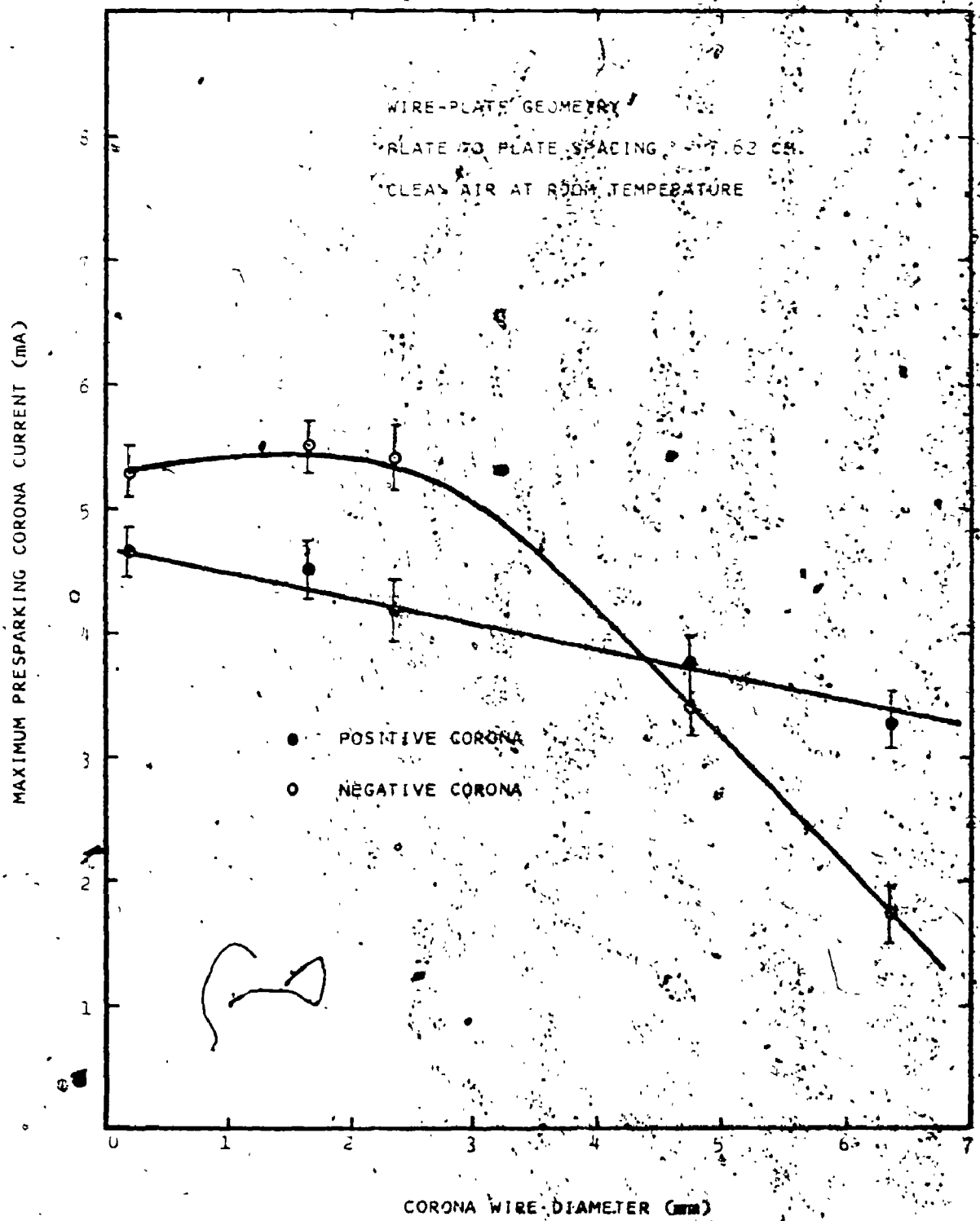
WIRE-PLATE GEOMETRY
PLATE TO PLATE SPACING = 7.62 CM.
CLEAN AIR AT ROOM TEMPERATURE
POSITIVE CORONA
NEGATIVE CORONA
MAXIMUM PRESPARKING CORONA CURRENT (mA)
CORONA WIRE DIAMETER (mm)
0
1
2
3
4
5
6
7

FIGURE (61)

corona current for this size range of wires where the electrostatic field component may be negligible. With a further increase in the corona wire diameter however, the electrostatic field component increases at the outer electrode and hence the space charge component and the maximum presparking corona current required to give a total field for triggering the breakdown streamers decreases.

8.3.2 Effect of the particle concentration on the sparking characteristics

As discussed in section (3.4.3), the build up of the particle space charge alters the electric field distribution in the gap between the two electrodes. Of primary importance are: the electric field enhancement at the outer electrode and the field reduction at the discharge electrode since they directly affect the sparking characteristics. In this section the results will be concentrated on the sparkover voltage and the maximum presparking corona current under conditions of corona quenching for both the tube and duct precipitators using different diameters of corona wires.

Figures (62) to (65) show the sparkover voltage as influenced by the inlet specific surface area of the suspended materials for different corona wire diameters under negative and positive polarities in tube and duct

FIGURE (62) WIRE-TUBE PRECIPITATOR (NEGATIVE CORONA)

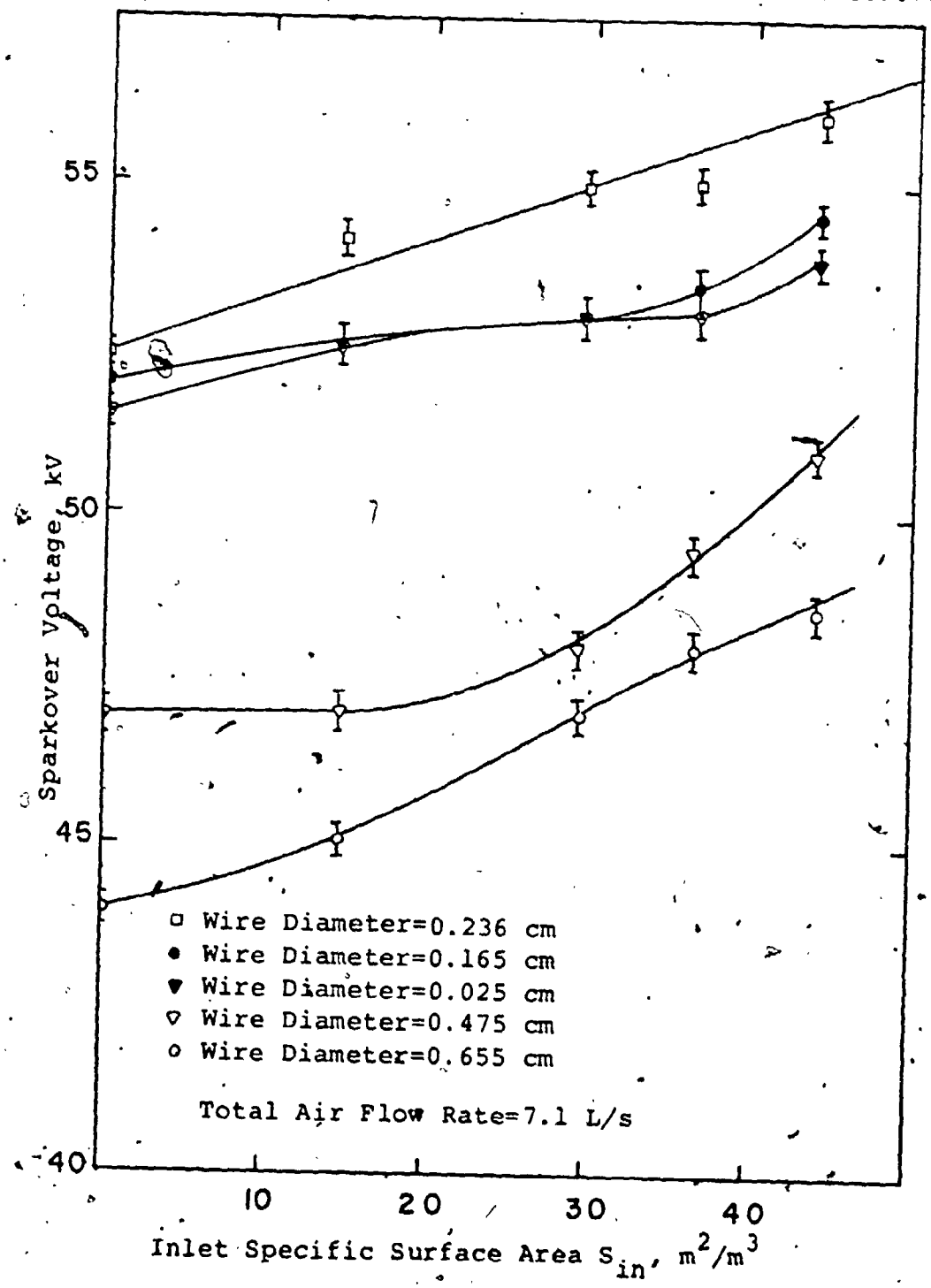

FIGURE (63) WIRE-TUBE PRECIPITATOR (POSITIVE CORONA)

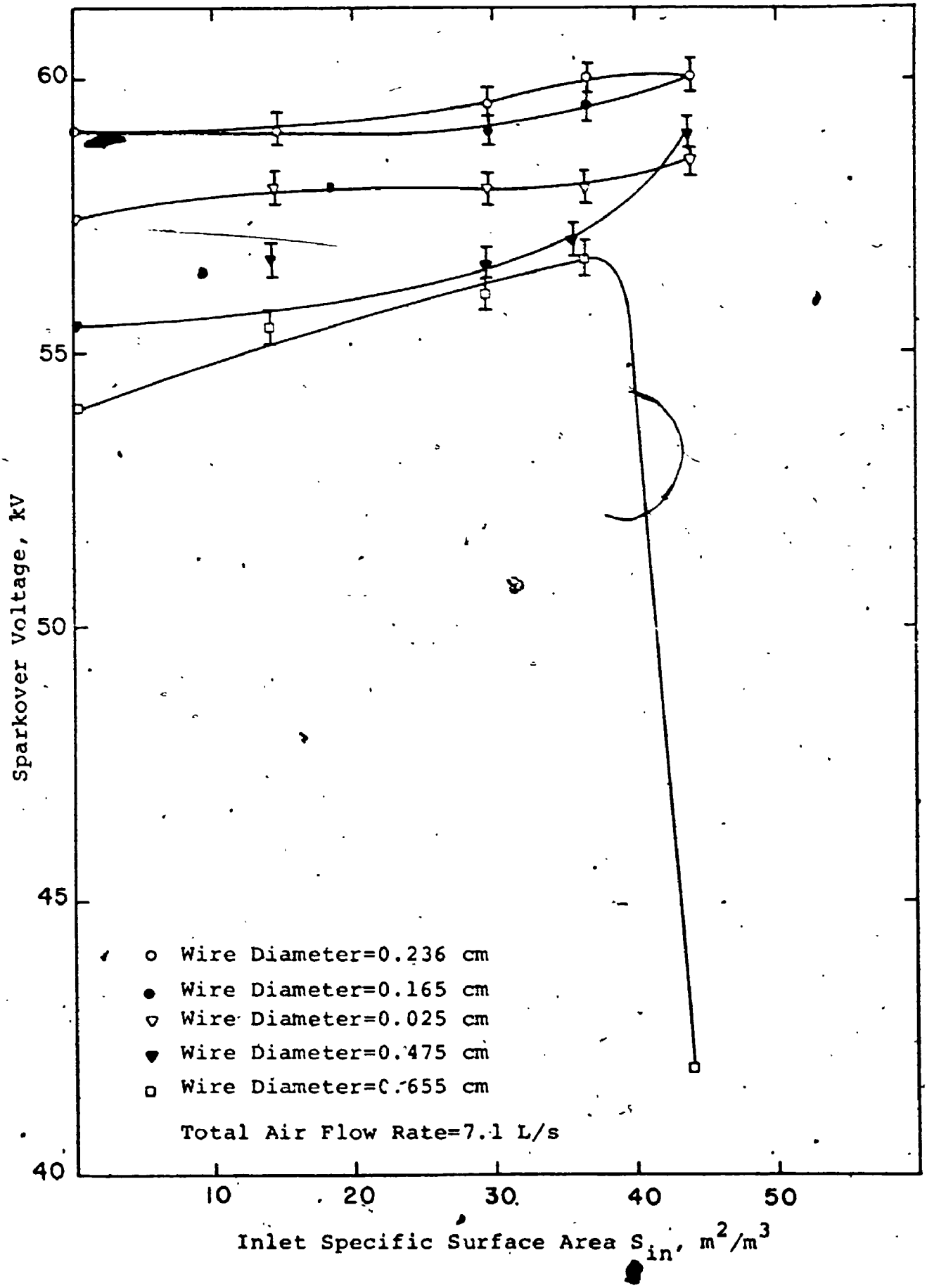

FIGURE (64) DUCT PRECIPITATOR (NEGATIVE CORONA)

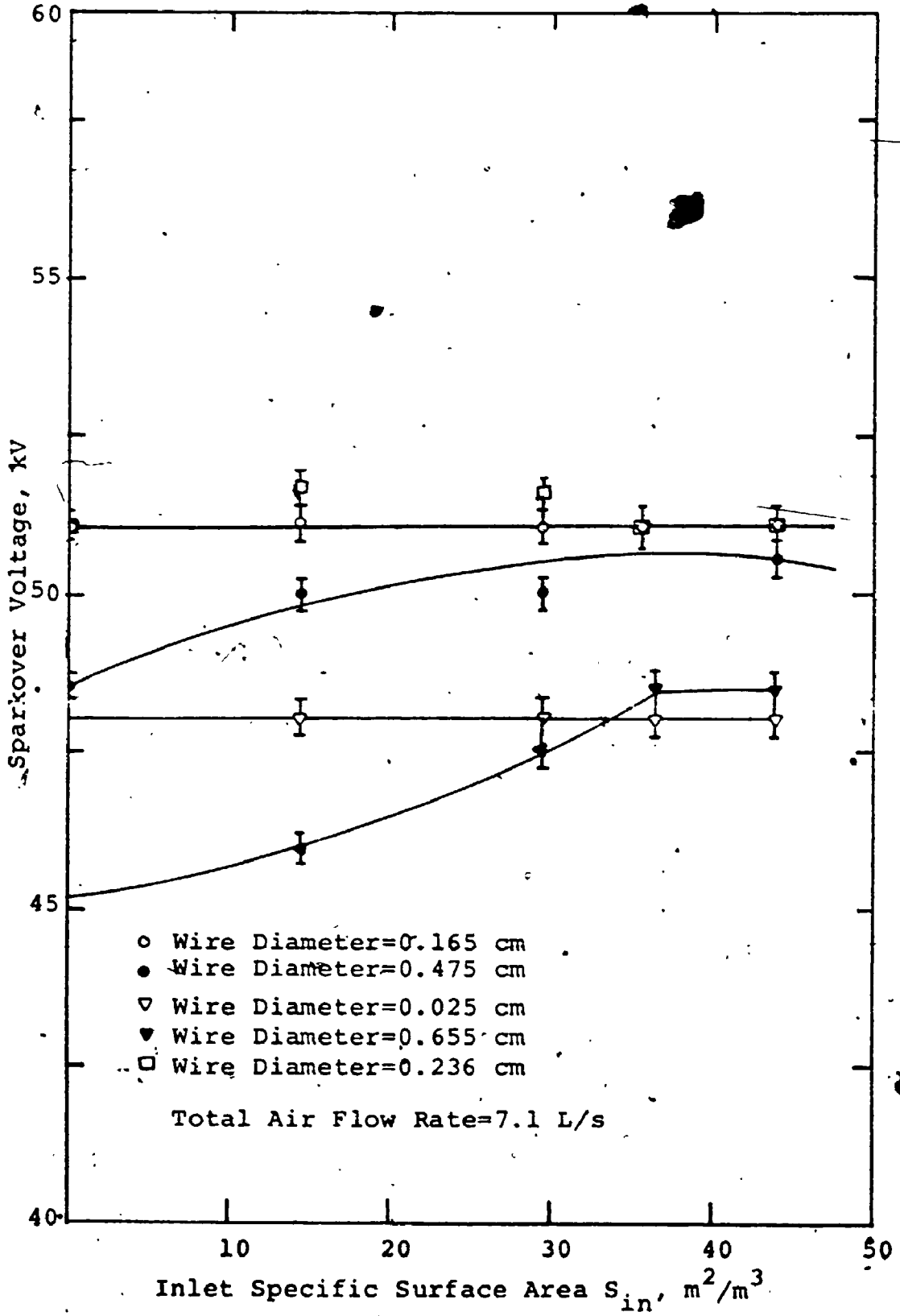

FIGURE (65) DUCT PRECIPITATOR (POSITIVE CORONA)

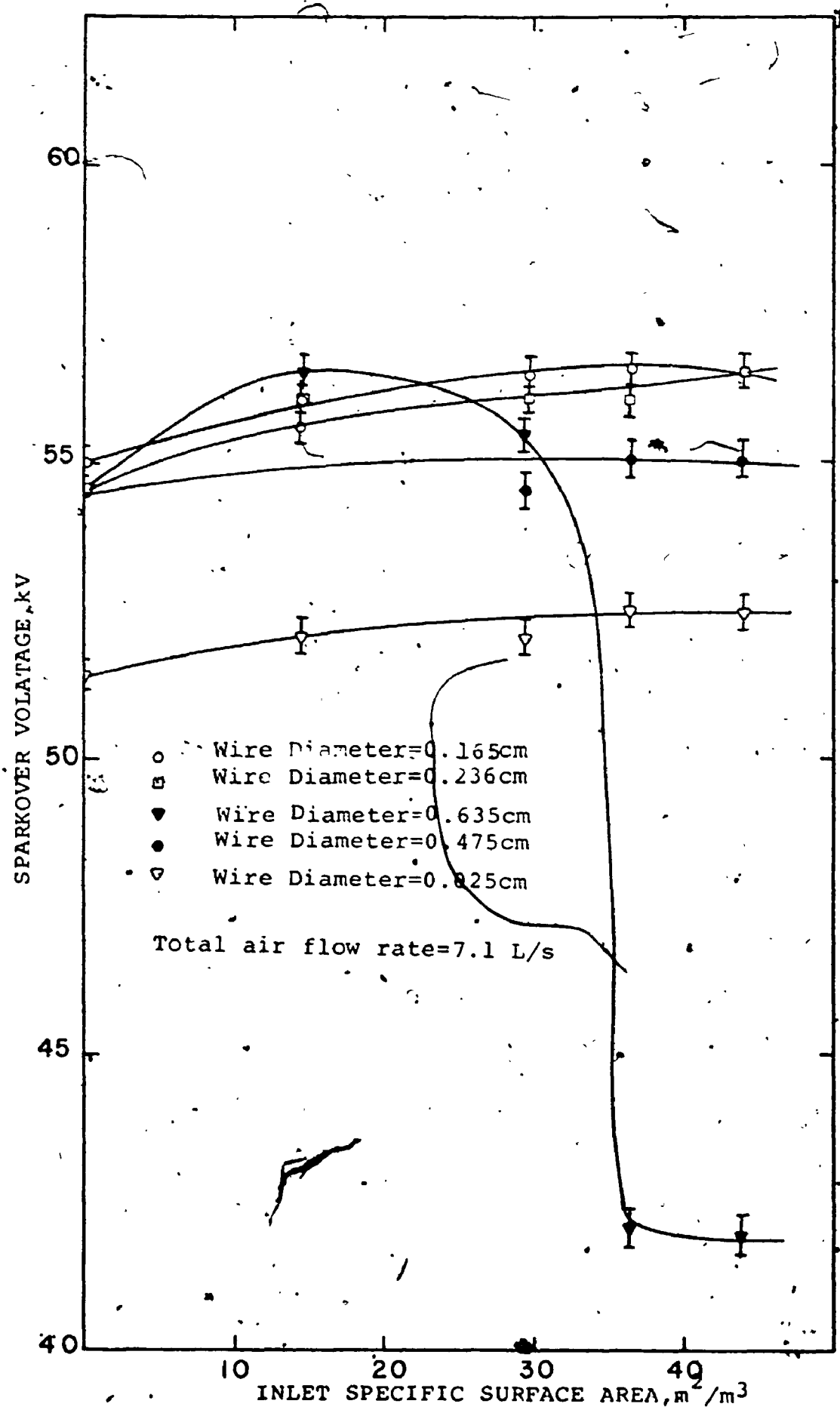

precipitators. From these figures one can see:

(1) For Negative Corona:

In the tube precipitator, as the inlet specific surface area increases the sparkover voltage slightly increases for the three smallest corona wires of diameters 0.025 cm (0.010"), 0.165 cm (0.065"), and 0.236 cm (0.093"). A larger increase in the sparkover voltage was obtained with the two biggest corona wires of diameters 0.475 cm (0.187") and 0.635 cm (0.25"). In the duct precipitator, the sparkover voltage stays almost constant with the increase in the inlet specific surface area for the three smallest corona wires of diameters 0.010", 0.065" and 0.093". A slight increase was obtained for the two largest corona wires of diameters 0.187" and 0.25". One can see that the trend is towards increasing the sparkover voltage with the increase in the specific surface area. However, since sparkover is a localized phenomenon that occurs at the point of the lowest breakdown strength and because of the very high efficiencies involved near sparkover and the presence of a zone of very low particle concentration, it is likely that the sparkover occurs at these sections. The two largest corona wires used had the lowest maximum pre-sparking corona current with clean air and the lowest collection efficiencies and therefore,

they showed larger increase in the sparkover voltage with the increase in the inlet specific surface area than the three smallest corona wires. For the same inlet specific surface area, as the collection efficiency decreases the specific surface area at the exit section increases and particle space charge effects will be more pronounced leading to greater increases in the sparkover voltage. Therefore, for example, if one used a cylindrical precipitator so that 99.99% of the particles are collected on a small portion at the entrance of the precipitator leaving the rest of it almost free from particles, the sparkover voltage should be almost the same as with clean air. Sectionalizing of a large precipitator such that each section is operated at its optimum sparkover level, is thus appreciably affected by the particle concentration in each section.

The increase in sparkover voltage due to the particle space charge effect in this case may be explained as follows: The positive streamers initiated from the outer electrode propagate towards the corona wire and meets with the negative streamers ("Feathers") bridging the gap. The particle space charge enchances the field at the outer electrode thus tending to reduce the sparkover voltage. The field at the outer electrode is a main factor but

there are other factors such as the creation of electrons near the outer electrode aided by the photo electric energy from the glow. The capture of these electrons by the particles may stabilize the discharge and hence increase the voltage required to trigger the sparkover. Therefore, these experimental results confirm that quenching of the free electron component is an important factor that results in increasing the sparkover. This may be compared in a similar way to the case of increasing the electronegativity of the gas and the suppression of free electrons and the increase in sparkover voltage[3].

(2) For Positive Corona:

The same trend can be observed in figures (63) and (65) for this case, similar to the negative corona i.e a slight increase in the sparkover voltage for the smallest three corona wires and larger increase in the case of the bigger wire of diameter 0.187" due to the lower collection efficiency. In these cases the slight increase in the sparkover voltage due to the particle space charge effect may be explained as follows:

The breakdown streamers triggering the sparkover are initiated from the ionization sheath around the corona wire and are governed by a critical field near the wire. The particle space charge reduces the field in

this region and hence increases the voltage required to cause sparkover.

For the special case of the biggest corona wire of diameter 0.635×10^{-2} m (0.25"), at the highest inlet specific surface area of 44 m^2/m^3 the sparkover voltage was drastically reduced. In this case the onset streamers produced were so strong that they caused complete sparkover. As mentioned in section (7.3.2), this is due to the decrease in the electric field at the corona wire surface which is equivalent to using a larger wire diameter wire than 0.25" in which case no corona regime can be obtained with the existing interelectrode spacing before sparkover. In other words the ratio (b/a) for the equivalent larger size will become close to 3 where corona can not be obtained before sparkover.

To check the idea that the collection efficiency through its effect on the particle concentration at the exit section may affect the sparkover voltage, experiments were made to reduce the collection efficiency by increasing the total air flow rate keeping the specific surface area of the particles at the input of the precipitator fixed. Figures (66) and (67) show the sparkover voltage versus the total air flow rate at fixed inlet specific surface area for both polarities and both geometries. These graphs show that with the reduction in the collection

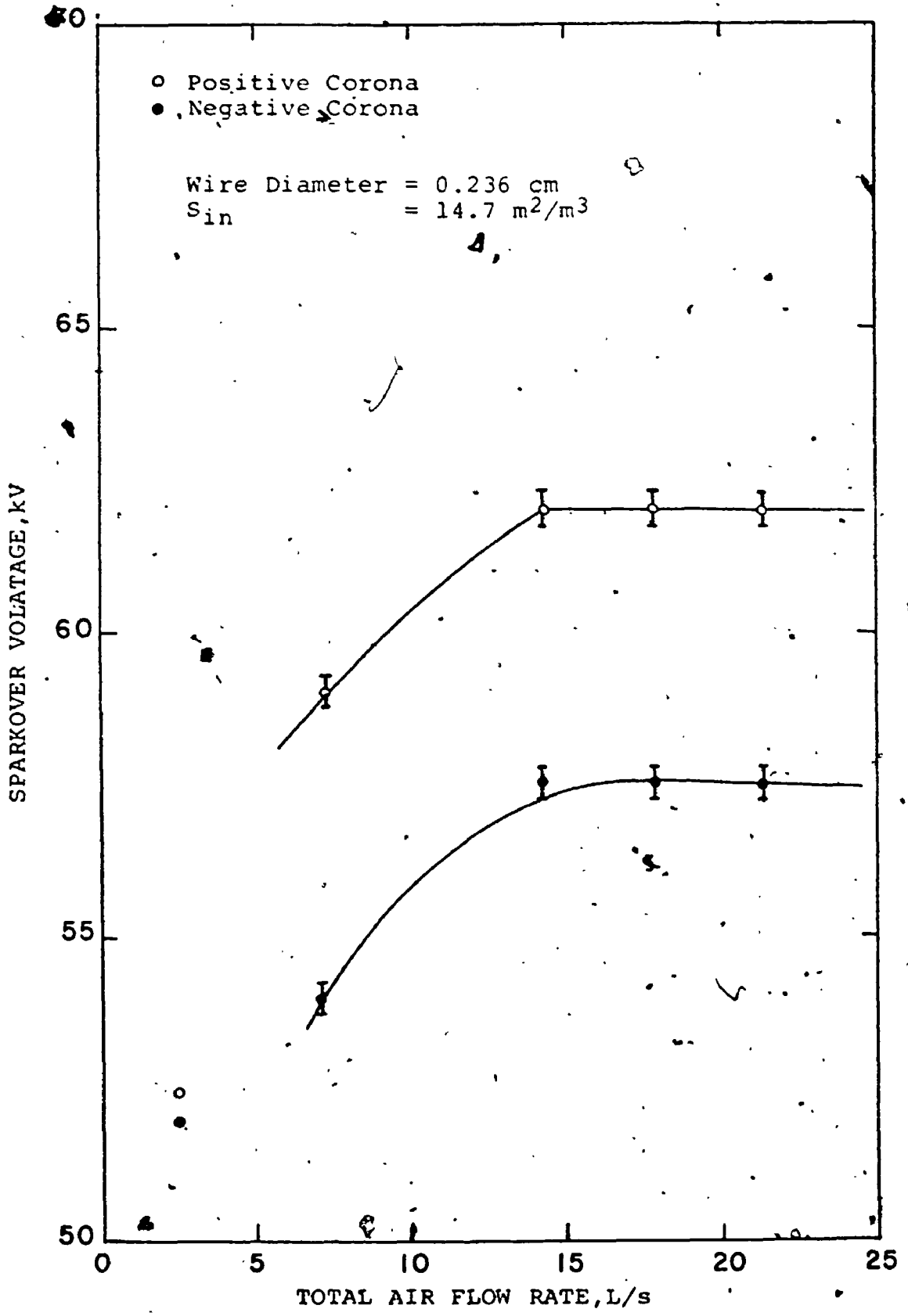

FIGURE(66) SPARKOVER VOLTAGE vs. TOTAL AIR FLOW RATE IN WIRE-TUBE PRECIPITATOR

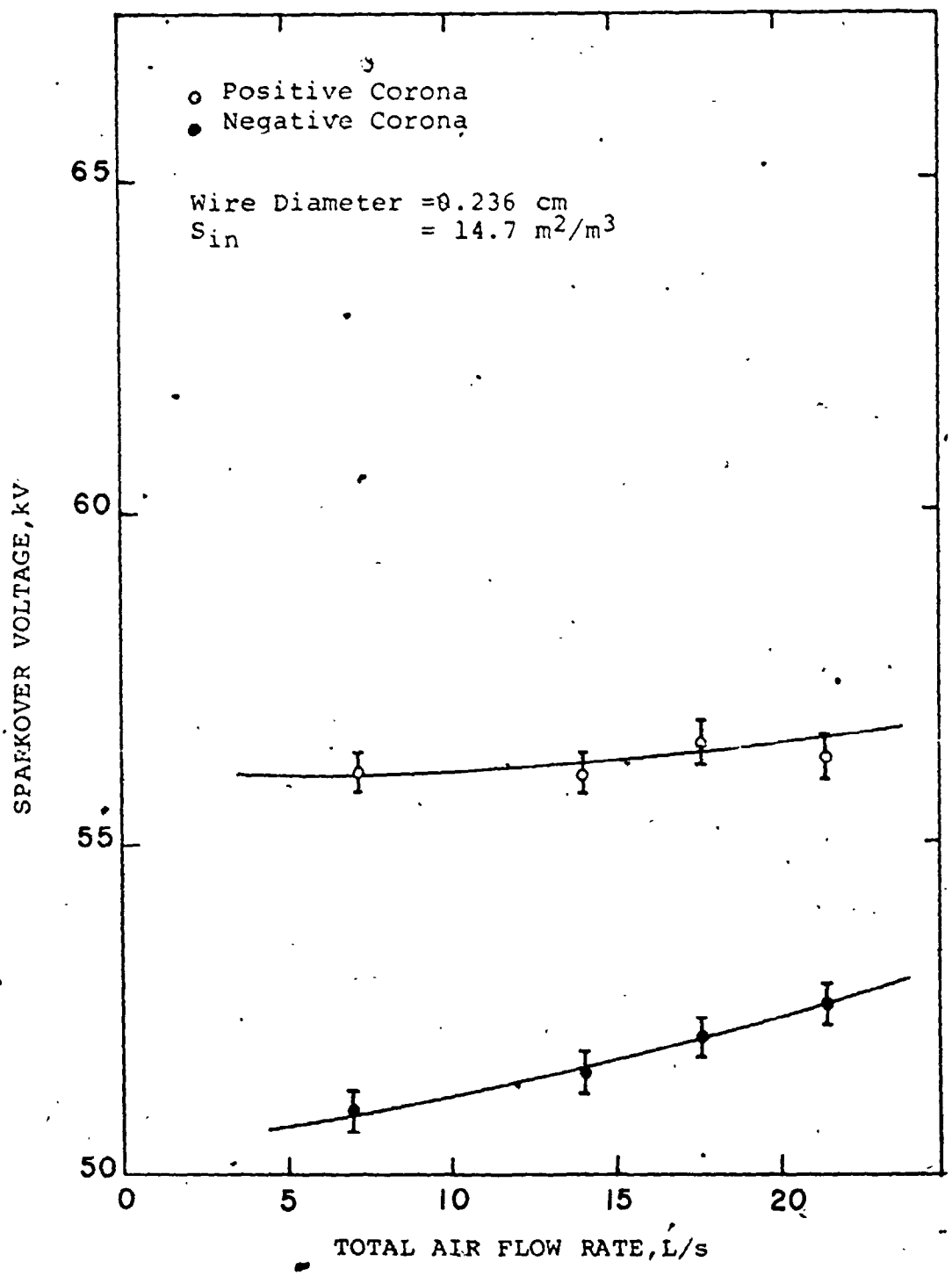

FIGURE(67) SPARKOVER VOLTAGE vs. TOTAL AIR FLOW RATE IN DUCT PRECIPITATOR

efficiency the sparkover voltage increases. The maximum increases in the sparkover voltage were 3.5 kV under the negative corona and 3 kV under the positive.

Figures (68) to (71) show the maximum pre-sparking corona current as affected by the inlet specific surface area S_{in}. From these figures note:

(1) Effect of the inlet specific surface area: As the inlet specific surface area increases, I_{max} decreases. The increase in the sparkover voltage due to the particle space charge does not compensate for the reduction in the corona current at fixed value of applied voltage.

(2) Effect of the corona wire diameter:

The results show that for the same inlet specific surface area, as the corona wire diameter decreases, I_{max} increases for both polarities in both geometries. The effect is relatively small for corona wire diameters less than 0.093". On the other hand, the effect appears appreciable for diameters larger than 0.093".

(3) Effect of polarity:

For the tube precipitator, the negative polarity gives higher values for I_{max} than the positive for the smallest three corona wires used. The reverse is true for the largest two corona wires.

For the duct precipitator, the negative polarity

FIGURE (68) WIRE-TUBE-PRECIPITATOR (NEGATIVE CORONA)

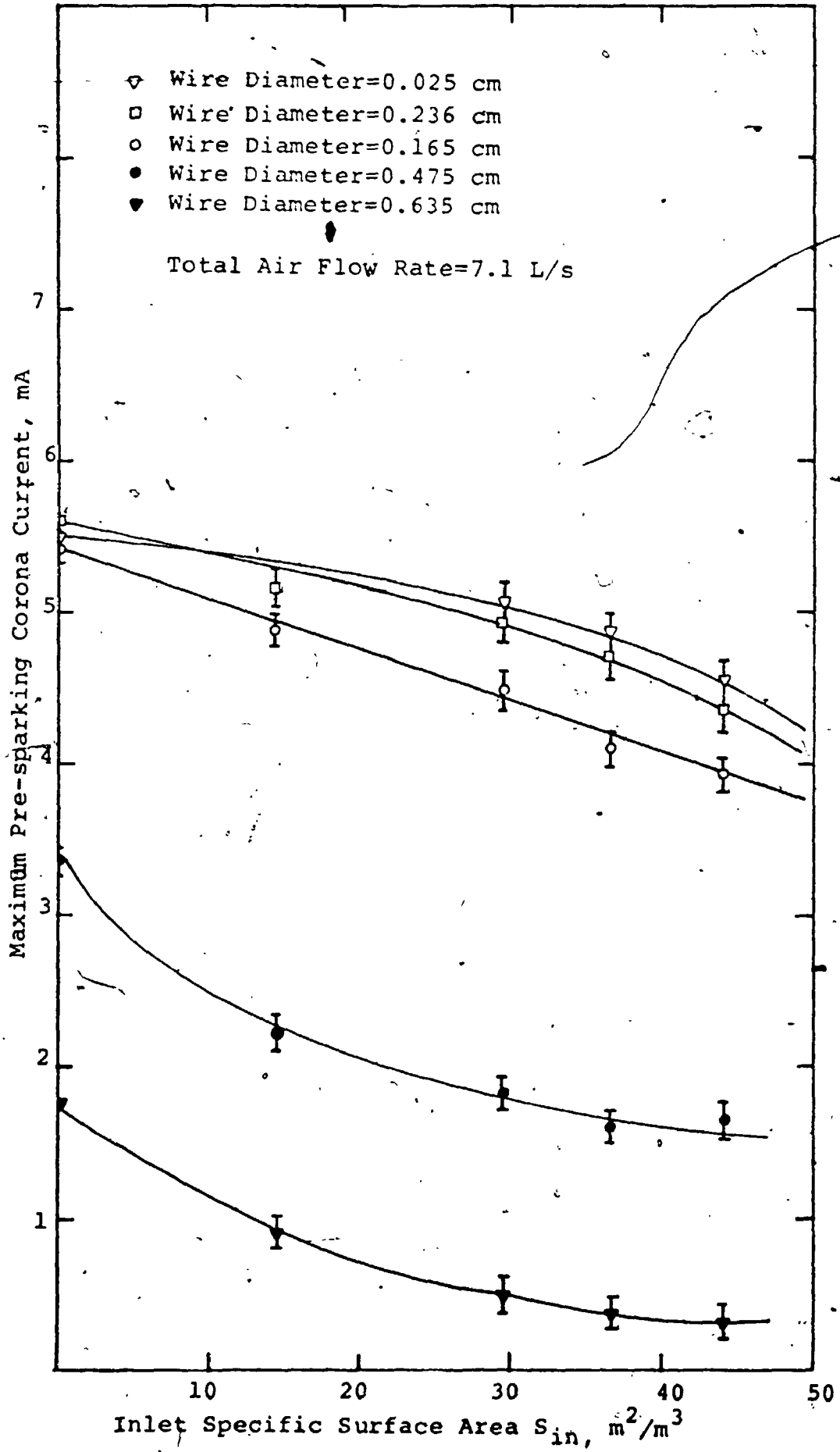

FIGURE (69) WIRE-TUBE PRECIPITATOR (POSITIVE CORONA)

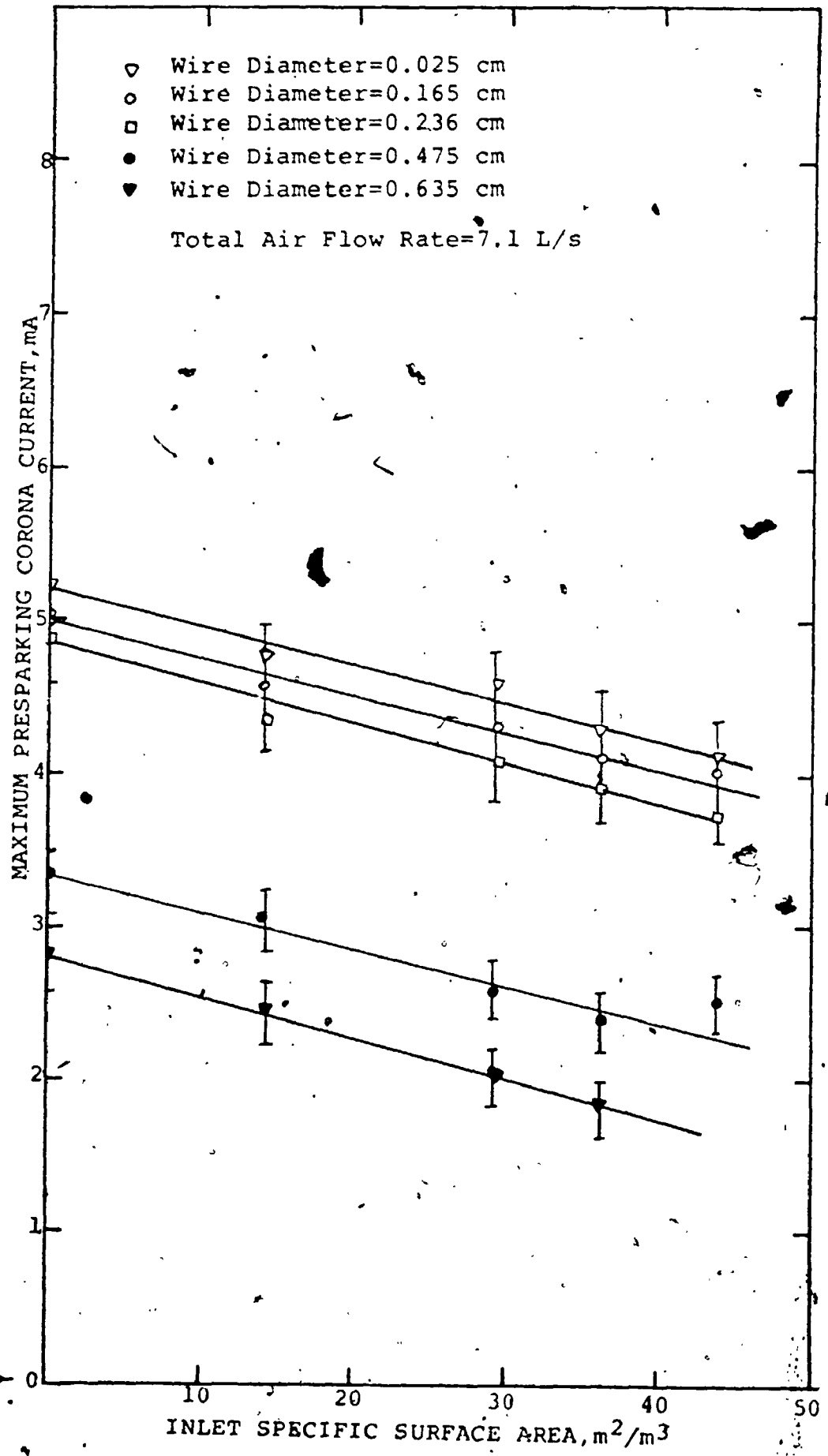

FIGURE (70) DUCT PRECIPITATOR (NEGATIVE CORONA)

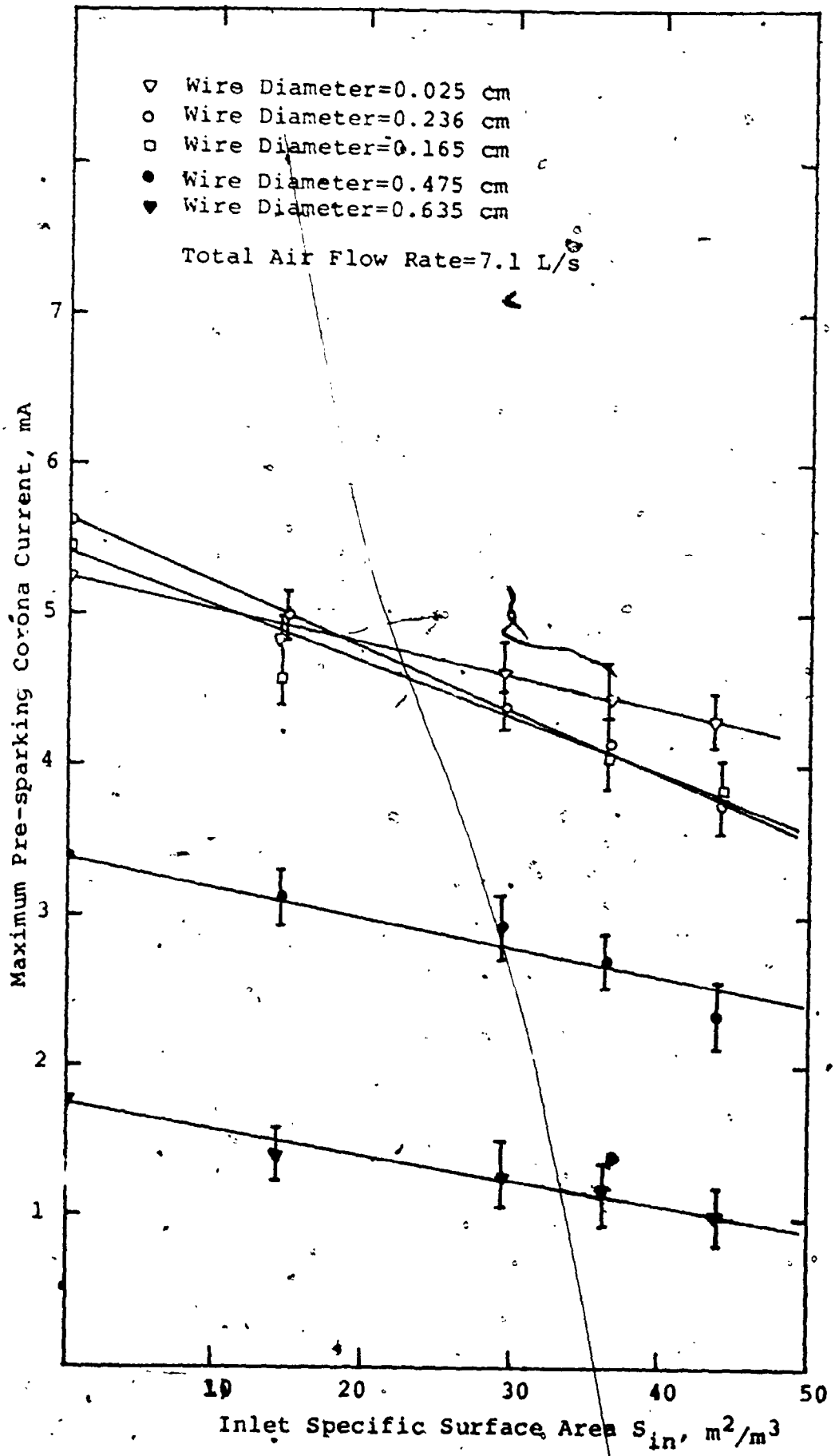

FIGURE (71) DUCT PRECIPITATOR (POSITIVE CORONA)

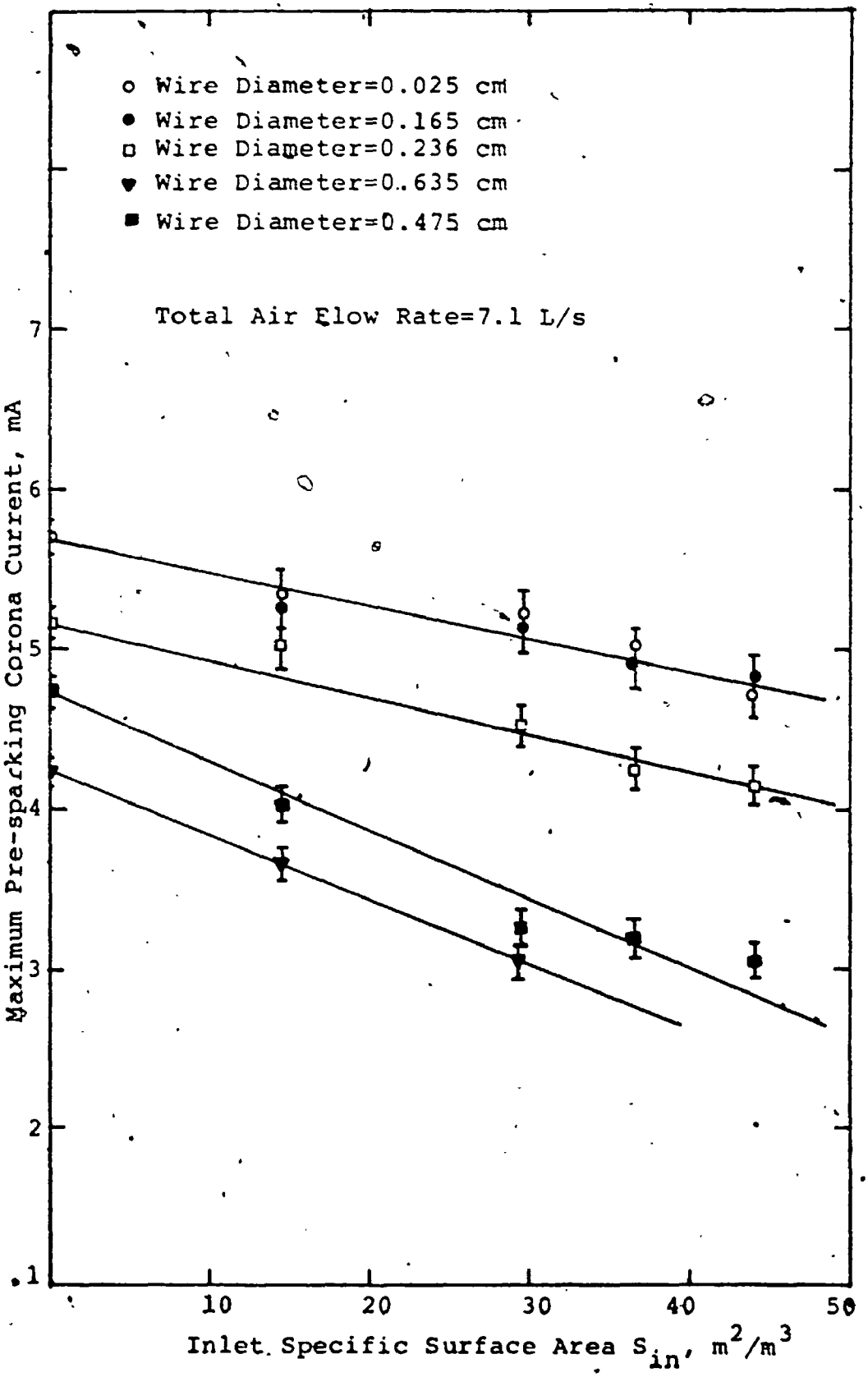

gives also higher values for I_{max} than the positive for the smallest four corona wires used. The reverse is true for the largest corona wire.

It is interesting to mention that on a larger scale precipitator, Tassicker[63] confirmed that higher sparkover voltages can be obtained with increasing the particle space charge density.

CHAPTER IX

Corona quenching and the sparkover phenomena with heated corona wire

9.1 General

The experimental results and their interpretation for the corona quenching and sparkover were presented in Chapters (7) and (8). It was shown that the electric field inside the ionized sheath affects the ionization rate and both of these phenomena. However, this ionization rate is also dependent upon the gas density in the vicinity of the corona wire. Therefore, a parameter that was believed to affect both of these phenomena was based upon heating the corona wire at the center of the wire-tube corona apparatus while keeping the gas flowing and the outer electrode practically at the room temperature.

9.2 Theory

By heating the corona wire to a temperature above the gas in which it is immersed, a temperature gradient is established across the ionized sheath with an average value T_{av}. The relative gas density inside this sheath is then reduced according to the relation:

$$\delta = (T_o/T_{av})$$

at constant pressure. There are two effects on the corona (V-I) characteristic due to this reduction in the average gas density in the ionized sheath under clean gas condition:

(1) The critical field intensity at the surface of the corona wire required for the corona onset is given by Peek's formula:

$$E_o = (300\ \delta + 9\sqrt{(\delta/a)}\ ) \times 10^4 \quad V/m$$

and the corona onset voltage for a cylindrical precipitator is given by:

$$V_o = aE_o \ln(b/a)$$

Therefore, as the relative gas density δ decreases, E_o decreases and the corona onset voltage decreases.

(2) The first Townsend's ionization coefficient α is known to be dependent on the electric field intensity and the relative gas density inside the ionized sheath. By reducing the relative gas density, the ionizing mean-free path of the electrons in the field decreases and hence the first Townsend's ionization coefficient α increases. This increase in α results in higher corona current with heating the corona wire than without heating at fixed value of applied voltage. See figure (2).

The above two effects will result in a shift in the (V-I) characteristic to the left, from position (1) to position (2), as in figure (72) [27].

As shown in section (7.3.1), the presence of certain particle concentration in the gas results in an apparent increase in the corona onset voltage, a reduction in the corona current at fixed value of applied voltage, and a shift in the (V-I) characteristic of the right from position (1) to position (3). So, it appears that heating the corona wire has an opposite effect on the (V-I) characteristic to that of the corona quenching. The question that arises is whether heating the corona wire under conditions of corona quenching can shift the (V-I) characteristic of position (3) to the left and compensate for the corona quenching effect, and to what extent?

Since a main factor that contributes to the corona quenching phenomenon is due to the reduction in the ionization field (and α) and the lower rate of current generation from the ionized sheath, then the increase in α due to the reduction in the relative gas density may compensate for the corona quenching effect. The extent of this compensation should be, of course, dependent on the particle concentration, coupled with the heating power to

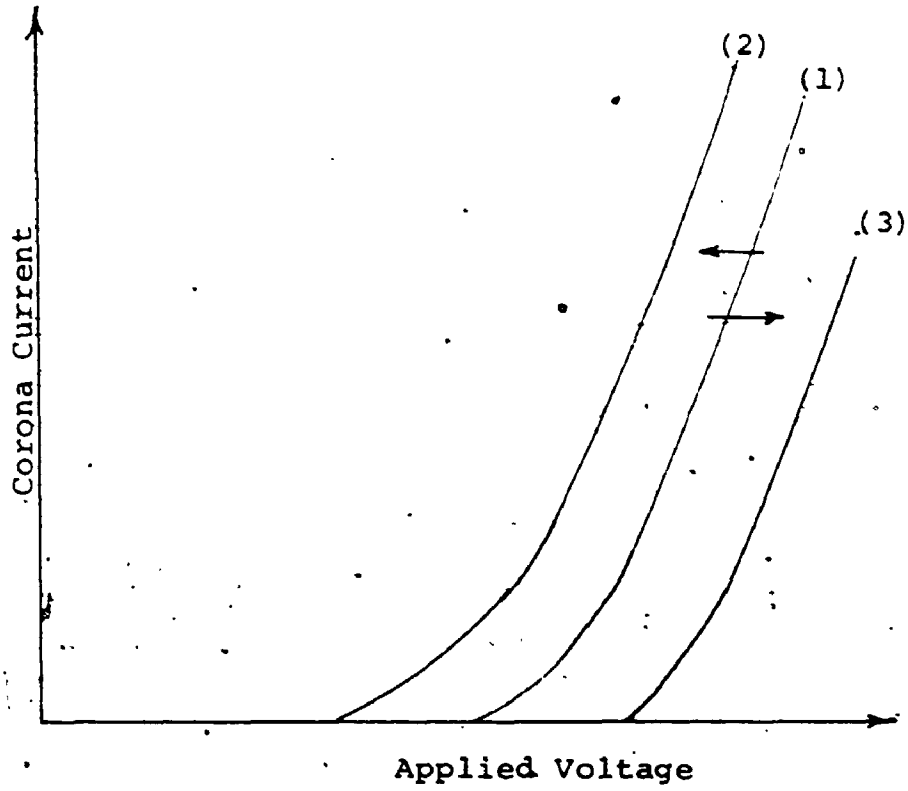

FIGURE (72) CORONA (V-I) CHARACTERISTIC

Curve (1) Clean Gas
Curve (2) Clean Gas With Heating The Corona Wire
Curve (3) Gas With Suspended Material

the corona wire and thus the increase in temperature inside the ionized sheath.

With regard to the collection efficiency under conditions of corona quenching as affected by heating the corona wire at fixed value of applied voltage, the following factors may be considered:

(1) As the heating power to the corona wire increases the corona current increases at fixed value of applied voltage and fixed inlet specific surface area. Since the electric field in the passive zone close to the outer electrode is mainly dependent on the corona current, then as the heating power to the corona wire increases the collection field increases.

(2) Since we are considering this heating effect at fixed total applied voltage, then the increase in the field in the outer region close to the collecting electrode is accompanied by a reduction in the field in a portion of the gap close to the corona wire so that

$$\int_a^b E \, dr = \text{Applied voltage}$$

In other words, the field distribution with and without heating the corona wire at fixed value of applied voltage may have the general trend shown in figure (73). The charge acquired by a particle is dependent upon the electric field prevailing in the gap and the ion space

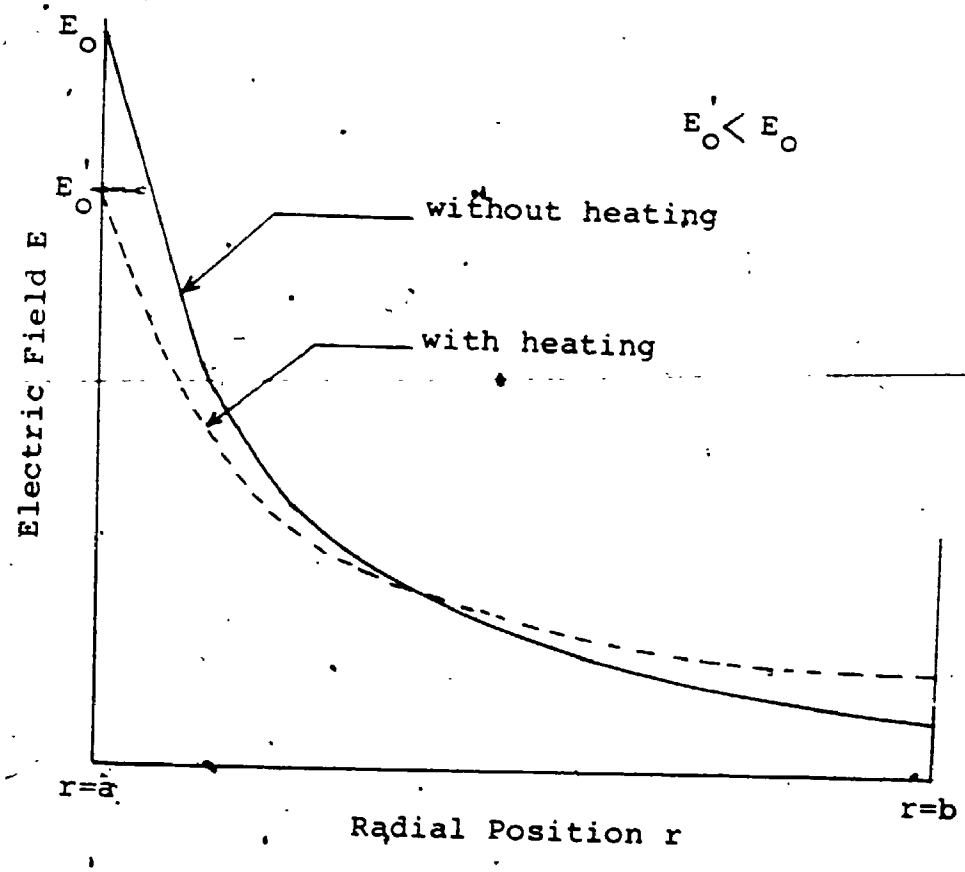

FIGURE (73) GENERAL TREND OF THE FIELD DISTRIBUTION WITH AND WITHOUT HEATING THE CORONA WIRE AT FIXED APPLIED VOLTAGE

charge density. Therefore, under this new electric field distribution with heated corona wire, the charge acquired by a particle may be different from the value obtained by the same particle without heating the corona wire.

(3) As the relative gas density in the vicinity of the negative corona wire decreases, electrons emanating from the ionized tufts can move longer distance before they become attached to form negative ions. Under the presence of suspended particles, these electrons may attach to the particles and participate in particle charging instead of forming negative ions. Note that the electrons are known to be more capable of charging than the negative ions because of their very high mobility.

In short, heating the corona wire at fixed value of applied voltage, although it increases the corona current, may or may not imply an increase in the collection efficiency.

Another part of the study of heating the corona wire was devoted to its effect on the sparking characteristics. As has been proposed in section (8.2) in the positive corona, the triggering of the breakdown streamers originates in the ionized sheath and is dependent upon the negative ion space charge density. As the heating power to the corona wire increases, the relative gas density in the vicinity of the corona wire decreases,

the electron attachment decreases and the negative ion space charge density decreases. With this decrease in the negative ion space charge density the probability of developing the breakdown streamers increases. Thus a reduction in the sparkover voltage and the maximum presparking corona current is anticipated with heating the corona wire in this positive case. In the negative corona however, the breakdown streamers are initiated from the outer electrode and hence one may expect negligible effect on the sparking characteristics due to heating the corona wire.

9.3 Results and discussion

9.3.1 Effect of heating the corona wire on the corona quenching characteristics

Two corona wires of diameters 0.165×10^{-2} m (0.065") and 0.235×10^{-2} m (0.093") were electricaly heated and used in the cylindrical corona apparatus. The heating circuit for the corona wire was as described in section (5.8). The (V-I) characteristics were measured with and without the presence of suspended particles of different concentrations. Figures (74) and (75) for positive and negative corona respectively show the (V-I) characteristic with and without heating the corona wire under the presence of the highest particle concentration used, (specific

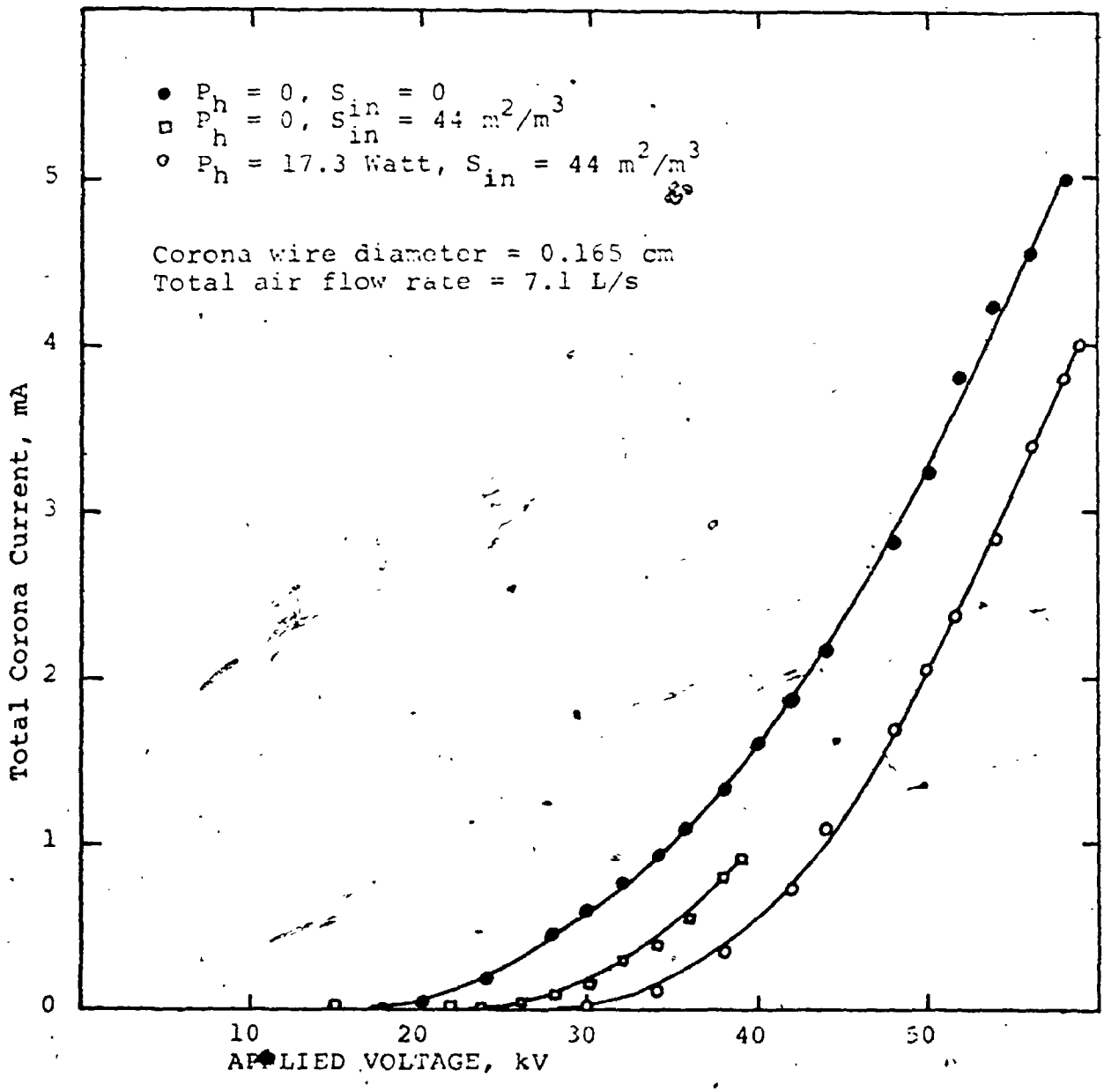

FIGURE (74) POSITIVE CORONA VOLTAGE CURRENT CHARACTERISTIC WITH AND WITHOUT HEATING THE CORONA WIRE

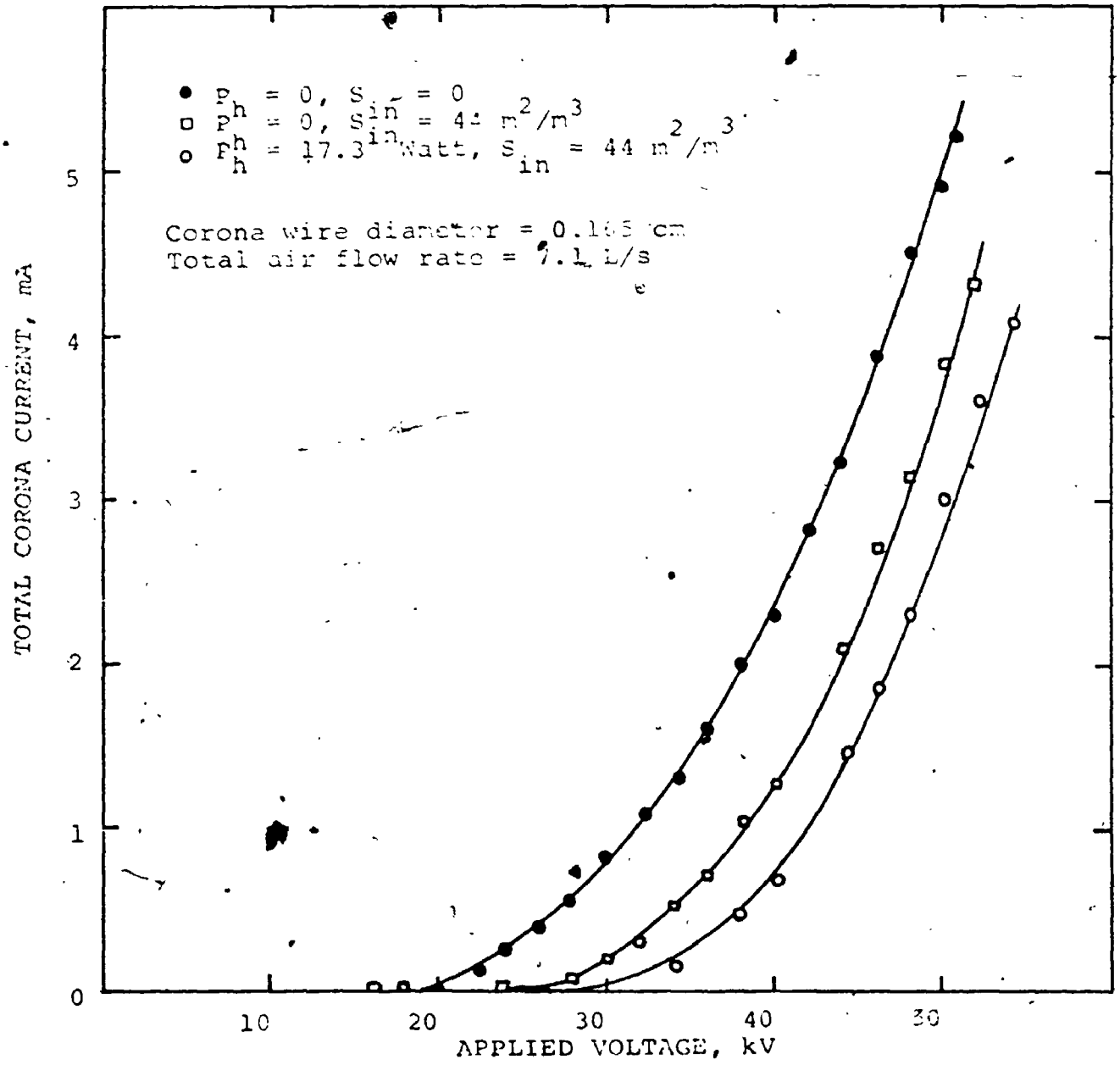

FIGURE (75) NEGATIVE CORONA VOLTAGE CURRENT CHARACTERISTIC WITH AND WITHOUT HEATING THE CORONA WIRE

ourface area of 44 m^2/m^3) compared with the original (V-I) characteristic with no particles and no heating. These figures show that, as the corona wire was heated and the temperature was increased inside the ionized sheath, in the presence of particles:

(1) The corona onset voltage decreased to a value even less than the corona onset voltage with clean air and no corona wire heating.

(2) At fixed value of applied voltage the corona current increased but did not completely compensate for the corona quenching of this particle concentration.

(3) The sparkover voltage and the maximum pre-sparking corona current were drastically reduced in the positive corona whereas in the negative case, these values are slightly affected. This will be explained in section (9.3.3) of this Chapter.

Similar trends were obtained using the other corona wire under all particle concentrations used.

Figure (76) shows the corona onset voltage versus the inlet specific surface area with and without heating for the positive and negative corona respectively. From this figure one can observe that at any of the particle concentrations used, the heating power to the corona wire and the corresponding rise in temperature inside the ionized sheath were more than sufficient to offset the

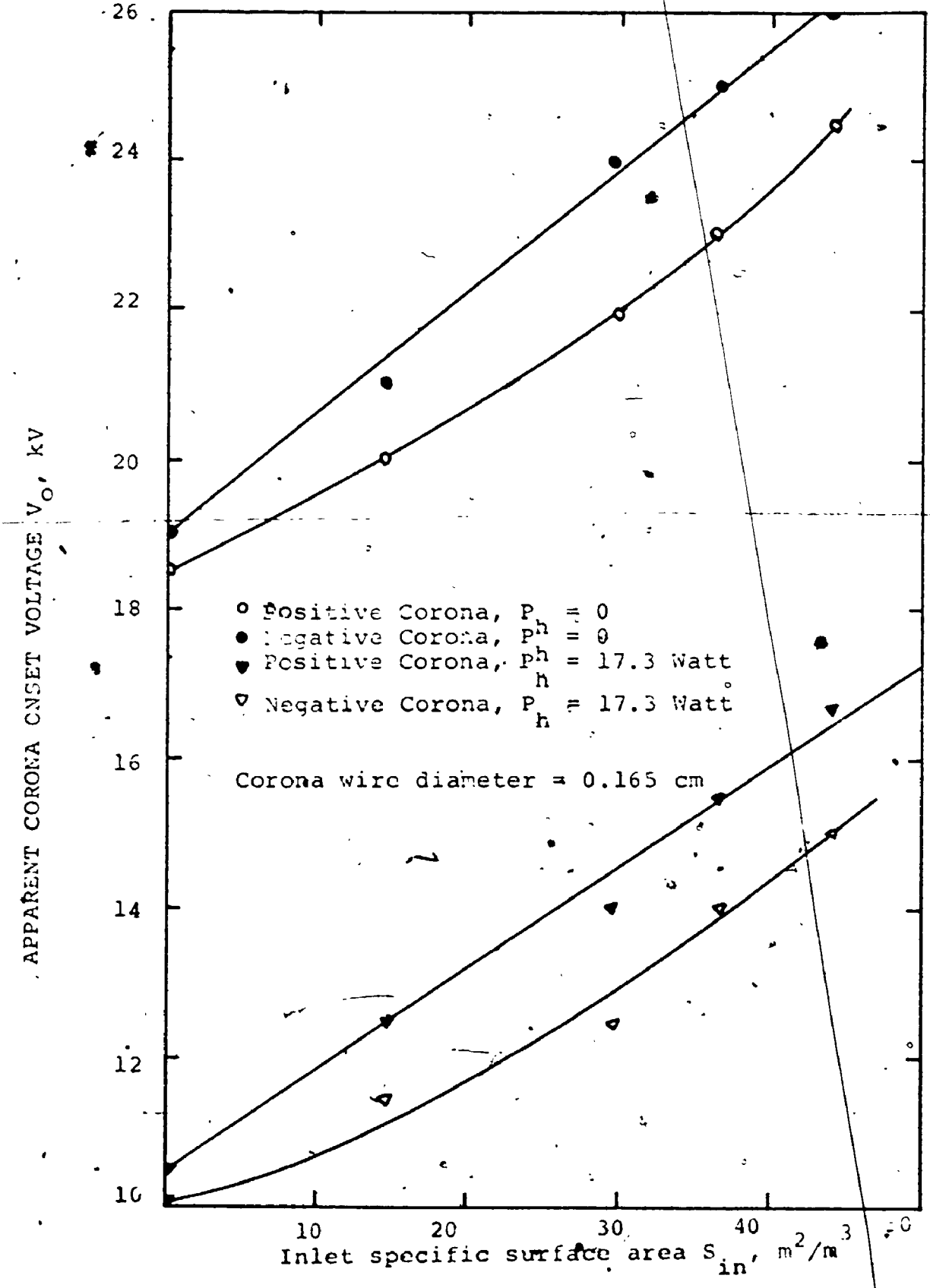

FIGURE(76) APPARENT CORONA ONSET VOLTAGE VERSUS THE INLET SPECIFIC SURFACE AREA WITH AND WITHOUT HEATING THE CORONA WIRE

increase in the apparent corona onset voltage due to the particle loading.

Figures (77) and (78) show the average linear corona current suppression ratio at a fixed intermediate voltage of 34 kV as influenced by heating the corona wire for positive and negative corona respectively. From these figures one can see that heating the corona wire leads to a reduction in the corona current suppression ratio and hence counteracts the corona quenching effect.

9.3.2 Effect of heating the corona wire on the collection efficiency under condition of corona quenching

The experimental results in the previous section have indicated that the method of heating the corona wire is successful in counteracting the particle space charge effect on reducing the corona current. However, from the practical point of view, it is the collection efficiency of an electrostatic precipitator that is of primary importance. The collection efficiency was measured at fixed values of applied voltages with and without heating the corona wire. Figures (79) and (80) for the negative and positive corona respectively, show the collection efficiency versus the inlet specific surface area of the suspended material at fixed voltages with and without

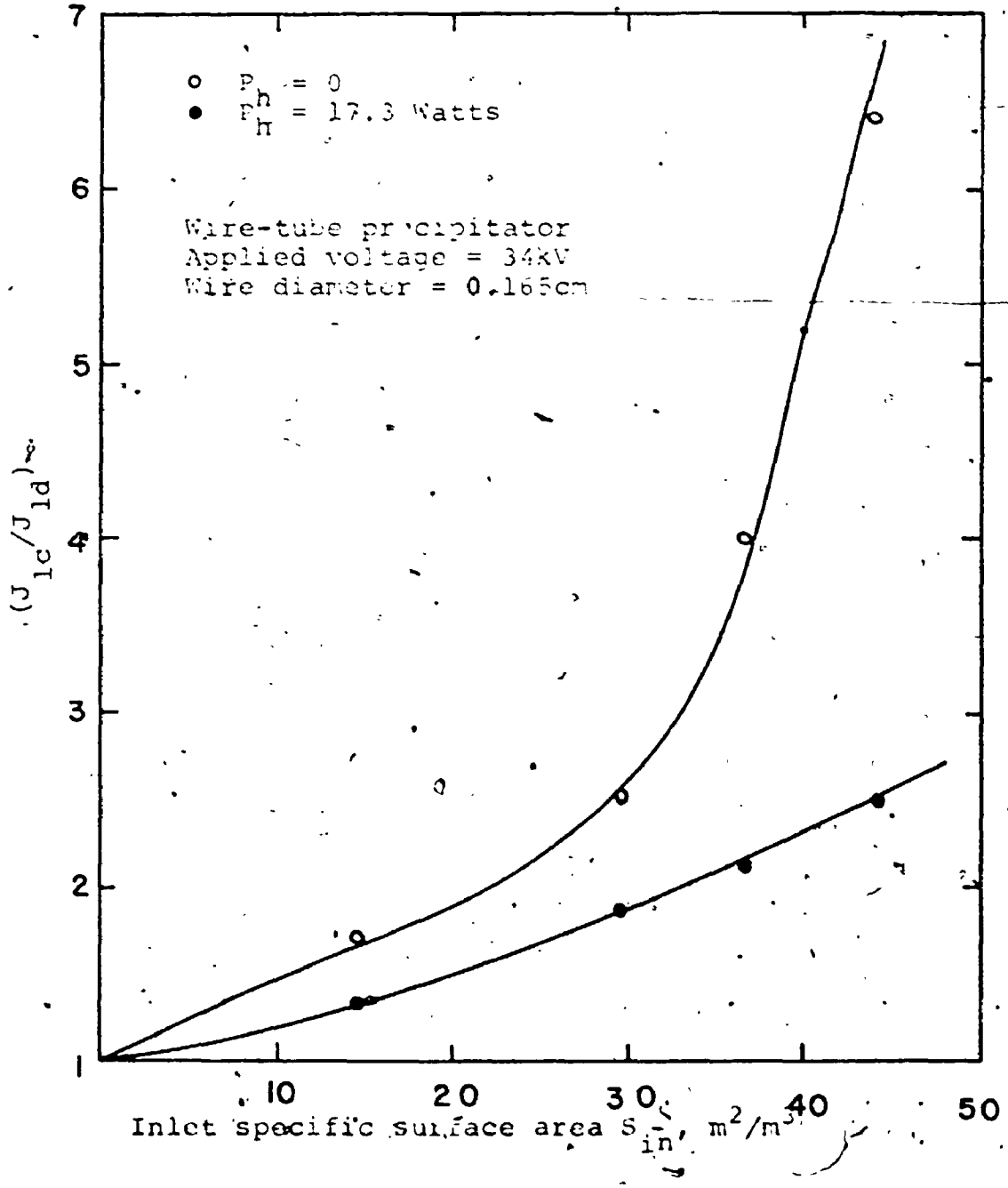

FIGURE (77) (J_{lc}/J_{ld}) VERSUS S_{in} WITH AND WITHOUT HEATING THE CORONA WIRE IN POSITIVE CORONA

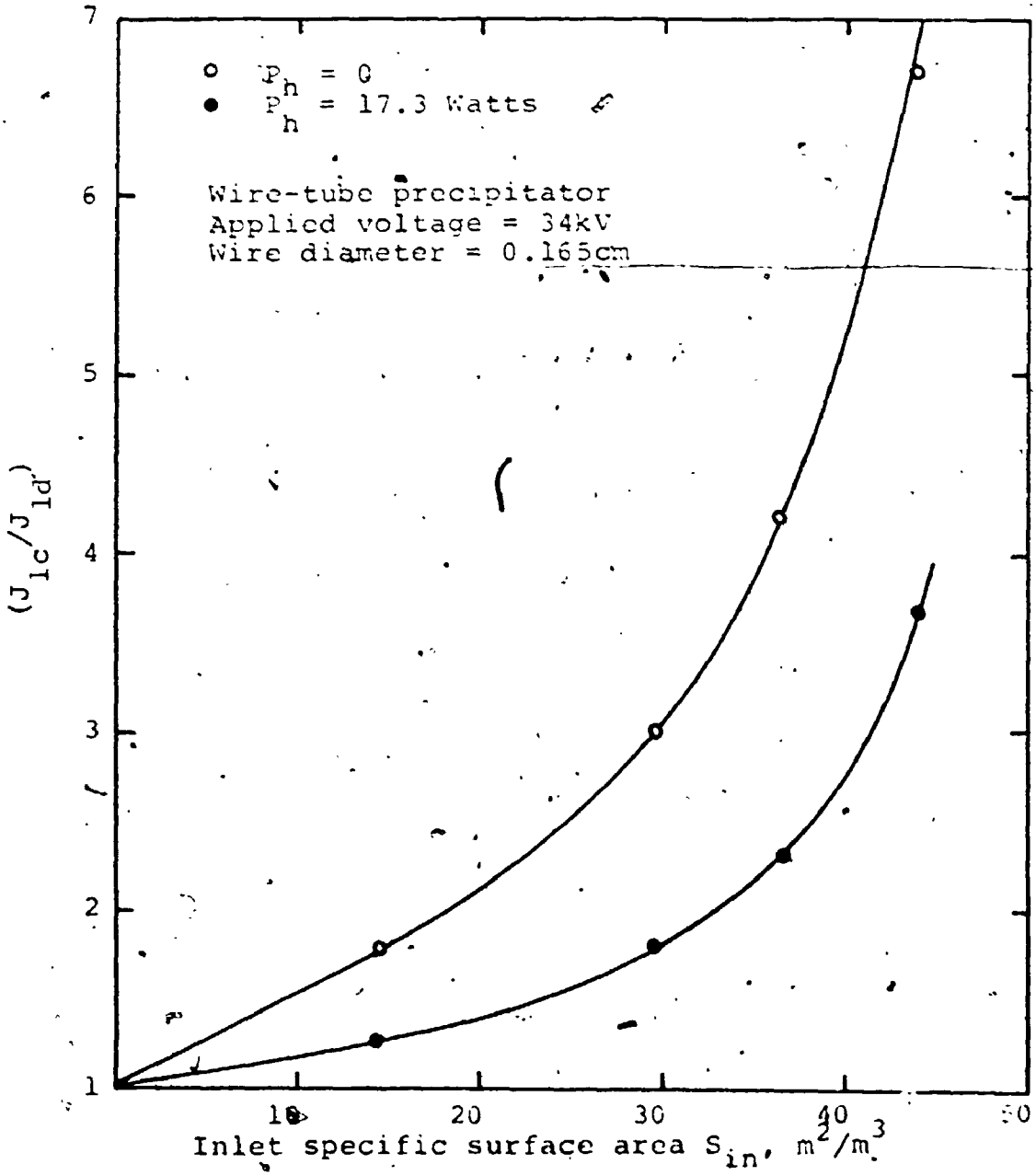

FIGURE (78) (J_{lc}/J_{ld}) VERSUS S_{in} WITH AND WITHOUT HEATING THE CORONA WIRE IN NEGATIVE CORONA

FIGURE (79) COLLECTION EFFICIENCY VERSUS INLET SPECIFIC SURFACE AREA WITH AND WITHOUT HEATING THE CORONA WIRE IN NEGATIVE CORONA

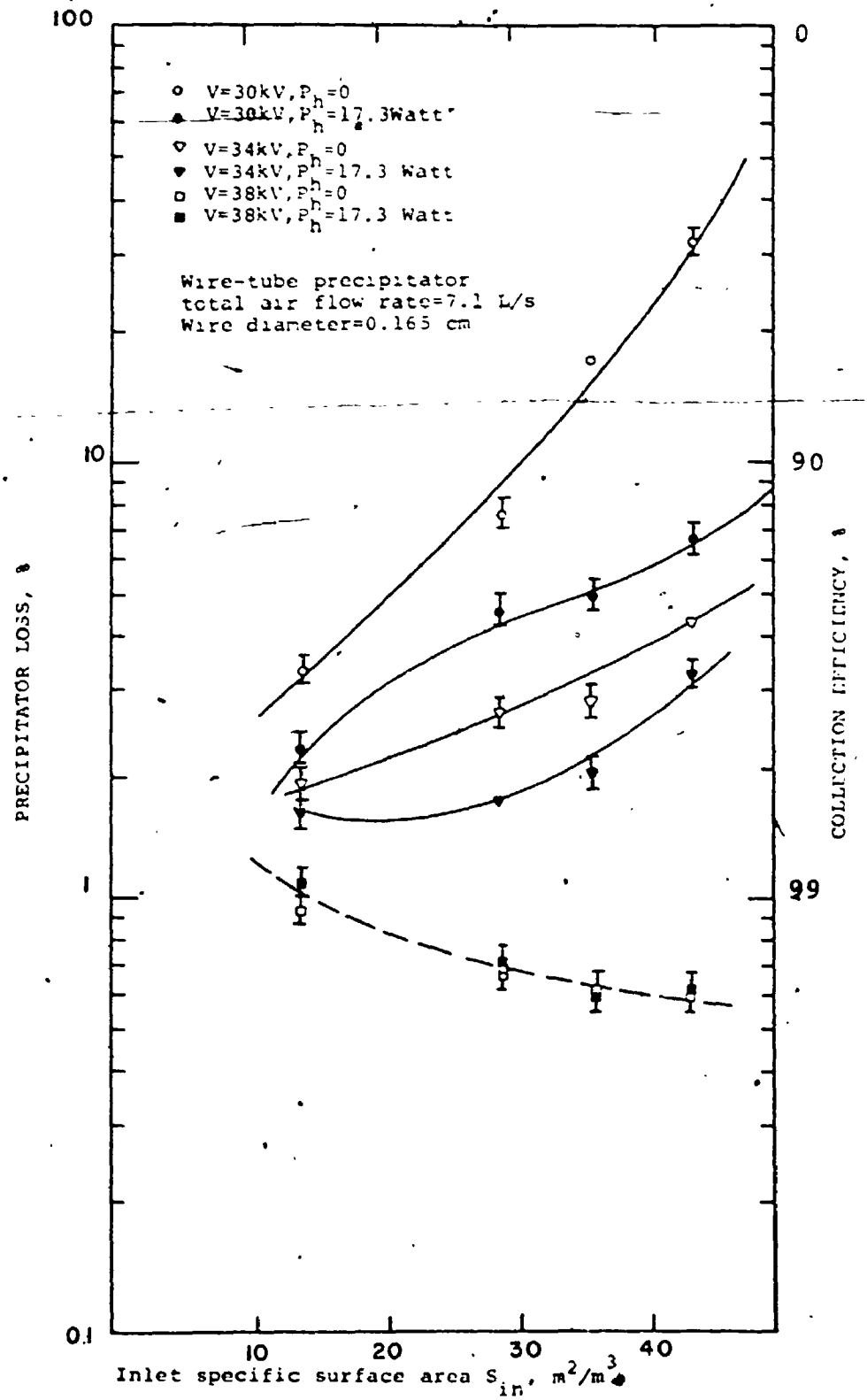

FIGURE (60) COLLECTION EFFICIENCY VERSUS INLET SPECIFIC SURFACE AREA WITH AND WITHOUT HEATING THE CORONA WIRE IN POSITIVE CORONA

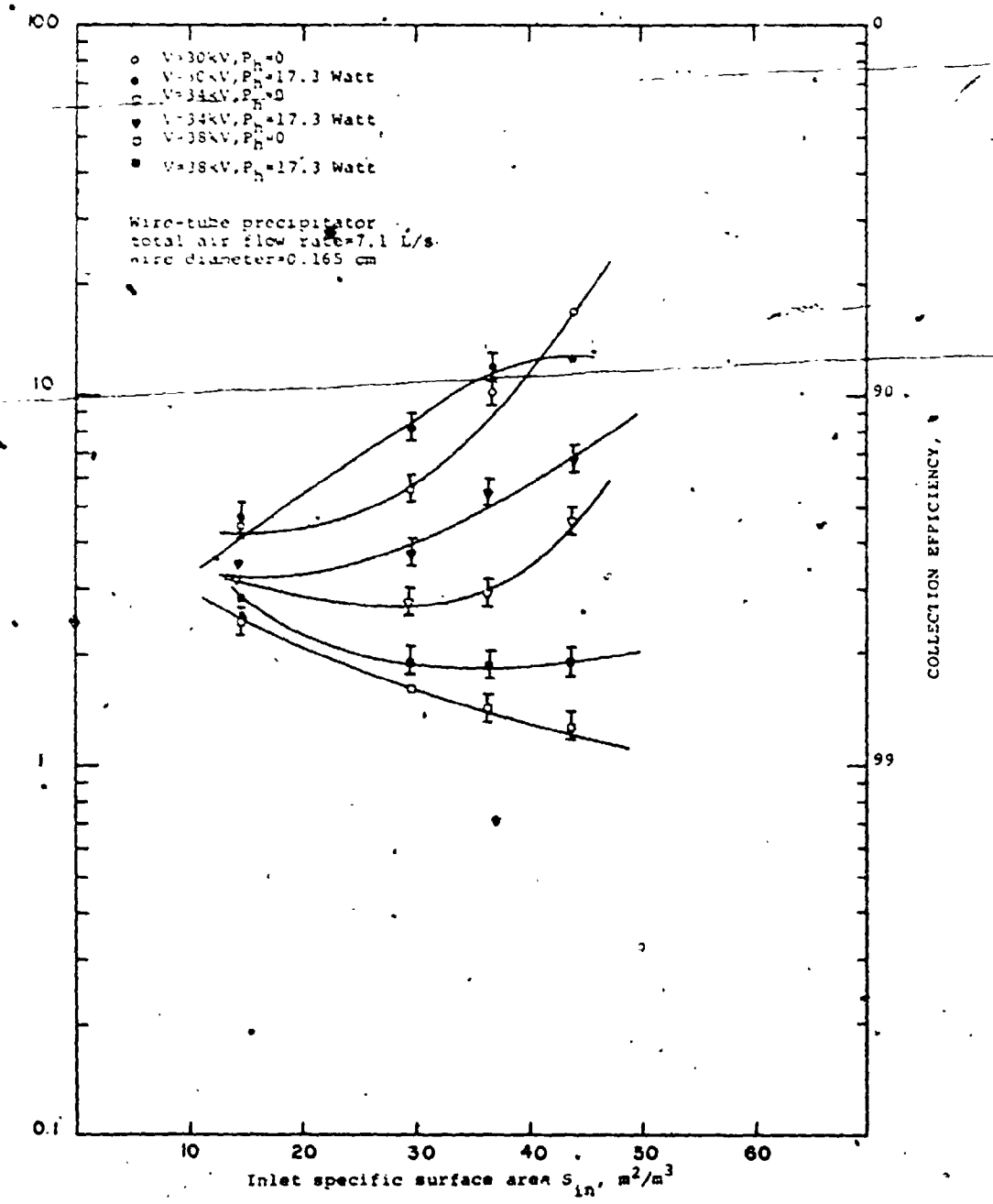

heating the corona wire of diameter 0.165×10^{-2} m (0.065"). The values of the average linear corona current densities are indicated between brackets beside each point. Note the increase in this corona current density at fixed applied voltage and fixed inlet specific surface area with heating the corona wire.

For negative corona, the increase in the average linear corona current density causes an increase in the collection efficiency at applied voltages of 30 and 34 kV. Apparently in this case, the increase in the field in the outer region close to the collecting electrode and the increase in particle charging due to electrons emanating from the tufts may offset any reduction in particle charging that may be caused by the new field pattern. At 38 kV however, the collection efficiencies were very close to those without heating the corona wire. Hence, it can be seen that heating the corona wire should result in an increase in the collection efficiency under negative coroha especially at low corona current densities.

For positive corona, figure (80) shows that under heating the corona wire the collection efficiency decreased compared to without heating. The reduction in the collection efficiency in this case is an evidence that the increase in the collection field due to the higher corona current

density with the heated corona wire may be offset by a reduction in the charge acquired by the particles. This reduction in particle charge may be essentially due to the new pattern of the electric field in the interelectrode spacing as shown in figure (73).

9.3.3 Effect of heating the corona wire on the sparking characteristics

This parameter is of importance for two reasons:

(1) As mentioned in section (4.2) that the industrial electrostatic precipitators normally operate close to sparkover condition. Therefore, for the method of heating the corona wire to be practically feasible in electrostatic precipitators operating under conditions of corona quenching, it should result in an increase in the maximum pre-sparking corona current with no appreciable reduction in the sparkover voltage.

(2) As noted in section (4.1) the origin of the breakdown streamers triggering the sparkover is not certain especially under negative corona. Therefore, it was believed that the experiments with heated corona wire may give better understanding for the origin of these breakdown streamers.

Table (2) shows the sparkover voltage with and without heating two corona wires under conditions of clean

air and different inlet specific surface areas. From this table one can observe:

(1) With heating the positive corona wire, the sparkover voltage appreciably decreases. Comparison of the results for the two wires show that, as the heating power to the corona wire increases the sparkover voltage decreases. This may be explained by the increase in the tendency of triggering the breakdown streamers at lower voltage because of the relatively low negative ion space charge density due to the reduction in the relative gas density in the vicinity of the ionization region. These results emphasize that under positive polarity, the electrical characteristics of the discharge in the active zone has the main role in originating the breakdown streamers.

(2) With heating the negative corona wire, the sparkover voltage decreases only very slightly in a few cases. The results show a reduction up to a maximum of 1.5 kV. These results indicate that under negative polarity, the main factor governing the sparkover is the positive streamers initiated from the outer electrode. There is only very slight effect due to the negative streamers "Feathers" initiated from the negative glow around the corona wire. In other words, the complete breakdown of the gap is not obtained unless the positive

streamers are initiated from the positive outer electrode even if the negative streamers are already present.

Table (3) shows the max. pre-sparking corona current with and without heating two corona wires under conditions of clean air and different inlet specific surface areas. In this table note:

(1) With the reduction in the sparkover voltage under positive polarity, a drastic reduction in the maximum pre-sparking corona current was obtained.

(2) Under negative polarity, the maximum pre-sparking corona current slightly increases by heating the corona wire. This result shows that the method of heating the corona wire may be suitable for industrial electrostatic precipitators under conditions of severe corona quenching where the maximum pre-sparking corona current density is very low and hence any increase in this current should result in higher collection efficiencies.

Table (2) Sparkover voltage with and without heating the corona wire under different particle concentrations

Particle concentration	Wire diameter = 0.165×10^{-2} m (0.065")				Wire diameter = 0.235×10^{-2} m (0.093")			
	Positive Corona		Negative Corona		Positive Corona		Negative Corona	
	$P_h=0$	$P_h=17.3$	$P_h=0$	$P_h=17.3$	$P_h=0$	$P_h=7.9$	$P_h=0$	$P_h=7.9$
$S_{in}=0$	59	39	52.0	51.5	59	51.5	52.5	52.5
$S_{in}=14.7\ m^2/m^3$	59	41	52.5	52	59	54	54	53.5
$S_{in}=29.4\ m^2/m^3$	59	40	53	53	59.5	54.5	55	54
$S_{in}=36.7\ m^2/m^3$	59.5	39	53.5	52	60	54.5	55	54
$S_{in}=44\ m^2/m^3$	60	40	54.5	53	60	55	56	54.5

P_h is in Watt

All voltages are in kV

Table (3) Maximum presparking corona current with and without heating the corona wire under different particle concentrations

Particle concentration	Wire diameter = 0.165×10^{-2} m(0.065")				Wire diameter = 0.235×10^{-2} m(0.093")			
	Positive Corona		Negative Corona		Positive Corona		Negative Corona	
	$P_h = 0$	$P_h =$ 17.3	$P_h = 0$	$P_h =$ 17.3	$P_h = 0$	$P_h =$ 7.9	$P_h = 0$	$P_h =$ 7.9
$S_{in} = 0$	5.0	1.6	5.45	5.6	4.85	3.25	5.75	6.0
$S_{in}=14.7\ m^2/m^3$	4.55	1.4	4.9	5.1	4.35	3.65	5.2	5.4
$S_{in}=29.4\ m^3/m^3$	4.25	1.15	4.5	4.65	4.15	3.35	5.0	5.2
$S_{in}=36.7\ m^2/m^3$	4.1	0.9	4.1	4.35	3.9	3.3	4.7	4.75
$S_{in}=44\ m^2/m^3$	4.0	0.85	4.05	4.3	3.7	3.2	4.5	4.65

P_h is in Watt

Corona currents are in mA

CHAPTER X

Conclusions

10.1 Summary

The detailed conclusions and implications of the experimental results have been discussed in the particular section in which they arose. The following describe the most significant points:

(A) Corona quenching in electrostatic precipitators

(i) Particles carried in suspension in the gas affect the electrical parameters in the corona and thus influence the charging and collection processes. This interaction is much more complex than generally assumed in the literature. The mathematical model found in the literature to predict the effect of the particle concentration on the apparent increase in the corona onset voltage and the quenching of the corona current is based upon several questionable assumptions and no quantitative agreement was obtained with the experimental results. The apparent increase in the corona onset voltage results from conditions of severe corona quenching because of the limited availability of free gaseous ions. For the same particle concentration negative corona results in larger increase in the apparent

corona onset voltage. Onset streamers have more chance to be formed in positive coronas experiencing the space charge suppression.

The linear corona current density in the presence of a given inlet particle concentration varies in the axial direction of the wire-tube precipitator depending upon the relative rate of particle charging and collection. Hence, the average linear corona current suppression ratio is dependent upon all the factors that affect the charging and collection processes such as the applied voltage, the diameter of the corona wire, the total gas flow rate, the polarity of the corona and the interelectrode spacing.

(ii) In the precipitator tested, the collection efficiency at a fixed voltage as influenced by the inlet specific surface area appears to be primarily dependent on the magnitude of the original corona current density with clean gas coupled with the inlet specific surface area. This dependence can be classified into two regimes: If the ratio of the linear corona current density with clean gas (J_{lc}) to the inlet specific surface area of the suspended material (S_{in}) is smaller than approximately 0.5 mA for the negative corona and 0.25 mA for the positive, then an increase in S_{in} for a certain original value of J_{lc} should result in a reduction in collection efficiency.

On the other hand if this ratio J_{lc}/S_{in} is higher than the above experimental limits, then an increase in S_{in} for a certain original value of J_{lc} should result in a slight increase in the collection efficiency. In this case, it appears that collection field enhancement due to the particle space charge effect offsets any reduction in the charge acquired per particle.

Measurements of the collection efficiency under relatively low corona current densities were shown to be dependent on both the applied voltage and the linear corona current density. This means that both the electrostatic and the ion space charge components of the electric field are significant. On the other hand, for relatively high values of linear corona current densities the main factor influencing the collection efficiency is the corona current with the magnitude of the applied voltage having only a slight effect.

(B) Sparking characteristics in electrostatic precipitators

From the experimental data for the sparkover voltage and the maximum pre-sparking corona current under both polarities in the laboratory models of wire-tube and wire-plate precipitators, the results indicate:

(i) Under clean gas conditions, for fine corona wires,

the presence of negative ions outside the ionization sheath in positive corona aids in the formation of a glow discharge and prevents the formation of positive streamers and hence stabilizes the discharge. For large corona wires in positive corona, because of the lower field gradient, onset streamers may be formed. In this case, the breakdown streamers may or may not be preceeded by a glow discharge depending on the diameter of the corona wire. In the negative corona, it is the field at the outer electrode that is of most importance in triggering breakdown streamers. At room temperature positive corona has higher sparkover voltage than the negative using corona wire diameters in the range of 0.25 mm to 6.3 mm.

(ii) Particle space charge enhances slightly the sparkover voltage for both polarities. The amount of increase is dependent on the particle concentration in the exit sections i.e on the collection efficiency. However, the increase in the sparkover voltage for all the cases tested was not sufficient to compensate for the reduction in the corona current due to the particles and hence the maximum pre-sparking corona current decreases as the inlet specific surface area increases.

current due to the particles and hence the maximum pre-sparking corona current decreases as the inlet specific surface area increases.

(C) Corona quenching and sparkover with heated corona wire

Heating the corona wire counteracts the particle space charge effect on the corona voltage-current characteristics i.e it reduces the apparent corona onset voltage and increases the corona current at fixed value of applied voltage. This is because of the reduction in the relative gas density inside the ionized sheath which gives rise to higher value for the first Townsend's ionization coefficient α and the ion production rate. The degree of compensation of the particle space charge effect by heating the corona wire is primarily dependent on the heating power coupled with the inlet specific surface area. The efficiency measurements with and without heating the corona wire at fixed applied voltage have shown an increase in the collection efficiency in the negative corona. The amount of increase is appreciable only for low corona current densities. In the positive corona however, the collection efficiency decreased with heating the corona wire.

Measurements of the sparkover voltage and the maximum pre-sparking corona current with heated corona wire in the negative case have shown a slight reduction in the sparkover

voltage and a slight increase in the maximum pre-sparking corona current. These results indicate that the main factor governing the sparkover under negative polarity is the positive streamers initiated in the vicinity of the outer electrode at certain critical field intensity. In the positive corona however, both the sparkover voltage and the maximum pre-sparking corona current are drastically reduced with heating the corona wire. These results emphasize that the electrical characteristics of the discharge in the vicinity of the corona wire have the main role in originating the breakdown streamers in this case.

10.2 Practical Applications

It is believed that the investigation presented in this thesis represents a contribution to the knowledge of the physical mechanisms of the corona quenching and sparkover phenomena. This better understanding should lead to a more successful design of electrostatic precipitators. For instance:

(1) Optimum collection efficiencies under conditions of corona quenching (mild or severe) can be achieved by using the smallest possible corona wire compatible with the mechanical strength. This is because the value of the sparkover voltage and the maximum pre-sparking corona current are maximum in this case.

(2) As the gas traverses an industrial electrostatic precipitator, the particle concentration, heavy at first, is reduced and may be very small at the outlet. The particle space charge interacts with the corona characteristics. The experimental results presented here indicate that the sparkover voltage and the maximum pre-sparking corona current are influenced by the particle space charge effect. Therefore, corona wires at the inlet sections should be electrically separated from the corona wires at the outlet. In other words, sectionalizing of a large precipitator such that each section is operated at its sparkover voltage should be matched as close as possible with the variation in the particle concentration for maximum collection efficiency. The higher the inlet specific surface area, the greater will be the electrical space charge effect and therefore, the greater degree of sectionalization required for optimum performance.

(3) In industrial precipitators operating under conditions of severe corona quenching, positive corona may be preferable to the generally accepted negative corona for the following reasons:

(a) The negative corona has a much greater relative corona current quenching than the positive especially at high gas temperatures.

(b) The results obtained from this study have shown that positive corona has higher sparkover voltage than the negative in the presence of different particle concentrations using corona wire diameters in the range of 0.25 mm (0.010") and 6.35 mm (0.250") in both the tube and the duct precipitators. The interelectrode spacing was 3.81 cm (1.5"). However, work found in the literature[52] under clean gas condition has indicated that for interelectrode spacings of 5 to 10 cm which are comparable with those found in large electrostatic precipitators, the corona wire diameter should not exceed 1.6 mm (0.063") for the sparkover voltage in the positive corona to exceed that of the negative. Combining the two results together, one can conclude that using a corona wire diameter 1.6 mm or less under certain particle concentration should give higher sparkover voltage with the positive polarity than the negative.

(c) The presence of high resistivity material at the outer electrode appreciably reduces the sparkover voltage in the negative corona but to a much less extent in the positive[3].

10.3 Recommendation for further work

(1) It is recommended that a further study is required to investigate the sparking characteristics at higher gas temperatures (200-300 ^{o}F) with and without particle space-charge effect in both polarities. Different corona wire diameters and interelectrode spacings should be used. The main purpose of these experiments should be to elucidate the mechanism that gives rise to the higher sparkover voltage in the negative corona than the positive in the industrial precipitators.

(2) An interesting study could be undertaken to find the effects of corona quenching on the back corona phenomenon. This can be carried out by using a thin perforated plate of high resistivity material on the collection electrode of a duct precipitator. The (V-I) characteristic should be measured at first with clean gas under the presence of back corona. Different concentrations of particles should be then injected and the (V-I) characteristic measured again. The author believes that an increase in the sparkover voltage and the maximum pre-sparking corona current should be achieved due to the corona quenching effect on the back corona. The reasons are as follows:

(i) the resistivity of the gas pockets close to the collecting electrode is equal to(E/j).The particle

space-charge enhances the field at the outer electrode E and reduces the corona current density j and hence raises the resistivity in these gas pockets. This effectively should reduce the probability of the back corona.

(ii) The pick-up by the dust particles of the ions of reverse sign produced by the back corona should stabilize the discharge and hence higher sparkover should be obtained.

(iii) The pick-up of the free electrons emanating from the negative corona tufts by the particles should also stabilize the discharge.

APPENDIX (A)

Some properties of the D.O.P.

Formula

$C_6 H_4 (COOCH_2 CH(C_2 H_5) C_4 H_9)_2$

Physical properties

A light-colored ordorless liquid, specific gravity 0.98 (at 20 C°); pour point -46 C°; refractive index* 1.48, flash point 425 $^{\circ}F$, viscosity 81.4 cp (20 C°); insoluble in water, molecular weight 392.

Derivation

Reaction of 2- ethylhexyl alchol and phthalic anhydride.

Chemical name

di(2- ethylhexyl) phthalate.

---

*The dielectric constant is the square of the refractive index. Therefore, the dielectric constant of the D.O.P. is 2.2

APPENDIX (B)

Specifications and Calibration for Fluorometer

The aerosol concentration, for a given run, was determined by analysing for the presence of uranine on a Turner Fluorometer, Model 111 (Section 5.4). The primary filter used on the incident (exciting) radiation were 2 A-15 and 47 B. Those used to filter the radiation emitted from the samples, secondary filters, were 2 A-15 and 65 A. The fluorometer is basically an optical bridge (analogous to the Wheatstone bridge in measuring electrical resistance) that detects the difference between light emitted by the sample and that from the rear light path (Figure B.1). A single photo-multiplier surrounded by a mechanical light interupter sees light alternatively from the sample and the rear light path. A phase sensitive detector whose output is either positive (excess light in the sample) or negative (excess light in the rear path) drives a servo amplifier. The servo motor connected to the servo amplifier drives the light cam (and hence the fluorescent dial until an equal amount of light reaches the photo-multiplier from both paths. The fluorescent dial indicates the amount of light required in the rear light path to balance that from the sample. Each

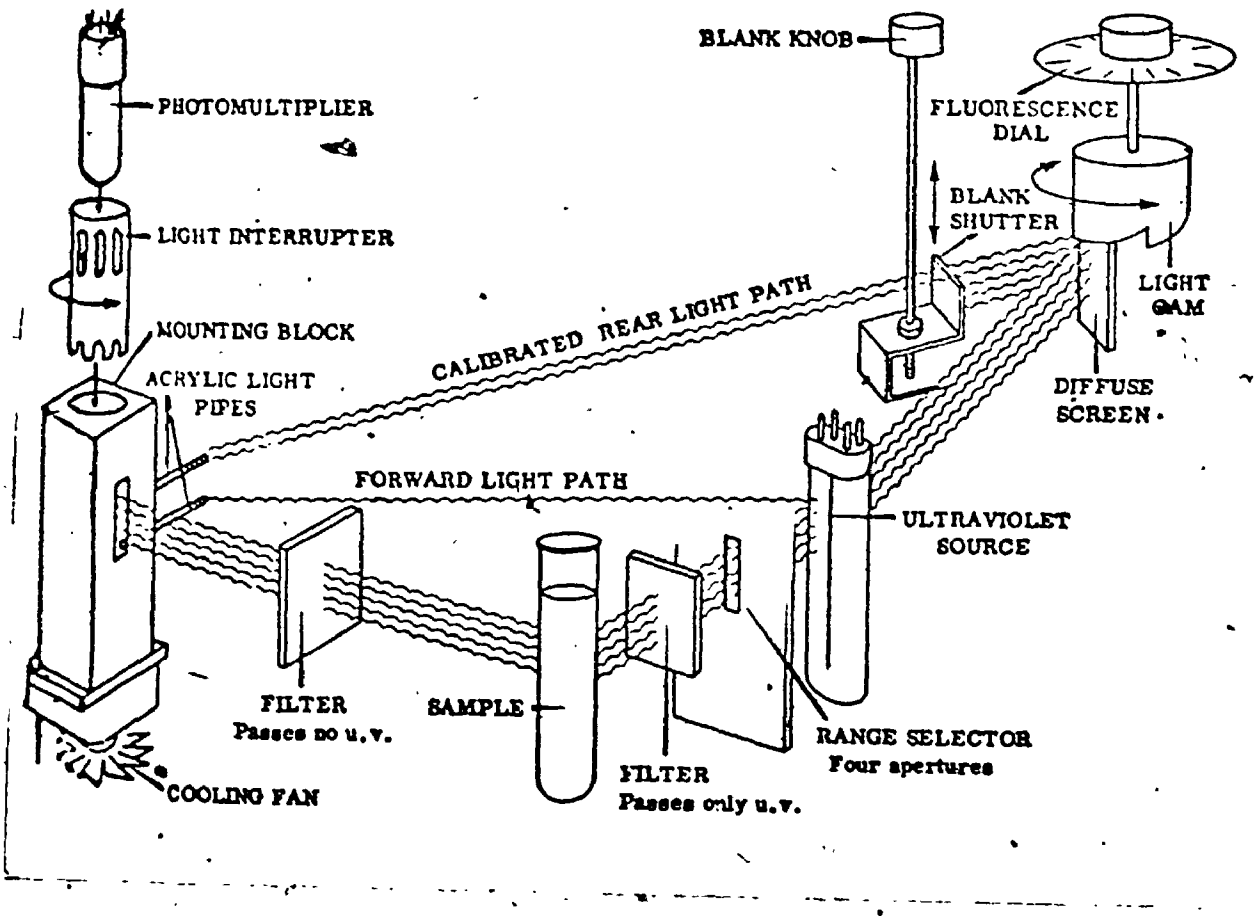

FIGURE (B1) OPTICAL SYSTEM

of the dial's 100 divisions add equal increments of light to the rear light path by means of the light cam. Equalization of the two light paths may also be adjusted normally with the blank control and the fluorescence dial set to zero. This blank reading is normally made with pure solvent.

A very wide range of concentrations can be measured with this instrument since one can select the amount of incident radiation (range selector positions of 1X, 3X, 10X and 30X) and choose various combinations of primary filters (passing only ultraviolet light) and secondary filters (passing no ultraviolet light). Very dilute concentrations may be measured with the same accuracy as three orders of magnitude higher concentrated solutions.

Typical calibrations curves are given in figures B.2 and B.3.

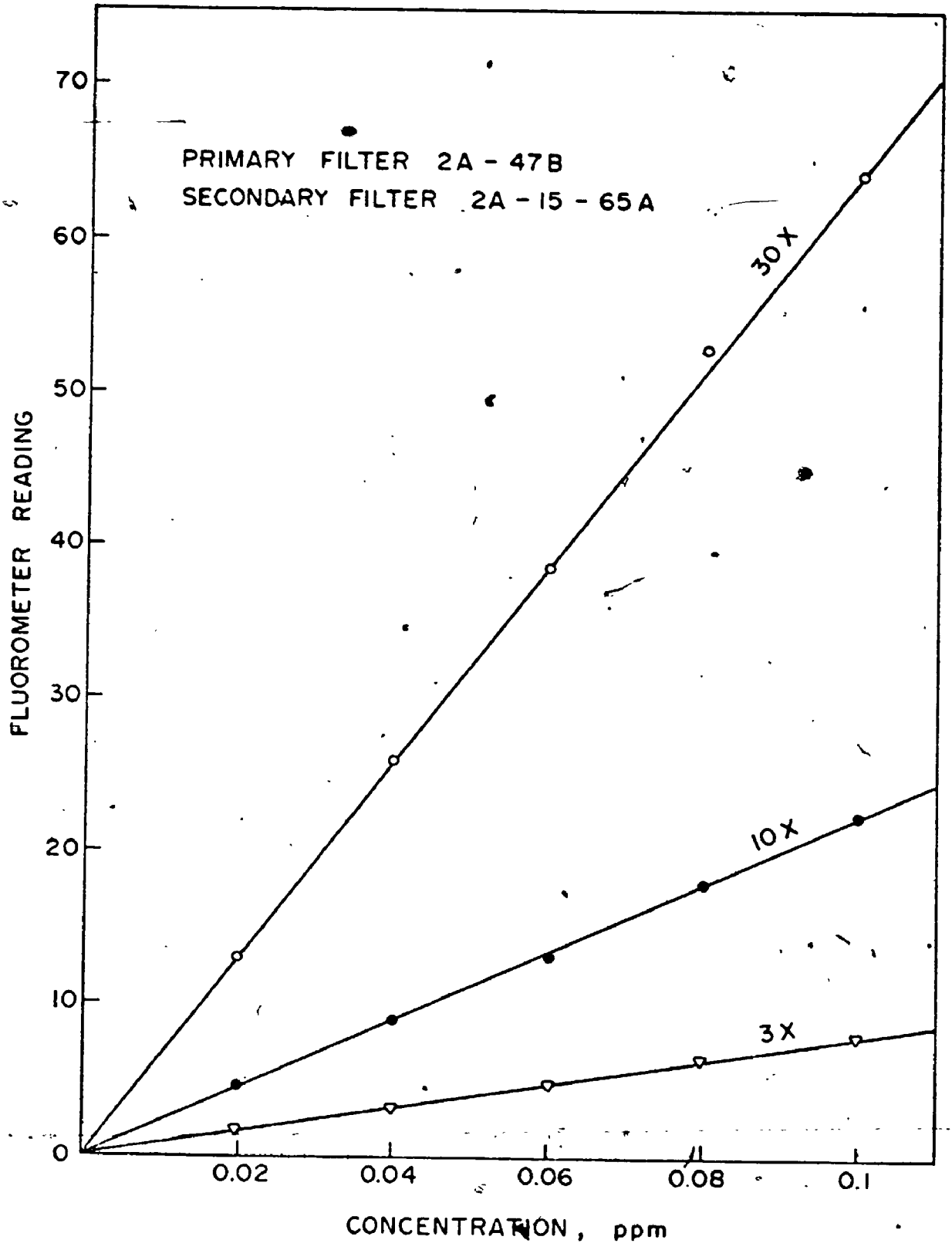

FIGURE (B2) CALIBRATION CHART FOR THE FLUOROMETER

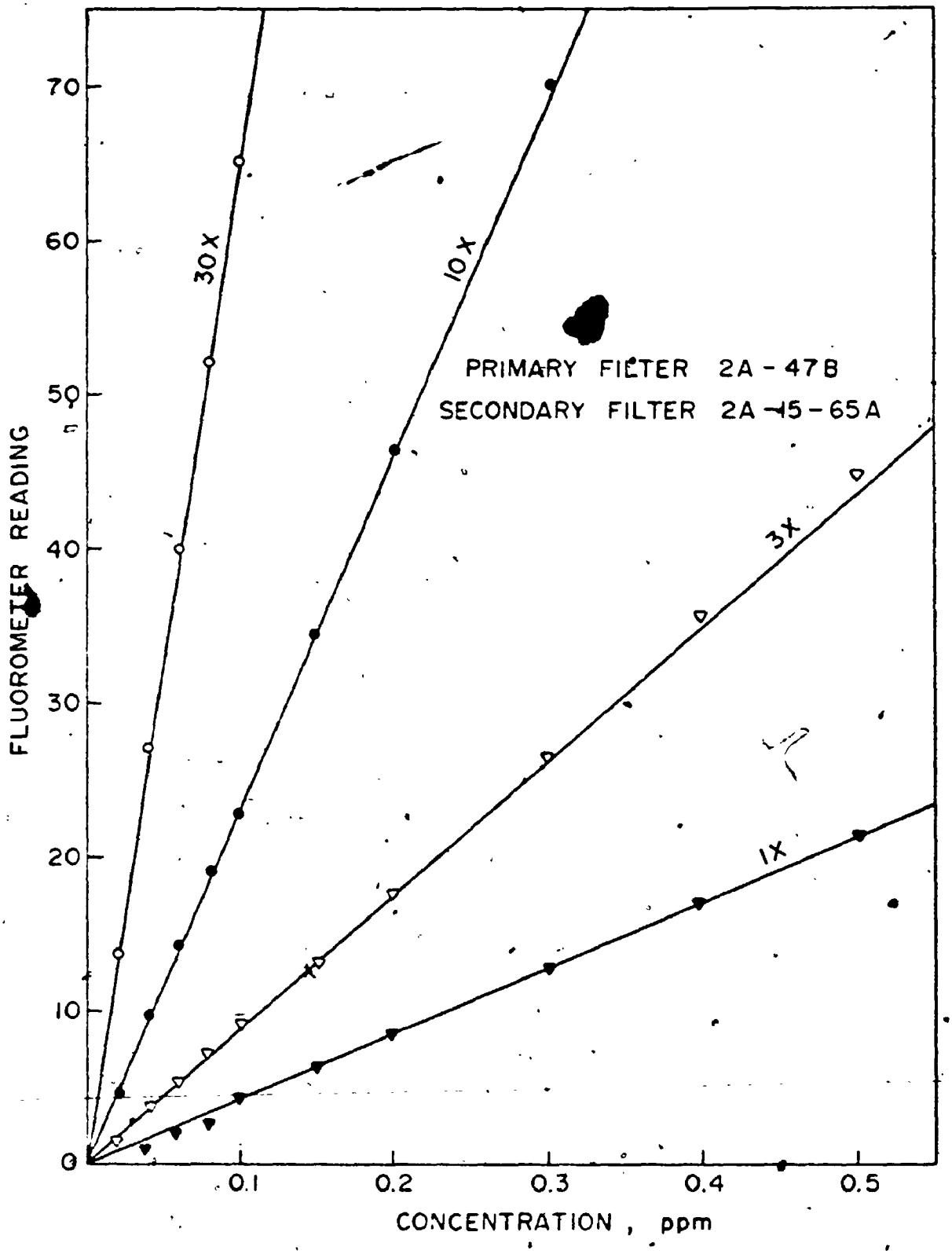

FIGURE(B3) CALIBRATION CHART FOR THE FLUOROMETER

APPENDIX (C)

Amount of the D.O.P. generated per minute

After dissolving certain amount of the uranine in the D.O.P., vacuum filteration was made to ensure the absence of any suspension of uranine particles which if present would clog the nozzle of the smoke generator. After this filtration the concentration of the uranine completely dissolved in the D.O.P. was determined by taking a sample of 1 milliliter in 500 milliliter of ethyl alchol. The readings obtained on the 10X scale and 30X scale were 28 and 84 respectively. Using the calibration curves it was found that

$$\text{D.O.P.} = \frac{\text{Uranine}}{64.3 \times 10^{-6}} \quad \text{gram.}$$

Running tests with 1,2,3 and 4 jets fully open for 10 minutes and washing the filter papers with 100 milliliter of ethyl alchol the readings obtained from the fluorometer on the 10X scale were:
12 for 1 jet, 24 for 2 jet, 30 for 3 jets and 36 for 4 jets. Using the calibration curves and the concentration of the uranine in the D.O.P. with the suction rate of 5 L/min, the concentration of the D.O.P. generated by one

jet was found to be 1.65 milligram per liter of air. For a total air flow rate of 7.1 L/s (15 ft.^{3}/min.), the amount of D.O.P. generated per minute was as indicated in Table (C1).

Table (C1) Amount of D.O.P. generated per minute

number of jets used	D.O.P. generated
1 jet	0.7 gram/min.
2 jets	1.4 gram/min.
3 jets	1.75 gram/min.
4 jets	2.1 gram/min.

APPENDIX (D), Table (D_1) Negative Corona Voltage-Current Characteristics for Three Corona Wires in Wire-Tube Precipitator

Applied Voltage (kV)	Total Corona Current (mA)														
	Wire Diameter=0.025cm.					Wire Diameter=0.236cm					Wire Diameter=0.475cm				
	S_{in} (m^2/m^3)					S_{in} (m^2/m^3)					S_{in} (m^2/m^3)				
	0.	14.7	29.4	36.7	44	0	14.7	29.4	36.7	44	0	14.7	29.4	36.7	44
10	.008														
14	.082	.021	.004	.002											
18	.195	.092	.030	.011	.005										
22	.422	.19	.087	.042	.018										
26	.785	.55	.325	.21	.115	.13	.606								
30	1.3	.81	.645	.452	.305	.48	.13	.040	.01	.002					
34	1.78	1.5	1.12	.87	168	1.15	.505	.21	.112	.045	.32	.002			
38	2.35	2	1.7	1.45	1.27	1.65	1.12	.6	.425	.23	1.05	.3	.16	.006	.004
42	3.07	2.77	2.4	2.17	1.92	2.42	2.22	1.35	1	.67	1.95	.95	.39	.16	.087
46	4	3.6	3.3	3	2.8	3.33	2.75	2.2	1.95	1.6	3.1	2.15	1.35	.82	.45
50	5.1	4.7	4.32	4	3.75	4.62	3.87	3.32	3	2.72					1.45
51	5.5	5	4.6	4.37	4.1	5	4.3	3.65	3.5	3					
52		5.27	4.95	4.75	4.3	5.32	4.6	4	3.75	3.25					
53					4.55	5.75	5	4.3	4	3.7					
54								4.7	4.5	4					

APPENDIX (D), Table (D_2) Positive Corona Voltage-Current Characteristics for Three Corona Wires in Wire-Tube Precipitator

Applied Voltage (kV)	Total Corona Current (mA)														
	Wire Diameter=0.025cm					Wire Diameter=0.236cm					Wire Diameter=0.475cm				
	S_{in} (m^2/m^3)					S_{in} (m^2/m^3)					S_{in} (m^2/m^3)				
	0	14.7	29.4	36.7	44	0	14.7	29.4	36.7	44	0	14.7	29.4	86.7	44
10	.012	.002													
14	.08	.028	.008	.003	.002										
18	.19	.095	.04	.018	.01										
22	.4	.245	.14	.087	.05										
26	.64	.435	.31	.12	.1	.12	.04	.003							
30	.95	.685	.53	.425	.32	.35	.15	.03	.015	.006					
34	1.3	1	.85	.7	.6	.69	.35	.19	.12	.03	.125	.007			
38	1.75	1.43	1.25	1.1	1	1.1	.75	.5	.4	.2	.48	.13	.025	.008	.005
42	2.28	1.92	1.75	1.6	1.45	1.6	1.25	.95	.78	.6	.95	.5	.2	.09	.05
46	2.9	2.46	2.3	2.2	2	2.15	1.8	1.5	1.45	1.15	1.55	1.05	.75	.5	.21
50	3.55	3.12	2.92	2.82	2.7	2.85	2.5	2.2	2	1.85	2.2	1.75	1.45	1.1	.75
54	4.4	3.92	3.72	3.6	3.5	3.7	3.3	2.95	2.8	2.7	3.1	2.55	2.25	1.9	1.45
56	4.85	4.4	4.2	4.1	3.95	4.15	3.75	3.45	3.3	2.95		3		2.25	1.95
58			4.6			4.6	4.25	3.95	3.7	3.35					2.30

APPENDIX (D), Table (D_3) Negative Corona Voltage-Current Characteristics for Three Corona Wires in Duct Precipitator

Applied Voltage (kV)	Total Corona Current (mA)														
	Wire Diameter=0.025cm					Wire Diameter=0.236cm					Wire Diameter=0.475cm				
	S_{in} (m^2/m^3)					S_{in} (m^2/m^3)					S_{in} (m^2/m^3)				
	0	14.7	29.4	36.7	44	0	14.7	29.4	36.7	44	0	14.7	29.4	36.7	44
12	.078	.014													
16	.24	.085	.05	.03	.015										
20	.48	.265	.15	.11	.06										
24	.85	.55	.43	.35	.26										
28	1.3	1	.75	.7	.54	.2	.07	.008							
32	1.85	1.55	1.35	1.15	1	0.75	.35	.17	.07	.04					
36	2.55	2.3	2	1.85	1.6	1.35	.8	.6	.45	.35	.14	.01			
40	3.35	2.95	2.75	2.65	2.5	2.1	1.7	1.5	1.25	0.95	1.05	.45	.135	.028	.008
44	4.3	3.9	3.65	3.5	3.4	3.1	2.7	2.35	2.2	1.85	2.2	1.55	1.1	.68	.535
48						4.3	3.85	3.5	3.3	2.95	3.4	2.9	2.3	1.95	1.65
50							4.5	4.05	3.9	3.5				2.5	2.3

APPENDIX (D), Table (D_4) Positive Corona Voltage-Current Characteristics for Three Corona Wires in Duct Precipitator

Applied Voltage (kV)	Total Corona Current (mA)														
	Wire Diameter=0.025cm					Wire Diameter=0.236cm					Wire Diameter=0.475cm				
	S_{in} (m^2/m^3)					S_{in} (m^2/m^3)					S_{in} (m^2/m^3)				
	0	14.7	29.4	36.7	44	0	14.7	29.4	36.7	44	0	14.7	29.4	36.7	44
10	.03	.002													
14	.135	.055	.05	.005	.002										
18	.3	.16	.1	.005	.04										
22	.52	.32	.25	.2	.15										
26	.85	.65	.5	.4	.32	.062	.004								
30	1.2	.92	.8	.7	.63	.3	.135	.08	.047	.002					
34	1.65	1.4	1.2	1.15	1	.65	.4	.285	.2	.165	.002				
38	2.2	1.85	1.7	1.6	1.5	1.1	.82	.65	.52	.435	.33	.112	.065	.02	.002
42	2.85	2.5	2.25	2.15	2	1.65	1.4	1.2	.95	.85	.8	.5	.32	.24	.18
46	3.55	3.15	2.85	2.75	2.65	2.32	2	1.8	1.6	1.5	1.45	1.1	.85	.7	.575
50	44	3.95	3.7	3.5	3.45	3.15	2.75	2.5	2.25	2.1	2.25	1.8	1.55	1.3	1.2
52			4.15	3.95	3.75	3.6	3.2	2.9	2.65	2.5	2.75	2.25	1.9	1.7	1.55
54						4.15	3.7	3.3	3.1	2.9	3.25	2.7	2.4	2.1	1.95

APPENDIX (E), Table (E_5) Positive Corona Voltage-Current Characteristics in the Segmented Wire-Tube Precipitator with S_{in}=44 m^2/m^3

V	Corona Current in Each Segment (A)														
	(1) enter	(2)	(3)	(4)	(5)	(6)	(7)	(8)	(9)	(10)	(11)	(12)	(13)	(14)	(15) exit
30	5	2	1.5	1.2	1.2	1.2	1.4	1.7	1.8	4	4.5	6	6	0.5	0.5
34	11	4.5	4.2	4.2	4.2	4.4	4.6	5.6	6.2	12	17	21	26	27	2
36	15.5	6.8	6.8	6.8	7.2	8	8.5	9	10	22.5	27.5	34	42	50	10
38	22	10	10	10.2	11	12	13	14	16	34	42	51	60	73	32
40	28.5	13	13.8	14.2	15.5	17	18.5	20	23	50	61	70	83	96	65
42	37	17	18	18.5	21	23	25.5	27.5	32	70	82	95	110	125	115
43	41	19.5	20	22	24	26	29	32	36	83	95	107	122	138	150

APPENDIX (E), Table (E_4) Positive Corona Voltage-Current Characteristics in the Segmented Wire-Tube Precipitator with S_{in}=36.7 m^2/m^3

V	Corona Current in Each Segment (A)														
	(1) enter	(2)	(3)	(4)	(5)	(6)	(7)	(8)	(9)	(10)	(11)	(12)	(13)	(14)	(15) exit
28	5	2	2	1.8	1.8	1.8	1.8	1.8	1.8	4	4.8	5.2	4	0.5	0.5
30	8.5	3.5	3.2	3	3	3.2	3.2	3.4	3.8	8	9.2	10.5	11.2	4	1
34	18.5	8.5	8.5	8.5	8.8	9.2	9.8	10	11	22.5	25.5	29	33	35.2	5.5
36	26	12	12	12.2	13	13.8	14.5	15	16.5	34	38.5	44	50	50	22
38	35	16	17	17	18	20	21	21	23	48	55	60	70	80	50
40	46	21	22	24	25	26	27	29	31	65	73	81	92	105	87
42	68	27	28	30	31	33	35	37	41	85	95	106	115	130	145

APPENDIX (E), Table (E_3) Positive Corona Voltage-Current Characteristics in the Segmented Wire-Tube Precipitator with S_{in}=29.4 m^2/m^3

V	Corona Current in Each Segment (A)														
	(1) enter	(2)	(3)	(4)	(5)	(6)	(7)	(8)	(9)	(10)	(11)	(12)	(13)	(14)	(15) exit
28	10	5	5	4.5	4	4	4.5	4.5	5	9.5	10	11	11.2	3	0
30	15.5	7.2	7.2	7	7	7	7.2	7.5	8	15.5	15.5	18	19	12	1
34	32	15	15.5	15.5	16	16	16.5	17	18	35	38	42	47	55	16
36	42	20	21	21	21	21	23	24	25	50	53	60	65	75	40
38	55	26	26	27	28	28	30	31	33	65	70	76	86	96	78
40	72	33	33	35	35	36	38	38	41	81	87	95	105	116	112
42	88	40	40	42	44	45	47	48	52	100	110	116	130	142	168

APPENDIX (E), Table (E_2) Positive Corona Voltage-Current Characteristics in the Segmented Wire-Tube Precipitator with S_{in}=14.7 m^2/m^3

V	Corona Current in Each Segment (A)														
	(1) enter	(2)	(3)	(4)	(5)	(6)	(7)	(8)	(9)	(10)	(11)	(12)	(13)	(14)	(15) exit
24	8	3.8	3.9	3.9	3.9	3.9	3.9	3.5	3.6	7.6	7.7	7.6	7.6	3	0
28	23.5	10.5	10.5	10.5	10.5	10.5	11	10.5	11	21	21.2	21.2	22	20	2
30	34	15	15	15	15	15	15	15	16	30	30.5	31	31.5	32	11.5
34	62	27	27	27	28	28	28	28	30	55	56	58	60	65	60
36	78	34	33	33	35	35	35	35	37	69	70	72	75	81	92
38	96	41	41	41	43	43	44	44	45	85	87	90	93	102	121
40	116	49	49	50	51	51	52	52	55	103	106	109	114	122	155
42	132	56	57	58	58	60	61	61	64	121	125	128	135	145	197

APPENDIX (E), Table (E_1) Positive Corona Voltage-Current Characteristics in the Segmented Wire-Tube Precipitator with $S'_{in}=0$

V	Corona Current in Each Segment (A)														
	(1) enter	(2)	(3)	(4)	(5)	(6)	(7)	(8)	(9)	(10)	(11)	(12)	(13)	(14)	(15) exit
20	1	1.8	2	2	2	1.5	2	2	2	2.5	2.8	3	3	2.5	0.5
24	20	8	8	8	8	8.5	8.5	8.5	8.5	16	16	16	16	16	20
28	45	20	20	20	20	20	20	20	20	38	38	38	38	38	46
30	60	26	26	26	26	26	26	26	26	50	50	50	50	50	65
34	96	40	40	40	40	40	40	40	40	77	76	76	77	80	105
36	118	50	50	50	50	50	50	50	50	95	95	95	95	97	120
38	127	60	60	60	60	60	60	60	60	112	112	112	112	117	145
40	150	70	70	70	70	70	70	70	70	132	132	132	132	140	165
42	172	80	80	80	80	80	80	80	80	152	152	152	157	155	195

APPENDIX (F)

Sulphur dioxide removal from flue gases using a spray drying technique and Electrostatic Precipitator

F.1 General

This part of study has been carried out under a P.R.A.I. grant by a research team from the University of Western Ontario consisting of Professor G.S. Peter Castle, Professor K.A. Shelstad, Dr. R.C.H. Huang, and the author in cooperation with Mr. George Lee of the Canadian Combustion Research Laboratory and Dr. N. Sekhar of Ontario Hydro.

The process under investigation consists of the introduction of a very fine spray of liquid absorbent into hot stack gases where it evaporates to dryness and simultaneously reacts with the SO_2 gas. The fine particles remaining in the gas are then collected in an electrostatic precipitator. Since this electrostatic precipitator is expected to deal with very fine particles of high specific surface area, it was felt necessary to carry out a thorough literature survey on the phenomenon of corona quenching and conduct an experimental study to answer some of the questions raised in the literature.

In the following sections the proposed process will be briefly discussed.

F.2 Desulphurization of flue gas

The desulphurization of flue gas is one of the most important problems for the prevention of air pollution due to sulphur dioxide. Many proposed processes for the desulphurization of such flue gas have been developed during the last few years but none of these have been entirely successful. Fuel desulphurization is also a potential solution to the problem. However, its technology is quite complex and a high degree of desulphurization is quite expensive.

In the removal of SO_2 from flue gases, the main problem results from the large volume of the gas to be treated and the low concentration of SO_2 in the gas. Examples of processes currently under consideration are lime slurry scrubbing[58] and absorption in various solutions such as sodium citrate or ammonia[59]. The main disadvantages of these processes are[60]:

(1) The stack plume rise and dispersion are disturbed because of the reduction of the flue gas temperature to the dew point of approximately 50 to 60° C, which necessitates reheating by an additional afterburner according to weather conditions.

(2) The volume of the solutions required per unit volume of the gas to be treated is very large.

(3) The technical problems of storage, transportation, recovery and disposal of large amounts of waste products from the desulphurization process have not been completely solved.

The process that has been under investigation here is based upon a spray drying technique using NaOH as the absorbing chemical. The advantage of using a fine spray is that the contact area between the absorbing chemical and the gas can be made much higher than in scrubbers. For a fixed volume of the absorbing chemical, as the droplet size decreases the specific surface area available for SO_2 absorption increases. A further advantage of this process is that by using a concentrated solution for the absorbing chemical and limiting the amount of water contained in the droplet the temperature drop of the flue gas may be reduced. Hence, the reduction in the flue gas temperature due to the latent heat can be minimized, keeping the gas temperature above the dew point. The droplet should participate in the absorption process only until evaporation stops and the droplet changes to a dry particle. One should actually design the absorbing chamber such that the actual contact time of the droplets in the chamber (i.e the gas flow rate divided by the volume of the chamber) to be approximately equal to the time required to dry the droplet. This should be the

criterion for the most efficient absorbing chamber. In the case of using very fine spray one should also avoid coalesence of the droplets with the walls and with each other. This may be done by optimum choice of the spray angle with respect to the direction of the flow. This can only be determined experimentally. Note that using a very fine spray in the absorption process although of great advantage, it may introduce a problem for its collection in the electrostatic precipitator due to the corona quenching phenomenon. However, it is felt that after this present study for this phenomenon one may achieve high collection efficiency by a proper design of the precipitator.

F.3. Brief Summary of the Experimental Equipment and Results

Preliminary tests on the spray chamber were carried out in the Chemical Engineering Laboratory. The main purpose of these tests was to determine the flow pattern of the gas, the injection rate of the spray, the number and position of the nozzles, different droplet sizes, and to check the chemical analysis for SO_2. Following these experiments, the equipment was installed in the University boiler house and connected to a source of high temperature flue gas. The equipment used was as shown schematically in figure (F) and the operation can be briefly described as follows:

Figure F1 Schematic Diagram of Equipment for Spray Absorption Tests

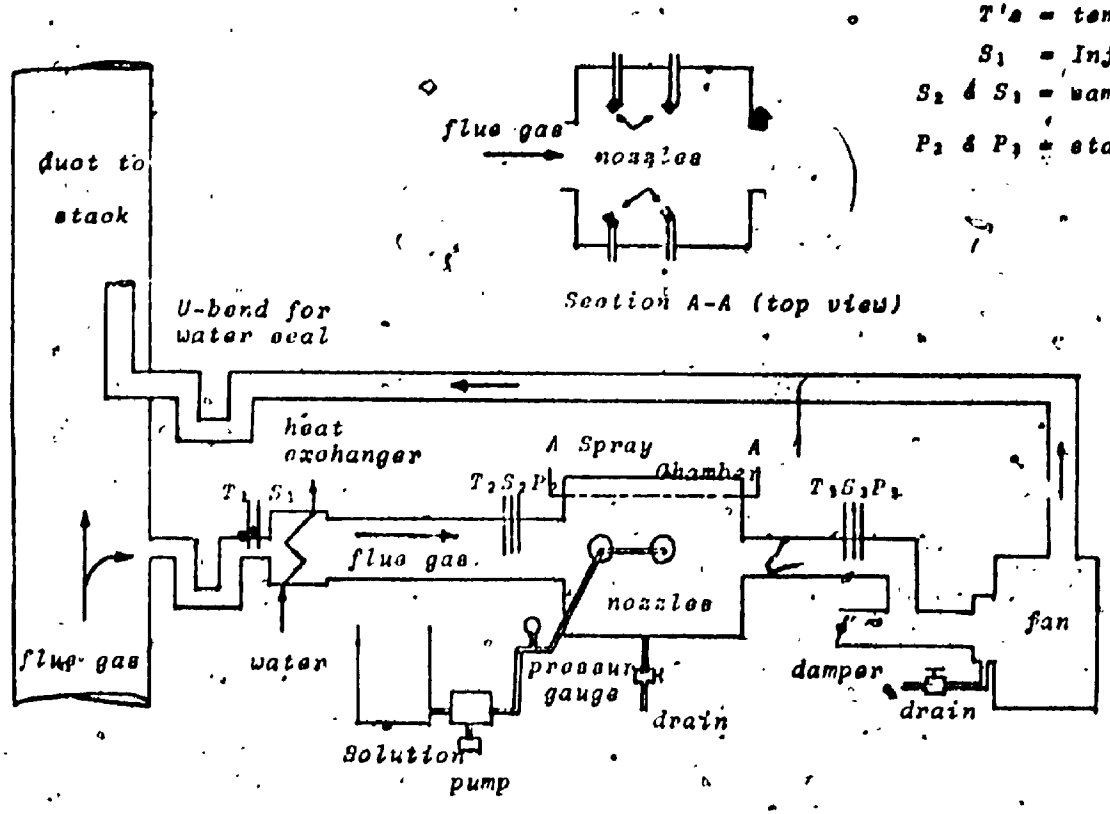

The flue gas was drawn into the system through a 4" I.D. insulated pipe and passed through a heat exchanger. The heat exchanger was capable of cooling the flue gas from 450°F to about 200°F at maximum flow. An insulated rectangular duct, 60x10x12 inch, conducted the flue gas into the spray chamber having the dimensions of 52x32x24 inch. At a position 48 inches downstream from the heat exchanger, a sampling probe, a thermocouple and a static pressure tap were installed. Parts for inserting spray nozzles were positioned at each side of the chamber. After this stage an electrostatic precipitator having the dimension of 40" long x 24" high x 10" wide was built to collect some of the product of the absorption process. On leaving the precipitator, the gas was conducted to an exhaust fan by a 6 inch I.D. insulating steel tube. Sampling, temperature, and static pressure measuring positions were located about 46 inches downstream from the chamber. Since the fan operated at constant capacity, the gas flow rate through the system could be adjusted by a damper in front of the fan over the range 180-320 SCFM.

A number of experiments were carried out using different nozzles. The results indicated that high efficiency absorption of SO_2 was possible provided very fine atonization of the liquid ocurred. This was acheived

by use of a sonic nozzle. The complete results from these experiments are contained in the final report to N.R.C.[61]

From the results obtained using this experimental model it was concluded that the spray drying technique for SO_2 absorption using an electrostatic precipitator for the collection of the dry material may have potential as a satisfactory process for the removal of SO_2.

REFERENCES

(1) Strauss, W., "Industrial Gas Cleaning", Pergamon Press, (1966).

(2) Danielson, J.A., (Editor), "Air Pollution Engineering Manual", U.S. Department of Health, Education, and Welfare, Cincinnati, Ohio, (1967).

(3) White, H.J., "Industrial Electrostatic Precipitation", Addison-Wesley, (1963).

(4) Sproull, W.T. and Nakada, Y., "Operation of Cottrell Precipitators (Effects of Moisture and Temperature)", Industrial and Engineering Chemistry, Vol. 43, No. 6, pp 1350-1358, (1951).

(5) Penney, G.W., "A new Electrostatic Precipitator", Elect. Engineering, 56 , pp 159-162, (1937).

(6) Robinson, M., "Electrostatic Precipitation", Wiley-Interscience, Part 1, pp 227-355

(7) Sproull, W.T., "Corona Quenching - its significance in Electrical Precipitation", Journal of the Air Pollution Control Association, Vol. 13, No. 12, pp 617-621, (1963).

(8) Winkel, A., and Schuetz, A., "Eletrische Abscheidung Feindisperser Gisenoxid-Staube bei Hoheren Temperaturen unter Besonderer Berucksichtigung des Eletrischen Staubwiderstandes", Staub, 22, 343, (1962).

(9) Low, H.J., and Lucas, D.H., "The Physics of Electrostatic Precipitation", British Journal of Applied Physics, Supplement No:2, 1953, pp S40-S47.

(10) Pauthenier, M., and Moreau-Hanot, M., "La Charge des Particules Spheriques dans un Champ Ionise", J. Physique et Radium 3, sgo, (1932).

(11) Cooperman, P., "Dust Space-charge in Electrical Precipitators", AIEE Conference paper CP62-253: Presented at AIEE Winter General Meeting, N.Y. (1962).

(12) Cooperman, P., "A Theory for Space Charge Limited Currents with Application to Electrical Precipitation", AIEE trans., 79, 47 (1960).

(13) Whitehead, J.B., "High-Voltage Corona" in "Internation Critical Tables", (McGraw-Hill, 1929).

(14) Peek, F.W., "Dielectric Phenomena in High-Voltage Engineering", (McGraw-Hill, 1929), Chapter 1V.

(15) Awad, M.B., and Castle, G.S.P., "Some parameters affecting the generation of Ozone in Positive and Negative Corona", Presented at the 1973 Annual meeting of the IEEE on Industrial Application Society. Accepted for the Journal of the IEEE trans. on IGA.

(16) Townsend, J.S., "Electricity in Gases", Oxford University Press, New York, (1914).

(17) Sarma, M.P., and Janischewsky, W., "D.C. Corona on Smooth Conductors in Air, Steady-state Analysis of the Ionization Layer", Proc. IEE, Vol. 116, No. 1, (1969).

(18) Khalifa, M., and Abdel-Salam, M., "Calculating the surface fields of conductors during corona", Proc. IEE, Vol. 120, No. 12, pp 1574-1575, December 1973.

(19) Pauthenier, M., "Lois de Charge des Particules Spheriques Conductrices dans un Champ Electrique Bi-Ionise", Colloque International-La Physique des Forces Electrostatiques et Leurs Applications (published by centre National de la Recherche Scientifique, Paris, 1961).

(20) Waters, R.T., et al. "Electric field measurements in D.C. Corona discharges", IEE Conference Publication, 1970, pp 188-190.

(21) Cobine, J.D., "Gaseous Conductors Theory and Engineering Applications", Dover Publications, New York, 1958, pp 256-270.

(22) Evans, R., "Electrostatic Charging in the Corona and subcorona regions', M.E.Sc. thesis, University of Western Ontario, (1975).

(23) Loeb, L.B., "Current Increase at Constant Amplification Factor in Steady Corona with Caxial cylindrical Geometry", Physical Review, Vol. 90, No. 1, pp 144-145, (1953).

(24) Colli, L., et al, "Dynamics of Corona Discharge Between Cylindrical Electrodes", J. of applied physics, Vol. 25, No. 4, pp 429-435, (1954).

(25) Troost, N., "A New Approach to the Theory and Operation of Electrostatic Precipitators for use on Pulverized-Fuel-Fired Boilers", Proc. of IEE, Power Engineering (London), 101, 369, (1954).

(26) Low, H.J., and Lucas, D.H., Discussion on reference (25), Proc. IEE, Power Engineering London, 385, (1954).

(27) Awad, M.B., and Castle, G.S.P., "Ozone Generation in an Electrostatic Precipitator with a Heated Corona Wire", J. of the Air Pollution Control Association, April 1975, Vol. 25, No. 4, pp 369-374.

(28) Khalifa, M., and Abdel Salam, M. "Improved method for calculating D.C. Corona losses", presented at the IEEE PES 1973 Summer meeting and EHV/UHV Conference, Vancouver, B.C., Canada, pp 720-726.

(29) Leutret, G., and Bohlen, B., "The Spatial Trend of Electric Field Strength and Space Charge Density in Plate-Type Electrostatic Precipitators", Staub-Reinhalt. Luft Vol. 32, No. 7, July 1972, pp 27-33.

(30) Cooperman, P., "A New Technique for the measurement of corona field strength and current density in Electrical Precipitation", AIEE Trans., Pt. I (Communication and Electronics), Vol. 75, March 1956, pp 64-66.

(31) Cooperman, P., Report No. 46, Research-Cottrell, Inc., Bound Brook, N.J., 1952.

(32) Sarma, M.P., and Janischewskyj, W. "Analysis of Corona Losses on D.C. Transmission Lines: I-Unipolar Lines", IEEE trans. on PAS, Vol. PAS-88, No. 5, May 1969, pp 718-731.

(33) Deutsch, W., "Uber die dichtverteilung unipolarer Ionenstrome", Ann. Physik, Vol. 5, pp 589-613, (1933).

(34) Khalifa, M., Discussion on Reference (32), IEEE trans., on PAS, May 1969, p 726.

(35) Arten, P., Discussion on Reference (32), IEEE trans, on PAS, May 1969, p 728.

(36) Felici, N., "Recent advances in the analysis of D.C. ionized electric field", direct current, Vol. 8, No. 9 and 10.

(37) Gall, C.F., and Lammer, W., "The lateral distribution of current from wire-to-plate coronas", IEEE trans. on Industry and General Applications, IGA-7, 426, (1971).

(38) Penney, G.W., and Matick, R.E., "Potentials in D.C. Corona fields", AIEE, May 1960, pp 91-99.

(39) Pauthenier, M., and Moreau-Hanot, M., "La Charge des Particules Spheriques dans un Champ Ionise", J. Physique et. Radium 3, 590, (1932).

(40) Arendt, P., and Kallmann, H., "The Mechanism of Charging Mist Particles", Z. Phys. 35, 421 (1926).

(41) Hignett, E.T., Proc. Inst. Elect. Engrs., 114, 1325, (1967).

(42) Liu, B.Y.H., et al, J. Colloid Interface Sci., 23, 367, (1967).

(43) Smith, R.L., and Penney, G.W., "The charging of non-spherical particles in a corona discharge", AIEE Conference paper presented at Winter General meeting, New York, February 1961.

(44) Cochet, R., "Lois de charge des Fines Particules (submicronique) Etudes Theoretiques, Controles Recents Spectre de Particules". Colloque International-La Physique des Forces Electrostatiques et Leurs Applications (published by Centre National de la Recherche Scientifique, Paris, 1961).

(45) Deutsch, W., Ann. der Physik 68, 335, (1922).

(46) Deutsch, W., "Uber die Raumladring-sbeschwerte Townsend-entladring [illegible]ichten Nebel", Ann. der. Phys., (5 Floge), 10: 847 (1931).

(47) Loeb, L.B., "Electrical Coronas, Their Basic Physical Mechanisms", Berkeley: University of California Press, 1965.

(48) Nasser, E., "Fundamentals of Gaseous Ionization and Plasma Electronics", Wiley-Interscience, 1971.

(49) Cottrell, F.G., "Art of Separating Suspended particles from Gaseous Bodies", U.S. Patent, 895, 729 (1908).

(50) Penney, G.W., and Craig, S.E., "Sparkover as influenced by surface conditions in D.C. Corona", AIEE trans. pt. I (Communication and Electronics), Vol. 79, May 1960, pp 112-118.

(51) Cooperman, P. "Positive polarity Operation of Electrostatic Precipitators", IEEE trans. on Communication and Electronics, Vol. 83, No. 75, November 1964.

(52) Vuhuu, Q., and Comsa, R.P., "Influence of gap length on wire-plane Corona", IEEE trans., PAS, Vol. 88, October 1969, pp 1462-1475.

(53) Penney, G.W., and Hewitt, J.G., "Some Measurements of Abnormal Corona", AIEE trans. pt.II, July 1958, pp 319-327.

(54) Chemical Engineering Dictionary, 1970, p 317.

(55) Pordi, V., and Melandri, C., "Size Spectrometery of D.O.P. Particles Using Low Temperature Separation and Replica Technique", Staub-Reinhalt Luft, Vol. 30, No. 3, March 1970, pp 31-34.

(56) Penney, G.W.; and Crynack, R., "Charging of fine particles in negative corona near sparkover", IEEE trans. IGA, July-August 1974, pp 524-532.

(57) Silverman, L.S. et al, "Particle Size Analysis in Industrial Hygiene", Academic Press, New York and London, pp 235-245, (1971).

(58) Strauss, W. (Editor), "Air Pollution Control", Wiley-Interscience, Part 1, 1971, pp 95-176.

(59) Rosenberg, H.S., et al, "The status of SO_2 Control Systems", Chemical Engineering Progress, Vol. 71, No. 5, 1975, pp 66-71.

(60) Isahayer, F., Staub Reinhalting der Luft (in English) 33 (4), 194 (1973).

(61) Shelstad, K.A., Castle, G.S.P., Huang, R.C., and Awad, M.B., "Final report to N.R.C. on PRAI grant Project, P 7305, August 1975.

(62) Tassicker, O.J. "Performance of cold side and hot side electrostatic precipitators", Research Report, Electric Power Research Institute, California, U.S.A. 1974.

(63) Mills, R.A., and Tassicker, O.J. "Analysis of Pilot Plant Electrostatic Precipitators Testing in Connection with Hintly Power Station", International Clean Air Conference, 1975, pp 67-91.